

QUANTUM TWO-PHOTON LASER IN KERR-LIKE MEDIUM

FAISAL HAMOOD AHMED MATHKOOR

**FACULTY OF SCIENCE
UNIVERSITI MALAYA
KUALA LUMPUR**

2020

QUANTUM TWO-PHOTON LASER IN KERR-LIKE MEDIUM

FAISAL HAMOOD AHMED MATHKOOR

**THESIS SUBMITTED IN FULFILMENT OF THE
REQUIREMENTS FOR THE DEGREE OF DOCTOR OF
PHILOSOPHY**

**DEPARTMENT OF PHYSICS
FACULTY OF SCIENCE
UNIVERSITI MALAYA
KUALA LUMPUR**

2020

UNIVERSITI MALAYA

ORIGINAL LITERARY WORK DECLARATION

Name of Candidate: **FAISAL HAMOOD AHMED MATHKOOR**

Name of Degree: **DOCTOR OF PHILOSOPHY**

Title of Project Paper/Research Report/Dissertation/Thesis ("this Work"):

QUANTUM TWO-PHOTON LASER IN KERR-LIKE MEDIUM

Field of Study: **THEORETICAL PHYSICS**

I do solemnly and sincerely declare that:

- (1) I am the sole author/writer of this Work;
- (2) This work is original;
- (3) Any use of any work in which copyright exists was done by way of fair dealing and for permitted purposes and any excerpt or extract from, or reference to or reproduction of any copyright work has been disclosed expressly and sufficiently and the title of the Work and its authorship have been acknowledged in this Work;
- (4) I do not have any actual knowledge nor do I ought reasonably to know that the making of this work constitutes an infringement of any copyright work;
- (5) I hereby assign all and every rights in the copyright to this Work to the University of Malaya ("UM"), who henceforth shall be owner of the copyright in this Work and that any reproduction or use in any form or by any means whatsoever is prohibited without the written consent of UM having been first had and obtained;
- (6) I am fully aware that if in the course of making this Work I have infringed any copyright whether intentionally or otherwise, I may be subject to legal action or any other action as may be determined by UM.

Candidate's Signature

Date:

Subscribed and solemnly declared before,

Witness's Signature Name:

Date:

Designation:

QUANTUM TWO-PHOTON LASER IN KERR-LIKE MEDIUM

ABSTRACT

In this thesis, we studied the Kerr nonlinearity effects on nonclassicality and statistics of the laser field besides the effects of detuning, injection rate, and intensity-dependent coupling (IDC). We developed a quantum theory of light generated from a two-photon laser (TPL) with nonlinear Kerr-like medium in a laser dissipative cavity. The full quantum mechanical approach with the density matrix of the particle-field system is used to derive the TPL master equation based on Scully-Lamb's quantum theory of laser. Various dynamical operators of interest for the cavity field are calculated analytically and computed numerically. The sophisticated computational program was developed to obtain the numerical solution for the nonlinear density matrix equation where the exact solution is not possible. We obtained an approximate soluble form of the photon number distribution equation using reasonable assumptions. The assumptions are justified by making a comparison with the exact numerical results that show a good agreement for small fluctuations in the field. We studied the dynamics and effects of injection rate, two-photon detuning, the Kerr parameters, and IDC on mean photon number, entanglement criterion, second-order correlation functions $g^{(2)}$, Mandel- Q parameter, and photon number distribution. In the absence of IDC, we found that the field behaves nonclassically for a wide range of the selected parameters. The results show that the injection rate and detuning decrease the inter-mode correlation and change the field statistics from sub-Poissonian to super-Poissonian. However, the Kerr parameters change the field statistics from super-Poissonian to sub-Poissonian. This means that the Kerr parameters reduce the fluctuations in the mean photon number below the Poissonian classical limit, which is for photon number squeezed light. Moreover, Kerr parameters transform the detuning to become intensity-dependent

and shift the field frequency through the effective detuning. In the presence of IDC, we found the effects of Kerr parameters and detuning are greatly suppressed, but the effects of the injection rate are enhanced. The nonlinearity of the Kerr effect results in a dramatic decrease in the mean photon number. However, the IDC rises mean photon numbers substantially. The generated photons have nonclassical properties that would last for a long time. Interestingly, statistics of the field are reversed and become super-Poissonian under the effects of Kerr parameters and sub-Poissonian under the injection rate, which is the opposite of the previous case of no IDC. The results show competition between the Kerr effect and both the two-photon detuning and the IDC with dominance in favor of the later. These competitions become important if we can exploit and control them to produce desirable nonclassical photons with acceptable photon number and photon number fluctuations that would be useful in certain applications in quantum metrology and quantum information.

Keywords: Two-Photon Laser, Kerr effect, Intensity-dependent coupling.

ABSTRAK

Di dalam tesis ini, kajian berkenaan kesan ketaklinearan Kerr ke atas keadaan tak klasik dan statistik medan laser dijalankan disamping mengkaji kesan pengurangan (detuning) laser, kadar masukan dan gandingan yang bergantung kepada keamatan (IDC). Teori kuantum cahaya yang dihasilkan dari laser dua foton (TPL) dengan ketaklinearan medium Kerr-like dalam laser rongga lesap. Pendekatan kuantum mekanik secara menyeluruh dengan ketumpatan matriks bagi sistem zarah-medan digunakan untuk menerbitkan persamaan master untuk TPL berdasarkan teori kuantum laser Scully-Lamb. Pelbagai operator dinamik terpilih bagi medan rongga dihitung secara analitik dan dikira secara berangka. Aturcara komputasi yang canggih telah dibangunkan untuk mendapatkan penyelesaian berangka bagi matriks ketumpatan tak linear dimana tiada kebarangkalian mendapatkan hasil yang tepat. Anggaran bentuk penyelesaian telah diperolehi bagi persamaan taburan bilangan foton menggunakan set andaian yang munasabah. Andaian tersebut adalah wajar dengan membuat perbandingan dengan hasil pengiraan berangka yang tepat, yang mana ianya menunjukkan keputusan yang selari dengan pergolakan kecil dalam medan. Kajian keatas kedinamikan dan kesan kadar masukan, detuning dua-foton, parameter Kerr, dan IDC keatas purata bilangan foton, kriteria kebergelutuan, fungsi korelasi tertib kedua $g^{(2)}$, parameter Mandel-Q, dan taburan bilangan foton. Tanpa kehadiran IDC, kami dapati bahawa medan bertindak secara tidak klasik dalam julat parameter yang terpilih. Keputusan menunjukkan kadar masukan dan detuning telah menurunkan nilai korelasi Antara mod dan mengubah statistic medan dari sub-Poissonian ke super-Poissonian. Walau bagaimanapun, parameter Kerr mengubah statistic medan dari super-Poissonian ke sub-Poissonian. Ini menunjukkan parameter Kerr mengurangkan pergolakan purata bilangan foton dibawah

had klasik Poissonian, iaitu untuk bilangan foton cahaya termampat. Tambahan pula, parameter Kerr mengubah keadaan detuning menjadi keadaan bergantung-keamatan, dan menganjak frekuensi medan melalui kaedah detuning yang berkesan. Dengan kehadiran IDC, didapati kesan parameter Kerr dan detuning dipadamkan, tetapi kesan kadar masukan dipertingkatkan. Ketaklinearan kesan Kerr mengakibatkan penurunan dramatik dalam purata bilangan foton. Walaubagaimanapun, IDC telah menaikkan bilangan foton dengan ketara. Foton-foton yang dijana mempunyai ciri-ciri tidak klasik yang akan kekal untuk tempoh masa yang panjang. Apa yang menarik, statistic medan diterbalikkan dan menjadi super-Poissonian di bawah kesan parameter Kerr dan menjadi sub-Poissonian bawah kesan kadar masukan, dimana perkara ini bertentangan dengan kes tanda IDC sebelum ini. Keputusan dari kajian menunjukkan persaingan antara kesan Kerr dengan kedua-dua detuning dua foton dan IDC dengan kesan dominan memihak kepada IDC. Persaingan ini penting jika kita dapat mengeksploitasi dan mengawal mereka untuk menghasilkan foton tak klasik yang dikehendaki dengan bilangan foton yang wajar dan pergolakan foton yang berguna dalam aplikasi-aplikasi tertentu dalam kuantum metrologi dan kuantum maklumat.

Kata kunci: Laser dua-foton, kesan Kerr, gandingan bergantung keamatan

ACKNOWLEDGEMENTS

The process of earning a Ph.D. and writing this thesis has been long and arduous. First of all, I would like to express my sincere gratitude to my supervisor, Professor Dr. Raymond Ooi for continuously pushing me to complete my Ph.D. study, as well as for his patience, motivation, and immense knowledge. His guidance has helped me in difficult times, in research and writing of this thesis, particularly through his insightful comments, wisdom, and encouragement.

My sincere appreciation is to my family for their prayers, encouragement, and patience. It is to my father who passed away during my study in Universiti Malaya who was my shoulder in this life and I miss him too much. It is also to my sisters, brothers, and cousins whose prayers and unlimited support were my strengths. Special thank you to my friends: Mujahed Al-Dheeb, Dr. Mohammed Qussailah, Dr. Marwan Alnamari, Dr. Mohammed Mofteh, Dr. Ameen Alqadasi, Dr. Jebreel, Dr. Gamal Almoaled, and Dr. Ahmed Nady. These great people are my best friends among many, which is hard to list all of them, whom I appreciate for their support.

My love and appreciation are to my wives, Um Fares and Um Ahmed for their patience, great support, understanding, and love. My love and appreciation go to my daughters, Aisha, Reem, and Sarah and my sons, Fares and Yackoob for their love, patience, and encouragement.

Finally, I would like to express my gratitude and appreciation to Sana'a University (in Yemen) for their support through the scholarship that was offered to me. I am highly indebted to the Universiti Malaya, particularly the Faculty of Science staff for the financial support and extension that enabled me to complete my study. I also would like to thank all members of the Quantum and Laser Science research group for stimulating discussions.

TABLE OF CONTENTS

ABSTRACT	iii
ABSTRAK	v
ACKNOWLEDGEMENTS	vii
TABLE OF CONTENTS	viii
LIST OF FIGURES	xiii
LIST OF TABLES	xvi
LIST OF SYMBOLS AND ABBREVIATIONS	xvii
LIST OF APPENDICES	xviii
CHAPTER 1: INTRODUCTION	1
1.1 Preface.....	1
1.2 Motivations.....	2
1.3 Aims and Objectives.....	6
1.4 Outline.....	6
1.5 Organization of the Thesis.....	7
CHAPTER 2: NONCLASSICALITY OF LIGHT	8
2.1 Introduction.....	8
2.2 Density Matrix.....	10
2.3 Quantization of the Electromagnetic Field.....	15
2.4 Quantum States of the Electromagnetic Field.....	24
2.4.1 Number State.....	25
2.4.2 Thermal State.....	28
2.4.3 Coherent State.....	30

2.4.4	Squeezed State.....	32
2.5	Nonclassical Measures of the Field.....	35
2.5.1	Mandel Q Parameter.....	35
2.5.2	Correlation Functions.....	36
2.5.3	Cauchy-Schwarz Inequality.....	41
2.6	Glauber-Sudarshan P -Representation.....	42
CHAPTER 3: QUANTUM THEORY OF THE LASER.....		45
3.1	Introduction and Background.....	45
3.2	Single Mode Field in Bosonic Reservoir.....	46
3.3	Quantum Theory of the Laser: The Gain Part.....	53
3.3.1	Gain Part of Laser Master Equation.....	53
3.3.2	Coarse Graining - Many Atoms.....	56
3.4	Nonlinear Laser Master Equation: Scully - Lamb Approach.....	57
3.5	Photon Statistics.....	59
3.5.1	Exact Photon Statistics.....	60
3.5.2	Far Above Threshold.....	63
3.5.3	Expansion of Nonlinear Terms.....	64
3.5.4	Below Threshold: Linear Approximation.....	64
3.5.5	Lowest-Order Nonlinearity.....	65
3.6	Laser Spectrum and Linewidth.....	66
CHAPTER 4: TWO-PHOTON LASER WITH SELF-KERR EFFECT.....		68
4.1	Introduction.....	68
4.2	Model and Laser Master Equation.....	70
4.3	The Laser Rate Equation.....	77

4.4	Characterization of the Cavity Field.....	81
4.4.1	Mean Photon Number.....	83
4.4.2	Nonclassicality by $G^{(2)}$ and CSI.....	87
4.4.3	Nonclassicality by Q	89
4.4.4	Fluctuations.....	90
4.4.5	Entanglement.....	92
4.4.6	Photon Statistics.....	93
4.5	The Computational Solution.....	96
4.6	Results and Discussion.....	99
4.6.1	Effects of Injection Rate.....	100
4.6.1.1	On Mean Photon Number.....	100
4.6.1.2	On $G^{(2)}$ and CSI.....	101
4.6.1.3	On Entanglement.....	106
4.6.1.4	On Mandel Q Parameter.....	107
4.6.1.5	On Distribution $P_{n_1 n_2}$	107
4.6.2	Effects of Detuning.....	109
4.6.2.1	On Mean Photon Number.....	109
4.6.2.2	On $G^{(2)}$ and CSI.....	110
4.6.2.3	On Entanglement.....	111
4.6.2.4	On Mandel Q Parameter.....	112
4.6.2.5	On Distribution $P_{n_1 n_2}$	112
4.6.3	Effects of Kerr parameter.....	113
4.6.3.1	On Mean Photon Number.....	113
4.6.3.2	On $G^{(2)}$ and CSI.....	113
4.6.3.3	On Entanglement.....	114

4.6.3.4	On Mandel Q Parameter	115
4.6.3.5	On Distribution $P_{n_1n_2}$	115
4.6.4	Approximate Solution: Agreement and Justification	116

CHAPTER 5: TWO-PHOTON LASER WITH (SELF & CROSS) KERR EFFECT AND IDC 119

5.1	Introduction.....	119
5.2	Model and Laser Master Equation.....	120
5.3	The Laser Rate Equation.....	122
5.4	Field Nonclassicality and its Measures.....	127
5.4.1	Moments	128
5.4.2	Mean Photon Number	132
5.4.3	$G^{(2)}$ and CSI.....	135
5.4.4	Mandel Q Parameter and Fluctuations	137
5.4.5	Entanglement.....	138
5.5	Results and Discussion	139
5.5.1	Effects of Injection Rate	140
5.5.1.1	On Mean Photon Number	140
5.5.1.2	On $G^{(2)}$ and CSI	140
5.5.1.3	On Entanglement	144
5.5.1.4	On Mandel Q Parameter	145
5.5.1.5	On Distribution $P_{n_1n_2}$	146
5.5.2	Effects of Detuning.....	147
5.5.2.1	On Mean Photon Number	147
5.5.2.2	On $G^{(2)}$ and CSI	147
5.5.2.3	On Entanglement	149

5.5.2.4	On Mandel Q Parameter	149
5.5.2.5	On Distribution $P_{n_1 n_2}$	149
5.5.3	Effects of Kerr parameters	150
5.5.3.1	On Mean Photon Number	150
5.5.3.2	On $G^{(2)}$ and CSI	150
5.5.3.3	On Entanglement	151
5.5.3.4	On Mandel Q Parameter	151
5.5.3.5	On Distribution $P_{n_1 n_2}$	152
5.5.4	Approximate Solution with IDC: Agreement and Justification	152
CHAPTER 6: CONCLUSION		154
REFERENCES		156
LIST OF PUBLICATIONS AND PAPERS PRESENTED		171
APPENDICES		175

LIST OF FIGURES

Figure 4.1: Energy levels of photon number states and probability flow corresponding to the diagonal elements of the density matrix, Equation (4.23).	78
Figure 4.2: Mean photon number $\langle n_1 \rangle$ (upper panel) and entanglement E (lower panel). The dynamics and parameter dependence for: (a) injection rate r_a ($\Delta = 0$, $\chi_1 = 50\kappa$), (b) detuning Δ ($r_a = 40\kappa$, $\chi_1 = 50\kappa$), and (c) Kerr parameter χ_1 ($r_a = 40\kappa$, $\Delta = 0$).....	101
Figure 4.3: Mean photon number $\langle n_1 \rangle$ (upper panel) and entanglement E (lower panel). The dynamics for: (a) $\Delta = 0$, $\chi_1 = 50\kappa$, (b) $r_a = 40\kappa$, $\chi_1 = 50\kappa$, and (c) $r_a = 40\kappa$, $\Delta = 0$	102
Figure 4.4: Mean photon numbers, $\langle n_1 \rangle, \langle n_2 \rangle$ (upper panel) and Q (lower panel); parameter dependence for: (a) injection rate r_a ($\Delta = 0$, $\chi_1 = 50\kappa$), (b) detuning Δ ($r_a = 40\kappa$, $\chi_1 = 50\kappa$), and (c) Kerr parameter χ_1 ($r_a = 40\kappa$, $\Delta = 0$).	102
Figure 4.5: $g_{11}^{(2)}$ (upper panel) and $g_{22}^{(2)}$ (lower panel). The dynamics and parameter dependence for: (a) injection rate r_a ($\Delta = 0$, $\chi_1 = 50\kappa$), (b) detuning Δ ($r_a = 40\kappa$, $\chi_1 = 50\kappa$), and (c) Kerr parameter χ_1 ($r_a = 40\kappa$, $\Delta = 0$).	104
Figure 4.6: $g_{11}^{(2)}$ (upper panel) and $g_{22}^{(2)}$ (lower panel). The dynamics for: (a) $\Delta = 0$, $\chi_1 = 50\kappa$, (b) $r_a = 40\kappa$, $\chi_1 = 50\kappa$, and (c) $r_a = 40\kappa$, $\Delta = 0$	104
Figure 4.7: $g_{12}^{(2)}$ (upper panel) and CSI (F_{cs} , lower panel). The dynamics and parameter dependence for: (a) injection rate r_a ($\Delta = 0$, $\chi_1 = 50\kappa$), (b) detuning Δ ($r_a = 40\kappa$, $\chi_1 = 50\kappa$), and (c) Kerr parameter χ_1 ($r_a = 40\kappa$, $\Delta = 0$).	105
Figure 4.8: $g_{12}^{(2)}$ (upper panel) and CSI (F_{cs} , lower panel). The dynamics for: (a) $\Delta = 0$, $\chi_1 = 50\kappa$, (b) $r_a = 40\kappa$, $\chi_1 = 50\kappa$, and (c) $r_a = 40\kappa$, $\Delta = 0$	105
Figure 4.9: (upper panel) $g_{ij}^{(2)}$; $i, j = 1, 2$ and (lower panel) CSI (F_{cs} , left-hand axis in red color) and entanglement E (right-hand axis in blue color). The parameter dependence for: (a) injection rate r_a ($\Delta = 0$, $\chi_1 = 50\kappa$), (b) detuning Δ ($r_a = 40\kappa$, $\chi_1 = 50\kappa$), and (c) Kerr parameter χ_1 ($r_a = 40\kappa$, $\Delta = 0$).....	106
Figure 4.10: Q_1 (upper panel) and Q_2 (lower panel). The dynamics and parameter dependence for: (a) injection rate r_a ($\Delta = 0$, $\chi_1 = 50\kappa$), (b) detuning Δ ($r_a = 40\kappa$, $\chi_1 = 50\kappa$), and (c) Kerr parameter χ_1 ($r_a = 40\kappa$, $\Delta = 0$).	108
Figure 4.11: Q_1 (upper panel) and Q_2 (lower panel). The dynamics for: (a) $\Delta = 0$, $\chi_1 = 50\kappa$, (b) $r_a = 40\kappa$, $\chi_1 = 50\kappa$, and (c) $r_a = 40\kappa$, $\Delta = 0$	108

Figure 4.12: The statistics distribution function $P_{n_1 n_2}$, its contours (ellipses) at FWHM, and the single-mode distributions P_{n_1} in black color and P_{n_2} in red color, for each mode for: (i) injection rate r_a , (ii) detuning Δ , and (iii) Kerr parameter χ_1 . The distributions and their contours are evaluated at each of the three values. The vertical (horizontal) line in contours represents width of the distribution P_{n_1} (P_{n_2}). The coordinate of the cross point of the two lines are the averages ($\langle n_1 \rangle$, $\langle n_2 \rangle$). 110

Figure 4.13: Agreement between the exact solution and the analytic approximation at steady-state: (a, b) real part of $\rho_{n_1 n_2; n_1+1 n_2+1}$ (Equations 4.12 and 4.26 at $n_1 = n_2 = 6$) and $\langle n_1 \rangle$ (solution of the quadratic and quintic expressions, Equation 4.44 and Equation 4.41) for (a) $r_a = 40\kappa$, $\chi_1 = 50\kappa$ and (b) $r_a = 40\kappa$, $\Delta = 0$. (c-d) for $r_a = 40\kappa$, $\Delta = 0$, $\rho_{bb} = 0$; $P_{n_1 n_2}$ (at $\chi_1 = 50\kappa$), $\langle n_1 \rangle$, and F_{CS} . 117

Figure 5.1: (i-iv) Mean photon number $\langle n_1 \rangle$ and (v-viii) entanglement E ; the dynamics and parameter dependence are for: (i, v) $\Delta = 0$, $\chi_1 = 50\kappa$, $\chi = 0$, (ii, vi) $r_a = 40\kappa$, $\chi_1 = 50\kappa$, $\chi = 0$, (iii, vii) $r_a = 40\kappa$, $\Delta = 0$, $\chi = 0$, and (iv, viii) $r_a = 40\kappa$, $\Delta = 0$, $\chi_1 = 50\kappa$. 141

Figure 5.2: (i-iv) Mean photon number $\langle n_1 \rangle$ and (v-viii) entanglement E ; the dynamics for: (i, v) $\Delta = 0$, $\chi_1 = 50\kappa$, $\chi = 0$, (ii, vi) $r_a = 40\kappa$, $\chi_1 = 50\kappa$, $\chi = 0$, (iii, vii) $r_a = 40\kappa$, $\Delta = 0$, $\chi = 0$, and (iv, viii) $r_a = 40\kappa$, $\Delta = 0$, $\chi_1 = 50\kappa$. 141

Figure 5.3: (i-iv) Mean photon numbers $\langle n_1 \rangle$, $\langle n_2 \rangle$, and (v-viii) Q_1 , Q_2 . The parameter dependence are for: (i, v) $\Delta = 0$, $\chi_1 = 50\kappa$, $\chi = 0$, (ii, vi) $r_a = 40\kappa$, $\chi_1 = 50\kappa$, $\chi = 0$, (iii, vii) $r_a = 40\kappa$, $\Delta = 0$, $\chi = 0$, and (iv, viii) $r_a = 40\kappa$, $\Delta = 0$, $\chi_1 = 50\kappa$. 142

Figure 5.4: (i-iv) Q_1 and (v-viii) $g_{11}^{(2)}$; the dynamics and parameter dependence for: (i, v) $\Delta = 0$, $\chi_1 = 50\kappa$, $\chi = 0$, (ii, vi) $r_a = 40\kappa$, $\chi_1 = 50\kappa$, $\chi = 0$, (iii, vii) $r_a = 40\kappa$, $\Delta = 0$, $\chi = 0$, and (iv, viii) $r_a = 40\kappa$, $\Delta = 0$, $\chi_1 = 50\kappa$. 143

Figure 5.5: (i-iv) $g_{11}^{(2)}$ and (v-viii) $g_{22}^{(2)}$; the dynamics for: (i, v) $\Delta = 0$, $\chi_1 = 50\kappa$, $\chi = 0$, (ii, vi) $r_a = 40\kappa$, $\chi_1 = 50\kappa$, $\chi = 0$, (iii, vii) $r_a = 40\kappa$, $\Delta = 0$, $\chi = 0$, and (iv, viii) $r_a = 40\kappa$, $\Delta = 0$, $\chi_1 = 50\kappa$. 143

Figure 5.6: (i-iv) $g_{12}^{(2)}$ and (v-viii) CSI (F_{CS}); the dynamics and parameter dependence for: (i, v) $\Delta = 0$, $\chi_1 = 50\kappa$, $\chi = 0$, (ii, vi) $r_a = 40\kappa$, $\chi_1 = 50\kappa$, $\chi = 0$, (iii, vii) $r_a = 40\kappa$, $\Delta = 0$, $\chi = 0$, and (iv, viii) $r_a = 40\kappa$, $\Delta = 0$, $\chi_1 = 50\kappa$. 144

Figure 5.7: (i-iv) $g_{12}^{(2)}$ and (v-viii) CSI (F_{CS}). The dynamics for: (i, v) $\Delta = 0$, $\chi_1 = 50\kappa$, $\chi = 0$, (ii, vi) $r_a = 40\kappa$, $\chi_1 = 50\kappa$, $\chi = 0$, (iii, vii) $r_a = 40\kappa$, $\Delta = 0$, $\chi = 0$, and (iv, viii) $r_a = 40\kappa$, $\Delta = 0$, $\chi_1 = 50\kappa$. 144

- Figure 5.8: (i-iv) $g_{11}^{(2)}, g_{22}^{(2)}, g_{12}^{(2)}$. (v-viii) CSI (F_{cs} , on the left-hand side in red color) and entanglement E (on the right-hand side in blue). The parameter dependence for: (i, v) $\Delta = 0, \chi_1 = 50\kappa, \chi = 0$, (ii, vi) $r_a = 40\kappa, \chi_1 = 50\kappa, \chi = 0$, (iii, vii) $r_a = 40\kappa, \Delta = 0, \chi = 0$, and (iv, viii) $r_a = 40\kappa, \Delta = 0, \chi_1 = 50\kappa$ 145
- Figure 5.9: (i-iv) Q_1 and (v-viii) Q_2 ; the dynamics for: (i, v) $\Delta = 0, \chi_1 = 50\kappa, \chi = 0$, (ii, vi) $r_a = 40\kappa, \chi_1 = 50\kappa, \chi = 0$, (iii, vii) $r_a = 40\kappa, \Delta = 0, \chi = 0$, and (iv, viii) $r_a = 40\kappa, \Delta = 0, \chi_1 = 50\kappa$ 146
- Figure 5.10: The statistics distribution function $P_{n_1 n_2}$, its contours at FWHM, and its two marginal distributions for each single mode for: (i) injection rate r_a , (ii) detuning Δ , (iii) Kerr parameter χ_1 , and (iv) Kerr parameter χ . The contours (ellipses) of the distributions and the single-mode distributions, P_{n_1} in black color and P_{n_2} in red color, for mode 1 and mode 2, respectively, evaluated at each of the three values. 148
- Figure 5.11: The distribution $P_{n_1 n_2}$ (upper panel for $\chi = 50\kappa$), $\langle n_1 \rangle$, and F_{cs} (lower panel) at $r_a = 40\kappa, \Delta = 0, \chi_1 = 0$. The approximate solutions are from Equation 5.39 for quadratic and from Equation 5.35 for quartic. 153

LIST OF TABLES

Table 2.1: Properties of coherent state.....	31
Table 2.2: Properties of squeezed coherent state.....	34

University of Malaya

LIST OF SYMBOLS AND ABBREVIATIONS

CSI : Cauchy-Schwarz Inequality

FWHM : Full Width at Half Maximum

IDC : Intensity-Dependent Coupling

TPL : Two-Photon Laser

University of Malaya

LIST OF APPENDICES

Appendix A: Useful Operator Transformation Formulas	175
Appendix B: The Hamiltonian in the Interaction Picture	180
Appendix C: Atom-Field Density Matrix Elements	183
Appendix D: The Gain Part of the Density Matrix	188
Appendix E: Effective Values of $\langle M_{n_1 n_2}^\pm \rangle_{ss}$ and $\langle L_{n_1+1, n_2+1} \rangle_{ss} - \langle L_{n_1, n_2} \rangle_{ss}$	193
Appendix F: The Generating Function $G(x_1, x_2; t)$	195
Appendix G: Derivation of the Statistics Function $P(n_1, n_2; t)$	199
Appendix H: A General Formula for Moments	201

University of Malaya

CHAPTER 1: INTRODUCTION

1.1 Preface

Light is a jewel of nature. It has been fascinating scientists as well as poets and artists. The man is exposed to the light that comes from the sun or stars. These sources of light were the main sources for a very long time. The curiosity of a man leads him to discover various sources of light for his benefits. The light was, and to somewhat still, a puzzle to scientists. It captivates so many people by its speed, diffraction, and interference. Researchers devoted their time to study its properties and there have been two different views on the nature of light, the wave nature, and the particle nature.

The study of the great scientists, Newton, Huygens, Young, Kirchhoff, and many others paved the way for understanding the nature of the light. Their efforts came to resounding success. It is James Clerk Maxwell, who, as a contributor as well, presented a set of beautiful equations that describe light, which later named after him. This was a revolution in science, and the next leap was at the beginning of the last century when the photon idea was proposed. Since then, and after discovering the quantum theory, the science community adopted the dual nature of the light, a particle, and a wave.

Light is the messenger by which researchers can explore the other worlds, from the microworld of atoms and molecules to the very distant galaxies. It is the light that makes the theory of relativity and quantum mechanics possible. Its behavior led to Lorentz's transformation and guided Einstein to the special theory of relativity. It is the light that led to the black body catastrophe that drove scientists to the quantum theory. The recent advances in understanding the nature came at the beginning of the 1960s when the laser (light amplification by stimulated emission radiation) was invented.

1.2 Motivations

The light from lasers has special characteristics that make it unique from the normal light that comes from the sun or lamps, for example. Uniqueness comes from its directionality and monochromaticity. The laser has versatile applications and becomes daily life technology. The laser light is based on stimulated radiation; an incident photon stimulates an atom from the upper level to the lower level and two photons are scattered by the atom. These scattered photons have the same phase, frequency, and direction of the incident photon.

The process of lasing is composed of three quantum processes: absorption, spontaneous emission, and stimulated emission. Shortly after the invention of the laser, researchers (Sorokin & Braslau, 1964; Prokhorov, 1965) suggested another kind of lasers, the TPL. This laser was based on a theoretical study performed by Göppert-Mayer (1931) almost three decades before the invention of the laser. In her investigation, Goepfert studied the probability of transitions made by the absorption of two quanta (two photons) at the same time.

In TPL, the lasing is accomplished by emitting two photons from an atomic transition between levels of identical parity. The quest for knowledge and curiosity led researchers to perform extensive studies on the possibility of realizing such a new kind of lasers. The TPL is distinguished from its counterpart standard single-photon laser. It promises to display a wealth of new and exciting nonlinear behavior that might lead to novel results (Prokhorov, 1965; Gauthier, 2003). This means that, with TPL, it is possible to achieve high-intensity light that is an unresisting need. The first realization of the two-photon process was measured by Kaiser & Garrett (1961) when they reported a blue fluorescence from two-photon-excited atoms in a europium-doped crystal. Two-photon quantum process idea became the basis for two-photon scanning microscopy (Denk et al., 1990), and the motive for multiphoton microscopy (Ustione & Piston, 2011).

A two-photon laser has attracted a considerable amount of theoretical interest in the literature, semiclassically (Wang & Haken, 1984a,b,c; Bay et al., 1995), and as well as quantum-mechanically (Cheng & Haken, 1988; Zhu & Li, 1987; Boone & Swain, 1990). Its quantum statistical properties such antibunching (Zubairy, 1980) and squeezing (Savage & Walls, 1986; Zubairy et al., 1983) are of great interest. The quantum theory of laser was developed in a series of papers by Scully & Lamb (1967, 1968, 1969); Scully et al. (1970); Kim et al. (1970); Wang & Lamb (1973) and by Haken (2012) and Lax & Louisell (1969). Haken and Lax developed sophisticated techniques to convert operator master equations into *c*-number Fokker-Planck equations or equivalent Langevin's equations. The quantum theory of the two-photon laser (Gauthier, 2003) (for review) has been studied many years ago.

The radiation field has different classical and nonclassical statistical properties, and the two-photon process is in the heart of nonlinear and quantum optics (Walther et al., 2006; Loudon, 1980). The nonclassical properties like squeezing, antibunching, and sub-Poissonian (Davidovich, 1996) can be achieved through nonlinear processes (Brambilla et al., 1992). Entangled photons can be generated through laser-driven schemes involving two-photon emissions and double Raman excitations (Ooi, 2007). The field distribution function obeys the super-Poissonian for thermal light, Poissonian for coherent light, and sub-Poissonian for squeezed light (Fabre, 1992; Kimble, 1992). It is desirable to produce nonclassical properties of light (Loudon, 1980; Walther et al., 2006) for experimental applications where precise measurements are required like gravitational-wave detection (Caves, 1980, 1981; Abadie et al., 2011; Aasi et al., 2013). In photodetection experiments, one difficulty is to overcome the noise in the light source which limits the measurement accuracy. Thus photon fluctuation's reduction is important (Orszag & Retamal, 1991; Orszag, 2016). It has been shown that the pumping statistics (Orszag & Retamal, 1991) and detuning have

significant effects on the statistical properties of the field and can be optimized to reduce the photon fluctuations (Bay et al., 1995).

There are many studies on the statistical properties for one-photon, two-photon, and multi-photon lasers (McNeil & Walls, 1975a,b), correspondingly, from one mode to multimode cases (Schrade et al., 1993; Eremeev et al., 2011). Two-photon transitions, related to the production of squeezed lights (Every, 1975; Knight & Pegg, 1982), and production of the widely used entangled photon pairs by parametric down-conversion, are more interesting than the usual one-photon transitions (Dodonov & Mizrahi, 1997a,b). Photon statistics have been studied in various systems, including single beam (Simaan & Loudon, 1975b, 1978) and double beam (Simaan & Loudon, 1975a), two-photon absorption and stimulated Raman processes (Simaan, 1975). Extensive theory of two-photon laser has been developed and studied for two-level systems (Gauthier, 2003) up to saturation level (Bandilla & Voigt, 1982; Wang & Haken, 1984a; Cheng & Haken, 1988). Exact solutions based on P -representation have been found (Kryuchkyan et al., 1996). In the case of lasing far above the threshold, researchers have obtained analytical expressions for the photon statistics, particularly the photon numbers, moments and correlations of higher orders (Dodonov et al., 1989). However, for the simple degenerate 3-level cascade scheme, analytical expressions of the photon statistics remain challenging and non-trivial (Bay et al., 1995).

The two-photon process is the simplest form of nonlinearity and introducing another nonlinearity to the two-photon atom-field interaction enriches the nonclassical properties of the system. One simple, but interesting, form of this nonlinearity is the Kerr-effect, which has paid much attention since the laser invention (Yurke & Stoler, 1986; Bužek & Jex, 1990; Semiao et al., 2009; Faghihi et al., 2013; Singh & Gilhare, 2016b; Ghorbani et al., 2017). Recently, the two-mode field in a non-dissipative cavity with Kerr-like medium is investigated (Singh & Ooi, 2018). Another nonlinearity which has been investigated by

many researchers is the deformed nonlinear coupling between the matter and the radiation field (Bužek & Jex, 1990; Bartzis, 1990; Napoli & Messina, 1996; Singh & Ooi, 2018).

These studies give us the motivation to investigate the effect of the nonlinearity of Kerr-type and the IDC on the dynamics and nonclassicality of the two-photon laser. By Kerr-effect, the study refers to the optical Kerr effect resulting from the interaction of the light field itself with the matter to distinguish it from other types (external electric or magnetic field). The Kerr-effect has two parts, self-Kerr, and cross-Kerr. The self-Kerr of a mode of the field is produced by the mode itself independently from the other modes. However, the cross-Kerr is the result of the interaction between the two modes through the nonlinear medium.

In the present thesis, the statistical properties and the role of the IDC of a nondegenerate TPL in the Kerr-like medium is studied. The laser cavity is filled with many atoms. To realize the system, the cavity becomes dispersive. To model the dispersion, the dissipation of the cavity through its walls is simulated by allowing the cavity to interact with its surroundings. Several observables of the cavity are calculated in terms of the parameters of the system. These observables are studied through their dependence on time and parameters of the system. Besides the effects of these various parameters, the impact of the IDC on the statistical properties and distribution function of two modes of the lasing photons is investigated.

In this study, the approach of Scully & Lamb (1967) to calculate the master equation for the laser is followed. Exact nonlinear quantum theory of laser for a system of N two-level atoms in a doubly resonant cavity is used. The master equation of the system is derived and from the resulting master equation, the photon statistics and equations for other measurable quantities to characterize the field are obtained. The mean photon number, the $G^{(2)}$, and the Mandel- Q parameter are calculated also. The nonclassicality of the TPL is investigated

through the violation of the Cauchy-Schwarz inequality (CSI) and values of the Q that determine the kind of statistics (Poissonian, sub-Poissonian, and super-Poissonian).

1.3 Aims and Objectives

The objectives of the present work are:

1. Deriving the full quantum master equation of the TPL using the Scully-Lamb approach.
2. Obtaining an analytic approximate solution to the rate equation and the moments of the photon distribution.
3. Solving the full density-matrix and various nonclassicality measures of the TPL numerically.
4. Studying the effects of the Kerr parameters on the statistical properties of the cavity field of the TPL.
5. Studying the impact of the injection rate and detuning on the nonclassical properties of the TPL in Kerr-like medium.
6. Investigating the role of the IDC on the statistical properties of the TPL.

1.4 Outline

The thesis covers the following main topics:

1. The density matrix: The focus is on the derivation of the density matrix from which all required observables are obtained.
2. The rate equation: The focus is on the derivation of an approximate expression for the rate equation. Off-diagonal elements in the rate equation are approximated by diagonal elements. The resulting expression makes the subsequent calculations an easier task.
3. The moments and correlations: In this topic, the main theme is on deriving and solving the first moments and calculation of the $G^{(2)}$ and Q . Analyzing the assumptions

behind the approximation and calculation of the mean photon number is given. The nonclassicality measures follow from the calculation of the moments.

4. The photon statistics: The main focus is on deriving an analytic approximate solution for the photon distribution.
5. The simulation: In this topic, an account of the algorithm used to solve the multi-dimensional density matrix and the computational challenges are provided.

1.5 Organization of the Thesis

The thesis has the following structure: The first chapter is the introduction in which the motivations behind the research work are given. It also gives an account of the aims and objectives of the study and the outline of the research. Chapter 1 is concluded by presenting a summary of the thesis structure. The second chapter is devoted to the literature review in which a review of the previous related published works is presented. Chapter 1 also contains a brief account of the background of the field of quantum and nonlinear optics. Chapter 3 is devoted to the quantum theory of the laser where more details on the calculation of the master equation of the laser are given. The main chapters are Chapter 4 and Chapter 5 where the effects of the injection rate, detuning, and self-Kerr parameters on the statistical properties of the TPL are studied. In Chapter 5, the role of IDC and the cross-Kerr effect are also studied. Finally, the conclusion of the research and suggestions for future work are presented in Chapter 6.

CHAPTER 2: NONCLASSICALITY OF LIGHT

2.1 Introduction

A nonclassical phenomenon is the which cannot be explained in the framework of classical physics, and have an explanation in quantum physics. Nonclassical light is light with characteristics that can be described only within quantum optics; a field of physics that concerns the study and applications of the quantum interactions of the electromagnetic field with the matter. Dodonov & Man'ko (2003, Chapter 1) presented a comprehensive review of nonclassical states of light. A brief review on different families of nonclassical states was presented but much detail is given to squeezed and Schrodinger's cat states. They provided a comprehensive list of bibliography to the material for researchers and interested people. Nonclassical states refers to the quantum states that cannot be produced in the usual sources of light, such as lasers or lamps, rather than those requiring more sophisticated apparatus for their production.

Nonclassical light shows nonclassical behavior such as entanglement (an aspect of highly nonclassical correlation) (Einstein et al., 1935; Schrödinger, 1935, 1936; Audretsch, 2008), squeezing (Walls, 1983; Loudon & Knight, 1987; Knight & Bužek, 2004; Lvovsky, 2015; Schnabel, 2017), and antibunching (Kimble et al., 1977; Loudon, 1980; Mandel, 1986; Zou & Mandel, 1990; Mandel & Wolf, 1995). Nonclassical light has nonclassical states (Tan & Jeong, 2019; Dodonov, 2002) such as squeezed states and Fock or number states. It has a sub-Poissonian statistics (Mandel, 1979; Short & Mandel, 1983) of no classical counterpart. According to the Web of Science electronic database of journals and articles in titles in the field of optics only, the phrases "nonclassical states" , "squeezed states", "squeezing", and "entanglement" appear 336, 1323, 3150, and 15998 times respectively. This shows the huge amount of interest in the subject.

Nonclassicality is relevant in fundamental quantum physics and also in the context of some high-precision measurements. Sub-Poissonian beams and quadrature-squeezed light have been envisaged in communications, in precise interferometric measurements, and in the detection of gravitational waves (Davidovich, 1996; Caves, 1980, 1981). The nonclassicality is an important resource in quantum metrology. It has been demonstrated that the nonclassicality of a continuous-variable state is a quantifiable resource for parameter estimation tasks (Kwon et al., 2019). In the field of quantum optics and quantum information, the non-classical effects of quantum states, such as sub-Poisson statistical distribution, the squeezing effect, and the photon anti-bunching effect are a research focus for both theorists and experimentalists. Their importance is due to their wide applications in various fields, such as quantum key distribution, quantum measurement, quantum computation, and quantum teleportation (Bouwmeester & Zeilinger, 2000; Vedral, 2006; Mermin, 2007; Barnett, 2009; Nielsen & Chuang, 2010; Yamamoto & Semba, 2015).

Squeezed light exhibits noise reduction in one quadrature component and increasing noise in the other conjugate quadrature component. The most familiar kinds of squeezed light have either reduced amplitude noise or reduced phase noise, with increased noise of the other component. Fock states (also called photon number states) have a well-defined number of photons (stored, e.g., in a cavity), while the phase is totally undefined (Kim et al., 2012). The most classical state of the quantum light is the coherent state (Glauber, 1963a,b) in which the noise in each quadrature of the field is equal to the minimum quantum uncertainty (Mandel & Wolf, 1995; Gardiner & Zoller, 2004).

The important question that should be asked is how can one know the light is nonclassical? To differentiate between classical and nonclassical light, scientists adopted several measures. One of these, which is considered a definitive measure of nonclassicality is that the Glauber-Sudarshan P -representation has a negative value or being more singular than

a Dirac delta function (Glauber, 1963a; Titulaer & Glauber, 1965; Mandel, 1986; Hillery, 1987; Mandel & Wolf, 1995; Richter & Vogel, 2002; Agarwal, 2013; Kwon et al., 2019). However, many researchers have found regular nonclassical states (Damanet et al., 2018; Kühn & Vogel, 2018). The P -representation helps deduce a set of inequalities for field properties that the classical field obeys. A violation of these inequalities indicates the nonclassicality of the field as can be seen for CSI (Titulaer & Glauber, 1965; Loudon, 1980; Zubairy, 1982). One more measure to study the nonclassicality of the light is the correlation functions introduced by Glauber soon after the invention of the laser (Glauber, 1963a,c; Loudon, 1980). Another measure is the Mandel- Q parameter (Mandel, 1979, 1986; Mandel & Wolf, 1995) which quantifies the field fluctuations. Kwon et al. (2019) introduced the metrological power as a new measure for nonclassicality and showed that any pure state with negativity in the P function provides metrological enhancement over all classical states in displacement estimation tasks.

Nonclassical light is often generated either in nonlinear devices such as sub-threshold optical parametric oscillators or frequency doublers or in systems with only a single atom or ion (or just a few such emitters), such as a single-atom laser. The interested reader may refer to other dedicated reviews of the subject for more indepth discussions (Braunstein & van Loock, 2005; Davidovich, 1996; Boyd et al., 2019).

2.2 Density Matrix

The density matrix was introduced by von Neumann (1927) to describe statistical concepts in quantum mechanics. Since then its use grows up from quantum mechanics and statistical physics to other fields (McWeeny, 1960; Haar, 1961). In quantum mechanics, the concern is almost on states of systems that are represented by state vectors. This is true for a single isolated or noninteracting system or a pure state. However, we are often confronted with situations where the system is coupled to another system and the interest

becomes in one of these two systems but not the other. Here, equations for this system alone are written and what happens to the other is ignored. The truncation of the total problem automatically reduces our knowledge and usually results in a mixture.

In the mixture case, we are completely ignorant about the states of the system but rather the classical probabilities for having various possible state vectors (Landau & Lifshitz, 1981; Louisell, 1973; Sargent III et al., 1974; Meystre & Sargent, 2007; Blum, 2012). In this case, the calculation of averages and wave functions of the physical quantities characterizing a given system using state vectors is extremely cumbersome. So, the primary reason to have an alternative and mathematically compact tool is to facilitate the treatment of many-particle interacting quantum systems. The second reason is that the physical system goes into various kinds of damping and one must include them for a valid and more complete description. Some of these can be incorporated directly into equations of motion for the probability amplitudes (the wave functions). However, for other damping mechanisms such as decoherence, we need a more general description than can be provided by the state vector (Sargent III et al., 1974; Schleich, 2001; Rand, 2016). For these reasons, the density matrix gains its importance.

For two noninteracting systems, A and B , the state vector of the combined system is the direct product of the pure state vectors of each subsystem

$$|\psi_{A+B}\rangle = |\psi_A = \phi_A\rangle \otimes |\psi_B = \phi_B\rangle = |\phi_A\rangle|\phi_B\rangle, \quad (2.1)$$

where $|\phi_A\rangle$ and $|\phi_B\rangle$ are eigenstates of the subsystems A and B , respectively. If at a specific point of time the two subsystems are allowed to interact, the state vector of the combined system $|\psi_{A+B}(t)\rangle$ can be expressed in terms of orthonormal basis vectors $|a_i\rangle$

and $|b_j\rangle$ of each subsystem

$$|\psi_{A+B}(t)\rangle = \sum_{ij} C_{ij}^{ab}(t) |a_i b_j\rangle \langle a_i b_j|, \quad (2.2)$$

where the coefficient $C_{ij}^{ab}(t)$ are the probability amplitude at time t of the subsystem A being in the state $|a_i\rangle$ and subsystem B in state $|b_j\rangle$. If the two subsystems have not interacted at all, the system state vector of the combined system, Equation 2.2, becomes the direct product of the state vectors of its subsystems and the system is in its pure state. The combined system is said to be *entangled* if its state vector cannot be factorized into a product of the states of its subsystems.

The density or statistical operator ρ , is a sum of projectors $|\psi_i\rangle\langle\psi_i|$ onto the possible state vectors $|\psi_i\rangle$, each weighted by a classical probability P_i

$$\rho = \sum_i P_i |\psi_i\rangle\langle\psi_i|. \quad (2.3)$$

Here the summation can take the form of several summations and integrals. The expectation value of an observable M is calculated by taking the quantum mechanical average then taking the ensemble average of all possible states. In another words, one has to sum up all the possible values of the observable from the quantum state $|\psi_i\rangle$ then taking the statistical average of the system in the state $|\psi_i\rangle$ with probability P_i

$$\langle M \rangle = \sum_i P_i \langle \psi_i | M | \psi_i \rangle. \quad (2.4)$$

In a chosen complete orthonormal set of basis ϕ_j , Equation 2.4 is written as

$$\begin{aligned}\langle M \rangle &= \sum_i P_i \langle \psi_i | M \sum_j |\phi_j\rangle \langle \phi_j| | \psi_i \rangle = \sum_{ij} P_i \langle \phi_j | \psi_i \rangle \langle \psi_i | M | \phi_j \rangle \\ &= \sum_j \langle \phi_j | \sum_i P_i | \psi_i \rangle \langle \psi_i | M | \phi_j \rangle = \text{Tr}(\rho M),\end{aligned}\quad (2.5)$$

where in the last equality, Equation 2.3 and trace notation are used. The result is independent of the basis used as it should be. For two subsystems in interaction, sometimes our interest becomes in knowing the behavior of only one of them, say A . Now, let $M^{(A)}$ be an operator in the space of subsystem A , where the superscript A denotes that the operator acts only on the variables of its subsystem A . Hence expectation value of $M^{(A)}$ is

$$\begin{aligned}\langle M^{(A)}(t) \rangle &= \text{Tr} \left[\rho(t) M^{(A)} \right] \\ &= \sum_{ij} \langle \psi_i^{(A)} \psi_j^{(B)} | \rho(t) M^{(A)} | \psi_i^{(A)} \psi_j^{(B)} \rangle \\ &= \sum_{ijkl} \langle \psi_i^{(A)} \psi_j^{(B)} | \rho(t) | \psi_k^{(A)} \psi_l^{(B)} \rangle \langle \psi_k^{(A)} \psi_l^{(B)} | M^{(A)} | \psi_i^{(A)} \psi_j^{(B)} \rangle \\ &= \sum_{ijkl} \langle \psi_i^{(A)} \psi_j^{(B)} | \rho(t) | \psi_k^{(A)} \psi_l^{(B)} \rangle \langle \psi_k^{(A)} | M^{(A)} | \psi_i^{(A)} \rangle \delta_{lj} \\ &= \sum_{ik} \left(\sum_j \langle \psi_i^{(A)} \psi_j^{(B)} | \rho(t) | \psi_k^{(A)} \psi_j^{(B)} \rangle \right) \langle \psi_k^{(A)} | M^{(A)} | \psi_i^{(A)} \rangle \\ &= \sum_{ik} \langle \psi_i^{(A)} | \rho^{(A)}(t) | \psi_k^{(A)} \rangle \langle \psi_k^{(A)} | M^{(A)} | \psi_i^{(A)} \rangle \\ &= \sum_i \langle \psi_i^{(A)} | \rho^{(A)}(t) M^{(A)} | \psi_i^{(A)} \rangle = \text{Tr}_B \left[\rho^{(A)}(t) M^{(A)} \right],\end{aligned}\quad (2.6)$$

where the relevant density matrix that contains only the variables of subsystem A is defined by the matrix elements

$$\langle \psi_i^{(A)} | \rho^{(A)}(t) | \psi_k^{(A)} \rangle = \sum_j \langle \psi_i^{(A)} \psi_j^{(B)} | \rho(t) | \psi_k^{(A)} \psi_j^{(B)} \rangle, \quad (2.7)$$

and Tr_B denotes the trace is over subsystem B variables. This relevant density matrix is called the reduced density matrix. It has the operator form

$$\rho^{(A)}(t) = \text{Tr}_B \rho(t). \quad (2.8)$$

The time evolution of the density operator is given by the *Liouville equation*

$$\frac{\partial}{\partial t} \rho = -\frac{i}{\hbar} [H, \rho]. \quad (2.9)$$

The solution of Equation 2.9 in terms of the unitary evolution operator $U(t, t_0)$ is given by

$$\rho(t) = U(t - t_0) \rho(t_0) U^\dagger(t - t_0). \quad (2.10)$$

For time-independent Hermitian Hamiltonian H , the evolution operator has the form

$$U(t - t_0) = e^{-i/\hbar H(t-t_0)}, \quad (2.11)$$

and Equation 2.10 has the solution

$$\rho(t) = e^{-i/\hbar H(t-t_0)} \rho(t_0) e^{i/\hbar H(t-t_0)}. \quad (2.12)$$

Here is a summarized list of a few important properties of the density operator. (Puri, 2001):

1. The density operator of a mixture is given by Equation 2.3 and for a pure state, it is reduced to a single quantum state $|\psi_i\rangle\langle\psi_i|$.
2. The density operator is Hermitian $\rho^\dagger = \rho$ with $\text{Tr}\rho = 1$.
3. The density operator is positive-definite $\langle\psi|\rho|\psi\rangle \geq 0$.
4. For mixed state, $\text{Tr}\rho^2 < 1$, but for pure state $\rho^2 = \rho$ and $\text{Tr}\rho^2 = 1$.
5. The diagonal elements of the density matrix are non-negative real numbers and repre-

sent the probability of the system being in particular states of a chosen representation.

6. The off-diagonal elements represent the coherence and are complex in general.

The main virtue of the density matrix is its analytical power in the construction of general formulas and the proof of general theorems. The use of density matrix methods also has the advantage of providing a uniform treatment of all quantum mechanical states, whether they are completely or incompletely known. For an elementary introduction, the interested reader may refer to Parker (2005), and for a good background and more details on the density matrix to Blum (2012). A great deal of how to use the density matrix in quantum and nonlinear optics is presented in Rand (2016).

2.3 Quantization of the Electromagnetic Field

Most of the properties of the light can be explained in the framework of semiclassical theory in which the matter is treated quantum mechanically while the field is described by classical electrodynamics. However, few phenomena, but very important, such as squeezing and antibunching cannot be explained within this theory and it becomes necessary to treat the electromagnetic (EM) field quantum mechanically on the same foot as the matter. In this section, an outline of the quantization of the free electromagnetic field (noninteracting, far from the sources, charges, and currents) is given. More details can be found in Louisell (1973, Chapter 4), Mandel & Wolf (1995, Chapter 10), Greiner & Reinhardt (1996, Chapter 1), Cohen-Tannoudji et al. (1997), Loudon (2000, Chapter 4), Schleich (2001, Chapter 10), Blaise & Henri-Rousseau (2011, Chapter 14), and Grynberg et al. (2010, Chapter 4). For a short survey for quantization in nonlinear quantum optics, one may refer to Hillery (2009).

The canonical quantization is starting by writing the classical Lagrangian and then obtaining the Hamiltonian of the system. This Lagrangian must be written in terms of

the conjugate canonical variables of the system q_1, q_2, \dots, q_N and p_1, p_2, \dots, p_N , a well-known solved problem in classical mechanics (Landau & Lifshitz, 1976; Goldstein et al., 2011). In the dynamics of a single particle, the two conjugate canonical variables are the position $q = x$ and momentum $p = mv$. For the sake of shortening the notation, the coordinates (the variables) are written collectively by $\mathbf{q} = (q_1, q_2, \dots, q_N)$ and $\mathbf{p} = (p_1, p_2, \dots, p_N)$. These variables characterize the physical system at each instant of time and from which its energy $E = H(q, \dot{q}, t)$ is obtained. The Hamiltonian H and the Lagrangian L are linked by

$$H(q, \dot{q}, t) = \sum_{j=1}^N \dot{q}_j p_j - L(q, \dot{q}, t). \quad (2.13)$$

The pairs of conjugate canonical variables (q_j, p_j) , $j = 1, \dots, N$ are connected by the Hamilton's canonical Equations

$$\dot{q}_j = \frac{\partial H}{\partial p_j}, \quad (2.14)$$

$$\dot{p}_j = -\frac{\partial H}{\partial q_j}. \quad (2.15)$$

The quantum version of the Hamiltonian is obtained by replacing the classical dynamical conjugate canonical variables (c-numbers, functions of space and time) by their corresponding observables (linear operators in a Hilbert space), $q_j \rightarrow \hat{q}_j$ and $p_j \rightarrow \hat{p}_j$. The classical Poisson brackets are replaced by their corresponding quantum commutation relations according to (Greiner & Reinhardt, 1996)

$$[q_j, p_j]_{\text{Poisson}} \rightarrow \frac{1}{i\hbar} [\hat{q}_j, \hat{p}_j]. \quad (2.16)$$

The procedure described above applies to the material particles, and a similar procedure to quantize the EM field is followed. This means that the conjugate canonical variables

satisfying the Hamilton's Equations 2.14 and 2.15 have to be identified. The same procedure cannot be applied directly since the dynamics of the EM field are governed by Maxwell's equations (a continuously infinite system of coupled linear partial differential equations) and the problem has to be reduced to a countable set of decoupled variables. For this purpose, the calculations will be performed in the k -space (spacial-reciprocal space) by using Fourier decomposition. In other words, the real EM field is expressed in terms of their complex Fourier components. The EM field in free space are governed by the four Maxwell's equations

$$\nabla \cdot \mathbf{E}(\mathbf{r}, t) = 0, \quad (2.17)$$

$$\nabla \cdot \mathbf{B}(\mathbf{r}, t) = 0, \quad (2.18)$$

$$\nabla \times \mathbf{E}(\mathbf{r}, t) = -\frac{\partial}{\partial t} \mathbf{B}(\mathbf{r}, t), \quad (2.19)$$

$$\nabla \times \mathbf{B}(\mathbf{r}, t) = \epsilon_0 \mu_0 \frac{\partial}{\partial t} \mathbf{E}(\mathbf{r}, t), \quad (2.20)$$

where ϵ_0 and μ_0 are the permittivity and permeability of free (vacuum) space, respectively.

The EM field can be expressed in terms of vector $\mathbf{A}(\mathbf{r}, t)$ and scalar $\phi(\mathbf{r}, t)$ potential fields

$$\mathbf{E}(\mathbf{r}, t) = -\frac{\partial}{\partial t} \mathbf{A}(\mathbf{r}, t) - \nabla \phi(\mathbf{r}, t), \quad (2.21)$$

$$\mathbf{B}(\mathbf{r}, t) = \nabla \times \mathbf{A}(\mathbf{r}, t). \quad (2.22)$$

The Maxwell's equations are gauge invariant (Jackson, 1999, p. 240; Parker, 2005, p. 356; Schleich, 2001, p. 257; Zangwill, 2013, p. 504). In quantum optics, the Coulomb gauge (or transversality gauge) condition is used, which is defined by

$$\nabla \cdot \mathbf{A}(\mathbf{r}, t) = 0. \quad (2.23)$$

From Equation 2.17, $\phi = 0$ is taken. From the vector identity $\nabla \times \nabla \times \mathbf{A} = \nabla \nabla \cdot \mathbf{A} - \nabla^2 \mathbf{A}$ and Equation 2.20, the vector potential satisfies the wave equation

$$\nabla^2 \mathbf{A} - \frac{1}{c^2} \frac{\partial^2 \mathbf{A}}{\partial t^2} = 0. \quad (2.24)$$

Solution of Equation 2.24 can be obtained by either by solving it in a region in space of volume V with real boundaries such as in a real cavity or in a large cavity without any real boundaries, called the quantization cavity. In the former case, the solution is represented by standing waves and in the later by running plane waves, in both situations periodic conditions at the walls of the cavity are imposed. Adopting the second case, the vector potential reads

$$\mathbf{A}(\mathbf{r}, t) = \frac{1}{\sqrt{V}} \sum_{\mathbf{k}} \mathcal{A}_{\mathbf{k}}(t) e^{i\mathbf{k} \cdot \mathbf{r}}, \quad (2.25)$$

with the Fourier components (amplitude)

$$\mathcal{A}_{\mathbf{k}}(t) = \frac{1}{\sqrt{V}} \int_V d^3r \mathbf{A}(\mathbf{r}, t) e^{-i\mathbf{k} \cdot \mathbf{r}}. \quad (2.26)$$

The sum in Equation 2.25 is over all the three integer number components of the vector $\mathbf{n} = (n_1, n_1, n_3)$ that define the wave vector \mathbf{k} according to

$$\mathbf{k} = \frac{2\pi}{L} \mathbf{n}, \quad (2.27)$$

and the volume V is, for simplicity, chosen to be $V = L^3$ for a cubic cavity. The Coulomb gauge Equation 2.23 or the transversality condition of the EM field in the k -space becomes

$$\mathbf{k} \cdot \mathcal{A}_{\mathbf{k}} = 0. \quad (2.28)$$

The reality of the field leads to the condition

$$\mathcal{A}_{-\mathbf{k}}(t) = \mathcal{A}_{\mathbf{k}}^*(t). \quad (2.29)$$

Using Equation 2.25 in to Equation 2.24, the amplitudes evolve according to

$$\frac{d^2 \mathcal{A}_{\mathbf{k}}}{dt^2} + \omega_{\mathbf{k}}^2 \mathcal{A}_{\mathbf{k}} = 0, \quad (2.30)$$

with the angular frequency $\omega_{\mathbf{k}} = c|\mathbf{k}|$ (c is the speed of light in the vacuum). The solution of Equation 2.30 is straight forward and from the reality of the field it reads

$$\mathcal{A}_{\mathbf{k}}(t) = \alpha_{\mathbf{k}} e^{-i\omega_{\mathbf{k}} t} + \alpha_{-\mathbf{k}}^* e^{i\omega_{\mathbf{k}} t}, \quad (2.31)$$

where $\alpha_{\mathbf{k}}$ is a constant vector. The transversality of the field means that, in infinitely many different ways, two mutually linearly-independent unit vectors $\boldsymbol{\varepsilon}_{\mathbf{k}s}$, $s = 1, 2$ can be chosen. These two unit vectors are the polarization vectors (for the same propagation vector) constitute with the unit propagation vector $\mathbf{k}/|\mathbf{k}|$ an orthonormal right-handed system. In this system, the vector potential is resolved into two components, along these polarization vectors, so the

$$\alpha_{\mathbf{k}} = \sum_{s=1}^2 \alpha_{\mathbf{k}s} \boldsymbol{\varepsilon}_{\mathbf{k}s}. \quad (2.32)$$

Using Equation 2.32 in Equation 2.31 and substituting the result in Equation 2.25, the vector potential has the expansion

$$\begin{aligned} \mathbf{A}(\mathbf{r}, t) &= \frac{1}{\sqrt{V}} \sum_{\mathbf{k}s} [\alpha_{\mathbf{k}s} \boldsymbol{\varepsilon}_{\mathbf{k}s} e^{-i\omega_{\mathbf{k}s} t} + \alpha_{-\mathbf{k}s}^* \boldsymbol{\varepsilon}_{-\mathbf{k}s}^* e^{i\omega_{\mathbf{k}s} t}] e^{i\mathbf{k} \cdot \mathbf{r}} \\ &= \frac{1}{\sqrt{V}} \sum_{\mathbf{k}s} [\beta_{\mathbf{k}s}(t) \mathbf{u}_{\mathbf{k}s}(\mathbf{r}) + \beta_{\mathbf{k}s}^*(t) \mathbf{u}_{\mathbf{k}s}^*(\mathbf{r})]. \end{aligned} \quad (2.33)$$

The vector potential $\mathbf{A}(\mathbf{r}, t)$ thus has expansion in terms of vector mode functions $\mathbf{u}_{\mathbf{k}s}$ with complex amplitude coefficients $\alpha_{\mathbf{k}s}$. In Equation 2.33, the mode functions and amplitudes are

$$\mathbf{u}_{\mathbf{k}s}(\mathbf{r}) = \varepsilon_{\mathbf{k}s} e^{i\mathbf{k}\cdot\mathbf{r}}, \quad (2.34)$$

$$\beta_{\mathbf{k}s}(t) = \alpha_{\mathbf{k}s} e^{-i\omega_{\mathbf{k}s}t}. \quad (2.35)$$

Each mode is labeled by a wave vector \mathbf{k} and polarization index s . From Equations 2.21 and 2.22, the fields $\mathbf{E}(\mathbf{r}, t)$ and $\mathbf{B}(\mathbf{r}, t)$ have the expansions

$$\mathbf{E}(\mathbf{r}, t) = \frac{i}{\sqrt{V}} \sum_{\mathbf{k}s} \omega_{\mathbf{k}s} [\beta_{\mathbf{k}s}(t) \mathbf{u}_{\mathbf{k}s}(\mathbf{r}) - \beta_{\mathbf{k}s}^*(t) \mathbf{u}_{\mathbf{k}s}^*(\mathbf{r})], \quad (2.36)$$

$$\mathbf{B}(\mathbf{r}, t) = \frac{i}{\sqrt{V}} \sum_{\mathbf{k}s} [\beta_{\mathbf{k}s}(t) \mathbf{k} \times \mathbf{u}_{\mathbf{k}s}(\mathbf{r}) - \beta_{\mathbf{k}s}^*(t) \mathbf{k} \times \mathbf{u}_{\mathbf{k}s}^*(\mathbf{r})]. \quad (2.37)$$

The energy of the EM field is obtained by substituting Equations 2.36 and 2.37 in the formula

$$H = \frac{\epsilon_0}{2} \int_V d^3r [\mathbf{E}^2(\mathbf{r}, t) + c^2 \mathbf{B}^2(\mathbf{r}, t)]. \quad (2.38)$$

Using the orthogonality relation of the basis functions $\mathbf{u}_{\mathbf{k}s}(\mathbf{r})$

$$\int_V d^3r \mathbf{u}_{\mathbf{k}'s'}^*(\mathbf{r}) \cdot \mathbf{u}_{\mathbf{k}s}(\mathbf{r}) = V \delta_{\mathbf{k}\mathbf{k}'} \delta_{ss'}, \quad (2.39)$$

and the vector relation $(\mathbf{a} \times \mathbf{b}) \cdot (\mathbf{c} \times \mathbf{d}) = (\mathbf{a} \cdot \mathbf{c})(\mathbf{b} \cdot \mathbf{d}) - (\mathbf{a} \cdot \mathbf{d})(\mathbf{b} \cdot \mathbf{c})$, the energy of the field reads

$$H = \epsilon_0 \sum_{\mathbf{k}s} \omega_{\mathbf{k}}^2 [\beta_{\mathbf{k}s}^*(t) \beta_{\mathbf{k}s}(t) + \beta_{\mathbf{k}s}(t) \beta_{\mathbf{k}s}^*(t)]. \quad (2.40)$$

The Hamiltonian, Equation 2.40, suggests a linear relation between the conjugate canonical

variables and the real and imaginary parts of the amplitude functions $\beta_{\mathbf{k}s}(t)$. These functions, Equation 2.35, satisfy the oscillator equation, Equation 2.30, and their real and imaginary parts are coupled by linear equations similar to the Hamilton equations. So, the amplitude functions are linear combination of the real canonical variables that can be written as

$$\beta_{\mathbf{k}s}(t) = \frac{1}{\sqrt{4\epsilon_0}} \left[q_{\mathbf{k}s}(t) + \frac{i}{\omega_{\mathbf{k}}} p_{\mathbf{k}s}(t) \right]. \quad (2.41)$$

By substituting Equation 2.41 in Equation 2.40, the Hamiltonian takes the form

$$H = \frac{1}{2} \sum_{\mathbf{k}s} [p_{\mathbf{k}s}^2(t) + \omega_{\mathbf{k}}^2 q_{\mathbf{k}s}^2(t)]. \quad (2.42)$$

The total energy is the energy of a system of independent harmonic oscillators of unit mass, each oscillator corresponds to the mode (\mathbf{k}, s) of the electromagnetic field. In terms of the conjugate canonical variables, the expansions of the classical electromagnetic fields become

$$\mathbf{A}(\mathbf{r}, t) = \frac{1}{\sqrt{4\epsilon_0 V}} \sum_{\mathbf{k}s} \left\{ \left[q_{\mathbf{k}s}(t) + \frac{i}{\omega_{\mathbf{k}}} p_{\mathbf{k}s}(t) \right] \boldsymbol{\varepsilon}_{\mathbf{k}s} e^{i\mathbf{k}\cdot\mathbf{r}} + \text{c.c.} \right\}, \quad (2.43)$$

$$\mathbf{E}(\mathbf{r}, t) = \frac{1}{\sqrt{4\epsilon_0 V}} \sum_{\mathbf{k}s} \left\{ \left[q_{\mathbf{k}s}(t) + \frac{i}{\omega_{\mathbf{k}}} p_{\mathbf{k}s}(t) \right] (i\omega_{\mathbf{k}} \boldsymbol{\varepsilon}_{\mathbf{k}s}) e^{i\mathbf{k}\cdot\mathbf{r}} + \text{c.c.} \right\}, \quad (2.44)$$

$$\mathbf{B}(\mathbf{r}, t) = \frac{1}{\sqrt{4\epsilon_0 V}} \sum_{\mathbf{k}s} \left\{ \left[q_{\mathbf{k}s}(t) + \frac{i}{\omega_{\mathbf{k}}} p_{\mathbf{k}s}(t) \right] (i\mathbf{k} \times \boldsymbol{\varepsilon}_{\mathbf{k}s}) e^{i\mathbf{k}\cdot\mathbf{r}} + \text{c.c.} \right\}. \quad (2.45)$$

Here c.c stands for the complex conjugate of the preceding term. The quantum version of the fields is straightforward after obtaining the quantum expressions for the dynamical variables q and p . The quantum mechanical conjugate canonical variables satisfy the

commutation relations

$$[\hat{q}_{\mathbf{k}s}(t), \hat{p}_{\mathbf{k}'s'}(t)] = i\hbar\delta_{\mathbf{k}\mathbf{k}'}\delta_{ss'}, \quad (2.46)$$

$$[\hat{q}_{\mathbf{k}s}(t), \hat{q}_{\mathbf{k}'s'}(t)] = 0, \quad (2.47)$$

$$[\hat{p}_{\mathbf{k}s}(t), \hat{p}_{\mathbf{k}'s'}(t)] = 0, \quad (2.48)$$

where the convention of putting carets on the same symbols of their classical corresponding variables is used. It is more convenient to work with non-Hermitian variables rather than the Hermitian operators as in the case of the quantum harmonic oscillator. For this purpose, the non-Hermitian annihilation (or destruction) $\hat{a}_{\mathbf{k}s}(t)$ and creation $\hat{a}_{\mathbf{k}s}^\dagger(t)$ operators for a quantum oscillator are defined by

$$\hat{a}_{\mathbf{k}s}(t) = \frac{1}{\sqrt{2\hbar\omega_{\mathbf{k}}}} [\omega_{\mathbf{k}}\hat{q}_{\mathbf{k}s}(t) + i\hat{p}_{\mathbf{k}s}(t)], \quad (2.49)$$

$$\hat{a}_{\mathbf{k}s}^\dagger(t) = \frac{1}{\sqrt{2\hbar\omega_{\mathbf{k}}}} [\omega_{\mathbf{k}}\hat{q}_{\mathbf{k}s}(t) - i\hat{p}_{\mathbf{k}s}(t)]. \quad (2.50)$$

The time evolution of operators $\hat{a}_{\mathbf{k}s}(t)$, $\hat{a}_{\mathbf{k}s}^\dagger(t)$ has the same form of Equation 2.35

$$\hat{a}_{\mathbf{k}s}(t) = \hat{a}_{\mathbf{k}s}(0)e^{-i\omega_{\mathbf{k}}t}, \quad (2.51)$$

$$\hat{a}_{\mathbf{k}s}^\dagger(t) = \hat{a}_{\mathbf{k}s}^\dagger(0)e^{i\omega_{\mathbf{k}}t}, \quad (2.52)$$

with commutation relations (using Equations 2.46-2.48 and Equations 2.49, 2.50)

$$\left[\hat{a}_{\mathbf{k}s}(t), \hat{a}_{\mathbf{k}'s'}^\dagger(t) \right] = \delta_{\mathbf{k}\mathbf{k}'}\delta_{ss'}, \quad (2.53)$$

$$[\hat{a}_{\mathbf{k}s}(t), \hat{a}_{\mathbf{k}'s'}(t)] = 0, \quad (2.54)$$

$$\left[\hat{a}_{\mathbf{k}s}^\dagger(t), \hat{a}_{\mathbf{k}'s'}^\dagger(t) \right] = 0. \quad (2.55)$$

In terms of the annihilation and creation operators, Equations 2.49, 2.50, and using the

commutation relation Equations 2.53-2.55 in Equation 2.42, the Hamiltonian takes the form

$$\hat{H} = \sum_{\mathbf{k}s} \hbar\omega_{\mathbf{k}} \left(\hat{a}_{\mathbf{k}s}^\dagger(t) \hat{a}_{\mathbf{k}s}(t) + \frac{1}{2} \right). \quad (2.56)$$

The term $\frac{1}{2}\hbar\omega_{\mathbf{k}}$ is the zero point energy contribution to the oscillator mode energy or the energy of the vacuum field of the corresponding mode. This term is usually dropped in many calculations and for this case Equation 2.56 takes the form

$$\hat{H} = \sum_{\mathbf{k}s} \hbar\omega_{\mathbf{k}} \hat{a}_{\mathbf{k}s}^\dagger(t) \hat{a}_{\mathbf{k}s}(t) = \sum_{\mathbf{k}s} \hbar\omega_{\mathbf{k}} \hat{n}_{\mathbf{k}s}(t), \quad (2.57)$$

where $\hat{n}_{\mathbf{k}s}(t) = \hat{a}_{\mathbf{k}s}^\dagger(t) \hat{a}_{\mathbf{k}s}(t)$ is the Hermitian *number operator*. The energy spectrum is therefore determined by the eigenvalues of the number operator which are non-negative integers. In the following section, a brief introduction to different states of the electromagnetic field, one of which is the number state (the eigenstate of the number operator) is presented. The quantum mechanical expressions for the EM fields corresponding to the classical EM fields, Equations 2.43-2.45 read

$$\mathbf{A}(\mathbf{r}, t) = \sum_{\mathbf{k}s} \sqrt{\frac{\hbar}{2\epsilon_0 V \omega_{\mathbf{k}}}} \left(\hat{a}_{\mathbf{k}s}(0) \boldsymbol{\varepsilon}_{\mathbf{k}s} e^{i(\mathbf{k}\cdot\mathbf{r} - \omega_{\mathbf{k}}t)} + \text{h.c.} \right), \quad (2.58)$$

$$\mathbf{E}(\mathbf{r}, t) = \sum_{\mathbf{k}s} \sqrt{\frac{\hbar\omega_{\mathbf{k}}}{2\epsilon_0 V}} \left(i\hat{a}_{\mathbf{k}s}(0) \boldsymbol{\varepsilon}_{\mathbf{k}s} e^{i(\mathbf{k}\cdot\mathbf{r} - \omega_{\mathbf{k}}t)} + \text{h.c.} \right), \quad (2.59)$$

$$\mathbf{B}(\mathbf{r}, t) = \sum_{\mathbf{k}s} \sqrt{\frac{\hbar}{2\epsilon_0 V \omega_{\mathbf{k}}}} \left(i\hat{a}_{\mathbf{k}s}(0) \mathbf{k} \times \boldsymbol{\varepsilon}_{\mathbf{k}s} e^{i(\mathbf{k}\cdot\mathbf{r} - \omega_{\mathbf{k}}t)} + \text{h.c.} \right). \quad (2.60)$$

Here h.c stands for the Hermitian conjugate of the preceding term. Usually vector fields are written as a sum of positive and negative frequency parts conjugate to each other. For

the electric field, Equation 2.59

$$\mathbf{E}(\mathbf{r}, t) = \mathbf{E}^{(+)}(\mathbf{r}, t) + \mathbf{E}^{(-)}(\mathbf{r}, t), \quad (2.61)$$

where

$$\mathbf{E}^{(+)}(\mathbf{r}, t) = i \sum_{\mathbf{k}s} \sqrt{\frac{\hbar\omega_{\mathbf{k}}}{2\epsilon_0 V}} \hat{a}_{\mathbf{k}s}(0) \boldsymbol{\varepsilon}_{\mathbf{k}s} e^{i(\mathbf{k}\cdot\mathbf{r} - \omega_{\mathbf{k}}t)}, \quad (2.62)$$

$$\mathbf{E}^{(-)}(\mathbf{r}, t) = -i \sum_{\mathbf{k}s} \sqrt{\frac{\hbar\omega_{\mathbf{k}}}{2\epsilon_0 V}} \hat{a}_{\mathbf{k}s}^{\dagger}(0) \boldsymbol{\varepsilon}_{\mathbf{k}s}^* e^{-i(\mathbf{k}\cdot\mathbf{r} - \omega_{\mathbf{k}}t)}. \quad (2.63)$$

The positive frequency $\mathbf{E}^{(+)}(\mathbf{r}, t)$ is a combination of annihilation operators only and the negative part is a combination of creation operators only. The field operators with $\mathbf{E}^{(-)}(\mathbf{r}, t) = \left(\mathbf{E}^{(+)}(\mathbf{r}, t)\right)^{\dagger}$ are non-Hermitian operators but the positive frequency part is the most used in experiments (absorption as in photoelectric effect) to measure the field not the real field itself, Equation 2.61.

2.4 Quantum States of the Electromagnetic Field

The quantized electromagnetic field can be in different states according to the values of fluctuations in its amplitude and phase. According to the amount of fluctuations, the field statistics can be classified also into super-Poissonian (where the variance is greater than the mean), sub-Poissonian (the variance is less than the mean), or Poissonian (the variance equals the mean). The classification will be discussed in more detail when the Mandel- Q parameter is explored in the next section. The main states are number state, coherent state, and squeezed states with many extensions and generalizations (Dodonov & Man'ko, 2003). Here, a very short summary of a few important properties of four states of the electromagnetic field is presented. The interested reader may refer to any textbook in quantum optics and Schleich (2001) is very useful.

2.4.1 Number State

In the quantization of the electromagnetic field in free space, the modes of the field are in a one-to-one correspondence with an infinite set of harmonic oscillators as have been shown in Section 2.3. The energy eigenstate of a single mode of the radiation field of n photons is the eigenstate of the harmonic oscillator of n excitations which is also the eigenstate of the number operator with eigenvalue n (Mandel & Wolf, 1995; Fox, 2006; Blaise & Henri-Rousseau, 2011). It is called the number state or Fock state $|n\rangle$ with $\hat{n}|n\rangle = n|n\rangle$. For multimode radiation field, the number state is the tensor product of the number state of each mode since the corresponding operators act on their each own subspace

$$\begin{aligned} |\{n_{\mathbf{k}_s}\}\rangle &= |n_{\mathbf{k}_1s_1}n_{\mathbf{k}_2s_2}, \dots, n_{\mathbf{k}_ls_l}, \dots\rangle \\ &= |n_{\mathbf{k}_1s_1}\rangle |n_{\mathbf{k}_2s_2}\rangle \cdots |n_{\mathbf{k}_ls_l}\rangle \cdots = \prod_{\mathbf{k}_s} |n_{\mathbf{k}_s}\rangle. \end{aligned} \quad (2.64)$$

The number state is the eigenstate of the number operator

$$\hat{n}_{\mathbf{k}_s} |n_{\mathbf{k}_s}\rangle = n_{\mathbf{k}_s} |n_{\mathbf{k}_s}\rangle. \quad (2.65)$$

The lowest energy of the field is when the field being in the vacuum state (ground state, no excitations) denoted by $|\text{vac}\rangle = |\{0_{\mathbf{k}_s}\}\rangle$. The number states are not eigenstates for the annihilation and creation operators; their operations on the number states are given by (Mandel & Wolf, 1995)

$$\hat{a}_{\mathbf{k}_s} |n_{\mathbf{k}_s}\rangle = \sqrt{n_{\mathbf{k}_s}} |n_{\mathbf{k}_s} - 1\rangle, \quad (2.66)$$

$$\hat{a}_{\mathbf{k}_s}^\dagger |n_{\mathbf{k}_s}\rangle = \sqrt{n_{\mathbf{k}_s} + 1} |n_{\mathbf{k}_s} + 1\rangle. \quad (2.67)$$

The operators $\hat{a}_{\mathbf{k}s}$ and $\hat{a}_{\mathbf{k}s}^\dagger$ sometimes are called lowering and raising operators, respectively, since they lower and raise the energy state of the field by unity as will be seen in the next section as shown in Equations 2.66 and 2.67. Since the operators in different modes act on each own subspace, their operations of the number states Equation 2.64 become

$$\hat{a}_{\mathbf{k}s}|\{n_{\mathbf{k}s}\}\rangle = \sqrt{n_{\mathbf{k}s}}|\cdots, n_{\mathbf{k}s} - 1, \cdots\rangle, \quad (2.68)$$

$$\hat{a}_{\mathbf{k}s}^\dagger|\{n_{\mathbf{k}s}\}\rangle = \sqrt{n_{\mathbf{k}s} + 1}|\cdots, n_{\mathbf{k}s} + 1, \cdots\rangle. \quad (2.69)$$

Any number state can be formed by repeated application of the raising operators on the vacuum state. From 2.69, the number states read

$$|\{n_{\mathbf{k}s}\}\rangle = \prod_{\mathbf{k}s} \left[(n_{\mathbf{k}s}!)^{-\frac{1}{2}} \left(\hat{a}_{\mathbf{k}s}^\dagger \right)^{n_{\mathbf{k}s}} \right] |\text{vac}\rangle. \quad (2.70)$$

The number state has a definite value of the amplitude (number of the photons) since it has vanishing variance so the phase is not defined according to Heisenberg uncertainty principle. The number states $|n_{\mathbf{k}s}\rangle$ are a complete and orthonormal set that serves as a basis for representation arbitrary states or operators

$$\sum_{n_{\mathbf{k}s}} |n_{\mathbf{k}s}\rangle \langle n_{\mathbf{k}s}| = \hat{1}, \quad (\text{completeness}) \quad (2.71)$$

$$\langle \{n_{\mathbf{k}s}\} | \{m_{\mathbf{k}s}\} \rangle = \prod_{\mathbf{k}s} \delta_{n_{\mathbf{k}s} m_{\mathbf{k}s}}, \quad (\text{orthonormality}) \quad (2.72)$$

where $\hat{1}$ is an identity operator. From the completeness relation Equation 2.71, the density operator reads

$$\hat{\rho} = \sum_{n_{\mathbf{k}s} m_{\mathbf{k}s}} \langle n_{\mathbf{k}s} | \hat{\rho} | m_{\mathbf{k}s} \rangle |n_{\mathbf{k}s}\rangle \langle m_{\mathbf{k}s}|. \quad (2.73)$$

A general pure state of the radiation field in the number state representation takes the form (Scully & Zubairy, 1997; Loudon, 2000; Grynberg et al., 2010; Schleich, 2001)

$$|\psi\rangle = \sum_{n_1 n_2 \dots n_j \dots} \psi_{n_1 n_2 \dots n_j \dots} |n_1 n_2 \dots n_j \dots\rangle, \quad (2.74)$$

where the probability amplitudes $\psi_{n_1 n_2 \dots n_j \dots}$ are arbitrary complex numbers. If the states $|\psi\rangle$ are products of individual modes states then they are called separable states otherwise they form what is called *entangled states* (non-separable states). Entanglement is coined by Schrödinger (1935, 1936) after the Einstein-Podolsky-Rosen paper (Einstein et al., 1935). Entangled states exhibit unique non-local correlation properties that are in the heart of quantum mechanics and extremely important in quantum information (Hillery & Zubairy, 2006; Audretsch, 2008; Horodecki et al., 2009; Ivan et al., 2011). Simple important pure states of this general form are obtained when the superposition is restricted to the number states of a single-mode. Examples of such states are coherent states and squeezed states that will be presented in the following subsections. It is important to calculate the average and fluctuations of the EM field in the number state representation. Using Equations 2.68, 2.69, and 2.72, the expectation values of the annihilation and creation operators vanishes

$$\langle \{n_{\mathbf{k}s}\} | \hat{a}_{\mathbf{k}s} | \{n_{\mathbf{k}s}\} \rangle = 0 = \langle \{n_{\mathbf{k}s}\} | \hat{a}_{\mathbf{k}s}^\dagger | \{n_{\mathbf{k}s}\} \rangle. \quad (2.75)$$

So the expectation values of the EM field Equation 2.61 vanishes too

$$\langle \{n_{\mathbf{k}s}\} | \hat{\mathbf{E}}(\mathbf{r}, t) | \{n_{\mathbf{k}s}\} \rangle = 0. \quad (2.76)$$

Again, using 2.68, 2.69, and 2.72, the expectation value of the fluctuations of the EM field becomes

$$\begin{aligned}
\langle \{n_{\mathbf{k}s}\} | (\Delta \hat{\mathbf{E}})^2 | \{n_{\mathbf{k}s}\} \rangle &= \langle \{n_{\mathbf{k}s}\} | \left[\hat{\mathbf{E}}^{(+)} \cdot \hat{\mathbf{E}}^{(+)} + \hat{\mathbf{E}}^{(-)} \cdot \hat{\mathbf{E}}^{(-)} \right] | \{n_{\mathbf{k}'s'}\} \rangle \\
&\quad + \langle \{n_{\mathbf{k}s}\} | \left[\hat{\mathbf{E}}^{(+)} \cdot \hat{\mathbf{E}}^{(-)} + \hat{\mathbf{E}}^{(-)} \cdot \hat{\mathbf{E}}^{(+)} \right] | \{n_{\mathbf{k}'s'}\} \rangle \\
&= \langle \{n_{\mathbf{k}s}\} | \left[\hat{\mathbf{E}}^{(+)} \cdot \hat{\mathbf{E}}^{(-)} + \hat{\mathbf{E}}^{(-)} \cdot \hat{\mathbf{E}}^{(+)} \right] | \{n_{\mathbf{k}'s'}\} \rangle \\
&= \sum_{\mathbf{k}s} \sum_{\mathbf{k}'s'} \frac{\hbar \sqrt{\omega_{\mathbf{k}} \omega_{\mathbf{k}'}}}{2\epsilon_0 V} \langle \{n_{\mathbf{k}s}\} | \hat{a}_{\mathbf{k}s}(0) \hat{a}_{\mathbf{k}'s'}^\dagger(0) | \{n_{\mathbf{k}'s'}\} \rangle f_{\mathbf{k}s\mathbf{k}'s'} \\
&\quad + \sum_{\mathbf{k}s} \sum_{\mathbf{k}'s'} \frac{\hbar \sqrt{\omega_{\mathbf{k}} \omega_{\mathbf{k}'}}}{2\epsilon_0 V} \langle \{n_{\mathbf{k}s}\} | \hat{a}_{\mathbf{k}s}^\dagger(0) \hat{a}_{\mathbf{k}'s'}(0) | \{n_{\mathbf{k}'s'}\} \rangle f_{\mathbf{k}s\mathbf{k}'s'}^* \\
&= \sum_{\mathbf{k}s} \sum_{\mathbf{k}'s'} \delta_{\mathbf{k}\mathbf{k}'} \delta_{s's'} \frac{\hbar \sqrt{\omega_{\mathbf{k}} \omega_{\mathbf{k}'}}}{2\epsilon_0 V} \left[(n_{\mathbf{k}s} + 1) f_{\mathbf{k}s\mathbf{k}'s'} + n_{\mathbf{k}s} f_{\mathbf{k}s\mathbf{k}'s'}^* \right] \\
&= \sum_{\mathbf{k}s} \frac{\hbar \omega_{\mathbf{k}}}{2\epsilon_0 V} (2n_{\mathbf{k}s} + 1) = \frac{1}{\epsilon_0 V} \langle \hat{H} \rangle, \tag{2.77}
\end{aligned}$$

where $f_{\mathbf{k}s\mathbf{k}'s'} = \boldsymbol{\varepsilon}_{\mathbf{k}s} \cdot \boldsymbol{\varepsilon}_{\mathbf{k}'s'}^* e^{i[(\mathbf{k}-\mathbf{k}') \cdot \mathbf{r} - (\omega_{\mathbf{k}} - \omega_{\mathbf{k}'}t)]}$ and in the last equality, Equation 2.56 is used.

So the vacuum field has fluctuations of magnitude

$$\langle \text{vac} | (\Delta \hat{\mathbf{E}})^2 | \text{vac} \rangle = \frac{1}{\epsilon_0 V} \sum_{\mathbf{k}} \hbar \omega_{\mathbf{k}}, \tag{2.78}$$

where summation over the two polarization states is performed. The vacuum fluctuations are important pure quantum result that explains many phenomena such as spontaneous emission, Casimir effect, and Lamb shift (Mandel & Wolf, 1995; Scully & Zubairy, 1997; Loudon, 2000; Schleich, 2001; Grynberg et al., 2010). These phenomena and the divergence problem in the vacuum energy and vacuum fluctuations are not discussed here.

2.4.2 Thermal State

Most fields commonly encountered in practice are produced by sources in thermal equilibrium and they are called thermal fields, fields are in a thermal state. A system with

energy \hat{H} and in thermal equilibrium at temperature T is described by a canonical ensemble

$$\hat{\rho} = \frac{\exp(-\beta\hat{H})}{\text{Tr} \exp(-\beta\hat{H})}, \quad (2.79)$$

where $\beta = 1/k_B T$ with k_B is the Boltzmann constant and \hat{H} is the free-field Hamiltonian Equation 2.56. Since operators associated with different modes are commute then it is easy to show that the density operator, Equation 2.79, becomes (Mandel & Wolf, 1995; Loudon, 2000)

$$\hat{\rho} = \prod_{\mathbf{k}s} \hat{\rho}_{\mathbf{k}s} = \prod_{\mathbf{k}s} \left(1 - e^{-\hbar\omega_{\mathbf{k}}\beta}\right) e^{-\hbar\omega_{\mathbf{k}}\beta \hat{n}_{\mathbf{k}s}}. \quad (2.80)$$

The density operator Equation 2.80 is diagonal in the number state representation and upon using the completeness relation Equation 2.71, it reads

$$\hat{\rho} = \sum_{n_{\mathbf{k}s}} \prod_{\mathbf{k}s} \left(1 - e^{-\hbar\omega_{\mathbf{k}}\beta}\right) e^{-\hbar\omega_{\mathbf{k}}\beta n_{\mathbf{k}s}} |n_{\mathbf{k}s}\rangle \langle n_{\mathbf{k}s}|. \quad (2.81)$$

From Equation 2.81, the joint probability $p(\{n_{\mathbf{k}s}\})$ is the product of the independent probabilities $p(n_{\mathbf{k}s})$ for $n_{\mathbf{k}s}$ photons in the mode (\mathbf{k}, s)

$$p(\{n_{\mathbf{k}s}\}) = \prod_{\mathbf{k}s} p(n_{\mathbf{k}s}), \quad (2.82)$$

with

$$p(n_{\mathbf{k}s}) = \left(1 - e^{-\hbar\omega_{\mathbf{k}}\beta}\right) e^{-\hbar\omega_{\mathbf{k}}\beta n_{\mathbf{k}s}}. \quad (2.83)$$

The mean of the distribution is found to be

$$\langle \hat{n}_{\mathbf{k}s} \rangle = \frac{1}{e^{\hbar\omega_{\mathbf{k}}/k_B T} - 1}, \quad (2.84)$$

and the variance reads

$$\langle \hat{n}_{\mathbf{k}s}^2 \rangle - \langle \hat{n}_{\mathbf{k}s} \rangle^2 = \langle \hat{n}_{\mathbf{k}s} \rangle (1 + \langle \hat{n}_{\mathbf{k}s} \rangle). \quad (2.85)$$

Equation 2.85 indicates that the thermal field distribution is wider than the Poisson distribution for the same mean. However, the deviation is small for optical fields at typical radiation temperature where the mean photon number Equation 2.84 is small (Mandel & Wolf, 1995). In terms of the mean photon number, the photon number distribution of the individual mode, Equation 2.83, reads

$$p(n_{\mathbf{k}s}) = \frac{\langle \hat{n}_{\mathbf{k}s} \rangle^{n_{\mathbf{k}s}}}{(1 + \langle \hat{n}_{\mathbf{k}s} \rangle)^{n_{\mathbf{k}s}+1}}. \quad (2.86)$$

So, the photon distribution in a thermal field is described by the Bose-Einstein distribution, Equation 2.86.

2.4.3 Coherent State

Coherent states (quasi-classical states) (Klauder & Skagerstam, 1985; Klauder & Sudarshan, 2006; Zhang et al., 1990) are of central importance to quantum mechanics and, in particular, to quantum optics. They are states of the harmonic oscillator, which demonstrate maximum coherence and almost classical behavior. They were discovered by E. Schrodinger in 1926 when he derived it as a minimum uncertainty Gaussian wavepacket. Coherent states have a great deal of interest since introduced for the quantized electromagnetic fields by R. Glauber, J. Klauder and E.C.G. Sudarshan in early 1960. The coherent state of a single-mode light, $|\alpha\rangle$ is defined to be the eigenstate of the annihilation operator, \hat{a} , of the electromagnetic field (Glauber, 1963a,b)

$$\hat{a} |\alpha\rangle = \alpha |\alpha\rangle, \quad (2.87)$$

Table 2.1: Properties of coherent state.

Quantity	Definition
creation operator	$\langle \alpha \hat{a}^\dagger = \langle \alpha \alpha^*$
number-operator mean	$\langle \hat{n} \rangle = \langle \alpha \hat{n} \alpha \rangle = \alpha ^2$
orthogonality	$\langle \alpha \beta \rangle = e^{\alpha^* \beta - \alpha ^2/2 - \beta ^2/2}$
completeness	$\frac{1}{\pi} \int d^2\alpha \alpha \rangle \langle \alpha = \hat{1}$
measure	$d^2\alpha = d(\text{Re } \alpha) d(\text{Im } \alpha)$
excitations	$ \alpha \rangle = e^{\alpha \hat{a}^\dagger - \alpha^* \hat{a}} 0 \rangle$
variance	$\langle (\Delta \hat{n})^2 \rangle = \langle \hat{n}^2 \rangle - \langle \hat{n} \rangle^2 = \alpha ^2$
density operator	$\rho = \alpha \rangle \langle \alpha $

where $\alpha = \text{Re } \alpha + i \text{Im } \alpha$ is a complex number. It is the state of a coherent field with well-defined phase and amplitude (Agarwal, 2013). Coherent states can be represented in terms of Fock or number states (Glauber, 1963a; Gardiner & Zoller, 2004).

$$| \alpha \rangle = e^{-|\alpha|^2/2} \sum_{n=0}^{\infty} \frac{\alpha^n}{\sqrt{n!}} | n \rangle \quad (2.88a)$$

$$= e^{-|\alpha|^2/2} \sum_{n=0}^{\infty} \frac{\alpha^n}{n!} (\hat{a}^\dagger)^n | 0 \rangle. \quad (2.88b)$$

The main properties of the coherent state are summarized in Table 2.1 (Carmichael, 2002).

The coherent state in Equation 2.88 can be generated using the unitary displacement operator $D(\alpha)$ on the vacuum state $| 0 \rangle$

$$| \alpha \rangle = D(\alpha) | 0 \rangle, \quad (2.89)$$

with the displacement operator

$$D(\alpha) = e^{\alpha \hat{a}^\dagger - \alpha^* \hat{a}}. \quad (2.90)$$

A few important properties of the displacement operator are (Scully & Zubairy, 1997; Walls

& Milburn, 2008)

$$D^\dagger(\alpha) \hat{a} D(\alpha) = \hat{a} + \alpha \hat{1}, \quad (2.91)$$

$$D^\dagger(\alpha) \hat{a}^\dagger D(\alpha) = \hat{a}^\dagger + \alpha^* \hat{1}, \quad (2.92)$$

$$D^\dagger(\alpha) = D^{-1}(\alpha) = D(-\alpha). \quad (2.93)$$

The coherent states minimize the uncertainty relation of two quadratures (dimensionless canonical conjugate operators, \hat{X}_1 and \hat{X}_2) of the field. These quadratures can be expressed in terms of the operators \hat{a} and \hat{a}^\dagger and they have the minimum value of $(\Delta\hat{X}_1)^2 = (\Delta\hat{X}_2)^2 = 1/4$ (Peřina et al., 1994; Mandel & Wolf, 1995; Fox, 2006; Walls & Milburn, 2008) (Note that the authors definition of the quadratures differs by a factor so one encounter $(\Delta\hat{X}_1)^2 = (\Delta\hat{X}_2)^2 = 1$ or $1/2$). The extension of the pure coherent state to an ensemble (multimode) of coherent states is straightforward Mandel & Wolf (1995).

2.4.4 Squeezed State

The coherent states are considered on the boundary between classical and nonclassical states of the light. Any uncertainty less than the minimum on any one of the two quadratures of the field mode will produce what is called a squeezed state of the field (Walls, 1983; Loudon & Knight, 1987; Knight & Buřek, 2004; Lvovsky, 2015; Schnabel, 2017; Bachor & Ralph, 2004). Squeezed states originally introduced by Yuen (1976) under the name two-photon coherent states before they bear the current name. When one of the quadratures of the field has less uncertainty than the minimum; the other quadrature will have greater uncertainty than the minimum according to uncertainty relation, $(\Delta\hat{X}_j)^2 < 1/4$ ($j = 1$ or 2) (Scully & Zubairy, 1997).

The squeezed states are nonclassical states and very important for highly precision

measurement such as gravitational waves measurement (Abadie et al., 2011). If the measurement interest is to measure one aspect of the electromagnetic field, for example, the amplitude then the noise in the amplitude quadrature must be suppressed on the expense of the phase quadrature. The squeezed state can be generated from the vacuum state by applying the squeeze operator on the coherent state (Scully & Zubairy, 1997)

$$|\alpha, \xi\rangle = S(\xi) |\alpha\rangle = S(\xi) D(\alpha) |0\rangle. \quad (2.94)$$

The unitary squeeze operator is given by

$$S(\xi) = e^{(\xi^* \hat{a}^2 - \xi \hat{a}^{\dagger 2})/2}, \quad (2.95)$$

with the following properties (Scully & Zubairy, 1997)

$$S^\dagger(\xi) \hat{a} S(\xi) = \mu \hat{a} - \nu \hat{a}^\dagger, \quad (2.96)$$

$$S^\dagger(\xi) \hat{a}^\dagger S(\xi) = \mu \hat{a}^\dagger - \nu^* \hat{a}, \quad (2.97)$$

$$S^\dagger(\xi) = S^{-1}(\xi) = S(-\xi). \quad (2.98)$$

The squeeze parameter $\xi = r e^{i\theta}$ is an arbitrary complex number. The modulus $r = |\xi|$ describes the amount of squeezing, and the phase θ determines the angle of the squeezing axis in phase space (Garrison & Chiao, 2008). In Table 2.2, a few of the main properties of the squeezed coherent state are listed.

Alternative definition of the squeezed state is the coherent squeezed state obtained by first squeezing the vacuum then displace it (Mandel & Wolf, 1995; Walls & Milburn, 2008;

Table 2.2: Properties of squeezed coherent state.

Quantity	Definition
number-operator mean	$\langle \hat{n} \rangle = \alpha ^2 (\mu^2 + \nu ^2) - \alpha^{*2} \mu \nu - \alpha^2 \mu \nu^* + \nu ^2$
orthogonality	$\langle \alpha, \xi \beta, \xi \rangle = \langle \alpha \beta \rangle = e^{\alpha^* \beta - \alpha ^2/2 - \beta ^2/2}$
completeness	$\frac{1}{\pi} \int d^2\alpha \alpha, \xi\rangle \langle \alpha, \xi = \hat{1}$
degree of squeezing	$r = \xi $
generator	$ \alpha, \xi\rangle = S(\xi) D(\alpha) 0\rangle$
density operator	$\rho = \alpha, \xi\rangle \langle \alpha, \xi $

Garrison & Chiao, 2008; Orszag, 2016)

$$|\alpha, \xi\rangle = D(\alpha) S(\xi) |0\rangle. \quad (2.99)$$

In this definition one can consider the squeezed state $|\alpha, \xi\rangle$ as an eigenstate of a generalized annihilation operator \hat{A} (Mandel & Wolf, 1995; Walls & Milburn, 2008; Garrison & Chiao, 2008; Orszag, 2016)

$$\hat{A} |\alpha, \xi\rangle = \alpha_+ |\alpha, \xi\rangle, \quad (2.100)$$

where

$$\hat{A} = S(\xi) \hat{a} S^\dagger(\xi) \quad (2.101)$$

$$= \mu \hat{a} + \nu \hat{a}^\dagger, \quad (2.102)$$

and

$$\alpha_\pm = \mu \alpha \pm \nu \alpha^*, \quad (2.103)$$

with $\mu = \cosh r$, $\nu = e^{i\theta} \sinh r$, $[\hat{A}, \hat{A}^\dagger] = \hat{1}$. Mandel & Wolf (1995) and Garrison & Chiao (2008) make a clear notation to distinguish between the two definitions. They wrote $|\xi, \alpha\rangle$

for the new definition as the squeezing of the vacuum operates first then displaces the state. The two definitions are related to each other by (Mandel & Wolf, 1995; Garrison & Chiao, 2008)

$$|\xi, \alpha\rangle = |\alpha_-, \xi\rangle, \quad (2.104)$$

$$|\alpha, \xi\rangle = |\xi, \alpha_+\rangle. \quad (2.105)$$

These quantum states and many others can be generated by different ways (Tan & Jeong, 2019; Braunstein & van Loock, 2005; Davidovich, 1996; Boyd et al., 2019).

2.5 Nonclassical Measures of the Field

To study the nonclassicality of the quantized electromagnetic field, a set of measures is needed to quantify the nonclassicality of the field (Tan & Jeong, 2019). The main measures that are adopted in this work to demonstrate the nonclassicality are the Mandel- Q parameter, the correlation functions, and the CSI. For a clear and concise introduction, a reader may refer to Agarwal (2013).

2.5.1 Mandel Q Parameter

In statistics, moments are very important quantities to study statistical probability distributions of random variables. Fluctuations in a physical quantity are unavoidable and it is required to be reduced most of the time. To quantify these fluctuations and to study characteristics of a statistical distribution the normalized moments are used. In practice, the important is the low-order moments such as variance. For the Poisson random process, variance equals the mean which is the case for statistics of the ideal laser. Statistics are called *super-Poissonian* when its width is larger than the width of Poisson distribution or the variance is greater than the mean. On the other hand, when the variance is less than the mean, it is called *sub-Poissonian* (Davidovich, 1996). To study the departure of photon

number distribution from Poisson statistics, many measures have been used. The most used measure is the Q parameter introduced by Mandel to characterize the statistics of photon distribution emitted in atomic resonance fluorescence (Mandel, 1979) which is given by

$$Q = \frac{\langle \hat{a}^{\dagger 2} \hat{a}^2 - (\hat{a}^{\dagger} \hat{a})^2 \rangle}{\langle \hat{a}^{\dagger} \hat{a} \rangle} = \frac{\langle \hat{n} (\hat{n} - \hat{1}) \rangle - \langle \hat{n} \rangle^2}{\langle \hat{n} \rangle} = \frac{\langle (\Delta \hat{n})^2 \rangle}{\langle \hat{n} \rangle} - 1. \quad (2.106)$$

The field in a coherent state is considered to be the closest one to a classical field for which $Q = 0$ is the boundary between a classical and a quantum field. For a thermal state, one has $Q > 0$, corresponding to a super-Poissonian distribution. For $Q < 0$, photon statistics are sub-Poissonian and the corresponding state is nonclassical. The most elementary example of non-classical states is number states. Since they are eigenstates of the number operator with vanishing fluctuations and the $Q = -1$. The Q is related to what is called Fano factor (Fano, 1947; Teich & Saleh, 1985; Pennini & Plastino, 2010) through $Q = F - 1$ but Q has wide use in quantum optics as an indicator for a nonclassical field. The light that has sub-Poissonian statistics is sometimes described as photon-number squeezed (Yamamoto et al., 1986).

2.5.2 Correlation Functions

Coherence plays an important role in optics. The coherence is represented by correlation functions that facilitate the study of interference due to fluctuations of the field. The classical theory was developed and studied extensively in the classic standard book, Principles of Optics by Born & Wolf (1999). Glauber (1963c) for the first time studied the quantum theory of coherence. Born and Wolf studied the coherence function of the first order while Glauber studied the quantum version of all orders. Correlation functions are essential tools to characterize the electromagnetic field. In the calculations, the field is assumed to be linearly

polarized, in which it is much simpler to deal with the scalar quantities $E^{(\pm)} = \boldsymbol{\varepsilon} \cdot \mathbf{E}^{(\pm)}$. The photoelectric effect is used in the local field measurements in the optical region where the photon absorption mechanism is used. For this reason, only the annihilation operators involved in the measurements. To obtain the counting rate probability, one has to obtain the transition probability that the detector (atom) absorbs a photon from the field at position r between times t and $t + dt$ (Glauber, 1963c). The calculation shows that the transition probability is governed by the first-order correlation function, $G^{(1)}$ defined by

$$\begin{aligned} G^{(1)}(\mathbf{r}_1, t_1; \mathbf{r}_2, t_2) &= \text{Tr} \left[\rho E^{(-)}(\mathbf{r}_1, t_1) E^{(+)}(\mathbf{r}_2, t_2) \right] \\ &= \left\langle E^{(-)}(\mathbf{r}_1, t_1) E^{(+)}(\mathbf{r}_2, t_2) \right\rangle. \end{aligned} \quad (2.107)$$

For a statistically stationary field (with measurement time delay, τ), the $G^{(1)} = G^{(1)}(\mathbf{r}, t; \mathbf{r}, t + \tau)$ forms a Fourier transform pair with the power spectrum $S(\mathbf{r}, \omega)$ (Scully & Zubairy, 1997).

$$S(\mathbf{r}, \omega) = \frac{1}{\pi} \text{Re} \int_0^{\infty} d\tau e^{i\omega\tau} G^{(1)}(\mathbf{r}, t; \mathbf{r}, t + \tau). \quad (2.108)$$

Statistically stationary field means that the expectation value of any function of the field operators is invariant under time translation. This means that the correlation functions depend on the time difference $\tau = t_2 - t_1$ and not on the time points themselves. For a detailed presentation and discussion of this time-translation symmetry and other symmetries, the interested reader may refer to (Mandel & Wolf, 1995, p. 601) and references therein. In the case of evaluating the transition rate for a joint absorption of photons at the two space-time points (two detectors) with $t_1 < t_2$, the result defines the $G^{(2)} = G^{(2)}(\mathbf{r}_1, t_1, \mathbf{r}_2, t_2, \mathbf{r}_3, t_3, \mathbf{r}_4, t_4)$

(Glauber, 1963c).

$$\begin{aligned} G^{(2)} &= \text{Tr} \left[\rho E^{(-)}(\mathbf{r}_1, t_1) E^{(-)}(\mathbf{r}_2, t_2) E^{(+)}(\mathbf{r}_3, t_3) E^{(+)}(\mathbf{r}_4, t_4) \right] \\ &= \left\langle E^{(-)}(\mathbf{r}_1, t_1) E^{(-)}(\mathbf{r}_2, t_2) E^{(+)}(\mathbf{r}_3, t_3) E^{(+)}(\mathbf{r}_4, t_4) \right\rangle. \end{aligned} \quad (2.109)$$

The $G^{(2)}$ is a measure of intensity correlations at two space-time points. The most general correlation function may have unequal number of creation and annihilation operators due to a nonlinear interaction in a dielectric (Mandel & Wolf, 1995). Here the simple general version of the correlation functions is presented. The n th-order correlation function $G^{(n)} = G^{(n)}(\mathbf{X}_1, \dots, \mathbf{X}_{2n})$ with $t_1 < t_2 < \dots < t_{2n}$ (Glauber, 1963c; Mandel & Wolf, 1995; Scully & Zubairy, 1997) is defined by.

$$\begin{aligned} G^{(n)} &= \text{Tr} \left[\rho E^{(-)}(\mathbf{X}_1), \dots, E^{(-)}(\mathbf{X}_n) E^{(+)}(\mathbf{X}_{n+1}), \dots, E^{(+)}(\mathbf{X}_{2n}) \right] \\ &= \left\langle E^{(-)}(\mathbf{X}_1), \dots, E^{(-)}(\mathbf{X}_n) E^{(+)}(\mathbf{X}_{n+1}), \dots, E^{(+)}(\mathbf{X}_{2n}) \right\rangle. \end{aligned} \quad (2.110)$$

For matter of convenience, the notation of the arguments of the correlation functions is abbreviated so \mathbf{X}_j is the pair (\mathbf{r}_j, t_j) . The field operators are in normal order, i.e. all creation operators are to the left and all destruction operators are to the right which is in consistent with the kind of measurement based on the photo-electric effect as was discussed. The n th-order correlation functions are used in multiple photo-detector experiments. The $G^{(2)}$ is the most used to characterize a quantum field. To quantify the field, it is convenient to use the normalized correlation functions (degrees of coherence) $g^{(2)}$. From now on, when $G^{(2)}$ is mentioned, it refers to $g^{(2)}$. For stationary quantized electromagnetic field, according to Glauber (1963c) and Mandel & Wolf (1995), the $G^{(2)}$ is defined by.

$$g_{ij}^{(2)}(\mathbf{r}, \tau) = \frac{\langle \hat{E}^{(-)}(\mathbf{r}, t) \hat{E}^{(-)}(\mathbf{r}, t + \tau) \hat{E}^{(+)}(\mathbf{r}, t + \tau) \hat{E}^{(+)}(\mathbf{r}, t) \rangle}{\langle \hat{E}^{(-)}(\mathbf{r}, t) \hat{E}^{(+)}(\mathbf{r}, t) \rangle \langle \hat{E}^{(-)}(\mathbf{r}, t + \tau) \hat{E}^{(+)}(\mathbf{r}, t + \tau) \rangle}. \quad (2.111)$$

For measurements on two distinct modes of the field, Equation 2.111 leads to simple forms of the $G^{(2)}$ for the modes (Loudon, 1980; Zubairy, 1982).

$$g_{ij}^{(2)}(\mathbf{r}, \tau) = \frac{\langle \hat{a}_i^\dagger(\mathbf{r}, t) \hat{a}_j^\dagger(\mathbf{r}, t + \tau) \hat{a}_j(\mathbf{r}, t + \tau) \hat{a}_i(\mathbf{r}, t) \rangle}{\langle \hat{a}_i^\dagger(\mathbf{r}, t) \hat{a}_i(\mathbf{r}, t) \rangle \langle \hat{a}_j^\dagger(\mathbf{r}, t + \tau) \hat{a}_j(\mathbf{r}, t + \tau) \rangle}; \quad i, j = 1, 2. \quad (2.112)$$

These modes may differ in their frequencies, polarization, or direction of propagation (Loudon, 2000), for example. There are two types of correlations in Equation 2.112: the intra-mode correlations (for $i = j$) and the inter-mode correlations (for $i \neq j$). For zero time-delay, the intra-mode and inter-mode $G^{(2)}$, Equation 2.112, take the form

$$g_{jj}^{(2)}(0) = \frac{\langle \hat{a}_j^{\dagger 2} \hat{a}_j^2 \rangle}{\langle \hat{a}_j^\dagger \hat{a}_j \rangle^2}; \quad j = 1, 2, \quad (2.113)$$

$$g_{12}^{(2)}(0) = \frac{\langle \hat{a}_1^\dagger \hat{a}_1 \hat{a}_2^\dagger \hat{a}_2 \rangle}{\langle \hat{a}_1^\dagger \hat{a}_1 \rangle \langle \hat{a}_2^\dagger \hat{a}_2 \rangle}. \quad (2.114)$$

For the calculations, Equations 2.113 and 2.114 are rewritten in terms of the photon number operator as

$$g_{jj}^{(2)}(0) = \frac{\langle \hat{n}_j (\hat{n}_j - \hat{1}) \rangle}{\langle \hat{n}_j \rangle^2}; \quad j = 1, 2, \quad (2.115)$$

$$g_{12}^{(2)}(0) = \frac{\langle \hat{n}_1 \hat{n}_2 \rangle}{\langle \hat{n}_1 \rangle \langle \hat{n}_2 \rangle}. \quad (2.116)$$

The quantum nature of the field appears clearly in Equation 2.115 as a result of non-commutativity of the EM field operators \hat{a}_j and \hat{a}_j^\dagger applied to Equation 2.113. Equation 2.115 can be rewritten in terms of Q , Equation 2.106, and it reads

$$g_{jj}^{(2)}(0) = 1 + \frac{Q_j}{\langle \hat{n}_j \rangle}; \quad j = 1, 2, \quad (2.117)$$

where Q_j is the Q for the mode j . So, $g_{jj}^{(2)}(0) = 1$ is the boundary between a classical and a quantum field and the statistics are Poissonian. For $g_{jj}^{(2)}(0) > 1$, the statistics are super-Poissonian and becomes sub-Poissonian for $g_{jj}^{(2)}(0) < 1$. There are various inequalities obeyed by correlation functions which can be established using, for example, the CSI. One important of these inequalities reads

$$g^{(2)}(\tau) \leq g^{(2)}(0). \quad (2.118)$$

The violation of this classical inequality is an indication of the nonclassicality of the field. The field is called *bunching* if $g^{(2)}(\tau) < g^{(2)}(0)$ as in chaotic thermal light and no bunching when $g^{(2)}(\tau) = g^{(2)}(0) = 1$ as in coherent light. The field manifests nonclassical properties when the above inequality, Equation 2.118, is violated and called *antibunching* as in photons emitted in resonance fluorescence (Kimble & Mandel, 1976, 1977; Kimble et al., 1977; Paul, 1982). The bunching refers to the tendency of photons to arrive in bunches (clusters) while the antibunching is the case when the photons tend to distribute themselves separately rather than in bunches (Mandel, 1976; Kozierowski, 1981; Paul, 1982; Zou & Mandel, 1990; Scully & Zubairy, 1997; Loudon, 2000). There are other measures for antibunching (Zou & Mandel, 1990; Dung et al., 1992); for example

$$g^{(2)}(0) < 1. \quad (2.119)$$

However, since there is no association between sub-Poissonian and antibunching as pointed in Singh (1983) and according to Zou & Mandel (1990), the more acceptable measure for antibunching is the violation of Equation 2.118 and for sub-Poissonian statistics is violation of Equation 2.119.

2.5.3 Cauchy-Schwarz Inequality

CSI is an important tool in mathematics and mathematical physics. It is a simple inequality useful in establishing mathematical proofs. The importance of this inequality increased after the use of its quantum version to study the nonclassicality of quantum systems. The violation of this inequality indicates the nonclassical behavior of the quantum system. For any pair of vectors A, B in an inner product space, the CSI (Mandel & Wolf, 1995; Puri, 2001; Hassani, 2013; Agarwal, 2013)

$$|\langle A|B\rangle|^2 \leq \langle A|A\rangle\langle B|B\rangle. \quad (2.120)$$

This inequality is valid for classical fields but violated for quantum fields. An example of these functions is the $G^{(2)}$ (Glauber, 1963c; Loudon, 1980). From Equation 2.112, the CSI for these functions (Kheruntsyan et al., 2012)

$$\left|g_{ij}^{(2)}\right|^2 \leq g_{ii}^{(2)} g_{jj}^{(2)}. \quad (2.121)$$

To quantify the nonclassical correlation, and for computational convenience (Ooi et al., 2007; Kheruntsyan et al., 2012), the function F_{cs} is defined by

$$F_{cs} = \frac{\left|g_{12}^{(2)}\right|}{\sqrt{g_{11}^{(2)} g_{22}^{(2)}}} - 1. \quad (2.122)$$

In terms of F_{cs} , the CSI, Equation 2.121, is equivalent to $F_{cs} \leq 0$. The violation of the CSI Equation 2.122 (i.e. $F_{cs} > 0$) is an indicator of the nonclassicality of the field. In this study, this inequality is violated as will be seen.

2.6 Glauber-Sudarshan P -Representation

It is interesting and desirable to have understanding of quantum aspects intuitively by setting a correspondence between quantum physics and classical physics. The statistical distributions in phase space is problematic in quantum physics unlike their classical counterpart. The difficulty comes from the fact that a particle cannot simultaneously have a well defined position and momentum due to the uncertainty principle. For this reason, a true phase space probability distribution cannot be defined for a quantum mechanical particle. However, "quasi-probability distribution functions" that have some resemblance to phase space distribution functions can be defined (Wigner, 1932; Glauber, 1963b; Sudarshan, 1963; Cahill & Glauber, 1969a,b; Agarwal & Wolf, 1970a,b,c; Drummond & Gardiner, 1980). A comprehensive review with numerous references is provided by Hillery et al. (1984). There are three simple kinds of these distributions with much use in quantum optics (Puri, 2001; Schleich, 2001; Carmichael, 2002, 2008). Here, the concern is only on one of these three which is called the P -representation of Glauber (1963b) and Sudarshan (1963). The density matrix operator ρ for any state of light can be written as (Glauber, 1963a; Sudarshan, 1963; Klauder & Sudarshan, 2006).

$$\rho = \int d^2\alpha |\alpha\rangle P(\alpha, \alpha^*) \langle\alpha|, \quad (2.123)$$

with

$$\int d^2\alpha P(\alpha, \alpha^*) = 1, \quad (2.124)$$

where $|\alpha\rangle$ is a coherent state. A classical state of light is one in which the P -representation, $P(\alpha, \alpha^*)$ is a probability density function. If it is not, the state is said to be nonclassical (Hillery, 2009). The aspects of $P(\alpha, \alpha^*)$ that would make it nonclassical are:

- a negative value at any point,
- being more singular than a Dirac delta function.

According to (Mandel & Wolf, 1995, p. 541), "The different coherent states are not orthogonal, so that even if $P(\alpha, \alpha^*)$ behaved like a true probability density, it would not describe probabilities of mutually exclusive states." The P -representation of both the number state and the coherent state is mentioned briefly. The number state has no functional form in the P -representation, except for the vacuum state which is given by a delta function. A generalized function (distribution) of singularity much more than the delta function can be given as a P -representation for the number state (Scully & Zubairy, 1997; Schleich, 2001; Gardiner & Zoller, 2004; Gerry & Knight, 2005; Agarwal, 2013).

$$P(\alpha, \alpha^*) = \frac{1}{n!} e^{|\alpha|^2} \left(\frac{\partial^2}{\partial \alpha \partial \alpha^*} \right)^n \delta^2(\alpha). \quad (2.125)$$

This is not a well-behaved P -representation; it involves 2nth derivative of the delta function. In the coherent state, $\rho = |\alpha_0\rangle\langle\alpha_0|$, the P -representation is much simpler and has a delta function form (Scully & Zubairy, 1997; Schleich, 2001; Gardiner & Zoller, 2004; Gerry & Knight, 2005; Agarwal, 2013)

$$P(\alpha, \alpha^*) = \delta^2(\alpha - \alpha_0). \quad (2.126)$$

The P -representation for squeezed states is more singular than that for number states. While the representation of number states involves a finite number of derivatives of the delta function, the representation for squeezed states has derivatives of all orders (Tan & Jeong, 2019; Schleich, 2001)

$$P(\alpha, \alpha^*) = \exp \left[\frac{1-s}{8s} \frac{\partial^2}{\partial (\text{Re } \alpha)^2} - \frac{1-s}{8} \frac{\partial^2}{\partial (\text{Im } \alpha)^2} \right] \delta^2(\alpha - \alpha_0). \quad (2.127)$$

The parameter $s > 0$ describes the width of the wave packet (squeezing parameter) and α_0 is a displacement. Equation 2.127 can be written as (Schleich, 2001)

$$P(\alpha, \alpha^*) = \exp \left[\frac{1-s}{32s} (L_+ - sL_-) \right] \delta^2(\alpha - \alpha_0), \quad (2.128)$$

$$L_{\pm} = \frac{\partial^2}{\partial \alpha^2} + \frac{\partial^2}{\partial \alpha^{*2}} \pm \frac{\partial^2}{\partial \alpha \partial \alpha^*}. \quad (2.129)$$

University of Malaya

CHAPTER 3: QUANTUM THEORY OF THE LASER

3.1 Introduction and Background

The inventions of maser and laser (optical maser) involve several notable physicists and engineers; Charles Hard Townes, Gordon Ziegler, Theodore Maiman, Alexander Prokhorov, and Nikolay Basov. There were a lot of efforts on theoretical and experimental sides relating to laser as a new tool with applications and "a solution looking for problems". There are various versions of the quantum theory of lasers: the Fokker-Planck method by Haken and Risken, the noise operator method by Lax and Louisell, and the density matrix technique by Scully and Lamb. Scully & Lamb's theory stands out to be correct, truly quantum and successfully describes the quantum statistical properties of laser light such as the photon statistics and the linewidth.

The principle of the laser was first described by Albert Einstein in 1917, in his theory of stimulated emission. It took more than 20 years later for engineers to begin to utilize this principle for practical purposes. Nobel laureates Charles Hard Townes, Nicolay Genadiyevich Basov and Aleksandr Mikhailovich Prokhorov published, independently, papers about the possibility of maser action. In 1958, Charles Hard Townes and Arthur Schawlow proposed to extend the maser theory to the visible regime. Two years later, the first laser was invented by T. Maiman. Since then, the laser has revolutionized our lives and provided a quantum leap to many aspects of science and technology. In the early 1960s, the physics of laser linewidth was not well understood. Einstein's theory could not provide the correct description. This is not surprising since lasing is a combination of quantum statistical and mechanical effects.

Could the photon statistics of the laser be the thermal distribution, a coherent state of radiation or something in between? It is the purpose of this chapter to review the

fundamental nature and the physical origin of the photon statistics of a laser using the quantum statistical approach based on the successful Scully-Lamb's quantum theory of laser (Scully & Lamb, 1967). A self-contained theoretical framework using the master equation for the quantized laser field coupled to a dissipative system outside the laser cavity is presented. Such a technique has been applied to atom-laser with Bose-Einstein condensation.

3.2 Single Mode Field in Bosonic Reservoir

The analogy between the quantum statistics of Bose-Einstein condensate (BEC) (Klaers et al., 2010) and the quantum theory of laser is built on two parts. The first is the damping of the Bosons coupled to a reservoir of harmonic oscillators. The second is the pumping process which gives nonlinear characteristics of the laser. In this section, a short account is presented for the calculation of the dissipation part in the master equation due to the coupling between a quantum system (the electromagnetic field in the present case) and the environment modeled by the reservoir. Many textbooks in quantum optics treat this subject but for a clear presentation with detailed derivation (for the damping atom which is similar to the present problem) can be found in Schleich (2001).

The derivation of the damping Liouvillean proceeds from the Liouville-von Neumann equation, Equation 2.9

$$\frac{\partial}{\partial t} \hat{\rho}(t) = \frac{1}{i\hbar} [\hat{V}_{sr}, \hat{\rho}(t)], \quad (3.1)$$

where, in the interaction picture, the Hamiltonian of the system (s) and the radiation reservoir (r) reads

$$\hat{V}_{sr} = \hbar \sum_{\mathbf{k}} g_{\mathbf{k}} \left(\hat{b}_{\mathbf{k}} \hat{a}^{\dagger} e^{i(\omega - \omega_{\mathbf{k}})t} + \hat{b}_{\mathbf{k}}^{\dagger} \hat{a} e^{-i(\omega - \omega_{\mathbf{k}})t} \right). \quad (3.2)$$

The system is a single mode oscillator with frequency ω and creation and annihilation operators, \hat{a}^\dagger, \hat{a} . The radiation reservoir is a collection of harmonic oscillators (multimode) with frequencies $\omega_{\mathbf{k}}$ and creation and annihilation operators, $\hat{b}_{\mathbf{k}}, \hat{b}_{\mathbf{k}}^\dagger$. The system harmonic oscillator couples to the k -th reservoir oscillator through a coupling constant $g_{\mathbf{k}}$. A closed form of the dynamical equation of the reduced density operator for the single mode oscillator $\hat{\rho}_s(t) = \text{Tr}_r\{\hat{\rho}(t)\}$ can be derived by tracing out degrees of freedom of the reservoir. This is accomplished by first integrating Equation 3.1

$$\hat{\rho}(t) = \hat{\rho}(0) + \frac{1}{i\hbar} \int_0^t [\hat{V}_{sr}(t'), \hat{\rho}(t')] dt'. \quad (3.3)$$

Then, by substituting the result, Equation 3.3, back inside the commutator in Equation 3.1, gives

$$\frac{\partial}{\partial t} \hat{\rho}_s(t) = \frac{1}{i\hbar} \text{Tr}_r [\hat{V}_{sr}, \hat{\rho}(0)] + \frac{1}{(i\hbar)^2} \text{Tr}_r \int_0^t dt' [\hat{V}_{sr}(t), [\hat{V}_{sr}(t'), \hat{\rho}(t')]]. \quad (3.4)$$

This may be repeated indefinitely, but owing to the weaknesses of the system-reservoir interaction, it is possible to ignore terms higher than second order in \hat{V}_{sr} . Furthermore, the system and reservoir are assumed to be approximately uncorrelated in the past, and the reservoir is so large that it remains practically in thermal equilibrium $\hat{\rho}_r^{th}$, so

$$\hat{\rho}(0) = \hat{\rho}_s(0) \otimes \hat{\rho}_r^{th}, \quad (3.5)$$

$$\hat{\rho}(t') \simeq \hat{\rho}_s(t') \otimes \hat{\rho}_r^{th}. \quad (3.6)$$

To simplify the calculations, the quantities $c_{\mathbf{k}} = g_{\mathbf{k}} e^{-i(\omega - \omega_{\mathbf{k}})t}$, $c_{\mathbf{k}'} = g_{\mathbf{k}'} e^{-i(\omega - \omega_{\mathbf{k}'})t'}$, and $\hat{A}_{\mathbf{k}} = c_{\mathbf{k}} \hat{b}_{\mathbf{k}}^\dagger \hat{a}$ are introduced. In terms of these quantities, the first term becomes

$$\frac{1}{i\hbar} \text{Tr}_r [\hat{V}_{sr}, \hat{\rho}] = -i \sum_{\mathbf{k}} \left\{ \text{Tr}_r [\hat{A}_{\mathbf{k}}, \hat{\rho}(0)] + \text{Tr}_r [\hat{A}_{\mathbf{k}}^\dagger, \hat{\rho}(0)] \right\}, \quad (3.7)$$

and the second term reads

$$\begin{aligned} \frac{1}{(i\hbar)^2} \text{Tr}_r [\hat{V}_{sr}(t), [\hat{V}_{sr}(t'), \hat{\rho}(t')]] &= - \text{Tr}_r \int_0^t dt' \sum_{\mathbf{k}\mathbf{k}'} \{ [\hat{A}_{\mathbf{k}}, [\hat{A}_{\mathbf{k}'}, \hat{\rho}(t')]] \\ &+ [\hat{A}_{\mathbf{k}}, [\hat{A}_{\mathbf{k}'}^\dagger, \hat{\rho}(t')]] + [\hat{A}_{\mathbf{k}}^\dagger, [\hat{A}_{\mathbf{k}'}, \hat{\rho}(t')]] \\ &+ [\hat{A}_{\mathbf{k}}^\dagger, [\hat{A}_{\mathbf{k}'}^\dagger, \hat{\rho}(t')]] \}. \end{aligned} \quad (3.8)$$

The commutators in Equation 3.8 are evaluated to

$$[\hat{A}_{\mathbf{k}}, [\hat{A}_{\mathbf{k}'}, \hat{\rho}(t')]] = \hat{A}_{\mathbf{k}} \hat{A}_{\mathbf{k}'} \hat{\rho}(t') - \hat{A}_{\mathbf{k}} \hat{\rho}(t') \hat{A}_{\mathbf{k}'} - \hat{A}_{\mathbf{k}'} \hat{\rho}(t') \hat{A}_{\mathbf{k}} + \hat{\rho}(t') \hat{A}_{\mathbf{k}'} \hat{A}_{\mathbf{k}}, \quad (3.9)$$

$$[\hat{A}_{\mathbf{k}}, [\hat{A}_{\mathbf{k}'}^\dagger, \hat{\rho}(t')]] = \hat{A}_{\mathbf{k}} \hat{A}_{\mathbf{k}'}^\dagger \hat{\rho}(t') - \hat{A}_{\mathbf{k}} \hat{\rho}(t') \hat{A}_{\mathbf{k}'}^\dagger - \hat{A}_{\mathbf{k}'}^\dagger \hat{\rho}(t') \hat{A}_{\mathbf{k}} + \hat{\rho}(t') \hat{A}_{\mathbf{k}'}^\dagger \hat{A}_{\mathbf{k}}, \quad (3.10)$$

$$[\hat{A}_{\mathbf{k}}^\dagger, [\hat{A}_{\mathbf{k}'}, \hat{\rho}(t')]] = [\hat{A}_{\mathbf{k}}, [\hat{A}_{\mathbf{k}'}^\dagger, \hat{\rho}(t')]]^\dagger, \quad (3.11)$$

$$[\hat{A}_{\mathbf{k}}^\dagger, [\hat{A}_{\mathbf{k}'}^\dagger, \hat{\rho}(t')]] = [\hat{A}_{\mathbf{k}}, [\hat{A}_{\mathbf{k}'}, \hat{\rho}(t')]]^\dagger. \quad (3.12)$$

The commutators in Equations 3.11 and 3.12 are obtained by using the fact that for any two operators $[A, B]^\dagger = -[A^\dagger, B^\dagger]$ and the Hermiticity of the density operator. Using Equation 3.6, the trace of commutators in Equation 3.7 reads

$$\begin{aligned} \text{Tr}_r [\hat{A}_{\mathbf{k}}, \hat{\rho}(0)] &= c_{\mathbf{k}} \text{Tr}_r (\hat{b}_{\mathbf{k}}^\dagger \hat{\rho}_r^{th}) \hat{a} \hat{\rho}_s(0) - c_{\mathbf{k}} \text{Tr}_r (\hat{\rho}_r^{th} \hat{b}_{\mathbf{k}}^\dagger) \hat{\rho}_s(0) \hat{a} \\ &= c_{\mathbf{k}} \langle \hat{b}_{\mathbf{k}}^\dagger \rangle [\hat{a}, \hat{\rho}_s(0)], \end{aligned} \quad (3.13)$$

and the trace of the commutators in Equations 3.9 and 3.10 is similarly evaluated to

$$\begin{aligned} \text{Tr}_r [\hat{A}_{\mathbf{k}}, [\hat{A}_{\mathbf{k}'}, \hat{\rho}(t')]] &= c_{\mathbf{k}}c_{\mathbf{k}'} \left\{ \text{Tr}_r [\hat{b}_{\mathbf{k}}^\dagger \hat{b}_{\mathbf{k}'}^\dagger \hat{\rho}_r^{th}] \hat{a} \hat{a} \hat{\rho}_s(t') - \text{Tr}_r [\hat{b}_{\mathbf{k}}^\dagger \hat{\rho}_r^{th} \hat{b}_{\mathbf{k}'}^\dagger] \hat{a} \hat{\rho}_s(t') \hat{a} \right. \\ &\quad \left. - \text{Tr}_r [\hat{b}_{\mathbf{k}'}^\dagger \hat{\rho}_r^{th} \hat{b}_{\mathbf{k}}^\dagger] \hat{a} \hat{\rho}_s(t') \hat{a} + \text{Tr}_r [\hat{\rho}_r^{th} \hat{b}_{\mathbf{k}}^\dagger \hat{b}_{\mathbf{k}'}^\dagger] \hat{\rho}_s(t') \hat{a} \hat{a} \right\}, \end{aligned} \quad (3.14)$$

$$\begin{aligned} \text{Tr}_r [\hat{A}_{\mathbf{k}}, [\hat{A}_{\mathbf{k}'}^\dagger, \hat{\rho}(t')]] &= c_{\mathbf{k}}c_{\mathbf{k}'}^* \left\{ \text{Tr}_r [\hat{b}_{\mathbf{k}}^\dagger \hat{b}_{\mathbf{k}'} \hat{\rho}_r^{th}] \hat{a} \hat{a}^\dagger \hat{\rho}_s(t') - \text{Tr}_r [\hat{b}_{\mathbf{k}}^\dagger \hat{\rho}_r^{th} \hat{b}_{\mathbf{k}'}] \hat{a} \hat{\rho}_s(t') \hat{a}^\dagger \right. \\ &\quad \left. - \text{Tr}_r [\hat{b}_{\mathbf{k}'} \hat{\rho}_r^{th} \hat{b}_{\mathbf{k}}^\dagger] \hat{a}^\dagger \hat{\rho}_s(t') \hat{a} + \text{Tr}_r [\hat{\rho}_r^{th} \hat{b}_{\mathbf{k}} \hat{b}_{\mathbf{k}'}^\dagger] \hat{\rho}_s(t') \hat{a}^\dagger \hat{a} \right\}. \end{aligned} \quad (3.15)$$

Using the property that the trace is invariant under cyclic permutations $\text{Tr}(ABC) = \text{Tr}(CAB) = \text{Tr}(BCA)$, Equations 3.14 and 3.15 become

$$\begin{aligned} \text{Tr}_r [\hat{A}_{\mathbf{k}}, [\hat{A}_{\mathbf{k}'}, \hat{\rho}(t')]] &= c_{\mathbf{k}}c_{\mathbf{k}'} \left\{ \langle \hat{b}_{\mathbf{k}}^\dagger \hat{b}_{\mathbf{k}'}^\dagger \rangle \hat{a} \hat{a} \hat{\rho}_s(t') - \langle \hat{b}_{\mathbf{k}'}^\dagger \hat{b}_{\mathbf{k}}^\dagger \rangle \hat{a} \hat{\rho}_s(t') \hat{a} \right. \\ &\quad \left. - \langle \hat{b}_{\mathbf{k}}^\dagger \hat{b}_{\mathbf{k}'}^\dagger \rangle \hat{a} \hat{\rho}_s(t') \hat{a} + \langle \hat{b}_{\mathbf{k}'}^\dagger \hat{b}_{\mathbf{k}}^\dagger \rangle \hat{\rho}_s(t') \hat{a} \hat{a} \right\}, \end{aligned} \quad (3.16)$$

$$\begin{aligned} \text{Tr}_r [\hat{A}_{\mathbf{k}}, [\hat{A}_{\mathbf{k}'}^\dagger, \hat{\rho}(t')]] &= c_{\mathbf{k}}c_{\mathbf{k}'}^* \left\{ \langle \hat{b}_{\mathbf{k}}^\dagger \hat{b}_{\mathbf{k}'} \rangle \hat{a} \hat{a}^\dagger \hat{\rho}_s(t') - \langle \hat{b}_{\mathbf{k}} \hat{b}_{\mathbf{k}'}^\dagger \rangle \hat{a} \hat{\rho}_s(t') \hat{a}^\dagger \right. \\ &\quad \left. - \langle \hat{b}_{\mathbf{k}'} \hat{b}_{\mathbf{k}}^\dagger \rangle \hat{a}^\dagger \hat{\rho}_s(t') \hat{a} + \langle \hat{b}_{\mathbf{k}} \hat{b}_{\mathbf{k}'}^\dagger \rangle \hat{\rho}_s(t') \hat{a}^\dagger \hat{a} \right\}. \end{aligned} \quad (3.17)$$

Substituting Equation 3.13 in Equation 3.7, the first term in Equation 3.4 becomes

$$\frac{1}{i\hbar} \text{Tr}_r [\hat{V}_{sr}, \hat{\rho}(0)] = -i \sum_{\mathbf{k}} \left\{ c_{\mathbf{k}} \langle \hat{b}_{\mathbf{k}}^\dagger \rangle [\hat{a}, \hat{\rho}_s(0)] + c_{\mathbf{k}}^* \langle \hat{b}_{\mathbf{k}} \rangle [\hat{a}^\dagger, \hat{\rho}_s(0)] \right\}. \quad (3.18)$$

The second term in Equation 3.4 is obtained by using Equations 3.16 and 3.17 in Equation 3.8, the result reads

$$\frac{1}{(i\hbar)^2} \text{Tr}_r [\hat{V}_{sr}(t), [\hat{V}_{sr}(t'), \hat{\rho}(t')]] = - \int_0^t dt' \sum_{\mathbf{k}\mathbf{k}'} \left\{ c_{\mathbf{k}}c_{\mathbf{k}'} \mathcal{L}_1 + c_{\mathbf{k}}c_{\mathbf{k}'}^* \mathcal{L}_2 + \text{h.c.} \right\}, \quad (3.19)$$

where

$$\begin{aligned} \mathcal{L}_1 = & \left\langle \hat{b}_{\mathbf{k}}^\dagger \hat{b}_{\mathbf{k}'}^\dagger \right\rangle \hat{a} \hat{a} \hat{\rho}_s(t') - \left\langle \hat{b}_{\mathbf{k}}^\dagger \hat{b}_{\mathbf{k}}^\dagger \right\rangle \hat{a} \hat{\rho}_s(t') \hat{a} - \left\langle \hat{b}_{\mathbf{k}}^\dagger \hat{b}_{\mathbf{k}'}^\dagger \right\rangle \hat{a} \hat{\rho}_s(t') \hat{a} \\ & + \left\langle \hat{b}_{\mathbf{k}}^\dagger \hat{b}_{\mathbf{k}}^\dagger \right\rangle \hat{\rho}_s(t') \hat{a} \hat{a}, \end{aligned} \quad (3.20)$$

$$\begin{aligned} \mathcal{L}_2 = & \left\langle \hat{b}_{\mathbf{k}}^\dagger \hat{b}_{\mathbf{k}'}^\dagger \right\rangle \hat{a} \hat{a}^\dagger \hat{\rho}_s(t') - \left\langle \hat{b}_{\mathbf{k}'} \hat{b}_{\mathbf{k}}^\dagger \right\rangle \hat{a} \hat{\rho}_s(t') \hat{a}^\dagger - \left\langle \hat{b}_{\mathbf{k}}^\dagger \hat{b}_{\mathbf{k}'} \right\rangle \hat{a}^\dagger \hat{\rho}_s(t') \hat{a} \\ & + \left\langle \hat{b}_{\mathbf{k}'} \hat{b}_{\mathbf{k}}^\dagger \right\rangle \hat{\rho}_s(t') \hat{a}^\dagger \hat{a}, \end{aligned} \quad (3.21)$$

where the result of Equations 3.11 and 3.12 for the last two terms represented by h.c. are used. Since the density matrix of the thermal reservoir is diagonal in the number state representation, Equation 2.81, so from Equations 2.75 and 2.65 these averages are evaluated to

$$\text{Tr}_r \left(\hat{b}_{\mathbf{k}} \hat{\rho}_r^{th} \right) = \langle \hat{b}_{\mathbf{k}} \rangle = 0, \quad (3.22)$$

$$\text{Tr}_r \left(\hat{b}_{\mathbf{k}}^\dagger \hat{\rho}_r^{th} \right) = \langle \hat{b}_{\mathbf{k}}^\dagger \rangle = 0, \quad (3.23)$$

$$\text{Tr}_r \left(\hat{b}_{\mathbf{k}}^\dagger \hat{b}_{\mathbf{k}'} \hat{\rho}_r^{th} \right) = \langle \hat{b}_{\mathbf{k}}^\dagger \hat{b}_{\mathbf{k}'} \rangle = n^{th} \delta_{\mathbf{k}\mathbf{k}'}, \quad (3.24)$$

$$\text{Tr}_r \left(\hat{b}_{\mathbf{k}} \hat{b}_{\mathbf{k}'}^\dagger \hat{\rho}_r^{th} \right) = \langle \hat{b}_{\mathbf{k}} \hat{b}_{\mathbf{k}'}^\dagger \rangle = (n^{th} + 1) \delta_{\mathbf{k}\mathbf{k}'}, \quad (3.25)$$

$$\text{Tr}_r \left(\hat{b}_{\mathbf{k}} \hat{b}_{\mathbf{k}'} \hat{\rho}_r^{th} \right) = \langle \hat{b}_{\mathbf{k}} \hat{b}_{\mathbf{k}'} \rangle = 0, \quad (3.26)$$

$$\text{Tr}_r \left(\hat{b}_{\mathbf{k}}^\dagger \hat{b}_{\mathbf{k}'}^\dagger \hat{\rho}_r^{th} \right) = \langle \hat{b}_{\mathbf{k}}^\dagger \hat{b}_{\mathbf{k}'}^\dagger \rangle = 0, \quad (3.27)$$

where $n^{th} = n^{th}(\omega_{\mathbf{k}}, T)$ is the mean thermal photon number with frequency $\omega_{\mathbf{k}}$ in thermal equilibrium at temperature T given by Equation 2.84, but the temperature dependence will not be written explicitly. From Equations 3.22 and 3.25, the left-hand side of Equation 3.18 vanishes, so the master equation reduces to

$$\begin{aligned} \frac{\partial}{\partial t} \hat{\rho}_s(t) = & \int_0^t dt' \sum_{\mathbf{k}} g_{\mathbf{k}}^2 e^{-i(\omega - \omega_{\mathbf{k}})(t-t')} \left\{ n^{th}(\omega_{\mathbf{k}}) \left[\hat{a}^\dagger \hat{\rho}_s(t') \hat{a} - \hat{a} \hat{a}^\dagger \hat{\rho}_s(t') \right] \right. \\ & \left. + \left(n^{th}(\omega_{\mathbf{k}}) + 1 \right) \left[\hat{a} \hat{\rho}_s(t') \hat{a}^\dagger - \hat{\rho}_s(t') \hat{a}^\dagger \hat{a} \right] + \text{h.c.} \right\}. \end{aligned} \quad (3.28)$$

It is noteworthy that the terms proportional to $c_{\mathbf{k}}c_{\mathbf{k}'} = g_{\mathbf{k}}g_{\mathbf{k}'}e^{-i[(\omega-\omega_{\mathbf{k}})t+(\omega-\omega_{\mathbf{k}'})t']}$ and $c_{\mathbf{k}}^*c_{\mathbf{k}'}^* = g_{\mathbf{k}}g_{\mathbf{k}'}e^{i[(\omega-\omega_{\mathbf{k}})t+(\omega-\omega_{\mathbf{k}'})t']}$ vanish for the thermal reservoir. These fast oscillating terms are neglected also in the secular approximation (Puri, 2001, p. 162). The sum over the modes is evaluated by moving to the continuum and using the correspondence

$$\sum_{\mathbf{k}} f_{\mathbf{k}} = \int_0^{\infty} d\Omega D(\Omega) f(\Omega), \quad (3.29)$$

where $D(\Omega)$ is the density of states. Using Equation 3.29 with $\tau = t - t'$, the master equation, Equation 3.28 becomes

$$\begin{aligned} \frac{\partial}{\partial t} \hat{\rho}_s(t) = \int_0^t d\tau \{ & G_{\bar{n}}(\tau) [\hat{a}^\dagger \hat{\rho}_s(t-\tau) \hat{a} - \hat{a} \hat{a}^\dagger \hat{\rho}_s(t-\tau)] \\ & + G_{\bar{n}+1}(\tau) [\hat{a} \hat{\rho}_s(t-\tau) \hat{a}^\dagger - \hat{\rho}_s(t-\tau) \hat{a}^\dagger \hat{a}] + \text{h.c.} \}, \end{aligned} \quad (3.30)$$

where

$$\begin{aligned} G_{\bar{n}}(\tau) &= \sum_{\mathbf{k}} g_{\mathbf{k}}^2 e^{-i(\omega-\omega_{\mathbf{k}})\tau} n^{th}(\omega_{\mathbf{k}}) \\ &= \int_0^{\infty} d\Omega e^{-i(\omega-\Omega)\tau} D(\Omega) |g(\Omega)|^2 n^{th}(\Omega), \end{aligned} \quad (3.31)$$

$$\begin{aligned} G_{\bar{n}+1}(\tau) &= \sum_{\mathbf{k}} g_{\mathbf{k}}^2 e^{-i(\omega-\omega_{\mathbf{k}})\tau} (n^{th}(\omega_{\mathbf{k}}) + 1) \\ &= \int_0^{\infty} d\Omega e^{-i(\omega-\Omega)\tau} D(\Omega) |g(\Omega)|^2 (n^{th}(\Omega) + 1). \end{aligned} \quad (3.32)$$

The integration in Equation 3.30 is dominated by times that are much shorter than the time scale for the evolution of ρ_s . It is true in vacuum, where the continuum property of the density of modes corresponds to the state of the system being independent of its past. This allows us to perform the short memory or *Markovian* approximation ($\rho_s(t-\tau) \simeq \rho_s(t)$) (Mandel & Wolf, 1995; Blum, 2012). In the Markovian approximation, the integration limit

are extended to ∞ and Equation 3.30 becomes

$$\begin{aligned} \frac{\partial \hat{\rho}_s}{\partial t} = & \mathcal{E}_1 [\hat{a}^\dagger \hat{\rho}_s \hat{a} - \hat{a} \hat{a}^\dagger \hat{\rho}_s] + (\mathcal{E}_0 + \mathcal{E}_1) [\hat{a} \hat{\rho}_s \hat{a}^\dagger - \hat{\rho}_s \hat{a}^\dagger \hat{a}] \\ & + \mathcal{E}_1^* [\hat{a}^\dagger \hat{\rho}_s \hat{a} - \hat{\rho}_s \hat{a} \hat{a}^\dagger] + (\mathcal{E}_0^* + \mathcal{E}_1^*) [\hat{a} \hat{\rho}_s \hat{a}^\dagger - \hat{a}^\dagger \hat{a} \hat{\rho}_s], \end{aligned} \quad (3.33)$$

where the damping coefficients are

$$\mathcal{E}_0 = \int_0^\infty d\Omega D(\Omega) |g(\Omega)|^2 \int_0^\infty d\tau e^{-i(\omega-\Omega)\tau} = \frac{1}{2}\kappa + i\xi_0, \quad (3.34)$$

$$\mathcal{E}_1 = \int_0^\infty d\Omega D(\Omega) |g(\Omega)|^2 n^{th}(\Omega, T) \int_0^\infty d\tau e^{-i(\omega-\Omega)\tau} = \frac{1}{2}\kappa n^{th} + i\xi_1, \quad (3.35)$$

with

$$\kappa = 2\pi D(\omega) |g(\omega)|^2, \quad (3.36)$$

$$\xi_0 = P \int_0^\infty d\Omega \frac{D(\Omega) |g(\Omega)|^2}{\Omega - \omega}, \quad (3.37)$$

$$\xi_1 = P \int_0^\infty d\Omega \frac{D(\Omega) |g(\Omega)|^2}{\Omega - \omega} n^{th}(\Omega, T). \quad (3.38)$$

In deriving Equations 3.34 and 3.35, the following relation is used (Puri, 2001, Appendix A)

$$\int_0^\infty dk e^{\pm ikx} = \pi \delta(x) \pm iP \frac{1}{x}. \quad (3.39)$$

In Equation 3.39, $\delta(x)$ and P are the delta function and the Cauchy principal value, respectively. In terms of the real and imaginary parts of the coefficients in Equations 3.34 and 3.35, the master equation, Equation 3.33, takes the form

$$\begin{aligned} \frac{\partial \hat{\rho}_s}{\partial t} = & \xi_0 [\hat{a}^\dagger \hat{a}, \hat{\rho}_s] - \frac{1}{2} \kappa n^{th} \left(\hat{a} \hat{a}^\dagger \hat{\rho}_s - 2 \hat{a}^\dagger \hat{\rho}_s \hat{a} + \hat{\rho}_s \hat{a} \hat{a}^\dagger \right) \\ & - \frac{1}{2} \kappa \left(n^{th} + 1 \right) \left(\hat{a}^\dagger \hat{a} \hat{\rho}_s - 2 \hat{a} \hat{\rho}_s \hat{a}^\dagger + \hat{\rho}_s \hat{a}^\dagger \hat{a} \right). \end{aligned} \quad (3.40)$$

For an ideal Markovian process, the commutator in Equation 3.40 is discarded, and the

dissipation master equation reduces to

$$\begin{aligned} \frac{\partial \hat{\rho}_s}{\partial t} = & -\frac{1}{2}\kappa n^{th} \left(\hat{a}\hat{a}^\dagger \hat{\rho}_s - 2\hat{a}^\dagger \hat{\rho}_s \hat{a} + \hat{\rho}_s \hat{a}\hat{a}^\dagger \right) \\ & -\frac{1}{2}\kappa \left(n^{th} + 1 \right) \left(\hat{a}^\dagger \hat{a} \hat{\rho}_s - 2\hat{a} \hat{\rho}_s \hat{a}^\dagger + \hat{\rho}_s \hat{a}^\dagger \hat{a} \right), \end{aligned} \quad (3.41)$$

where κ is the cavity decay rate. To understand the meaning of each term in the density matrix Equation 3.41, it is rewritten as follows

$$\begin{aligned} \frac{\partial \hat{\rho}_s}{\partial t} = & \frac{1}{2}\kappa n^{th} \left[\underbrace{-\left(\hat{a}\hat{a}^\dagger \hat{\rho}_s + \hat{\rho}_s \hat{a}\hat{a}^\dagger \right)}_{\text{loss to above (emission)}} + \underbrace{2\hat{a}^\dagger \hat{\rho}_s \hat{a}}_{\text{gain from below(emission)}} \right] \\ & + \frac{1}{2}\kappa \left(n^{th} + 1 \right) \left[\underbrace{-\left(\hat{a}^\dagger \hat{a} \hat{\rho}_s(t) + \hat{\rho}_s \hat{a}^\dagger \hat{a} \right)}_{\text{loss to below (emission)}} + \underbrace{2\hat{a} \hat{\rho}_s \hat{a}^\dagger}_{\text{gain from above (absorption)}} \right] \end{aligned} \quad (3.42)$$

3.3 Quantum Theory of the Laser: The Gain Part

In the previous section, the derivation of the damping part of the master equation is presented. The pumping dynamics are governed by the laser coupling which leads to gain in the photon number. In this section, the nonlinear theory that gives the gain part in the laser master equation is provided.

3.3.1 Gain Part of Laser Master Equation

Assume that a two-level atom with upper level $|a\rangle$ and lower level $|b\rangle$ interacts with a single-mode quantum field of creation and annihilation operators \hat{a}^\dagger and \hat{a} , respectively. If the atom-field coupling constant is g , the atom-field interaction Hamiltonian at resonance becomes

$$V = \hbar g \left(|a\rangle\langle b| \hat{a} + |b\rangle\langle a| \hat{a}^\dagger \right), \quad (3.43)$$

where $|a\rangle\langle b|$ is the atom transition operator from the lower level $|b\rangle$ to the upper level $|a\rangle$ and $|b\rangle\langle a|$ is the transition operator from the upper level $|a\rangle$ to the lower level $|b\rangle$. The internal state vector of the atom-field as a superposition of the two states becomes

$$|\psi\rangle = \sum_n (C_{an}|a\rangle + C_{bn}|b\rangle) |n\rangle, \quad (3.44)$$

where $|n\rangle$ is the field number state with n photons. The Schrödinger equation gives the coupled equations

$$\frac{d}{dt}C_{an} = -ig\sqrt{n+1}C_{b,n+1}, \quad (3.45)$$

$$\frac{d}{dt}C_{b,n+1} = -ig\sqrt{n+1}C_{an}. \quad (3.46)$$

Laplace transform gives

$$sC_{an}(s) = C_{an}(0) - ig\sqrt{n+1}C_{b,n+1}(s), \quad (3.47)$$

$$sC_{b,n+1}(s) = C_{b,n+1}(0) - ig\sqrt{n+1}C_{an}(s). \quad (3.48)$$

The solution of these algebraic coupled equations is straightforward. By doing the inverse Laplace transform, the general solution is

$$C_{an}(t_0 + \tau) = C_{an}(t_0) \cos(g\tau\sqrt{n+1}) - iC_{b,n+1}(t_0) \sin(g\tau\sqrt{n+1}), \quad (3.49)$$

$$C_{b,n+1}(t_0 + \tau) = C_{b,n+1}(t_0) \cos(g\tau\sqrt{n+1}) - iC_{an}(t_0) \sin(g\tau\sqrt{n+1}), \quad (3.50)$$

The density matrix elements are constructed as follows

$$\begin{aligned}
\rho_{an,an'}(t + \tau) &= C_{an}(t + \tau)C_{an'}^*(t + \tau) \\
&= \rho_{an,an'}(t) \cos(g\tau\sqrt{n+1}) \cos(g\tau\sqrt{n'+1}) \\
&\quad + \rho_{bn+1,bn'+1}(t) \sin(g\tau\sqrt{n+1}) \sin(g\tau\sqrt{n'+1}) \\
&\quad + i\rho_{an,bn'+1}(t) \cos(g\tau\sqrt{n+1}) \sin(g\tau\sqrt{n'+1}) \\
&\quad - i\rho_{bn+1,an'}(t) \sin(g\tau\sqrt{n+1}) \cos(g\tau\sqrt{n'+1}),
\end{aligned} \tag{3.51}$$

$$\begin{aligned}
\rho_{bn+1,bn'+1}(t + \tau) &= C_{bn+1}(t + \tau)C_{bn'+1}^*(t + \tau) \\
&= \rho_{bn+1,bn'+1}(t) \cos(g\tau\sqrt{n+1}) \cos(g\tau\sqrt{n'+1}) \\
&\quad + \rho_{an,an'}(t) \sin(g\tau\sqrt{n+1}) \sin(g\tau\sqrt{n'+1}) \\
&\quad + i\rho_{bn+1,an'}(t) \cos(g\tau\sqrt{n+1}) \sin(g\tau\sqrt{n'+1}) \\
&\quad - i\rho_{an,bn'+1}(t) \sin(g\tau\sqrt{n+1}) \cos(g\tau\sqrt{n'+1}),
\end{aligned} \tag{3.52}$$

where, in the adiabatic approximation (Sargent III et al., 1974), $t_0 = t$ is assumed. Assume initially no population in level b as well as no coherence, $\rho_{an,an'}(t) = \rho_{n,n'}(t)$, others are zero,

$$\rho_{an,an'}(t + \tau) = \rho_{n,n'}(t) \cos(g\tau\sqrt{n+1}) \cos(g\tau\sqrt{n'+1}), \tag{3.53}$$

$$\rho_{bn+1,bn'+1}(t + \tau) = \rho_{n,n'}(t) \sin(g\tau\sqrt{n+1}) \sin(g\tau\sqrt{n'+1}). \tag{3.54}$$

An alternative method using evolution operator can also give the same results. The density matrix elements in Equations 3.51 and 3.52 are obtained for the resonant case when the field frequency ω matches the atom transition frequency ω_0 (zero detuning, $\Delta = \omega_0 - \omega = 0$). The general case for an arbitrary detuning can be obtained in a similar way. The corresponding

Hamiltonian and probability amplitude coefficients take the form

$$V = \hbar g \left(e^{i\Delta t} |a\rangle \langle b| \hat{a} + e^{-i\Delta t} |b\rangle \langle a| \hat{a}^\dagger \right), \quad (3.55)$$

and

$$C_{a,n}(t) = e^{i\Delta t/2} \left\{ C_{a,n}(0) \left[\cos\left(\frac{\Omega_n t}{2}\right) - \frac{i\Delta}{\Omega_n} \sin\left(\frac{\Omega_n t}{2}\right) \right] - \frac{i2g\sqrt{n+1}}{\Omega_n} \sin\left(\frac{\Omega_n t}{2}\right) C_{b,n+1}(0) \right\}, \quad (3.56)$$

$$C_{b,n+1}(t) = e^{-i\Delta t/2} \left\{ C_{b,n+1}(0) \left[\cos\left(\frac{\Omega_n t}{2}\right) + \frac{i\Delta}{\Omega_n} \sin\left(\frac{\Omega_n t}{2}\right) \right] - \frac{i2g\sqrt{n+1}}{\Omega_n} \sin\left(\frac{\Omega_n t}{2}\right) C_{a,n}(0) \right\}, \quad (3.57)$$

where $\Omega_n^2 = \Delta^2 + 4g^2(n+1)$. More details are given in Scully & Zubairy (1997).

3.3.2 Coarse Graining - Many Atoms

Let an atom enters the cavity at time t . The change in the field due to one atom (say j) when it transits through the cavity in time τ is obtained by the trace on the atomic degrees of freedom and is given by

$$\delta \hat{\rho}_f^j(t) = \text{Tr}_a \{ \hat{\rho}^j(t+\tau) - \hat{\rho}^j(t) \} \quad (3.58)$$

$$= \hat{\rho}_{aa}^j(t+\tau) + \hat{\rho}_{bb}^j(t+\tau) - \hat{\rho}_{aa}^j(t) - \hat{\rho}_{bb}^j(t). \quad (3.59)$$

The change in the field due to all N atoms in the cavity from time t to $t + \Delta t$ is

$$\Delta \hat{\rho}_f(t) \simeq \sum_{j=1}^N \delta \hat{\rho}_f^j(t). \quad (3.60)$$

Assuming that all atoms are essentially identical, the injection rate can be defined by

$r_a = N/\Delta t$ and hence

$$\frac{\Delta \hat{\rho}_f}{\Delta t} \simeq r_a \delta \hat{\rho}_f. \quad (3.61)$$

The atoms fly by the cavity and assumed to have a transit lifetime γ . Coarse graining (Fischer, 2018; Phoenix & Knight, 1988) gain over the transit time gives gain contribution

$$\frac{d\rho_f}{dt}_{gain} \simeq \int_0^\infty P(\tau) \frac{\Delta \hat{\rho}_f}{\Delta t} d\tau = \int_0^\infty P(\tau) r_a \delta \hat{\rho}_f d\tau \quad (3.62)$$

$$\begin{aligned} &= \int_0^\infty P(\tau) r_a \text{Tr}_a \{ \hat{\rho}(t + \tau) - \hat{\rho}(t) \} d\tau \\ &= r_a \int_0^\infty P(\tau) \sum_x \{ \hat{\rho}_{xx}(t + \tau) - \hat{\rho}_{xx}(t) \} d\tau, \end{aligned} \quad (3.63)$$

where $P(\tau) = \gamma e^{-\gamma\tau}$ is the weighting function, probability of an atom having a decay rate γ of being in the cavity, and the trace is over atoms states. The elements of the density matrix are given in Equations 3.51 and 3.52 for the resonance case and directly obtained from Equations 3.56 and 3.57.

3.4 Nonlinear Laser Master Equation: Scully - Lamb Approach

In this section, a brief introduction to the nonlinear master equation of the laser is presented. The main focus is on the Scully-Lamb approach for its clarity and simplicity; it is adopted in the analysis.

Scully-Lamb master equation can be obtained simply by using the coarse graining method Equation 3.63 and the density matrix elements from Equations 3.51 and 3.52. For the Scully-Lamb result, where the atoms are initially in excited state and in resonance with

the field, Equations 3.53 and 3.54 are used to obtain

$$\begin{aligned}
\langle n|\delta\hat{\rho}_f(t)|n'\rangle &= \langle n|\text{Tr}_a [\hat{\rho}(t+\tau) - \hat{\rho}(t)] |n'\rangle \\
&= \rho_{an,an'}(t+\tau) + \rho_{bn,bn'}(t+\tau) - \rho_{an,an'}(t) - \rho_{bn,bn'}(t) \\
&= \rho_{n,n'}(t) \cos\left(g\tau\sqrt{n+1}\right) \cos\left(g\tau\sqrt{n'+1}\right) \\
&\quad + \rho_{n-1,n'-1}(t) \sin\left(g\tau\sqrt{n}\right) \sin\left(g\tau\sqrt{n'}\right) - \rho_{n,n'}(t),
\end{aligned} \tag{3.64}$$

where $\rho_{n,n'}(t) = \rho_{an,an'}(t)$ and $\rho_{bn,bn'}(t) = 0$ are assumed and the field reduced density matrix is used

$$\rho_{n,n'}(t+\tau) = \rho_{bn,bn'}(t+\tau) + \rho_{an,an'}(t+\tau). \tag{3.65}$$

Performing the integration on τ , the gain part (Equation 3.63) of the laser master equation is obtained (Sargent III et al., 1974)

$$\left(\frac{\partial p_{nn'}}{\partial t}\right)_{\text{gain}} = -\left(\frac{\mathcal{M}_{nn'}\mathcal{A}}{1 + \mathcal{N}_{nn'}\mathcal{B}/\mathcal{A}}\right)p_{nn'} + \left(\frac{\mathcal{A}\sqrt{nn'}}{1 + \mathcal{N}_{n-1,n'-1}\mathcal{B}/\mathcal{A}}\right)p_{n-1,n'-1}, \tag{3.66}$$

where

$$\mathcal{A} = \frac{2rg^2}{\gamma^2}, \quad \mathcal{B} = \frac{4g^2}{\gamma^2}\mathcal{A}, \tag{3.67}$$

$$\mathcal{M}_{nn'} = \frac{1}{2}(n+1+n'+1) + (n-n')^2\frac{\mathcal{B}}{8\mathcal{A}}, \tag{3.68}$$

$$\mathcal{N}_{nn'} = \mathcal{M}_{nn'} - (n-n')^2\frac{\mathcal{B}}{16\mathcal{A}} = \frac{1}{2}(n+1+n'+1) + (n-n')^2\frac{\mathcal{B}}{16\mathcal{A}}, \tag{3.69}$$

where \mathcal{A} and \mathcal{B} are the linear gain and self-saturation coefficients, respectively. After

including the damping part, Equation 3.41, the overall master equation for laser is

$$\frac{\partial p_{nn'}}{\partial t} = \left(\frac{\partial p_{nn'}}{\partial t} \right)_{\text{gain}} + \left(\frac{\partial p_{nn'}}{\partial t} \right)_{\text{damping}} \quad (3.70)$$

$$\begin{aligned} &= - \left(\frac{\mathcal{M}_{nn'} \mathcal{A}}{1 + \mathcal{N}_{nn'} \mathcal{B} / \mathcal{A}} \right) p_{nn'} + \left(\frac{\mathcal{A} \sqrt{nn'}}{1 + \mathcal{N}_{n-1, n'-1} \mathcal{B} / \mathcal{A}} \right) p_{n-1, n'-1} \\ &\quad - \frac{1}{2} \kappa n^{th} \left[(n+1) p_{n, n'} - 2\sqrt{nn'} p_{n-1, n'-1} + (n'+1) p_{n, n'} \right] \\ &\quad - \frac{1}{2} \kappa (n^{th} + 1) \left[n p_{n, n'} - 2\sqrt{(n+1)(n'+1)} p_{n+1, n'+1} + n' p_{n, n'} \right]. \end{aligned} \quad (3.71)$$

In the analysis a simple three-level system is considered where the cavity field couples between level a and level b of particles in a molecular beam injected into a cavity at a rate r ; this is an effective two-level system. The particles undergo non-radiative decay from level b to level g . A pumping mechanism established between level g up to level a can produce gain to the single mode field. The pumping process drives the single mode field and introduces nonlinearity in the new master equation. The diagonal elements of the density matrix Equation 3.71 evolve according to

$$\begin{aligned} \frac{\partial p_{nn}}{\partial t} &= - \left(\frac{(n+1) \mathcal{A}}{1 + (n+1) \frac{\mathcal{B}}{\mathcal{A}}} \right) p_n + \left(\frac{n \mathcal{A}}{1 + n \frac{\mathcal{B}}{\mathcal{A}}} \right) p_{n-1} \\ &\quad - \kappa n \left[(n^{th} + 1) p_n - n^{th} p_{n-1} \right] + \kappa (n+1) \left[(n^{th} + 1) p_{n+1} - n^{th} p_n \right]. \end{aligned} \quad (3.72)$$

This is a nonlinear equation compared to the classic Pauli master equation (Kreuzer, 1981) linear in photon number, n .

3.5 Photon Statistics

The photon statistics of the laser are found by considering the steady-state of the diagonal elements. Statistics equation becomes much easier to solve in the absence of coherence (vanishing of density matrix off-diagonal elements). In this section, exact the photon number distribution p_n for zero and nonzero thermal mean photon number n^{th} . Also, two limiting cases will be discussed; the distribution below the laser threshold (when the gain in laser

medium equals the loss) and the far above the laser threshold.

3.5.1 Exact Photon Statistics

Assuming atoms are prepared initially in the excited state only as in the Scully-Lamb result considered above, the exact photon statistics function (photon number distribution) can be obtained. From Equation 3.72, the steady-state equation results in the detailed balance set of equations

$$\frac{(n+1)\mathcal{A}}{1+(n+1)\frac{\mathcal{B}}{\mathcal{A}}}p_n = \kappa(n+1) \left[(n^{th}+1)p_{n+1} - n^{th}p_n \right], \quad (3.73)$$

$$\frac{n\mathcal{A}}{1+n\frac{\mathcal{B}}{\mathcal{A}}}p_{n-1} = \kappa n \left[(n^{th}+1)p_n - n^{th}p_{n-1} \right]. \quad (3.74)$$

From Equation 3.74, the statistics function p_n is calculated by iteration

$$p_n = \frac{1}{(n^{th}+1)} \left(\frac{\mathcal{A}/\kappa}{1+n\frac{\mathcal{B}}{\mathcal{A}}} + n^{th} \right) p_{n-1}. \quad (3.75)$$

The iteration of Equation 3.75 gives

$$p_n = \frac{p_0}{(n^{th}+1)^n} \prod_{m=1}^n \left(\frac{\mathcal{A}/\kappa}{1+m\frac{\mathcal{B}}{\mathcal{A}}} + m^{th} \right). \quad (3.76)$$

where the constant p_0 is determined from the normalization condition $\sum_{n=0}^{\infty} p_n = 1$. The product can be evaluated after some arrangement, which results in

$$\begin{aligned} p_n &= p_0 \left(\frac{n^{th}}{n^{th}+1} \right)^n \prod_{m=1}^n \frac{m + \frac{\mathcal{A}^2}{n^{th}\kappa\mathcal{B}} + \frac{\mathcal{A}}{\mathcal{B}}}{m + \frac{\mathcal{A}}{\mathcal{B}}} \\ &= p_0 \left(\frac{n^{th}}{n^{th}+1} \right)^n \frac{\Gamma\left(\frac{\mathcal{A}}{\mathcal{B}}+1\right) \Gamma\left(n + \frac{\mathcal{A}^2}{n^{th}\kappa\mathcal{B}} + \frac{\mathcal{A}}{\mathcal{B}} + 1\right)}{\Gamma\left(\frac{\mathcal{A}^2}{n^{th}\kappa\mathcal{B}} + \frac{\mathcal{A}}{\mathcal{B}} + 1\right) \Gamma\left(n + \frac{\mathcal{A}}{\mathcal{B}} + 1\right)}, \end{aligned} \quad (3.77)$$

where $\Gamma(z+1) = z\Gamma(z)$ is the gamma function and the constant p_0 is

$$p_0 = \left[\sum_0^{\infty} \left(\frac{n^{th}}{n^{th}+1} \right)^n \frac{\Gamma\left(\frac{\mathcal{A}}{\mathcal{B}}+1\right) \Gamma\left(\frac{\mathcal{A}^2}{n^{th}\kappa\mathcal{B}} + \frac{\mathcal{A}}{\mathcal{B}} + 1 + n\right)}{\Gamma\left(\frac{\mathcal{A}^2}{n^{th}\kappa\mathcal{B}} + \frac{\mathcal{A}}{\mathcal{B}} + 1\right) \Gamma\left(\frac{\mathcal{A}}{\mathcal{B}} + 1 + n\right)} \right]^{-1}. \quad (3.78)$$

The expressions Equations 3.77 and 3.78 take simple forms in the case of zero thermal mean photon number $n^{th} \rightarrow 0$ (n^{th} is almost zero in the optical region). In this case, Equations 3.77 and 3.78 are reduced to

$$p_n = p_0 \frac{\left(\frac{\mathcal{A}^2}{\mathcal{B}\kappa}\right)^n \Gamma\left(\frac{\mathcal{A}}{\mathcal{B}}+1\right)}{\Gamma\left(\frac{\mathcal{A}}{\mathcal{B}}+1+n\right)}, \quad (3.79)$$

$$p_0 = \left[\sum_{n=0}^{\infty} \frac{\left(\frac{\mathcal{A}^2}{\mathcal{B}\kappa}\right)^n \left(\frac{\mathcal{A}}{\mathcal{B}}\right)!}{\left(n + \frac{\mathcal{A}}{\mathcal{B}}\right)!} \right]^{-1} = \left[F\left(1; \frac{\mathcal{A}}{\mathcal{B}}+1; \frac{\mathcal{A}^2}{\mathcal{B}\kappa}\right) \right]^{-1}, \quad (3.80)$$

where

$$F(a; b; z) = \sum_{n=0}^{\infty} \frac{\Gamma(b) \Gamma(a+n) z^n}{\Gamma(a) \Gamma(b+n) n!} \quad (3.81)$$

is confluent hypergeometric function.

The mean photon number $\langle n \rangle$ and second moment $\langle n^2 \rangle$ are evaluated as follows

$$\langle n \rangle = \sum_{n=0}^{\infty} n p_n, \quad (3.82)$$

$$\langle n^2 \rangle = \sum_{n=0}^{\infty} n^2 p_n. \quad (3.83)$$

Instead of using Equation 3.77 or to evaluate the sum, it is easier to use Equation 3.75 after rearrangement

$$\left(1 + n \frac{\mathcal{B}}{\mathcal{A}}\right) p_n = \left(\frac{\mathcal{A}/\kappa}{n^{th}+1} + \frac{n^{th}}{n^{th}+1} \left(1 + n \frac{\mathcal{B}}{\mathcal{A}}\right)\right) p_{n-1}. \quad (3.84)$$

The mean is obtained from Equation 3.84 by sum over n and the second moment is obtained by multiplying Equation 3.84 by n and sum over n

$$\sum_{n=0}^{\infty} \left(1 + n \frac{\mathcal{B}}{\mathcal{A}}\right) p_n = \sum_{n=0}^{\infty} \left(\frac{\mathcal{A}/\kappa}{n^{th} + 1} + \frac{n^{th}}{n^{th} + 1} \left(1 + n \frac{\mathcal{B}}{\mathcal{A}}\right)\right) p_{n-1}$$

$$\sum_{n=0}^{\infty} \left(n + n^2 \frac{\mathcal{B}}{\mathcal{A}}\right) p_n = \sum_{n=0}^{\infty} \left(\frac{\mathcal{A}/\kappa}{n^{th} + 1} n + \frac{n^{th}}{n^{th} + 1} \left(n + n^2 \frac{\mathcal{B}}{\mathcal{A}}\right)\right) p_{n-1}$$

or

$$1 + \langle n \rangle \frac{\mathcal{B}}{\mathcal{A}} = \frac{\mathcal{A}/\kappa}{n^{th} + 1} + \frac{n^{th}}{n^{th} + 1} \left(1 + \langle n + 1 \rangle \frac{\mathcal{B}}{\mathcal{A}}\right), \quad (3.85)$$

$$\langle n \rangle + \langle n^2 \rangle \frac{\mathcal{B}}{\mathcal{A}} = \frac{\mathcal{A}/\kappa}{n^{th} + 1} \langle n + 1 \rangle + \frac{n^{th}}{n^{th} + 1} \left(\langle n + 1 \rangle + \langle (n + 1)^2 \rangle \frac{\mathcal{B}}{\mathcal{A}}\right). \quad (3.86)$$

From Equations 3.85 and 3.86, the mean and variance are

$$\langle n \rangle = \frac{\mathcal{A}}{\kappa} \left(\frac{\mathcal{A} - \kappa}{\mathcal{B}}\right) + n^{th}, \quad (3.87)$$

$$\langle n^2 \rangle - \langle n \rangle^2 = \left(n^{th} + 1\right) \left(\langle n \rangle + \frac{\mathcal{A}}{\mathcal{B}}\right). \quad (3.88)$$

In the above analysis, the laser is working above threshold in which $\mathcal{A} > \kappa$.

The laser statistics can be classified according to Q as follows.

$$Q = \frac{\langle n^2 \rangle - \langle n \rangle^2}{\langle n \rangle} - 1 = n^{th} + \frac{\kappa \mathcal{A} (n^{th} + 1)}{\mathcal{A} (\mathcal{A} - \kappa) + n^{th} \kappa \mathcal{B}}. \quad (3.89)$$

In the above threshold regime, laser statistics are super-Poissonian ($Q > 0$) like thermal state. When the laser is working far from threshold $\mathcal{A} \gg \kappa$, the laser is in coherent state and the statistics become Poissonian $\langle n \rangle \rightarrow \frac{\mathcal{A}^2}{\mathcal{B}\kappa}$ and $Q \rightarrow 0$ as will be shown in the next section.

3.5.2 Far Above Threshold

Far above threshold, $\mathcal{A} \gg \mathcal{C}$, the saturation becomes large in which $\mathcal{B}\langle n \rangle / \mathcal{A} \gg 1$ so the unity term in the denominator on the right-hand side of Equation 3.76 can be ignored. This corresponds to canceling the \mathcal{A}/\mathcal{B} term from the numerator and denominator in Equations 3.77 and 3.78. In this case the distribution p_n becomes

$$p_n = p_0 \left(\frac{n^{th}}{n^{th} + 1} \right)^n \frac{\Gamma(\mathcal{A}^2/n^{th}\kappa\mathcal{B} + 1 + n)}{\Gamma(\mathcal{A}^2/n^{th}\kappa\mathcal{B} + 1) n!}, \quad (3.90)$$

with

$$p_0 = \left[\sum_0^{\infty} \left(\frac{n^{th}}{n^{th} + 1} \right)^n \frac{\Gamma(\mathcal{A}^2/n^{th}\kappa\mathcal{B} + 1 + n)}{\Gamma(\mathcal{A}^2/n^{th}\kappa\mathcal{B} + 1) n!} \right]^{-1}. \quad (3.91)$$

Equations 3.90 and 3.91 take simple form when thermal mean photon number $n^{th} = 0$. In this case, the distribution reduces to Poissonian

$$p_n = p_0 \frac{(\mathcal{A}^2/\kappa\mathcal{B})^n}{n!}, \quad (3.92)$$

$$p_0 = \left[\sum_0^{\infty} \frac{(\mathcal{A}^2/\kappa\mathcal{B})^n}{n!} \right]^{-1} = e^{-\mathcal{A}^2/\kappa\mathcal{B}}. \quad (3.93)$$

The mean and variance of the distribution are reduced form of the expressions in Equations 3.87 and 3.88 read

$$\langle n \rangle = \frac{\mathcal{A}^2}{\kappa\mathcal{B}}, \quad \langle n^2 \rangle - \langle n \rangle^2 = \frac{\mathcal{A}^2}{\kappa\mathcal{B}}. \quad (3.94)$$

Using Equation 3.94, the distribution far above threshold is

$$P_n = e^{-\langle n \rangle} \frac{\langle n \rangle^n}{n!}, \quad (3.95)$$

and $Q = 0$ as it would be expected.

3.5.3 Expansion of Nonlinear Terms

In this subsection, the role of linear and nonlinear terms in the gain part of the distribution equation p_n is discussed. Near threshold and for weak saturation, $n \frac{\mathcal{B}}{\mathcal{A}} < 1$, Equation 3.72 for the distribution function is expanded in terms of n and written as

$$\begin{aligned} \frac{\partial p_n}{\partial t} &= - (n+1) \mathcal{A} \sum_{m=0}^{\infty} \left(- (n+1) \frac{\mathcal{B}}{\mathcal{A}} \right)^m p_n + n \mathcal{A} \sum_{m=0}^{\infty} \left(- n \frac{\mathcal{B}}{\mathcal{A}} \right)^m p_{n-1} \\ &\quad - \kappa n \left[(n^{th} + 1) p_n - n^{th} p_{n-1} \right] + \kappa (n+1) \left[(n^{th} + 1) p_{n+1} - n^{th} p_n \right] \\ &= - (n+1) \mathcal{A} p_n + n \mathcal{A} p_{n-1} \quad \text{Linear approximation} \end{aligned} \quad (3.96a)$$

$$+ (n+1)^2 \mathcal{B} p_n - n^2 \mathcal{B} p_{n-1} \quad \text{First order nonlinearity} \quad (3.96b)$$

⋮

$$+ \underbrace{(-1)^{m+1} (n+1)^{m+1} \frac{\mathcal{B}^m}{\mathcal{A}^{m-1}} p_n + (-1)^m n^{m+1} \frac{\mathcal{B}^m}{\mathcal{A}^{m-1}} p_{n-1}}_{m\text{th-order approximation}} \quad (3.96c)$$

⋮

$$- \kappa n \left[(n^{th} + 1) p_n - n^{th} p_{n-1} \right] + \kappa (n+1) \left[(n^{th} + 1) p_{n+1} - n^{th} p_n \right]. \quad (3.96d)$$

In the following two subsections, the distribution is discussed in the linear and first nonlinear terms for zero thermal mean photon number.

3.5.4 Below Threshold: Linear Approximation

If $n^{th} = 0$ is assumed, and the expansion in Equation 3.96 is truncated and only the first linear term of the gain, Equation 3.96a is maintained, the detailed balance gives

$$p_n = \frac{\mathcal{A}}{\kappa} p_{n-1}. \quad (3.97)$$

The solution for Equation 3.75 exists only for $\mathcal{A} < \kappa$ (below threshold) and by iteration the distribution becomes

$$p_n = p_0 \left(\frac{\mathcal{A}}{\kappa} \right)^n. \quad (3.98)$$

The normalization p_0 is found from $\sum_{n=0}^{\infty} p_n = p_0 \left(1 - \frac{\mathcal{A}}{\kappa} \right)^{-1}$, and the distribution becomes

$$p_n = \left(1 - \frac{\mathcal{A}}{\kappa} \right) \left(\frac{\mathcal{A}}{\kappa} \right)^n. \quad (3.99)$$

Below threshold $\mathcal{A} < \kappa$, the laser is in thermal state and the statistics are of the black body radiation, Equation 2.83 with an effective temperature defined by $e^{-\hbar\omega/k_B T} = \frac{\mathcal{A}}{\kappa}$.

3.5.5 Lowest-Order Nonlinearity

From Equation 3.96, it can be seen that the terms associated with \mathcal{B} introduce the lowest order nonlinearity, Equation 3.96b. The question arises: How does this nonlinearity affect the photon number distribution? Would it remain to be thermal? To answer these questions, the detailed balance equation between level $n - 1$ and n is obtained

$$\left(\mathcal{A}n - \mathcal{B}n^2 \right) p_{n-1} - \kappa n p_n = 0. \quad (3.100)$$

By iteration

$$p_n = \left(\frac{\mathcal{A} - \mathcal{B}n}{\kappa} \right) p_{n-1} = p_0 \prod_{m=1}^n \frac{\mathcal{A} - \mathcal{B}m}{\kappa} = p_0 \left(\frac{\mathcal{B}}{\kappa} \right)^n \prod_{m=1}^n (\mathcal{A}/\mathcal{B} - m). \quad (3.101)$$

Note that Equation 3.101 is valid for $n \frac{\mathcal{B}}{\mathcal{A}} < 1$ and can be rewritten as

$$p_n = p_0 \left(\frac{\mathcal{B}}{\kappa} \right)^n \frac{\Gamma(\mathcal{A}/\mathcal{B})}{\Gamma(\mathcal{A}/\mathcal{B} - n)}, \quad (3.102)$$

and the normalization constant

$$p_0 = \left[\sum_{n=0}^{n_c} \left(\frac{\mathcal{B}}{\kappa} \right)^n \frac{\Gamma(\mathcal{A}/\mathcal{B})}{\Gamma(\mathcal{A}/\mathcal{B} - n)} \right]^{-1}, \quad (3.103)$$

where the cutoff photon number $n \leq n_c = \mathcal{A}/\mathcal{B}$. The cutoff is the largest photon number allowed in this regime determined by the laser parameters: the gain, saturation, and loss. The photon statistics of the laser are not Poissonian, Equation 3.95, as would be expected for a coherent state. This shows that the consequence of coherent in laser is due to higher order nonlinearities.

3.6 Laser Spectrum and Linewidth

The fluctuations have to parts; fluctuations in intensity or the number of photons and fluctuations in the phase of the laser field. The fluctuations in the phase lead to widening the finite linewidth of the laser spectrum. While the photon number distribution of the laser is associated with the diagonal elements of the density matrix, the off-diagonal elements of the density matrix are associated with the coherence or the phase. The calculation of the linewidth is not an easy task; it requires the calculation of the Fourier transform of $G^{(1)}$, Equation 2.108. Calculation of $G^{(1)}$ requires evaluation of a two-time average which needs a solution of the full density matrix, Equation 3.71, and use of the regression theorem (Carmichael, 1993). In this section, the main simple result of laser linewidth is present.

According to the regression theorem (which is satisfied in the Markovian approximation), the two-time average in $G^{(1)}$ is reduced to a single time average of the field $\langle E^{(+)}(t) \rangle$. The field of a single-mode laser of frequency ν and amplitude E_0 and its average are

$$\hat{E}^{(+)}(t) = E_0 \hat{a} e^{-i\nu t}, \quad (3.104)$$

$$\langle \hat{E}^{(+)}(t) \rangle = E_0 e^{-i\nu t} \sum_n \langle n | \hat{a} \hat{\rho} | n \rangle = E_0 e^{-i\nu t} \sum_n \sqrt{n+1} \rho_{n+1,n}. \quad (3.105)$$

Equation 3.105 shows that the decay in the off-diagonal elements of the density matrix (decoherence) yields laser linewidth. So, evaluating the off-diagonal elements $\rho_{n+1,n}$, determines the laser linewidth. Since it is difficult to obtain analytic solution for the density matrix, various approximations are used. One approach is to use P -representation and solve Fokker-Planck equation by calculating the diffusion coefficient. Another method using an ansatz approximation after some arrangement on the equation of the off-diagonal elements to allow using the detailed balance (Scully & Zubairy, 1997). The Lorentzian spectrum $S(\omega)$ that gives the laser linewidth D is

$$S(\omega) \propto \text{Re} \int_0^{\infty} d\tau e^{i\omega\tau} \langle E^{(-)}(t) E^{(+)}(t + \tau) \rangle \propto \frac{1}{(\omega - \nu)^2 + D^2}, \quad (3.106)$$

$$D \simeq \frac{\mathcal{A} + \kappa}{\langle n \rangle}. \quad (3.107)$$

The result shows that the damping κ and the spontaneous emission associated coefficient \mathcal{A} increase the laser linewidth.

CHAPTER 4: TWO-PHOTON LASER WITH SELF-KERR EFFECT

4.1 Introduction

The quantum theory of TPL [for review, see Gauthier (2003) and Scully & Zubairy (1997)] has been studied many years ago and laser statistics have attracted a great deal of attention. The radiation field has different classical and nonclassical statistical properties and the two-photon process is in the heart of nonlinear and quantum optics (Walther et al., 2006; Reid & Walls, 1986; Kozirowski, 1981; Loudon, 1980). The nonclassical properties like squeezing, antibunching and sub-Poissonian can be achieved through nonlinear processes (Brambilla et al., 1992). Entangled photons can be produced through laser-driven schemes involving two-photon emissions and double Raman excitations (Ooi, 2007). The field distribution function obeys the super-Poissonian for thermal light, Poissonian for coherent light, and sub-Poissonian for squeezed light (Fabre, 1992; Kimble, 1992). It is desirable to produce nonclassical properties of light (Loudon, 1980; Walther et al., 2006) for experimental applications where precise measurements are required like gravitational wave detection. In photodetection experiments, one difficulty is to overcome the noise in the light source which limits the measurement accuracy. Thus photon fluctuations reduction is important (Orszag & Retamal, 1991; Orszag, 2016). It has been shown that the pumping statistics (Orszag & Retamal, 1991) and detuning have significant effects on the statistical properties of the field and can be optimized to reduce the photon fluctuations (Bay et al., 1995). There are many studies on the statistical properties for one-photon, two-photon, and multi-photon lasers (McNeil & Walls, 1975a,b), correspondingly, from one mode to multimode cases (Schrade et al., 1993; Ereemeev et al., 2011). Two-photon transitions, related to the generation of squeezed light (Every, 1975; Knight & Pegg, 1982), and generation of the widely used entangled photon pairs by parametric down-conversion, are more interesting than the usual

one-photon transitions (Dodonov & Mizrahi, 1997a,b). Photon statistics have been studied in various systems, including single beam (Simaan & Loudon, 1975b, 1978) and double beam (Simaan & Loudon, 1975a), two-photon absorption and stimulated Raman processes (Simaan, 1975). An extensive theory of TPL has been developed and studied for two-level systems (Gauthier, 2003), up to saturation level (Bandilla & Voigt, 1982; Wang & Haken, 1984a; Cheng & Haken, 1988). Exact solutions based on P-representation have been found (Kryuchkyan et al., 1996). In the case of lasing far above the threshold, researchers have obtained analytical expressions for the photon statistics, particularly the photon numbers, moments and correlations of higher orders (Dodonov et al., 1989). However, for the simple degenerate 3-level cascade scheme, analytical expressions of the photon statistics remain challenging and non-trivial (Bay et al., 1995). The two-photon process is the simplest form of nonlinearity and introducing another nonlinearity to the two-photon atom-field interaction enriches the nonclassical properties of the system. One simple, but interesting, form of this nonlinearity is the Kerr-effect which has paid much attention since the laser invention (Yurke & Stoler, 1986; Bužek & Jex, 1990; Semiao et al., 2009; Faghihi et al., 2013; Singh & Gilhare, 2016b; Ghorbani et al., 2017). A recent study for two modes cavity-field non-dissipative system in Kerr-like medium is investigated (Singh & Ooi, 2018). These studies give us the motivation to study the effect of the nonlinearity of Kerr-type on the dynamics and nonclassicality of the TPL.

In this chapter, the statistical properties of a nondegenerate TPL in Kerr-like medium in a dissipative cavity are studied and analyze the effects of injection rate, two-photon detuning, and Kerr parameters on the statistical properties and distribution function of two modes of lasing photons. Exact nonlinear quantum theory of laser for the system of N two-level atoms in a doubly resonant cavity is used. The use of effective two-level Hamiltonian to represent the actual three-level scheme is realistic and acceptable under specific conditions (when

the laser field and the intermediate level are far off-resonance in which one can drop the slow variation of this low populated level) (Bay et al., 1995; Boone & Swain, 1989a,b, 1990; Singh et al., 2012). The density matrix master equation of the system was derived using the Scully-Lamb approach. Equations of the photon statistics are derived and an approximate form of equation was presented. From the approximate equation of the photon statistics, a general equation of the moments was given and the first moments' expressions are derived. Analytic expressions for mean photon numbers, $G^{(2)}$, and Q are obtained in elegant forms. Two expressions for the mean photon-number are obtained. One of these expressions is more reliable over a long range of the parameters of the system. Moreover, for a special case, photon statistics are calculated using the generating function method and a general formula for the moments is derived. The exact full density matrix was solved numerically using MATLAB. A justification of the analytic solution by making a comparison between the analytic results and those of the exact solution is presented. Nonclassicality of the field such as squeezing, sub-Poissonian statistics, and violation of the CSI is documented. A discussion of the numerical computations is given.

4.2 Model and Laser Master Equation

In this chapter and the following chapters, and to lower the cost of notation by having hats on quantum operators, the hat will be dropped and it will be understood from the context that they are operators not classical c -numbers. For example, the creation and annihilation operators \hat{a}^\dagger and \hat{a} become a^\dagger and a ; therefore, $\langle \hat{n} \rangle = \langle n \rangle$. The model in this study is an open system of a collection of two-level atoms placed in a cavity. The ensemble of noninteracting identical effective two-level atoms interacts with a two-mode cavity field. The atoms have excited level $|a\rangle$ and ground level $|b\rangle$ of with frequencies ω_a and ω_b , respectively. The atom transition frequency $\omega = \omega_a - \omega_b$ and the two-mode cavity field have frequencies, ν_1 and ν_2 . The subsystems (atoms and cavity field) are coupled

through the coupling constants g_1, g_2 , for simplicity, taken to be real and equal to g which is acceptable in most cases. In addition to that, the two-mode cavity field has nonlinear interaction with the medium (the atoms in the cavity) through the parameters χ_1 and χ_2 , which are proportional to the third-order susceptibility of the medium $\chi^{(3)}$ (optical Kerr effect). The cavity field modes interact with the environment (mode of the universe). The effective Hamiltonian of the system in the dipole (Parker, 2005, p. 719; Puri, 2001, p. 137) and rotating wave approximation (Parker, 2005, p. 489; Puri, 2001, p. 140) is the sum of the free Hamiltonian H_0 and the interaction Hamiltonian H_I and has the form

$$H = H_0 + H_I, \quad (4.1a)$$

where

$$H_0 = \frac{\hbar\omega}{2} \sum_j \sigma_j^z + \hbar \sum_{f=1,2} \left(v_f a_f^\dagger a_f + \chi_f a_f^{\dagger 2} a_f^2 \right), \quad (4.1b)$$

$$H_I = \sum_j \hbar g \left(\sigma_j^+ a_1 a_2 + \sigma_j^- a_1^\dagger a_2^\dagger \right), \quad (4.1c)$$

where $a_f^\dagger(a_f)$, $f = 1, 2$ are creation (annihilation) operator of the field in mode f and σ_j^z, σ_j^\pm are the j^{th} - atom transition operators with

$$\sigma_j^+ = |a_j\rangle \langle b_j|, \quad (4.2a)$$

$$\sigma_j^- = \left(\sigma_j^+ \right)^\dagger = |b_j\rangle \langle a_j|, \quad (4.2b)$$

$$\sigma_j^z = \left[\sigma_j^+, \sigma_j^- \right]. \quad (4.2c)$$

Without the Kerr terms, the model is a two-mode version of the Jaynes-Cummings model (Jaynes & Cummings, 1963; Shore & Knight, 1993). Using the unitary transformation $U_0 = e^{-iH_0 t/\hbar}$, the Hamiltonian, Equation 4.1a, in the interaction picture, after setting the

cross-Kerr parameter $\chi = 0$ and the IDC, $F = 1$ (discussed in the next chapter) takes the form (see Appendix B for the derivation)

$$V = U_0^\dagger H_I U_0 = \sum_j V_j, \quad (4.3a)$$

$$V_j = \hbar g e^{-i2\left(\frac{\Delta}{2} + \chi_1 a_1^\dagger a_1 + \chi_2 a_2^\dagger a_2\right)t} a_1 a_2 \sigma_j^+ + \text{h.c.} \quad (4.3b)$$

where V_j is the Hamiltonian of a single atom, and the two-photon detuning is

$$\Delta = \nu_1 + \nu_2 - \omega. \quad (4.4)$$

The dynamics of the TPL can be described completely by knowing the reduced density matrix of the field $\rho = \text{Tr}_{\text{atoms}} \rho_t$, which can be obtained by tracing over the atomic degrees of freedom of the total (atom+field) density matrix ρ_t of the system. The dynamics of the reduced density matrix ρ is governed by the master equation

$$\frac{d}{dt} \rho = \frac{1}{i\hbar} \text{Tr}_{\text{atoms}} [V, \rho_t] + \sum_{f=1,2} \mathcal{L}_f \rho. \quad (4.5)$$

The first and second terms on the right side of Equation 4.5 represent the gain and loss contributions to the reduced density matrix ρ respectively. The super-operator \mathcal{L}_f in the loss (second term) part is obtained in the standard method of a system in a reservoir.

For a thermal field, the loss term takes the Lindblad form given in Equation 3.41 (Sargent III et al., 1974; Scully & Zubairy, 1997)

$$\begin{aligned} \mathcal{L}_f \rho = & -\frac{\kappa_f}{2} \bar{n}_f^{th} \left(a_f a_f^\dagger \rho - 2a_f^\dagger \rho a_f + \rho a_f a_f^\dagger \right) \\ & -\frac{\kappa_f}{2} \left(\bar{n}_f^{th} + 1 \right) \left(a_f^\dagger a_f \rho - 2a_f \rho a_f^\dagger + \rho a_f^\dagger a_f \right), \end{aligned} \quad (4.6)$$

where κ_f is the decay constant of mode $f = 1, 2$ of the field, and \bar{n}_f^{th} is the mean number

of quanta in the thermal reservoir. The hard work, now, in obtaining the master equation of the density matrix resides in calculating the gain or lasing part represented by the trace over the atomic variables in the first term of Equation 4.5. Fortunately, the goal is reached easily using the Scully-Lamb method (Scully & Lamb, 1967; Sargent III et al., 1974), in which the calculations reduced to finding the density matrix of one atom then doing a sum (integral). The calculation of the field density matrix ρ for one atom in a cavity is straight forward; using the evolution operator (for a single atom), or obtaining the wave function by solving Schrodinger equation. It is assumed that the atoms are initially prepared in a coherent superposition of the ground state $|a\rangle$ and the excited state $|b\rangle$, and the atoms and the field are uncoupled so the initial one-atom density matrix of the system is the direct product of the each subsystem

$$\rho_t(t_0) = \rho^{atom}(t_0) \otimes \rho(t_0) = \begin{pmatrix} \rho_{aa}(t_0)\rho(t_0) & \rho_{ab}(t_0)\rho(t_0) \\ \rho_{ba}(t_0)\rho(t_0) & \rho_{bb}(t_0)\rho(t_0) \end{pmatrix}. \quad (4.7)$$

According to the Scully-Lamb laser theory, the gain part of the field density matrix is calculated as follows

$$\dot{\rho}_{n_1 n_2; n'_1 n'_2}^{(gain)} = r_a \int_0^\infty \gamma d\tau e^{-\gamma\tau} \left[\sum_{x=a,b} \rho_{x n_1 n_2; x n'_1 n'_2}(t + \tau) - \rho_{n_1 n_2; n'_1 n'_2}(t) \right], \quad (4.8)$$

where γ is the atomic decay constant, r_a rate of atomic injection. In this theory, it is assumed that the effect on an atom by other atoms in the medium comes only through the laser field, i.e. they are independent, and the cavity decay time κ^{-1} is much longer than the atomic lifetime γ^{-1} . The time τ is assumed to be long compared with an atomic lifetime γ^{-1} , but short compared to the time characterizing the growth or decay of the laser radiation κ^{-1} . So in this coarse-grained time rate of change (Phoenix & Knight, 1988) for the gain part in the field operator $\dot{\rho}^{gain}$ is readily found from Equation 4.8 where the condition $\gamma \gg \kappa_1, \kappa_2$,

i.e. the laser field does not change appreciably on a time scale of an atomic lifetime, and the approximation $\rho(t_0) \approx \rho(t)$ for the field operator is made. To this end, it is required to obtain the single-atom and field density matrix, ρ .

The single-atom density matrix can be obtained in straight forward and Schrodinger equation will be used to obtain it. To achieve this, the elements $\rho_{\alpha n_1 n_2; \alpha' n'_1 n'_2}$, $\rho_{b n_1 n_2; b n'_1 n'_2}$ are evaluated. These elements are defined by

$$\rho_{\alpha n_1 n_2 \beta n'_1 n'_2}(t) = C_{\alpha n_1 n_2}(t) C_{\beta n'_1 n'_2}^*(t); \alpha, \beta = a, b. \quad (4.9)$$

The coefficients $C_{\alpha n_1 n_2}(t)$ are the probability amplitude of the wave function that can be obtained from solution of Schrödinger equation

$$\frac{d}{dt} |\psi\rangle = -\frac{i}{\hbar} V_j |\psi\rangle. \quad (4.10)$$

. The wave function is the superposition of the two states $|a n_1, n_2\rangle$ (atom is in the excited state $|a\rangle$ and the field in $|n_1, n_2\rangle$ state) and $|b n_1, n_2\rangle$ (atom is in the ground state $|b\rangle$ and the field in $|b n_1, n_2\rangle$ state).

$$|\psi\rangle = \sum_{n_1 n_2} [C_{a n_1 n_2} |a n_1, n_2\rangle + C_{b n_1 n_2} |b n_1, n_2\rangle]. \quad (4.11)$$

A detailed derivation of the density matrix elements $\rho_{\alpha n_1 n_2 \beta n'_1 n'_2}(t)$ is given in Appendix C. By substituting Equations C.26 and C.27 from Appendix C into Equation 4.8, employing the argument above, and performing the integration, the gain part of the laser master equation based on Scully-Lamb theory is obtained (detailed derivation is presented in Appendix D). By taking the elements of the dissipation part, Equation 4.6 at zero-temperature, and adding it to the gain part of the maser equation given by Equation D.30, the full master

equation of the field is found to be

$$\begin{aligned}
\frac{d}{dt}\rho_{n_1 n_2; n'_1 n'_2} = & -r_a \left(\rho_{aa} L_{n_1+1 n_2+1; n'_1+1 n'_2+1} + \rho_{bb} L_{n_1 n_2; n'_1 n'_2}^* \right) \rho_{n_1 n_2; n'_1 n'_2} \\
& + e^{2i(D_{n_1 n_2} - D_{n'_1 n'_2})\gamma t} r_a \rho_{aa} S_{n_1 n_2; n'_1 n'_2}^* \rho_{n_1-1 n_2-1; n'_1-1 n'_2-1} \\
& + e^{-2i(D_{n_1+1 n_2+1} - D_{n'_1+1 n'_2+1})\gamma t} r_a \rho_{bb} S_{n_1+1 n_2+1; n'_1+1 n'_2+1} \rho_{n_1+1 n_2+1; n'_1+1 n'_2+1} \\
& + i e^{2i D_{n'_1+1 n'_2+1} \gamma t} r_a \rho_{ab} M_{n_1+1 n_2+1; n'_1+1 n'_2+1} \rho_{n_1 n_2; n'_1+1 n'_2+1} \\
& - i e^{2i D_{n_1 n_2} \gamma t} r_a \rho_{ab} K_{n_1 n_2; n'_1 n'_2}^* \rho_{n_1-1 n_2-1; n'_1 n'_2} \\
& - i e^{-2i D_{n_1+1 n_2+1} \gamma t} r_a \rho_{ba} K_{n_1+1 n_2+1; n'_1+1 n'_2+1} \rho_{n_1+1 n_2+1; n'_1 n'_2} \\
& + i e^{-2i D_{n'_1 n'_2} \gamma t} r_a \rho_{ba} M_{n_1 n_2; n'_1 n'_2}^* \rho_{n_1 n_2; n'_1-1 n'_2-1} \\
& + \kappa_1 \sqrt{(n_1+1)(n'_1+1)} \rho_{n_1+1, n_2; n'_1+1, n'_2} \\
& + \kappa_2 \sqrt{(n_2+1)(n'_2+1)} \rho_{n_1, n_2+1; n'_1, n'_2+1} \\
& - \frac{1}{2} \left[\kappa_1 (n_1 + n'_1) + \kappa_2 (n_2 + n'_2) \right], \tag{4.12}
\end{aligned}$$

where

$$K_{n_1 n_2; n'_1 n'_2} = \frac{B_{n_1 n_2}}{R_{n_1 n_2; n'_1 n'_2}} \left(W_{n_1 n_2; n'_1 n'_2}^{+-} - i 2 D_{n'_1 n'_2} \lambda_{n_1 n_2; n'_1 n'_2} \right), \tag{4.13}$$

$$L_{n_1 n_2; n'_1 n'_2} = 1 - \frac{1}{R_{n_1 n_2; n'_1 n'_2}} \left[\begin{array}{l} \lambda_{n_1 n_2; n'_1 n'_2} \left(W_{n_1 n_2; n'_1 n'_2}^{++} + 2 D_{n_1 n_2} D_{n'_1 n'_2} \right) \\ + i D_{n_1 n_2} W_{n_1 n_2; n'_1 n'_2}^{+-} - i D_{n'_1 n'_2} W_{n_1 n_2; n'_1 n'_2}^{-+} \end{array} \right], \tag{4.14}$$

$$M_{n_1 n_2; n'_1 n'_2} = \frac{B_{n'_1 n'_2}}{R_{n_1 n_2; n'_1 n'_2}} \left(W_{n_1 n_2; n'_1 n'_2}^{-+} + i 2 D_{n_1 n_2} \lambda_{n_1 n_2; n'_1 n'_2} \right), \tag{4.15}$$

$$S_{n_1 n_2; n'_1 n'_2} = \frac{2 B_{n_1 n_2} B_{n'_1 n'_2} \lambda_{n_1 n_2; n'_1 n'_2}}{R_{n_1 n_2; n'_1 n'_2}}, \tag{4.16}$$

and

$$\lambda_{n_1 n_2; n'_1 n'_2} = 1 + i \left(D_{n_1 n_2} - D_{n'_1 n'_2} \right), \quad (4.17)$$

$$R_{n_1 n_2; n'_1 n'_2} = W_{n_1 n_2; n'_1 n'_2}^{++2} - 4\Omega_{n_1 n_2}^2 \Omega_{n'_1 n'_2}^2, \quad (4.18)$$

$$W_{n_1 n_2; n'_1 n'_2}^{\alpha\beta} = \lambda_{n_1 n_2; n'_1 n'_2}^2 + \alpha \Omega_{n_1 n_2}^2 + \beta \Omega_{n'_1 n'_2}^2; \alpha, \beta = \pm 1, \quad (4.19)$$

with

$$D_{n_1 n_2} = \gamma^{-1} \left[\frac{1}{2} \Delta + \chi_1 (n_1 - 1) + \chi_2 (n_2 - 1) \right], \quad (4.20)$$

$$B_{n_1 n_2} = \gamma^{-1} g \sqrt{n_1 n_2}, \quad (4.21)$$

$$\Omega_{n_1 n_2} = \sqrt{D_{n_1 n_2}^2 + B_{n_1 n_2}^2}. \quad (4.22)$$

The oscillating nature in the density matrix elements Equation 4.12 of the system appears clearly in the coefficients. The source of the oscillation comes from $D_{n_1 n_2}$ which contains the detuning and the nonlinearity in the system, i.e. the Kerr term in the Hamiltonian. The Hamiltonian in the interaction picture Equation 4.3b manifests this oscillation through the strength of the cavity field and the optical Kerr effect. The Hamiltonian in the interaction picture gives the dependence of the coupling on photon numbers or intensity and time. This kind of interaction is the cause of many effects as was mentioned above. The explanation of these effects (and others that may occur) requires further information from the analysis of the density matrix elements.

The solution of the density matrix Equation 4.12 contains all the information needed to describe the field in the cavity completely. Unfortunately, there is no solution in a closed form for the density matrix, Equation 4.12, even in the special case for the diagonal elements, as will be seen later.

To gain some understanding of the dynamics of the system considered, the photon

statistics, $P_{n_1 n_2} = \rho_{n_1 n_2; n_1 n_2}$, will be studied. The computation of $P_{n_1 n_2}$ function is much easier than the total density matrix though some information is lost that can be obtained from the off-diagonal terms that disappear in the distribution function.

4.3 The Laser Rate Equation

The time evolution of the diagonal elements of the density matrix from Equation 4.12 reads

$$\begin{aligned}
\dot{P}_{n_1 n_2} = & -r_a (\rho_{aa} L_{n_1+1 n_2+1} + \rho_{bb} L_{n_1 n_2}) P_{n_1 n_2} \\
& + r_a (\rho_{aa} L_{n_1 n_2} P_{n_1-1 n_2-1} + r_a \rho_{bb} L_{n_1+1 n_2+1} P_{n_1+1 n_2+1}) \\
& - i r_a (\rho_{ba} K_{n_1+1 n_2+1} \rho_{n_1+1 n_2+1; n_1 n_2} e^{-i2D_{n_1+1 n_2+1} \gamma t} + \text{h.c.}) \\
& + i r_a (\rho_{ba} K_{n_1 n_2} \rho_{n_1 n_2; n_1-1 n_2-1} e^{-i2D_{n_1 n_2} \gamma t} + \text{h.c.}) \\
& + \kappa_1 (n_1 + 1) P_{n_1+1, n_2} + \kappa_2 (n_2 + 1) P_{n_1, n_2+1} - \kappa_1 n_1 P_{n_1 n_2} - \kappa_2 n_2 P_{n_1 n_2},
\end{aligned} \tag{4.23}$$

with population and coherence coupling strength coefficients

$$K_{n_1, n_2} = \frac{\gamma^{-1} g \sqrt{n_1 n_2} [1 + i2\gamma^{-1} (\Delta/2 + \chi_1 (n_1 - 1) + \chi_2 (n_2 - 1))]}{1 + 4\gamma^{-2} (\Delta/2 + \chi_1 (n_1 - 1) + \chi_2 (n_2 - 1))^2 + 4\gamma^{-2} g^2 n_1 n_2}, \tag{4.24a}$$

$$L_{n_1, n_2} = \frac{2\gamma^{-2} g^2 n_1 n_2}{1 + 4\gamma^{-2} (\Delta/2 + \chi_1 (n_1 - 1) + \chi_2 (n_2 - 1))^2 + 4\gamma^{-2} g^2 n_1 n_2}. \tag{4.24b}$$

Unfortunately, it is difficult to obtain an analytic solution in a closed form for the photon-statistics function, $P_{n_1 n_2}$ from Equation 4.23 even in the steady state, $\dot{P}_{n_1 n_2} = 0$ case. The difficulty comes from the absence of detailed balance where the element P_{n_1, n_2} is coupled to other elements such that the values of n_1, n_2 do not change by the same amount (as the elements of the first line do). The terms that cause this difficulty are the coherence terms (the third and fourth lines) and the first two terms of the fourth line where the absorption is one photon in each mode. For this reason, Equation 4.23 has to be solved numerically. However, an analytic approximation for the solution could be found under reasonable

conditions as will be shown in the next section. To have some understanding of Equation

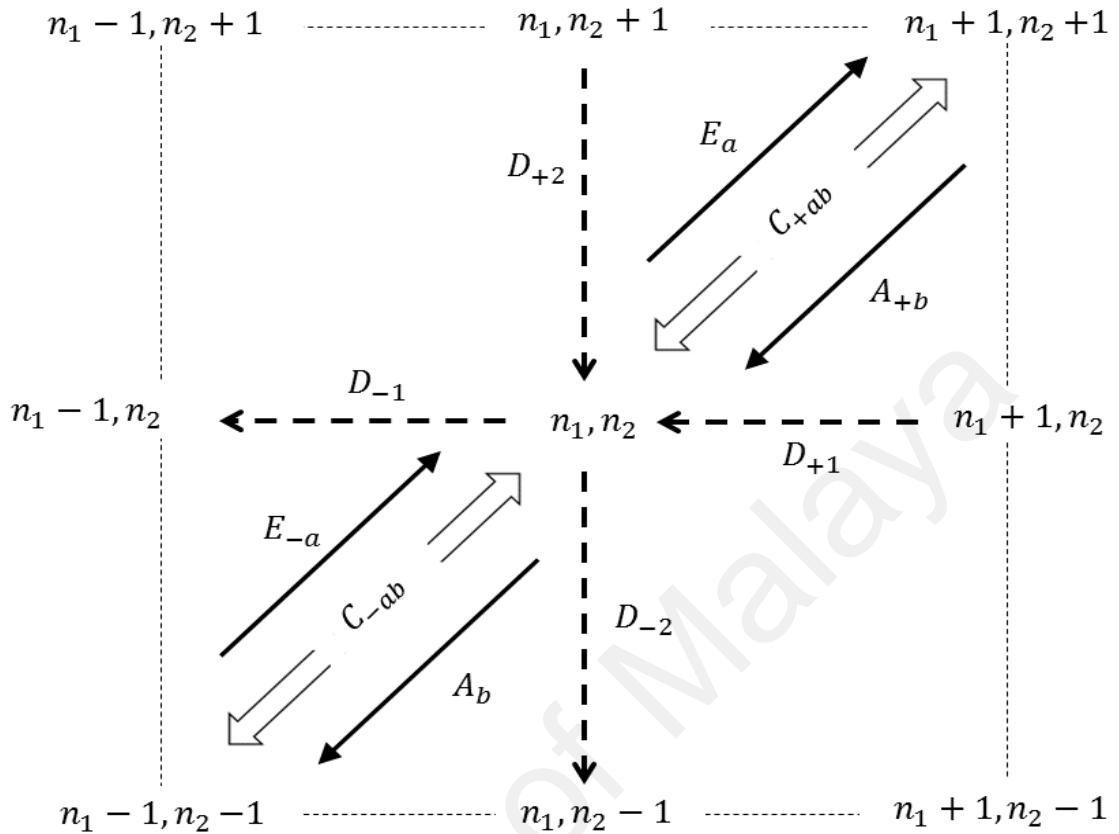


Figure 4.1: Energy levels of photon number states and probability flow corresponding to the diagonal elements of the density matrix, Equation (4.23).

4.23, one should interpret its various elements. The rate of probability of the state that there are n_1 photons of the first mode and n_2 photons of the second mode in the cavity, $\dot{P}_{n_1 n_2}$, consists of twelve terms. The transitions and mechanisms of these terms are depicted in Figure 4.1. The eight terms on the first, second, third, and fourth lines are the lasing terms; contributions of populations and coherence. The contribution from populations comes from the first four terms on the first and second lines. The first (second) term represents the two-photon emission (absorption) one in each mode by the lasing media to state of $|n_1 + 1, n_2 + 1\rangle$ ($|n_1 - 1, n_2 - 1\rangle$) represented by E_a (E_{-a}) on the figure. The third (fourth) term represents the two-photon emission (absorption) one in each mode by the lasing media from state $|n_1 - 1, n_2 - 1\rangle$ ($|n_1 + 1, n_2 + 1\rangle$) represented by E_{-a} (A_{+b}) on the figure.

The four terms on the third and fourth lines are the coherence contribution. The fifth and sixth terms (C_{+ab} on the figure) are the coherence of the states $|n_1, n_2\rangle$ and $|n_1 + 1, n_2 + 1\rangle$ of the field and ρ_{ba} of the atom (as being in a superposition of its ground and excited states). The same can be said about the seventh and eighth terms (C_{-ab} on the figure) as coherence between states $|n_1, n_2\rangle$ and $|n_1 - 1, n_2 - 1\rangle$. The last four terms on the last line represent the loss due to interaction with the environment stimulated by one-photon absorption. The first (second) term on the last line is the loss of a single photon (absorbed by the cavity walls) of the first (second) mode in the state $|n_1 + 1, n_2\rangle$ ($|n_1, n_2 + 1\rangle$) where the field state changes to $|n_1, n_2\rangle$ (increasing its population), represented by D_{+1} (D_{+2}) in the figure. The third and fourth terms are the loss of population in $|n_1, n_2\rangle$ state for the first and second modes (D_{-1} and D_{-2}). This section is concluded by approximating the coherence part of Equation 4.23 in terms of the populations. This approximation will allow us to derive analytic expressions for the moments to simplify the study of photons statistics. Equation of the density matrix element $\dot{\rho}_{n_1-1, n_2-1; n_1, n_2}$ can be easily obtained from the density matrix equation Equation 4.12 by shifting indices. By neglecting the small contribution of coherence terms compared to population contributions in the resulting equation, an adequate approximation for $\dot{\rho}_{n_1-1, n_2-1; n_1, n_2}$ in terms of populations takes the form

$$\begin{aligned}
\dot{\rho}_{n_1-1, n_2-1; n_1, n_2} \approx & - \left(r_a \rho_{aa} L_{n_1 n_2; n_1+1, n_2+1} + r_a \rho_{bb} L_{n_1-1, n_2-1; n_1, n_2}^* \right) \rho_{n_1-1, n_2-1; n_1, n_2} \\
& - \sum_{j=1,2} \kappa_j \left(n_j - \frac{1}{2} \right) \rho_{n_1-1, n_2-1; n_1, n_2} - i r_a \rho_{ba} e^{-i2D_{n_1 n_2} \gamma t} \\
& \times \left(K_{n_1 n_2; n_1+1, n_2+1} \rho_{n_1 n_2; n_1, n_2} - M_{n_1-1, n_2-1; n_1, n_2}^* \rho_{n_1-1, n_2-1; n_1-1, n_2-1} \right).
\end{aligned} \tag{4.25}$$

In the vicinity of steady-state, it can be written as

$$\rho_{n_1-1n_2-1;n_1n_2} \approx \frac{i\rho_{ba}e^{-i2D_{n_1n_2}\gamma t}}{\Gamma_{n_1-1n_2-1;n_1n_2}} \left(M_{n_1-1n_2-1;n_1n_2}^* P_{n_1-1n_2-1} - K_{n_1n_2;n_1+1n_2+1} P_{n_1n_2} \right), \quad (4.26)$$

where

$$\Gamma_{n_1-1n_2-1;n_1n_2} = \rho_{aa}L_{n_1n_2;n_1+1n_2+1} + \rho_{bb}L_{n_1-1n_2-1;n_1n_2}^* + \frac{1}{r_a} \sum_{j=1,2} \kappa_j \left(n_j - \frac{1}{2} \right). \quad (4.27)$$

This expression tells us that the coherence between two states is approximated by the weighted difference of populations of these states. It also shows the rule of detuning and Kerr parameters in the oscillating nature of the coherence. Making use of Equation 4.26 in Equation 4.23, it gives the approximated rate equation

$$\begin{aligned} \dot{P}_{n_1n_2} = & - \left(r_a \rho_{aa} L_{n_1+1,n_2+1} + r_a \rho_{bb} L_{n_1,n_2} + 2r_a |\rho_{ab}|^2 M_{n_1n_2}^+ \right) P_{n_1,n_2} \\ & + r_a \left[\rho_{aa} L_{n_1,n_2} + |\rho_{ab}|^2 \left(M_{n_1-1n_2-1}^+ + M_{n_1-1n_2-1}^- \right) \right] P_{n_1-1,n_2-1} \\ & + r_a \left[\rho_{bb} L_{n_1+1,n_2+1} + |\rho_{ab}|^2 \left(M_{n_1+1n_2+1}^+ - M_{n_1+1n_2+1}^- \right) \right] P_{n_1+1n_2+1} \\ & + \kappa_1 (n_1 + 1) P_{n_1+1n_2} + \kappa_2 (n_2 + 1) P_{n_1n_2+1} - (\kappa_1 n_1 + \kappa_2 n_2) P_{n_1,n_2}, \end{aligned} \quad (4.28)$$

with

$$M_{n_1n_2}^\pm = \text{Re} \left(\frac{K_{n_1+1n_2+1}^* K_{n_1+1n_2+1;n_1n_2}}{\Gamma_{n_1n_2;n_1+1n_2+1}} \pm \frac{K_{n_1n_2}^* K_{n_1n_2;n_1+1n_2+1}}{\Gamma_{n_1-1n_2-1;n_1n_2}} \right). \quad (4.29)$$

This is the main result in this section. This formula relates not only the diagonal elements of the density matrix, but it includes the coherence contributions. The statistics rate equation, Equation 4.23, is still hard to solve in this form, but if few assumptions are made, analytic approximate solution could be found (e.g., a simple solution could be obtained for the case $\rho_{bb} = 0$). From Equation 4.28 an analytic approximation for the moments will be derived.

Moments and $G^{(2)}$ will be the subjects of the next section.

4.4 Characterization of the Cavity Field

To characterize and study the nonclassical properties of the field, four measures are used. The $G^{(2)}$, CSI, Q , and the photon number fluctuations as was discussed in Chapter 2. More insights into the characteristics of a quantum electromagnetic field can be drawn from the study of quantum coherence (Mandel & Wolf, 1995). It is interesting to explore the effect of Kerr nonlinearity on the nonclassicality of the light through the study of these measures. For this goal, the first moments are derived using Equation 4.28.

From Equation 4.28, analytic calculations of photon statistics and the moments under specific conditions are presented. The approximation, within this model, that is presented is more effective over others presented in the literature (Zubairy, 1982; Bay et al., 1995), for example. The effectiveness is in the sense it takes into account the coherence and differences in photon number of adjacent states to the second order (i.e. $L_{n+1} - L_n = l_1 n^{-1} + l_2 n^{-2} + O(n^{-3})$). The first few moments are easily found by multiplying Equation 4.28 by n_j , n_j^2 , and $n_1 n_2$ then doing the sum. After making the right shift in the indices, the moments are found to be

$$\begin{aligned} \frac{d}{dt} \langle n_j \rangle = & -\kappa_j \langle n_j \rangle + r_a \rho_{aa} \langle L_{n_1+1, n_2+1} \rangle - r_a \rho_{bb} \langle L_{n_1, n_2} \rangle \\ & + 2r_a |\rho_{ab}|^2 \langle M_{n_1 n_2}^- \rangle, \end{aligned} \quad (4.30a)$$

$$\begin{aligned} \frac{d}{dt} \langle n_j^2 \rangle = & -2\kappa_j \langle n_j^2 \rangle + \kappa_j \langle n_j \rangle + 2r_a |\rho_{ab}|^2 (\langle M_{n_1 n_2}^+ \rangle + 2\langle n_j M_{n_1 n_2}^- \rangle) \\ & + r_a \rho_{aa} \langle (2n_j + 1) L_{n_1+1, n_2+1} \rangle - r_a \rho_{bb} \langle (2n_j - 1) L_{n_1, n_2} \rangle, \end{aligned} \quad (4.30b)$$

$$\begin{aligned} \frac{d}{dt} \langle n_1 n_2 \rangle = & -(\kappa_1 + \kappa_2) \langle n_1 n_2 \rangle + 2r_a |\rho_{ab}|^2 (\langle M_{n_1 n_2}^+ \rangle + \langle (n_1 + n_2) M_{n_1 n_2}^- \rangle) \\ & + r_a \rho_{aa} \langle (n_1 + n_2 + 1) L_{n_1+1, n_2+1} \rangle - r_a \rho_{bb} \langle (n_1 + n_2 - 1) L_{n_1, n_2} \rangle. \end{aligned} \quad (4.30c)$$

It is not easy to solve this system unless a few simplifications are made. The difficulty is in obtaining the averages such as $\langle L_{n_1, n_2} \rangle$ and $\langle M_{n_1, n_2}^\pm \rangle$. In principle, the system could be integrated if one decorrelates these averages to the first order such that the system of equations is closed. This process is still complicated since it consists of a system of coupled nonlinear equations, but a simpler procedure with several additional simplifications are adopted.

Above threshold, the averages $\langle L_{n_1, n_2} \rangle$ and $\langle M_{n_1, n_2}^\pm \rangle$ are slowly varying functions (asymptotically). Taking this into account, their values can be approximated by their steady-state values $\langle L_{n_1, n_2} \rangle \approx \langle L_{n_1, n_2} \rangle_{ss}$, $\langle M_{n_1, n_2}^\pm \rangle \approx \langle M_{n_1, n_2}^\pm \rangle_{ss}$. The averages $\langle n_j L_{n_1, n_2} \rangle_{ss}$ and $\langle n_j M_{n_1, n_2}^- \rangle_{ss}$ are decorrelated such that $\langle n_j L_{n_1, n_2} \rangle_{ss} \approx \langle L_{n_1, n_2} \rangle_{ss} \langle n_j \rangle$ and $\langle n_j M_{n_1, n_2}^- \rangle_{ss} \approx \langle M_{n_1, n_2}^- \rangle_{ss} \langle n_j \rangle$. The resulting steady-state averages are decorrelated to the zeroth-order (their variables are uncorrelated), $\langle L_{n_1, n_2} \rangle_{ss} \approx L_{\langle n_1 \rangle_{ss} \langle n_2 \rangle_{ss}}$, $\langle M_{n_1, n_2}^\pm \rangle_{ss} \approx M_{\langle n_1 \rangle_{ss} \langle n_2 \rangle_{ss}}^\pm$ (replacing a photon number by its average which is reasonable above the threshold and for a sharp enough distribution function). Employing these arguments, the moments in Equation 4.30 take the simple form

$$\frac{d}{dt} \langle n_j \rangle = r_a \langle \lambda_{-n_1, n_2} \rangle_{ss} - \kappa_j \langle n_j \rangle, \quad (4.31a)$$

$$\frac{d}{dt} \langle n_j \rangle^2 = -2\kappa_j \langle n_j \rangle^2 + (2r_a \langle \lambda_{-n_1, n_2} \rangle_{ss} + \kappa_j) \langle n_j \rangle + r_a \langle \lambda_{+n_1, n_2} \rangle_{ss}, \quad (4.31b)$$

$$\frac{d}{dt} \langle n_1 n_2 \rangle = -(\kappa_1 + \kappa_2) \langle n_1 n_2 \rangle + r_a \langle \lambda_{-n_1, n_2} \rangle_{ss} \langle n_1 + n_2 \rangle + r_a \langle \lambda_{+n_1, n_2} \rangle_{ss}, \quad (4.31c)$$

where

$$\lambda_{\pm n_1, n_2} = \rho_{aa} L_{n_1+1, n_2+1} \pm \rho_{bb} L_{n_1, n_2} + 2 |\rho_{ab}|^2 M_{n_1, n_2}^\pm. \quad (4.32)$$

Integrating Equation 4.31a, yields

$$\langle n_j \rangle = \frac{r_a \langle \lambda_{-n_1, n_2} \rangle_{ss}}{\kappa_j} (1 - e^{-\kappa_j t}). \quad (4.33)$$

Using this result back in Equations 4.31b, 4.31c, and integrating for $\langle n_1 n_2 \rangle$ and $\langle n_j \rangle^2$ gives

$$\langle n_1 n_2 \rangle - \langle n_1 \rangle \langle n_2 \rangle = \frac{r_a \langle \lambda_{+n_1, n_2} \rangle_{ss}}{\kappa_1 + \kappa_2} (1 - e^{-(\kappa_1 + \kappa_2)t}), \quad (4.34a)$$

$$\langle n_j^2 \rangle - \langle n_j \rangle^2 - \langle n_j \rangle = \frac{r_a}{2\kappa_j} (\langle \lambda_{+n_1, n_2} \rangle_{ss} - \langle \lambda_{-n_1, n_2} \rangle_{ss}) (1 - e^{-2\kappa_j t}). \quad (4.34b)$$

The moments in Equation 4.34, along with Equation 4.32, tell us that statistics are super-Poissonian and the coherence increases the correlation, but Kerr parameter decreases this correlation. The variances say that the coherence widens both the joint and the marginal photon distribution functions. This is clear since the right-hand side is non-negative, $\langle \lambda_{+n_1, n_2} \rangle_{ss} - \langle \lambda_{-n_1, n_2} \rangle_{ss} \geq 0$ (the equality holds when $\rho_{bb} = 0$, which means the atoms are prepared in their excited states). In this case, the variance becomes $\langle n_j^2 \rangle - \langle n_j \rangle^2 = \langle n_j \rangle$ and statistics are Poissonian. The correlations reach their maximum at steady-state and the spread of the distribution is enhanced by the atomic coherence. The moments are one method of characterizing a probability distribution and here they characterize the field distribution.

4.4.1 Mean Photon Number

From Equations 4.31a and 4.32, the steady-state mean photon-number can be calculated as

$$\kappa_j \langle n_j \rangle_{ss} = r_a \left(\rho_{aa} \langle L_{n_1+1, n_2+1} \rangle_{ss} - \rho_{bb} \langle L_{n_1, n_2} \rangle_{ss} + 2 |\rho_{ab}|^2 \langle M_{n_1 n_2}^- \rangle_{ss} \right). \quad (4.35)$$

This result enables us to express $\langle n_j \rangle_{ss}$ in terms of the total mean-photon number $\langle n \rangle_{ss} = \langle n_1 + n_2 \rangle_{ss}$

$$\kappa_j \langle n_j \rangle_{ss} = \kappa \langle n \rangle_{ss}, \quad (4.36)$$

where the effective decay constant

$$\kappa = \frac{\kappa_1 \kappa_2}{\kappa_1 + \kappa_2}. \quad (4.37)$$

The relation in Equation 4.36 is useful since it simplifies the calculations for effective expressions of the averages $\langle L_{n_1, n_2} \rangle_{ss}$, $\langle L_{n_1+1, n_2+1} \rangle_{ss}$, and $\langle M_{n_1 n_2}^\pm \rangle_{ss}$. To the orders $O(\langle n \rangle_{ss}^{-2})$, $O(\langle n \rangle_{ss}^{-3})$, and $O(\langle n \rangle_{ss}^{-3})$, respectively, effective expressions for $\langle M_{n_1 n_2}^+ \rangle_{ss}$, $\langle M_{n_1 n_2}^- \rangle_{ss}$, and $\langle L_{n_1+1, n_2+1} \rangle_{ss} - \langle L_{n_1, n_2} \rangle_{ss}$ can be written as

$$\langle M_{n_1 n_2}^+ \rangle_{ss} = \frac{m_1}{\langle n \rangle_{ss}}, \quad (4.38a)$$

$$\langle M_{n_1 n_2}^- \rangle_{ss} = \frac{m_2}{\langle n \rangle_{ss}^2}, \quad (4.38b)$$

$$\langle L_{n_1+1, n_2+1} \rangle_{ss} = \langle L_{n_1, n_2} \rangle_{ss} + \frac{l_1}{\langle n \rangle_{ss}} + \frac{l_2}{\langle n \rangle_{ss}^2}. \quad (4.38c)$$

with

$$\langle L_{n_1, n_2} \rangle_{ss} = \frac{2K \langle n \rangle_{ss}^2}{1 + \gamma^{-2} \delta^2 + 4\gamma^{-1} E \delta \langle n \rangle_{ss} + 4B \langle n \rangle_{ss}^2}, \quad (4.39)$$

and

$$K = \left(\frac{g}{\gamma}\right)^2 \frac{\kappa^2}{\kappa_1 \kappa_2}, \quad (4.40a)$$

$$E = \frac{\kappa}{\gamma} \left(\frac{\chi_1}{\kappa_1} + \frac{\chi_2}{\kappa_2}\right), \quad (4.40b)$$

$$B = K \left[1 + \frac{\kappa_1 \kappa_2}{g^2} \left(\frac{\chi_1}{\kappa_1} + \frac{\chi_2}{\kappa_2}\right)^2\right], \quad (4.40c)$$

$$\delta = \Delta - 2q, \quad (4.40d)$$

$$q = \chi_1 + \chi_2. \quad (4.40e)$$

The coefficients l_j, m_j are presented with their derivation in Appendix E.

By using Equation 4.38 and Equation 4.39 in Equation 4.35, it is straight forward to write the mean photon-number, $\langle n \rangle_{ss}$, as a solution of the quintic equation

$$\langle n \rangle_{ss}^5 - C_4 \langle n \rangle_{ss}^4 - C_3 \langle n \rangle_{ss}^3 - C_2 \langle n \rangle_{ss}^2 - C_1 \langle n \rangle_{ss} - C_0 = 0, \quad (4.41)$$

with

$$C_0 = \frac{r_a}{4\kappa B} \left(1 + \frac{\delta^2}{\gamma^2}\right) (\rho_{aa} l_2 + 2 |\rho_{ab}|^2 m_2), \quad (4.42a)$$

$$C_1 = \frac{r_a}{4\kappa B} \left(\rho_{aa} \left(\left(1 + \frac{\delta^2}{\gamma^2}\right) l_1 + 4 \frac{\delta}{\gamma} E l_2\right) + 8 |\rho_{ab}|^2 \frac{\delta}{\gamma} E m_2\right), \quad (4.42b)$$

$$C_2 = \frac{r_a}{4\kappa B} \left(4 \rho_{aa} \left(\frac{\delta}{\gamma} E l_1 + B l_2\right) + 8 |\rho_{ab}|^2 B m_2\right), \quad (4.42c)$$

$$C_3 = \frac{r_a}{4\kappa B} \left(4 \rho_{aa} B l_1 - \frac{\kappa}{r_a} \left(1 + \frac{\delta^2}{\gamma^2}\right)\right), \quad (4.42d)$$

$$C_4 = \frac{r_a}{4\kappa B} \left(2 (\rho_{aa} - \rho_{bb}) K - 4 \frac{\kappa \delta}{\gamma r_a} E\right). \quad (4.42e)$$

Equation 4.41 has, in general, five real roots, three real roots and two complex conjugate roots, or only one real root and four complex conjugate roots. The real physical solution is found to be in a good agreement with the numerical solution. The coherence contributes

through the low-order coefficients, C_0 , C_1 , C_2 that means it is negligible for large intensities. A special and simpler expression for the mean, yet still in a good agreement with the numerical solution for not very large values of the detuning and Kerr parameters is obtained by ignoring coherence contribution and the correction in the difference $\langle L_{n_1+1, n_2+1} \rangle - \langle L_{n_1, n_2} \rangle$ (derived in Appendix E). For this special case, the fifth-degree polynomial reduces to the quadratic equation

$$\langle n \rangle_{ss}^2 - C_4 \langle n \rangle_{ss} + \frac{1}{4B} (1 + \gamma^{-2} \delta^2) = 0. \quad (4.43)$$

The stable solution of Equation 4.43 is

$$\langle n_j \rangle_{ss} = \frac{\kappa}{2\kappa_j} C_4 \left(1 + \sqrt{1 - \frac{1 + \gamma^{-2} \delta^2}{BC_4^2}} \right), \quad (4.44)$$

and the other solution is unstable and diminishes far above threshold. This expression gives the threshold condition, $C_4 > \sqrt{(1 + \gamma^{-2} \delta^2) B^{-1}}$, explicitly

$$\frac{r_a g^2 (\rho_{aa} - \rho_{bb}) - 2 (\chi_1 \kappa_2 + \chi_2 \kappa_1) \delta}{\sqrt{(\gamma^2 + \delta^2) ((\chi_1 \kappa_2 + \chi_2 \kappa_1)^2 + g^2 \kappa_1 \kappa_2)}} \geq 2. \quad (4.45)$$

The threshold condition Equation 4.45 predicts that the Kerr parameter and positive detuning raise the threshold, but negative detuning lowers it. It also predicts the necessity of population inversion to sustain steady-state production of photons. The role of the sign of the detuning can be explained as follows: Kerr effect makes a shift in the field frequency (scattering photons) (He & Liu, 2017). From the definition of detuning, Equation 4.4), negative detuning represents low-energy photons (red-photons), and positive detuning represents high-energy photons. So, combining the energy from these red-scattering photons (from the optical Kerr effect) to the field energy will drive the atom and field far from resonance in the case of positive detuning but bring them close to resonance for the

negative detuning case (Mathkoo et al., 2020). So, in the presence of the Kerr effect, the mean photon number will be greater than for positive detuning.

Far from threshold (large $\langle n_j \rangle_{ss}$), the means take the simpler form

$$\langle n_j \rangle_{ss} = \frac{1}{2\kappa_j} \frac{r_a g^2 (\rho_{aa} - \rho_{bb}) - 2(\chi_1 \kappa_2 + \chi_2 \kappa_1) \delta}{g^2 + (\chi_1 \sqrt{\kappa_2/\kappa_1} + \chi_2 \sqrt{\kappa_1/\kappa_2})^2}. \quad (4.46)$$

Expression in Equation 4.46 (zeroth approximation in $(1 + \gamma^{-2} \delta^2) / BC_4^2$) anticipates a linear decrease of the mean with increasing detuning towards positive values. It says that the Kerr parameter and positive detuning lessen the mean photon number and the negative values for detuning, enhanced by the Kerr effect, increase the mean. However, the Kerr effect is dominant and the overall result is decreasing the mean photon number. This means that low-energy photons enhance the mean photon number while high-energy photons reduce the mean.

It is worth to state comparison between the solution in Equation 4.44 and its approximation given by Equation 4.46 as the solution to the fifth degree polynomial given by Equation 4.41. First, the solution of Equation 4.41 takes into account the coherence, but Equations 4.44 and 4.46 neglect the coherence. Second, the numerical solution of Equation 4.41 is in agreement with both Equations 4.44 and 4.46 and for a longer range of the parameters as shown in the discussion.

4.4.2 Nonclassicality by $G^{(2)}$ and CSI

The field correlation functions are useful tools to analyze the quantized electromagnetic field (Glauber, 1963c). The $G^{(2)}$ is one measure for nonclassical properties of the field, among other measures such as violation of CSI for $G^{(2)}$ (Loudon, 1980; Reid & Walls, 1986; Klyshko, 1996; Walther et al., 2006). From Equations 2.115 and 2.116, the $G^{(2)}$ in

simple elegant form is

$$g_{jj}^{(2)} = 1 + \left(g_{jj}^{(2)ss} - 1 \right) \coth \left(\frac{1}{2} \kappa_j t \right), \quad (4.47a)$$

$$g_{12}^{(2)} = 1 + \frac{1}{2} \left(g_{12}^{(2)ss} - 1 \right) \left[\coth \left(\frac{1}{2} \kappa_1 t \right) + \coth \left(\frac{1}{2} \kappa_2 t \right) \right]. \quad (4.47b)$$

These equations give a better agreement after a specific long time. This is a consequence of the assumption and validity of the approximation, e.g., far from threshold which is a point that needs more time to reach. By ignoring the fast decaying terms and using $\coth(x) \approx 1 + 2 \exp(-2x)$, $x \gg 1$, so $g^{(2)}$ near the steady-state takes the form

$$g_{jj}^{(2)} = 1 + \left(g_{jj}^{(2)ss} - 1 \right) (1 + 2e^{-\kappa_j t}), \quad (4.48a)$$

$$g_{12}^{(2)} = 1 + \left(g_{12}^{(2)ss} - 1 \right) (1 + e^{-\kappa_1 t} + e^{-\kappa_2 t}). \quad (4.48b)$$

From Equations 4.33 and 4.34, the steady-state $g^{(2)}$ are

$$g_{jj}^{(2)ss} = 1 + \frac{r_a}{2\kappa_j} \frac{\langle \lambda_{+n_1, n_2} \rangle_{ss} - \langle \lambda_{-n_1, n_2} \rangle_{ss}}{\langle n_j \rangle_{ss}^2}, \quad (4.49a)$$

$$g_{12}^{(2)ss} = 1 + \frac{r_a}{\kappa_1 + \kappa_2} \frac{\langle \lambda_{+n_1, n_2} \rangle_{ss}}{\langle n_1 \rangle_{ss} \langle n_2 \rangle_{ss}}. \quad (4.49b)$$

Equation 4.48 states that the correlations reach their lowest values at steady-state given by Equation 4.49. These expressions say that $g_{ij}^{(2)} > 1$ at all times and the field is super-Poissonian. These functions violate the CSI as will be shown soon. In the case $\rho_{bb} = 0$, the averages $\langle \lambda_{\pm n_1, n_2} \rangle_{ss}$ are reduced to $\langle \lambda_{+n_1, n_2} \rangle_{ss} = \langle \lambda_{-n_1, n_2} \rangle_{ss} = \langle L_{n_1+1, n_2+1} \rangle_{ss} = r_a^{-1} \kappa_j \langle n_j \rangle_{ss}$ (from Equation 4.32 and using the steady-state of Equation 4.31a). In this case and from

Equation 4.48, the $G^{(2)}$ reduce to

$$g_{jj}^{(2)} = 1, \quad (4.50a)$$

$$g_{12}^{(2)} = 1 + \frac{r_a}{\kappa_1 + \kappa_2} \frac{\langle \lambda_{+n_1, n_2} \rangle_{ss}}{\langle n_1 \rangle_{ss} \langle n_2 \rangle_{ss}} (1 + e^{-\kappa_1 t} + e^{-\kappa_2 t}). \quad (4.50b)$$

In the steady-state, $g_{12}^{(2)}$ takes the form

$$g_{12}^{(2)} = 1 + \frac{1}{\langle n_1 \rangle_{ss} + \langle n_2 \rangle_{ss}}. \quad (4.51)$$

Equation 4.51 is identical with Zubairy's result (Zubairy, 1982); The violation of CSI is of order $(\langle n_1 \rangle_{ss} + \langle n_2 \rangle_{ss})^{-1}$. It is convenient to use the function F_{cs} , as was discussed in Chapter 2, to quantify the correlation and to measure the nonclassicality through its violation of CSI, or $F_{cs} > 0$. For the case $\rho_{bb} = 0$, and from Equation 4.50, the function F_{cs} takes the form

$$F_{cs} = \frac{1}{\langle n_1 \rangle_{ss} + \langle n_2 \rangle_{ss}} (1 + e^{-\kappa_1 t} + e^{-\kappa_2 t}) > 0. \quad (4.52)$$

The function is always positive and takes its lowest value at the steady-state. So, $G^{(2)}$ violates CSI all the time. Another important measure that is adopted here is the Q parameter.

4.4.3 Nonclassicality by Q

As was discussed in Chapter 2, the statistics of the field are determined by quantifying Q . It measures the departure of the statistics from Poissonian $Q = 0$ or $\langle n_j^2 \rangle = \langle n_j \rangle^2$ (the variance equals the mean). So, Q indicates the nonclassicality when $Q < 0$ which corresponds to the sub-Poissonian statistics (Mandel, 1979). The Q parameter and the intra-mode correlations are related by Equation 2.117 which is written as

$$Q_j = \langle n_j \rangle (g_{jj}^{(2)} - 1). \quad (4.53)$$

By substituting Equation 4.47a in Equation 4.53, the dynamics of Q are

$$Q_j = Q_j^{ss} (1 + e^{-\kappa_j t}). \quad (4.54)$$

Equation 4.54 states that the Q -parameter reaches its lowest value at the steady-state.

The explicit expression of Q at steady-state is obtained from by substituting Equation 4.49a in Equation 4.53 giving

$$Q_j^{ss} = \frac{r_a}{2\kappa_j} \frac{\langle \lambda_{+n_1, n_2} \rangle_{ss} - \langle \lambda_{-n_1, n_2} \rangle_{ss}}{\langle n_j \rangle_{ss}}. \quad (4.55)$$

Equation 4.55 indicates that $Q_j^{ss} > 0$, so the statistics are super-Poissonian. When $\rho_{bb} = 0$ (atoms are initially in their excited states) and from Equation 4.50b, $Q_j = 0$. So, Q cannot tell about the nonclassicality of the field that is already found from the violation of the CSI at all times. Thus the approximate solution predicts that the statistics of the field are super-Poissonian and become Poissonian only when $\rho_{bb} = 0$, but the nonclassicality is witnessed through the violation of CSI.

4.4.4 Fluctuations

The relative fluctuations of the number of photons in j -mode is

$$\frac{\langle (\Delta n_j)^2 \rangle}{\langle n_j \rangle} = \frac{\langle n_j^2 \rangle - \langle n_j \rangle^2}{\langle n_j \rangle} = Q_j + 1. \quad (4.56)$$

It was thought that the relative fluctuations of the number of photons in a TPL cannot be smaller than the fluctuations in the coherent emission. Zubairy (1980) and Bay et al. (1995) calculated the photon number fluctuations high above the threshold and found the fluctuations in the photon number of TPL $\langle (\Delta n)^2 \rangle / \langle n \rangle = 3/2$. This is greater than that of the one-photon which means that spectral distribution for the TPL is wider than the

Poissonian that describes the standard one-photon laser. This increase in the width attains the maximum when the two photons have the same decay rates. The TPL is bunched (Cheng & Haken (1988) and the references therein). However, under some conditions, the fluctuations could be reduced and antibunching is observed (Bay et al., 1995; Loudon, 1980; Kozierowski, 1981). From Equation 4.55, the relative fluctuations for single-mode statistics, Equation 4.56, are

$$\frac{\langle (\Delta n_j)_{ss}^2 \rangle}{\langle n_j \rangle_{ss}} = 1 + \frac{r_a}{2\kappa_j} \frac{\langle \lambda_{+n_1, n_2} \rangle_{ss} - \langle \lambda_{-n_1, n_2} \rangle_{ss}}{\langle n_j \rangle_{ss}}. \quad (4.57)$$

The fluctuations in the single mode distribution take their lowest value 1 when $\rho_{bb} = 0$. It is interesting to see the fluctuations in the total photon number distribution, $\langle n \rangle = \langle n_1 \rangle + \langle n_2 \rangle$.

The relative noise could be written as

$$\frac{\langle (\Delta n)_{ss}^2 \rangle}{\langle n \rangle_{ss}} = 1 + \frac{2\kappa}{\kappa_1 + \kappa_2} + \frac{r_a}{2\kappa} \left(1 + \frac{4\kappa}{\kappa_1 + \kappa_2} \right) \frac{\langle \lambda_{+n_1, n_2} \rangle_{ss} - \langle \lambda_{-n_1, n_2} \rangle_{ss}}{\langle n \rangle_{ss}}. \quad (4.58)$$

The lowest value of the relative total fluctuations (for $\rho_{bb} = 0$) is

$$\frac{\langle (\Delta n)_{ss}^2 \rangle}{\langle n \rangle_{ss}} = 1 + \frac{2\kappa_1 \kappa_2}{(\kappa_1 + \kappa_2)^2}, \quad (4.59)$$

which has the maximum value of 3/2 when the two modes have the same decay rate and the known result (Zubairy, 1980; Bay et al., 1995) is recovered. This relation is also reduced to the known value of 1 (for coherent state) for the one-photon laser when one mode has a very small decay rate and becomes dominant over the other mode.

4.4.5 Entanglement

It is interesting to investigate the role of Kerr parameters on the entanglement. To study the entanglement, it is convenient to define $E = E(a_1, a_2)$ by

$$E(a_1, a_2) = |\langle a_1 a_2 \rangle|^2 - \langle a_1^\dagger a_1 \rangle \langle a_2^\dagger a_2 \rangle. \quad (4.60)$$

According to Hillery & Zubairy (2006), the criterion for entanglement is $E > 0$. The criterion states that the positivity of E implies entanglement. The computational form of Equation 4.60 in terms of the density matrix elements is

$$E(n_1, n_2) = \left| \sum_{n_1 n_2} \sqrt{(n_1 + 1)(n_2 + 1)} \rho_{n_1+1, n_2+1; n_1 n_2} \right|^2 - \langle n_1 \rangle \langle n_2 \rangle. \quad (4.61)$$

An approximate expression for Equation 4.61 can be obtained by using Equation 4.26 in Equation 4.60. The off-diagonal elements $\rho_{n_1+1, n_2+1; n_1 n_2}$ are written as

$$\rho_{n_1+1, n_2+1; n_1 n_2} \approx \frac{i \rho_{ab} e^{i2D_{n_1+1, n_2+1} \gamma t}}{\Gamma_{n_1 n_2; n_1+1, n_2+1}^*} \left(K_{n_1+1, n_2+1; n_1+2, n_2+2}^* P_{n_1+1, n_2+1} - K_{n_1+1, n_2+1; n_1 n_2}^* P_{n_1 n_2} \right). \quad (4.62)$$

Using Equation 4.62 in Equation 4.61, E can be written as

$$E(n_1, n_2) = \left| \rho_{ab} \langle \Xi_{n_1+1, n_2+1} K_{n_1+1, n_2+1; n_1 n_2}^* - \Xi_{n_1, n_2} K_{n_1 n_2; n_1+1, n_2+1}^* \rangle \right|^2 - \langle n_1 \rangle \langle n_2 \rangle, \quad (4.63)$$

where

$$\Xi_{n_1, n_2} = \frac{\sqrt{n_1 n_2}}{\Gamma_{n_1 n_2; n_1-1, n_2-1}} e^{i2D_{n_1 n_2} \gamma t}. \quad (4.64)$$

It worth to notice that the atomic coherence supports the entanglement. However, the expression in absolute value is smaller than the last term. This removes any possibility for entanglement. However, the model exhibits nonclassicality. It has been found that, in metrological tasks, nonclassicality rather than entanglement is a necessary resource to achieve quantum advantages (Kwon et al., 2019; Sahota & Quesada, 2015; Friis et al., 2015; Ge et al., 2018). This section is concluded by presenting a solution for the statistics function.

4.4.6 Photon Statistics

In this section, a solution for the statistics function using the generating function method is presented (Simaan & Loudon, 1975a,b, 1978; Zubairy, 1980; Dodonov & Mizrahi, 1997b). It is instructive to rewrite the statistics equation, Equation 4.28, in a simple form to simplify the calculations. From Equation 4.28 and Equation 4.32 the statistics equation is

$$\begin{aligned}
 \dot{P}_{n_1 n_2} = & - (r_a \lambda_{+n_1, n_2} + \kappa_1 n_1 + \kappa_2 n_2) P_{n_1, n_2} \\
 & + \frac{1}{2} r_a (\lambda_{+n_1-1, n_2-1} + \lambda_{-n_1-1, n_2-1}) P_{n_1-1, n_2-1} \\
 & + \frac{1}{2} r_a (\lambda_{+n_1+1, n_2+1} - \lambda_{-n_1+1, n_2+1}) P_{n_1+1, n_2+1} \\
 & + \kappa_1 (n_1 + 1) P_{n_1+1, n_2} + \kappa_2 (n_2 + 1) P_{n_1, n_2+1}.
 \end{aligned} \tag{4.65}$$

Using the generating function, $G = G(x_1, x_2; t)$, in two variables x_1, x_2 with t as a parameter

$$G(x_1, x_2; t) = \sum_{n_1 n_2=0} P_{n_1, n_2}(t) x_1^{n_1} x_2^{n_2}, \tag{4.66}$$

along with the assumptions employed in solving the moments, the generating function takes the form (for the derivation, see Appendix F)

$$\begin{aligned} \partial_t G = & \left[-r_a \langle \lambda_{+n_1, n_2} \rangle_{ss} + \kappa_1 (1 - x_1) \partial_{x_1} + \kappa_2 (1 - x_2) \partial_{x_2} \right] G \\ & + \frac{1}{2} r_a \left(\langle \lambda_{+n_1-1, n_2-1} \rangle_{ss} + \langle \lambda_{-n_1-1, n_2-1} \rangle_{ss} \right) x_1 x_2 G \\ & + \frac{1}{2} r_a \left(\langle \lambda_{+n_1+1, n_2+1} \rangle_{ss} - \langle \lambda_{-n_1+1, n_2+1} \rangle_{ss} \right) (\partial_{x_1} \partial_{x_2} x_1 x_2)^{-1} \partial_{x_1} \partial_{x_2} G, \end{aligned} \quad (4.67)$$

where $\partial_x = \frac{\partial}{\partial x}$; $x = t, x_1, x_2$. The third line of Equation 4.67 makes the solution complicated. A simple solution is easy to obtain for the case $\rho_{bb} = 0$ where this term disappears. So, a solution for this special case when the atoms are prepared in excited states is presented. This solution provides some insight on the effects of Kerr parameters and detuning on the dynamics of the system. Under this assumption, the solution can be approached as follows. The generating function G is rewritten in terms of a new auxiliary generating function Y such that

$$G = \exp(Y). \quad (4.68)$$

Equation of the new generating function is

$$\partial_t Y = \kappa \langle n \rangle_{ss} (x_1 x_2 - 1) + \left[\kappa_1 (1 - x_1) \partial_{x_1} + \kappa_2 (1 - x_2) \partial_{x_2} \right] Y. \quad (4.69)$$

Using Laplace transform and power series expansion, the solution of Equation 4.69 is (the derivation is given in Appendix F)

$$Y = \langle n_1 \rangle (x_1 - 1) + \langle n_2 \rangle (x_2 - 1) + C_{12} (x_1 - 1)(x_2 - 1), \quad (4.70)$$

where the mean $\langle n_j \rangle$ and covariance are C_{12}

$$\langle n_j \rangle = \langle n_j \rangle_{ss} (1 - e^{-\kappa_j t}), \quad (4.71)$$

$$C_{12} = \left(\langle n_1 n_2 \rangle_{ss} - \langle n_1 \rangle_{ss} \langle n_2 \rangle_{ss} \right) \left[1 - e^{-(\kappa_1 + \kappa_2)t} \right]. \quad (4.72)$$

It has to be remembered that the mean photon number that appears in this calculation for the distribution P_{n_1, n_2} is evaluated for the case $\rho_{bb} = 0$ otherwise the result is not correct.

The statistics function, P_{n_1, n_2} , is obtained directly by performing a series expansion for G ; it is the coefficient of the term $x_1^{n_1} x_2^{n_2}$ in the expansion. The calculations are presented in Appendix G and the result is

$$\begin{aligned} P_{n_1 n_2} &= \frac{\langle n_1 \rangle^{n_1} \langle n_2 \rangle^{n_2}}{n_1! n_2!} \exp(-\langle n_1 \rangle - \langle n_2 \rangle) \\ &\times \exp(C_{12}) \left(1 - \frac{C_{12}}{\langle n_1 \rangle} \right)^{n_1} \left(1 - \frac{C_{12}}{\langle n_2 \rangle} \right)^{n_2} \xi_{n_1 n_2} \left(\frac{C_{12}}{(\langle n_1 \rangle - C_{12})(\langle n_2 \rangle - C_{12})} \right), \end{aligned} \quad (4.73)$$

where

$$\xi_{n_1 n_2}(x) = \sum_{k=0}^{\min(n_1, n_2)} k! \binom{n_1}{k} \binom{n_2}{k} x^k, \quad (4.74)$$

and $\binom{k}{l}$ is binomial coefficient. The first line of the function in Equation 4.73 is the product of two independent ($C_{12} = 0$) Poissonian distributions and the second line is the correlation of the two modes. Departure of the distribution from a two-dimensional Poissonian is a measure of the statistics resulting from the correlation between the two modes. One interesting observation is the symmetric form of the distribution in the two modes variables. This symmetry will break when the average photon number in the two mode are different, $\langle n_1 \rangle \neq \langle n_2 \rangle$. This breaking of symmetry comes from the two factors in the middle of the second line. For example, if $\langle n_1 \rangle > \langle n_2 \rangle$, then the first factor will be the dominant and

contributions of the first mode is greater than the contribution of the second mode and the reverse is true when $\langle n_1 \rangle < \langle n_2 \rangle$. Thus the distribution function is symmetric in n_1 and n_2 when $\langle n_1 \rangle = \langle n_2 \rangle$. The implication of this symmetry-breaking in $P_{n_1 n_2}$ is photon number squeezing as a result of reduction in the fluctuations of one mode. In this case, the single-mode distribution (or the marginal distribution) can be obtained by projecting the two dimensional distribution on one dimension. Similarly to calculation of a reduced density matrix, the single-mode distribution is

$$P_{n_1} = \sum_{n_2=0}^{\infty} P_{n_1 n_2}, \quad P_{n_2} = \sum_{n_1=0}^{\infty} P_{n_1 n_2}. \quad (4.75)$$

In this section, analytic expressions for moments and photon statistics in a special case are derived. $G^{(2)}$ and Q are calculated and discussed. One of the main results of this section is the mean photon number expressed in Equation 4.41 which is in a very good agreement with the numerical solution over a large range of the parameters. In the next section, the results from the numerical solution are discussed and the analytic solution is compared to these results.

4.5 The Computational Solution

In this section, a numerical solution to Equation 4.23 is presented, and the moments and $G^{(2)}$ as tools used to study the characteristics of the field are computed. For the numerical solution, the whole density matrix in Equation 4.12 has to be solved since the system of equations in Equation 4.23 is not closed to the diagonal elements.

To solve a problem numerically, one must truncate the infinite-dimensional space to a finite one. This truncation causes a small error in the computations at the boundaries but this error decreases as the dimension of the finite space increases. In solving the density matrix equation, the four-dimensional density matrix ρ is rewritten in a column

vector form, ϱ . The density matrix equation took the form $\dot{\varrho} = M\varrho$ where the matrix M is time-dependent. The size of the system becomes large when the number of photons in each mode is increased and make the computations a challenge in the cost of memory and time. The maximum number of photons in the first mode and the second mode are considered to be equal to N . The vector ϱ has $(N + 1)^4$ elements and the matrix M has $(N + 1)^8$ elements. Fortunately, most of the elements of M are zeros (sparse matrix). Equations are solved using the adaptive Runge-Kutta-Fehlberg method (RKF45) algorithm (Esfandiari, 2017) on Matlab. The algorithm of the solution is explained as follows.

The 4-dimensional density matrix $(\rho_{n_1 n_2; n'_1 n'_2}), n_j, n'_j = 0 \cdots N$ is rewritten in a vector form. The vectorization is performed in two steps. First, the pair of indices $(n_1 n_2), (n'_1 n'_2)$ are transformed to the pair (nn') which are

$$n = (N + 1) n_2 + n_1 + 1, \quad n' = (N + 1) n'_2 + n'_1 + 1, \quad (4.76)$$

for $n, n' = 1, \dots, (N + 1)^2$. The density matrix becomes $\rho_{n_1 n_2; n'_1 n'_2} \rightarrow \rho_{nn'}$. Then, the later is transformed into a single-index, k

$$k = (N + 1)^2 (n' - 1) + n; \quad k = 1, \dots, (N + 1)^4, \quad (4.77)$$

and the density matrix transforms as $\rho_{nn'} \rightarrow \rho_k$. So the matrix is transformed from a 4-dimensional form into a single column matrix (vector).

$$\underbrace{(\rho_{n_1 n_2; n'_1 n'_2})}_{(N+1) \times (N+1) \times (N+1) \times (N+1)} \rightarrow \underbrace{(\rho_k)}_{(N+1)^4 \times 1} = \varrho. \quad (4.78)$$

Using this final form of the density matrix, Equation 4.12 is rewritten in a matrix equation as

$$\dot{\varrho} = M\varrho, \quad (4.79)$$

where ϱ is the (column) vector form of the the density operator ρ and M is a $(N + 1)^4 \times (N + 1)^4$ matrix, the Jacobian of the matrix equation, that contains the coefficients in the master equation. It is clear how fast the the system size is growing as N increases. For example, for $N = 9$, the size of ϱ and M are $10^4 \times 1$ and $10^4 \times 10^4$, respectively. In the calculations, $N = 15$ is used, in which ϱ and M have, roughly and respectively, the dimensions of $6.55(10^4 \times 1)$ and $42.95(10^4 \times 10^4)$. As can be seen, when N increased by about 50%, the matrices ϱ and M increased by about 6.55 and 42.95, respectively. This drastic increase in the size of the problem was an instrumental factor to limit the computations to not large values of N . In principle, the matrix equation Equation 4.79 can be solved analytically. The solution is formally, $\varrho(t) = e^{M(t-t_0)} \varrho(t_0)$. The difficulty is in the calculation of the exponential matrix. The algorithm is to calculate the eigenvalues and eigenvectors of the matrix M , which is a difficult task as N increases. Another way is to use Laplace transform but again the difficulty lies in calculation the inverse of a matrix that has the same size as of M . More complication in calculation of inverse Laplace transform, which is normally using the diagonalization procedure and the problem is reduced to calculation of the eigenvalues and eigenvectors. From these considerations, the numerical solution is the preferable procedure. In the numerical solution, the matrix M is computed at each set of values of the parameters and then using the vacuum initial density matrix, $\varrho(0)$, Equation 4.79 is solved using the Runge-Kutta fourth-order on Matlab. The vacuum initial density matrix is calculated as

$$\rho(0) = |n_1 = 0, n_2 = 0\rangle \langle n'_1 = 0, n'_2 = 0|, \quad (4.80)$$

with the vacuum states are

$$|n_1 = 0, n_2 = 0\rangle = |n_1 = 0\rangle \otimes |n_2 = 0\rangle, \quad (4.81a)$$

$$|n_j = 0\rangle = (1 \ 0 \ 0 \cdots 0)^T. \quad (4.81b)$$

The column matrix ϱ becomes $(1 \ 0 \ 0 \cdots 0)^T$ (T for transpose).

4.6 Results and Discussion

So far in this chapter, the density matrix is derived and from which the photon distribution equation and its approximated form Equation 4.28 are obtained. The solution of this equation and its results were studied. In this section, the exact results from the computational solution are provided as well as a justification for the analytic results from the approximated solution. The justification is through a comparison between the exact results and the results of the analytic approximation. The effects of injection rate r_a , detuning Δ , and the Kerr parameters χ_1 and χ_2 on mean photon number, $G^{(2)}$, CSI through the F_{cs} function, Q , entanglement, and photon distribution are studied. To study the dynamics of these quantities, 2D and 3D figures are presented. The 3D figures show the dynamics as well as the parameter dependence of the quantities. The 2D figures present the dynamics but at three chosen values of one of these parameters to make the effect quantitatively noticeable. The effect of these parameters on the steady-state of these quantities is studied also. Through these quantities, photon statistics and nonclassicality of the field are studied. For simplicity, the two modes are assumed to have the same decay rate. So, from the symmetry of system, the mean photon number $\langle n_1 \rangle$, $\langle n_2 \rangle$; correlation functions, $g_{11}^{(2)}(0)$, $g_{22}^{(2)}(0)$; and Mandel Q parameters, Q_1 , Q_2 of the two modes are equal whenever they have the same Kerr parameter. Also, from this symmetry, only one Kerr parameter χ_1 is allowed to change values because the other produces the same effects. If the two modes have different decay

rates, the mode of the smaller decay rate will dominate and the other will die if its decay rate is too high and the problem reduces to the normal single-photon laser (Eremeev et al., 2011).

A prototype realistic values of the parameters to show the main features of the field are selected. As expected, and verified by the exact solution, the injection rate increases the average of photon number, approximately, linearly as will be shown. Due to limiting computational capacity, as it discussed in the previous section, the researcher was confined to select a small range of values for the injection rate. The selected parameters are:

$$\begin{aligned} \rho_{aa} = 0.9, \quad \rho_{bb} = 0.1, \quad \rho_{ab} = -0.3i, \quad \rho_{ba} = 0.3i, \\ \gamma = 100\kappa, \quad g = 70\kappa, \quad \chi_2 = 50\kappa, \quad \kappa_1 = 2\kappa, \quad \kappa_2 = 2\kappa, \quad \kappa = 10^6\text{s}^{-1}. \end{aligned} \quad (4.82)$$

The other parameters (r_a , Δ , χ_1) are given in figure captions. The initial atomic state selection is based on that the system becomes more nonclassical as the inversion $\rho_{aa} - \rho_{bb}$ increases (Mathkoor et al., 2020). In the justification, computation of $P_{n_1 n_2}$ is performed for $\rho_{bb} = 0$. The time range of the simulation is chosen to be $\kappa t = 6$ since the field reaches steady-state earlier and the main features of the field are shown.

4.6.1 Effects of Injection Rate

In this subsection, the effects of injection rate r_a on all quantities under the study mentioned above are discussed.

4.6.1.1 On Mean Photon Number

The effects of r_a on dynamics of the mean photon numbers $\langle n_1 \rangle$, $\langle n_2 \rangle$ are shown on the upper panels of Figure 4.2(a) and Figure 4.3(a). Mean photon number starts from zero and reaches steady-state in time about $\kappa t \approx 1.3$ or $t = 1.3 \times 10^{-6}$ s. The increase in injection rate results in rising mean photon number which is understood since number of excited

atoms in the cavity will increase and they emit more photons. This rise is approximately linear as can be seen from Figure 4.3(a). The increase mean photon number when injection rate increases from $r_a = 20\kappa$ to $r_a = 35\kappa$ is almost similar to the increase when r_a rises from $r_a = 35\kappa$ to $r_a = 50\kappa$. The dependence of mean photon number on injection rate appears clearly in the steady-state, Figure 4.4, where a linear growth in photon number is observed. This confirms the analytic result, Equation 4.46, when the laser is above threshold with an excess of photons. What about the effects of r_a on $G^{(2)}$?

Effects of injection rate, detuning, and Kerr parameter on dynamics of the mean photon number and entanglement.

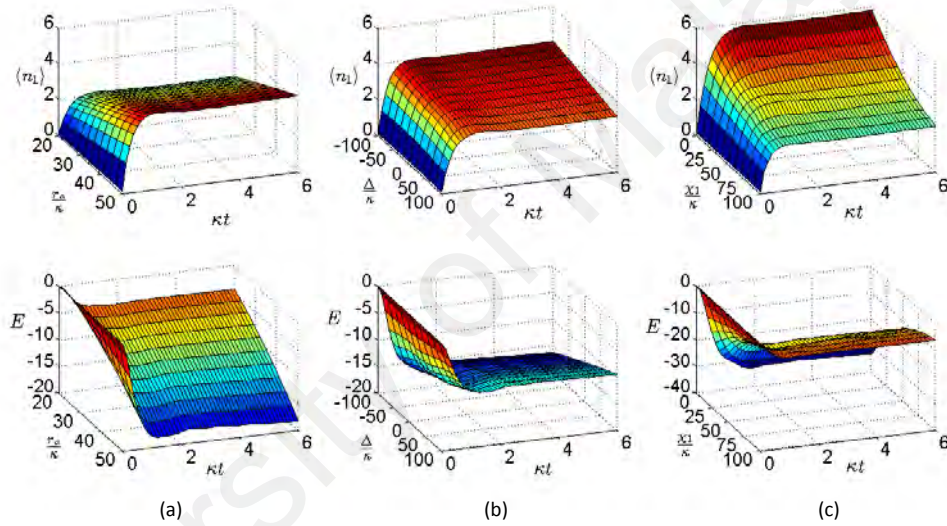


Figure 4.2: Mean photon number $\langle n_1 \rangle$ (upper panel) and entanglement E (lower panel). The dynamics and parameter dependence for: (a) injection rate r_a ($\Delta = 0$, $\chi_1 = 50\kappa$), (b) detuning Δ ($r_a = 40\kappa$, $\chi_1 = 50\kappa$), and (c) Kerr parameter χ_1 ($r_a = 40\kappa$, $\Delta = 0$).

4.6.1.2 On $G^{(2)}$ and CSI

The $G^{(2)}$ is the most important measure of nonclassicality of the field, and here a discussion and analysis of the results and its response to changes in the injection rate are given. The effects of r_a on dynamics of $G^{(2)}$ and consequently on CSI (demonstrated through F_{cs}) are presented in Figure 4.5(a), and Figure 4.6(a) for single-mode (or intra-mode) $g_{11}^{(2)}$, $g_{22}^{(2)}$; and in Figure 4.7(a), Figure 4.8(a) for inter-mode correlation $g_{12}^{(2)}$ and CSI. In steady-state, the results are shown in Figure 4.9(a) for $g_{12}^{(2)}$ and F_{cs} . The results

**Dynamics of the mean photon number and entanglement:
Effects of injection rate, detuning, and Kerr parameter.**

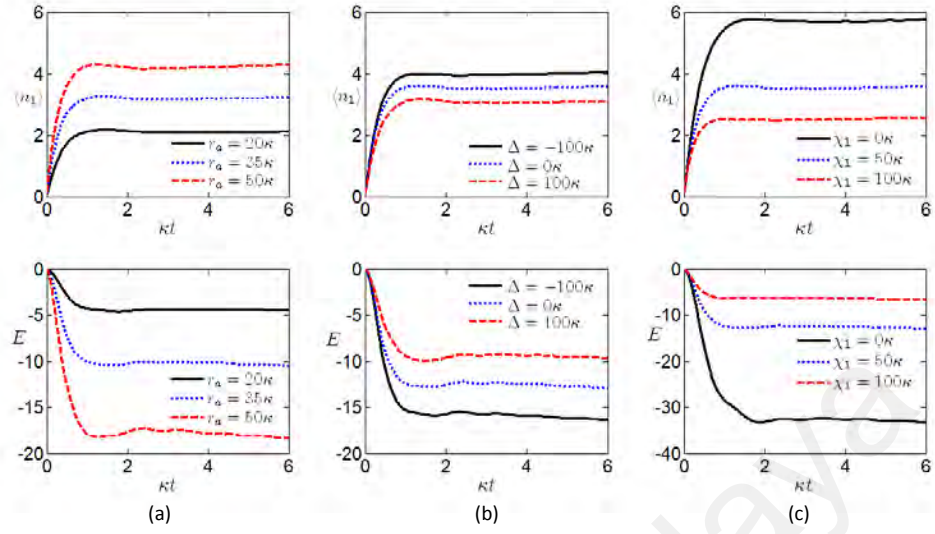


Figure 4.3: Mean photon number $\langle n_1 \rangle$ (upper panel) and entanglement E (lower panel). The dynamics for: (a) $\Delta = 0$, $\chi_1 = 50\kappa$, (b) $r_a = 40\kappa$, $\chi_1 = 50\kappa$, and (c) $r_a = 40\kappa$, $\Delta = 0$.

**Mean photon number and sub-Poissonian statistics ($Q_{1,2} < 0$):
Effects of injection rate, detuning, and Kerr parameter.**

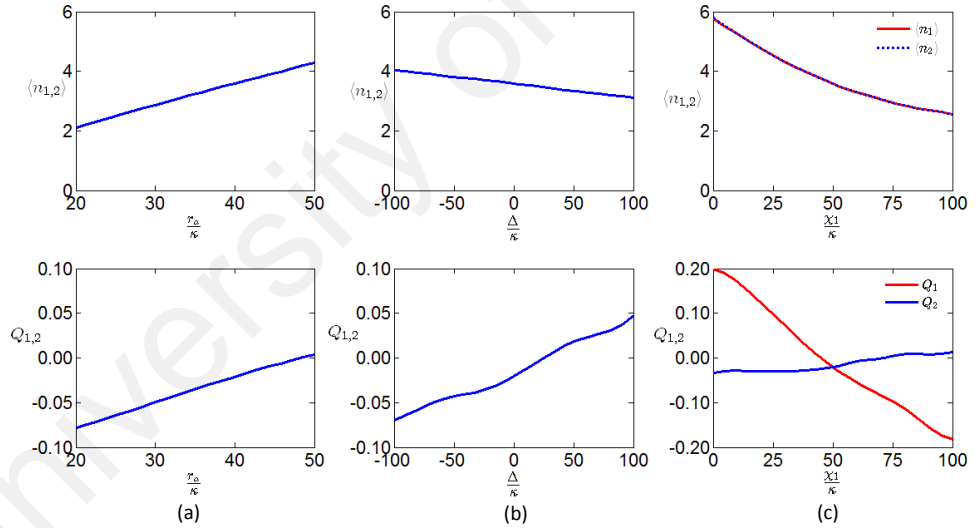


Figure 4.4: Mean photon numbers, $\langle n_1 \rangle, \langle n_2 \rangle$ (upper panel) and Q (lower panel); parameter dependence for: (a) injection rate r_a ($\Delta = 0$, $\chi_1 = 50\kappa$), (b) detuning Δ ($r_a = 40\kappa$, $\chi_1 = 50\kappa$), and (c) Kerr parameter χ_1 ($r_a = 40\kappa$, $\Delta = 0$).

for $G^{(2)}$ time-dependence show that the intra-mode correlations start from values below the classical limit for Poissonian statistics $g_{11}^{(2)} = 1 (= g_{22}^{(2)})$. Then, quickly, they reach their lowest value of around 0.9 at the kink before they grow up with small oscillations and reach their steady-state. This indicates that, initially, the relative fluctuations are small before they

grow up. They take their minimum at the kink where mean photon number $\langle n_1 \rangle \approx 1 (= \langle n_2 \rangle)$. It can be observed how the kink shifts to the right by increasing the injection rate. The shift gives time for the field to grow and reach the mean value of $\langle n_1 \rangle = 1$. At this particular time, the cavity has a mixture of one photon in each mode; the field in the two-photon state. The result reminds us that the lowest allowed value for $g_{11}^{(2)}$ is that for single-photon Fock state which is $g_{11}^{(2)} = 0$. As time goes on, $g_{11}^{(2)}$ increases and finally reaches its steady-state. When r_a continues to increase, $g_{11}^{(2)}$ increases too and becomes $g_{11}^{(2)} > 1$ for large values of r_a before it decreases again due to reduction in fluctuations for reaching a kind of equilibrium state between gain and loss. For example, at $r_a = 50\kappa$, $g_{11}^{(2)}$ reaches a maximum value at $\kappa t = 2.2$. The rise of correlation, is understood, and can be explained, as follows: The cavity photons build up with the time that results in a tendency of the cavity to have more photons as time passes. This leads to a high probability to find photons in higher states and fluctuations increase. As soon as the cavity reaches its saturation state, fluctuations response is delayed. This behavior can be understood as inertia and photon fluctuations need time to respond. So, statistics of the field change from sub-Poissonian at the initial time to super-Poissonian before reaching steady-state with statistics of sub-Poissonian, or Poissonian, depending on the value of injection rate. For weak values of r_a (and then $\langle n_1 \rangle$), the field maintains its statistics to be sub-Poissonian Figure 4.9(a). However, for large r_a , $g_{11}^{(2)}$ attains the classical value and the statistics become Poissonian. The dynamics for $g_{12}^{(2)}$, Figure 4.7(a) and Figure 4.8(a), it starts from large values at initial time. So, initially, $g_{11}^{(2)}$ is higher than $g_{11}^{(2)} \cdot g_{12}^{(2)}$ drops fast as fluctuations weaken when the cavity reaches an equilibrium between absorption and emission. In this case, the two modes become close to be independent and $g_{12}^{(2)}$ reaches its lowest values. This result becomes more realistic at strong injection rate when mean photon number becomes significantly large. The large $g_{12}^{(2)}$ and the slow change in $g_{11}^{(2)}, g_{22}^{(2)}$ (≈ 1) explain the dynamics of F_{cs} on the

Effects of injection rate, detuning, and Kerr parameter on the dynamics of the single-mode correlation functions.

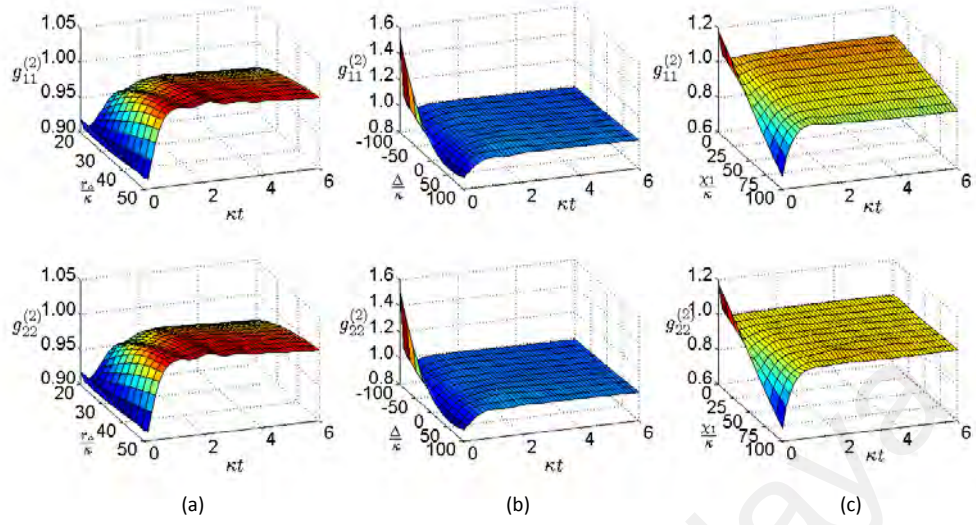


Figure 4.5: $g_{11}^{(2)}$ (upper panel) and $g_{22}^{(2)}$ (lower panel). The dynamics and parameter dependence for: (a) injection rate r_a ($\Delta = 0, \chi_1 = 50\kappa$), (b) detuning Δ ($r_a = 40\kappa, \chi_1 = 50\kappa$), and (c) Kerr parameter χ_1 ($r_a = 40\kappa, \Delta = 0$).

Dynamics of the single-mode correlation functions:
Effects of injection rate, detuning, and Kerr parameter.

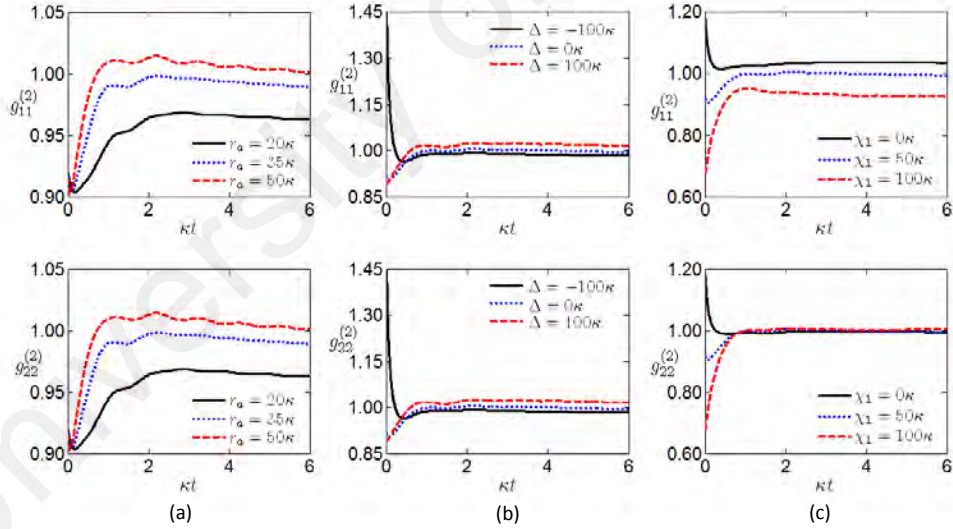


Figure 4.6: $g_{11}^{(2)}$ (upper panel) and $g_{22}^{(2)}$ (lower panel). The dynamics for: (a) $\Delta = 0, \chi_1 = 50\kappa$, (b) $r_a = 40\kappa, \chi_1 = 50\kappa$, and (c) $r_a = 40\kappa, \Delta = 0$.

same figures, Figure 4.7(a) and Figure 4.8(a). The function F_{cs} is always positive and this means that CSI is violated all the time and the field is nonclassical. In steady-state 4.9(a), $g_{11}^{(2)}$ and $g_{22}^{(2)}$ increase but the $g_{12}^{(2)}$ decreases as injection rate builds up. This shows that the amount of violation of CSI becomes less as r_a gets large. Thus the effect of r_a

is to increase fluctuations and reduce $G^{(2)}$ which leads to driving the statistics towards super-Poissonian and weaken nonclassicality of the field.

Effects of injection rate, detuning, and Kerr parameter on dynamics of the correlation function and violation of CSI.

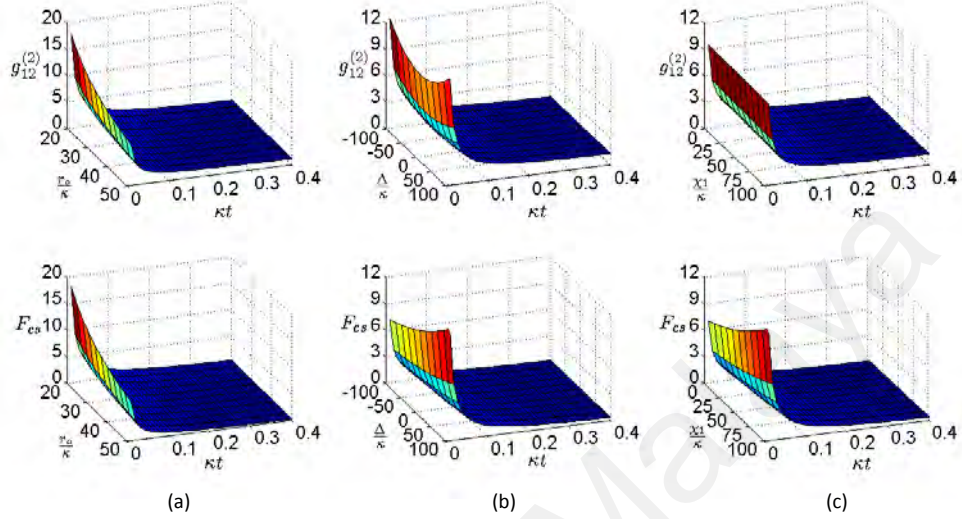


Figure 4.7: $g_{12}^{(2)}$ (upper panel) and CSI (F_{cs} , lower panel). The dynamics and parameter dependence for: (a) injection rate r_a ($\Delta = 0, \chi_1 = 50\kappa$), (b) detuning Δ ($r_a = 40\kappa, \chi_1 = 50\kappa$), and (c) Kerr parameter χ_1 ($r_a = 40\kappa, \Delta = 0$).

**Dynamics of the correlation function and violation of CSI:
Effects of injection rate, detuning, and Kerr parameter.**

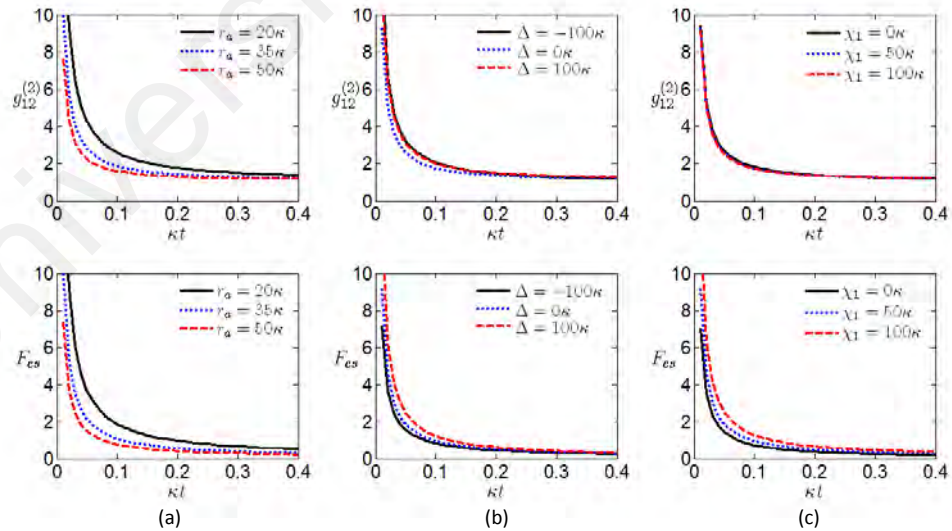


Figure 4.8: $g_{12}^{(2)}$ (upper panel) and CSI (F_{cs} , lower panel). The dynamics for: (a) $\Delta = 0, \chi_1 = 50\kappa$, (b) $r_a = 40\kappa, \chi_1 = 50\kappa$, and (c) $r_a = 40\kappa, \Delta = 0$.

**Correlation functions and violation of CSI:
Effects of injection rate, detuning, and Kerr parameter.**

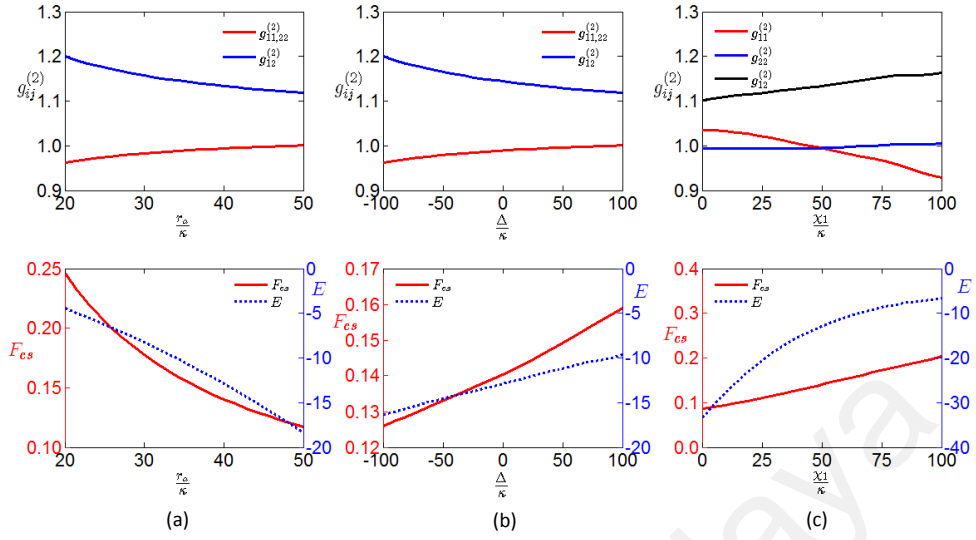


Figure 4.9: (upper panel) $g_{ij}^{(2)}$; $i, j = 1, 2$ and (lower panel) CSI (F_{cs} , left-hand axis in red color) and entanglement E (right-hand axis in blue color). The parameter dependence for: (a) injection rate r_a ($\Delta = 0, \chi_1 = 50\kappa$), (b) detuning Δ ($r_a = 40\kappa, \chi_1 = 50\kappa$), and (c) Kerr parameter χ_1 ($r_a = 40\kappa, \Delta = 0$).

4.6.1.3 On Entanglement

Since inter-mode correlations decrease by the increase in r_a , weak entanglement is expected if it is available. The results reveal that there is no entanglement and the injection rate makes entanglement hard to exist (increase of E , but in negative) as Figure 4.2(a) and Figure 4.3(a) show its dynamics. The increase in r_a lowers photon correlation and the two modes constitute two separable systems. The field density matrix becomes a tensor product of the single-mode density-matrix of the two modes. The response of E to the increase in r_a is nonlinear as shown in these figures. Figure 4.3(a) confirms that the contribution to E comes from the last term in Equation 4.63. since the off-diagonal elements $\rho_{n_1+1n_2+1;n_1n_2}$ are small, the average in absolute value is very small and has no effect. The smallest value is $E = 0$, which can be reached only at the initial time when the field in its vacuum state and entanglement criterion $E > 0$ is not satisfied. In steady-state E changes almost quadratically as demonstrated in Figure 4.9(a). This is confirmed by combining Equation 4.63, and Equation 4.46. From these two equations, E dependence

on r_a , approximately, follows a quadratic formula.

4.6.1.4 On Mandel Q Parameter

Since r_a reduces correlation and increases fluctuations, an increase in Q is expected and this is the case as results exhibit in Figures 4.10(a), 4.11(a) for its dynamics and in Figure 4.4(a) for its steady-state. Again, the kink at which the lowest values of fluctuations take place is seen. The Q and $g_{11}^{(2)}, g_{22}^{(2)}$ are sensitive to fluctuations so oscillations appear clearly at maximum fluctuations then they fade when the cavity approaches steady-state as exhibited in the figures. In the beginning, $Q_1 = 0$ which means that mean photon number and its fluctuations vanishes. Then Q_1 drops quickly to its smallest value at the kink and the shift of the kink is clear as was discussed above. As r_a increases, Q rises and statistics remain sub-Poissonian for the whole range of time while the injection rate is not high enough for fluctuations to exceed the mean. As soon as r_a becomes large, Q_1 turns to be positive and statistics of the field are super-Poissonian. The response of Q to the variation in the injection rate in steady-state is depicted in Figure 4.4(a). It is increasing almost linearly and the statistics change from sub-Poissonian at small values of r_a to super-Poissonian at large values of r_a . Since the mean increases also, the increase in Q_1 means higher fluctuations according to Equation 4.56.

4.6.1.5 On Distribution $P_{n_1 n_2}$

Since the width of the distribution indicates the number of fluctuations, the photon distribution is expected to be wide as the mean photon number increases due to injection. This is clearly represented in the 3D plot of the function $P_{n_1 n_2}$ in Figure 4.12i. The figure shows the variation of the distribution at three values of r_a : (a) $r_a = 20\kappa$, (b) $r_a = 35\kappa$, and (c) $r_a = 50\kappa$. In the same figure, the marginal or single-mode distribution is plotted for the two modes, P_{n_1} in black color and P_{n_2} in red color projected on their corresponding

Effects of injection rate, detuning, and Kerr parameter on dynamics of the Mandel parameter (sub-Poissonian statistics, $Q_{1,2} < 0$).

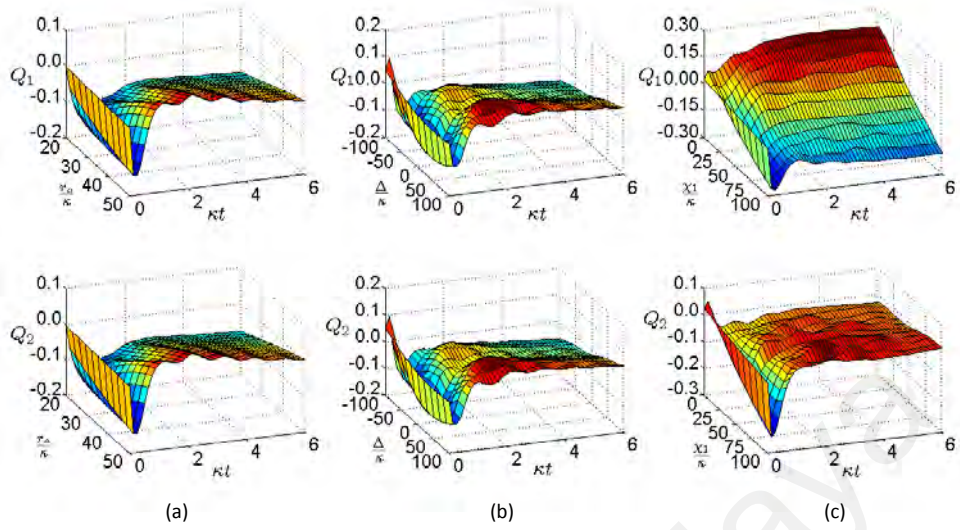


Figure 4.10: Q_1 (upper panel) and Q_2 (lower panel). The dynamics and parameter dependence for: (a) injection rate r_a ($\Delta = 0$, $\chi_1 = 50\kappa$), (b) detuning Δ ($r_a = 40\kappa$, $\chi_1 = 50\kappa$), and (c) Kerr parameter χ_1 ($r_a = 40\kappa$, $\Delta = 0$).

Dynamics of the Mandel parameter (sub-Poissonian statistics, $Q_{1,2} < 0$): Effects of injection rate, detuning, and Kerr parameter.

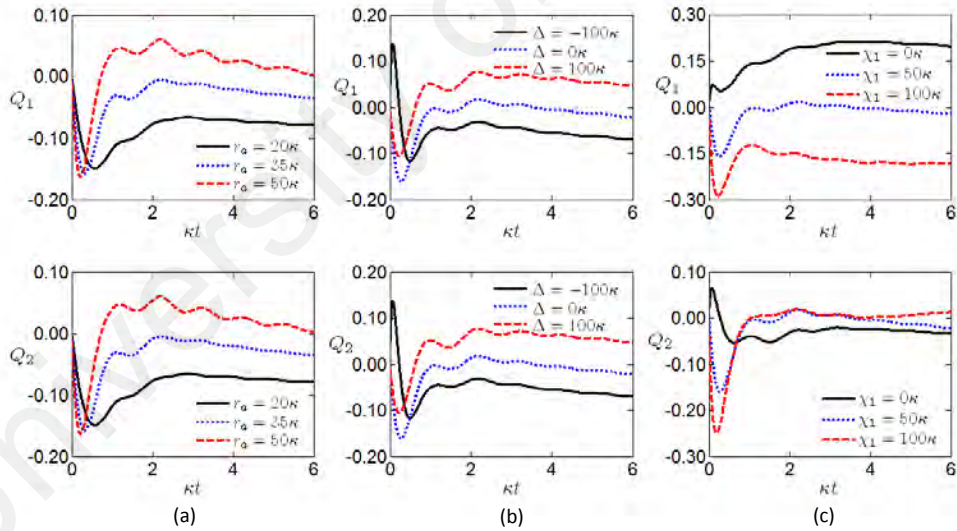


Figure 4.11: Q_1 (upper panel) and Q_2 (lower panel). The dynamics for: (a) $\Delta = 0$, $\chi_1 = 50\kappa$, (b) $r_a = 40\kappa$, $\chi_1 = 50\kappa$, and (c) $r_a = 40\kappa$, $\Delta = 0$.

axis. Also, to study the width of the distribution, its FWHM is shown through the contour lines represented by the ellipses. The two crossed lines, in Figures 4.12i(a) and 4.12i(c), represent projection of the width on each axis, i.e. they represent the width of each single-mode distribution. The vertical line is the width of the first mode and the horizontal line is the

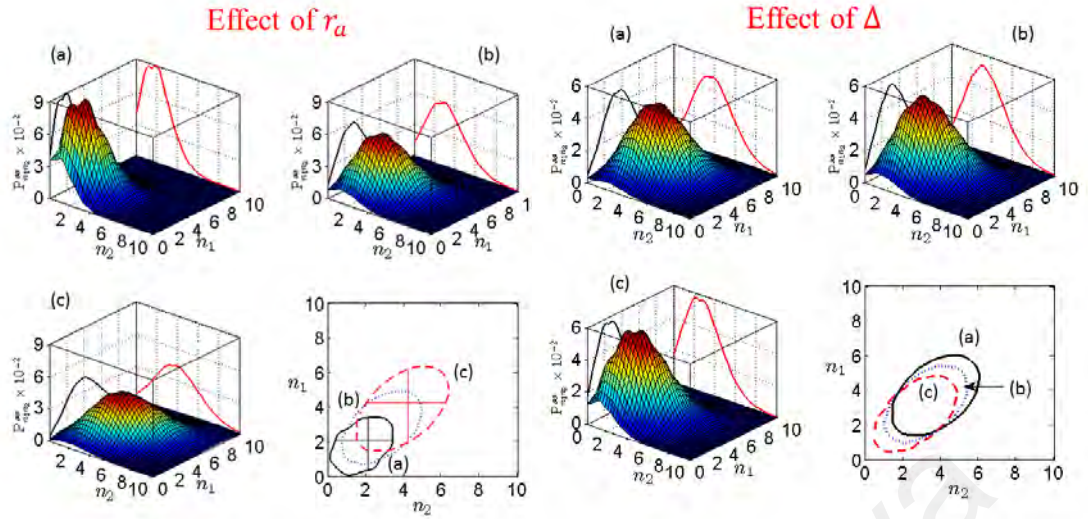
width of the second mode. The mean values $\langle n_1 \rangle$ and $\langle n_2 \rangle$ lie on the cross point of the two lines. Width of first mode distribution, P_{n_1} , is equal to width of the second mode distribution, P_{n_2} because the system is symmetric for the two modes, and $P_{n_1} = P_{n_2}$. This symmetry will break when the effect of χ_1 is discussed. By looking at Figure 4.12 an increase in size of the contours is observed which indicates that width of the distribution $P_{n_1 n_2}$ is increasing when injection rate increases from $r_a = 20\kappa$ in Figure 4.12i(a) to $r_a = 50\kappa$ in Figure 4.12i(c). So, the injection rate widens photon number distribution which is consistent with the effect on both mean photon number and Q . This result explains and supports the discussion on increasing fluctuations.

4.6.2 Effects of Detuning

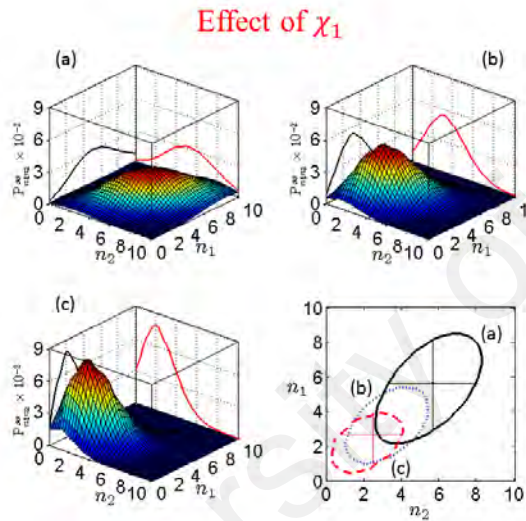
In this subsection, the effects of detuning Δ are discussed in a similar way to the discussion for the effect of the injection rate.

4.6.2.1 On Mean Photon Number

The effects of detuning on dynamics of the mean photon number are shown on the upper panels of Figure 4.2(b) and Figure 4.3(b). The increase in detuning lowers the mean photon number as can be seen when detuning changes from $\Delta = 0$ to $\Delta = 100\kappa$. It is interesting to notice the effect of the sign of detuning. The results show that the mean photon number is greater for negative detuning, $\Delta < 0$, than for positive detuning, $\Delta > 0$ which supports the early discussion. This is true due to the frequency-shift made by the Kerr effect as was shown previously. The effect of detuning on mean photon number is clearly shown for the steady-state in Figure 4.4 that demonstrates the argument presented and confirms the prediction of Equations 4.44 and 4.46. The decrease in the average, $\langle n_j \rangle$, $j = 1, 2$ due to detuning, is linear as Equation 4.46 predicts and Figure 4.4 confirms. How this result will affect other quantities will be shown.



- (i) Statistics at $\chi_1 = 50\kappa$, $\Delta = 0$ for: (ii) Statistics at $r_a = 40\kappa$, $\chi_1 = 50\kappa$ for:
 (a) $r_a = 20\kappa$, (b) $r_a = 35\kappa$, and (c) $r_a = 50\kappa$ (a) $\Delta = -100\kappa$, (b) $\Delta = 0$, and (c) $\Delta = 100\kappa$



- (iii) Statistics at $r_a = 40\kappa$, $\Delta = 0$ for:
 (a) $\chi_1 = 0\kappa$, (b) $\chi_1 = 50$, and (c) $\chi_1 = 100\kappa$

Figure 4.12: The statistics distribution function $P_{n_1 n_2}$, its contours (ellipses) at FWHM, and the single-mode distributions P_{n_1} in black color and P_{n_2} in red color, for each mode for: (i) injection rate r_a , (ii) detuning Δ , and (iii) Kerr parameter χ_1 . The distributions and their contours are evaluated at each of the three values. The vertical (horizontal) line in contours represents width of the distribution P_{n_1} (P_{n_2}). The coordinate of the cross point of the two lines are the averages $(\langle n_1 \rangle, \langle n_1 \rangle)$.

4.6.2.2 On $G^{(2)}$ and CSI

The dynamics of $g_{11}^{(2)}$ and $g_{22}^{(2)}$ in Figures 4.5(b), 4.6(b) are, initially, larger for negative detuning than for positive detuning before the situation is swiftly reversed. The results manifest, in the case of negative detuning, a fast change of statistics from super-Poissonian (at initial time) to sub-Poissonian. For non-negative detuning, statistics start from sub-Poissonian before they change, in a time not longer than $\kappa t \approx 0.8$, to Poissonian, for not large detuning, and to super-Poissonian for large detuning. The field maintains its statistics,

for the rest of time, to be super-Poissonian, for large positive detuning, and sub-Poissonian for negative or small detuning. In steady-state, $G^{(2)}$ shown in Figure 4.9(b) exhibit this obviously. For $g_{12}^{(2)}$, depicted on Figures 4.7(b) and 4.8(b), initially, it becomes stronger at high detuning and reaches its lowest value when $\Delta = 0$ but later it reduces as detuning changes from the far negative to the far positive which is demonstrated well in Figure 4.9(b). This result may be explained by the fact that close to resonance ($\Delta < 0$ in the present study) coupling becomes stronger. So, correlations are reduced as Δ increases negative to positive. The consequence of detuning effects on $g_{11}^{(2)}$, $g_{22}^{(2)}$, and $g_{12}^{(2)}$ is demonstrated by their violation for CSI ($F_{cs} > 0$) that demonstrates nonclassicality of the field shown in Figures 4.7(b), 4.8(b), and 4.9(b). Violation increases gradually as detuning takes its values from negative to positive. The violation is stronger in the beginning but it becomes weak when the system approaches steady-state. The increase in F_{cs} is due to the reduction in $g_{12}^{(2)}$. It is interesting to notice that statistics are more sub-Poissonian for negative values of detuning but more nonclassical for positive values. This is understood since statistics come from $g_{11}^{(2)}$ and $g_{22}^{(2)}$ which inform us about fluctuations but violations depends mostly on inter-mode correlations which comes from $g_{12}^{(2)}$.

4.6.2.3 On Entanglement

The probe of entanglement through the function E shows that the two modes are not entangled since $E < 0$ for the whole time as shown in Figures 4.2(b) and 4.3(b). The increase in detuning reduces correlations which excludes any possibility for entanglement. The effect of detuning, in this sense, is similar to that is discussed for the effect of the injection rate. However, as results presented in Figure 4.9(b) shows, the function E increases when Δ changes from negative to positive.

4.6.2.4 On Mandel Q Parameter

Effects of detuning on Mandel Q parameter are exhibited in Figures 4.10(b), 4.11(b), and 4.4(b). The dynamics show a drop in Q in the beginning and the noticeable kink at which the lowest values of fluctuations take place as was found previously. Later, Q rises and statistics remain sub-Poissonian for the whole range of time while detuning is negative or has small values. In a short time and for large detuning, the field statistics change from sub-Poissonian to super-Poissonian for the whole range of time. The effect is more important in the steady-state that is demonstrated in Figure 4.4(b). As detuning changes from the far negative to the far positive, Q increases and statistics show a transition from sub-Poissonian to super-Poissonian. However, according to 4.56, the relative fluctuations increase but the fluctuations decrease since the drop in mean photon number is greater than the rise in Q .

4.6.2.5 On Distribution $P_{n_1 n_2}$

The effect of detuning on the two-mode distribution function $P_{n_1 n_2}$ and the single-mode distribution functions P_{n_1} , P_{n_2} are shown in Figure 4.12ii. The effect of detuning is similar to the injection rate effect. As was discussed earlier, fluctuations are reduced by increasing detuning as can be seen from the shrinking in size of the contours, though they are small. Figure shows reduction in widths of the distributions as detuning increases and mean photon number decrease starting from $\Delta = -100\kappa$ in Figure 4.12ii(a) to $\Delta = 100\kappa$ in Figure 4.12ii(c). This reduction in the width is accompanied by a reduction in the mean number of photons. So, there is no contradiction with the fact that statistics become super-Poissonian when detuning increases. The peaks of the distributions increase and shifted towards smaller values of photon numbers, which is the opposite effect to their counterparts when the influence of the injection rate was discussed.

4.6.3 Effects of Kerr parameter

It is interesting to see the effect of Kerr parameter χ_1 on the quantities that already were discussed above and how much different the effect on properties of each mode will be. Kerr parameter χ_1 (and analogously χ_2) has a stronger effect on the field properties. It has some similarities with detuning effects as can be observed from their corresponding figures. However, the difference is significant since the Kerr parameter takes its role through the intensity.

4.6.3.1 On Mean Photon Number

The effects of injection rate and detuning on mean photon numbers are found to be almost linear. However, a noticeable nonlinear dependence is expected in the case of the Kerr parameter because it is combined with the intensity. Mean photon number $\langle n_1 \rangle$ dynamics with Kerr parameter dependence is shown in Figures 4.2(c) and Figure 4.3(c). The effect is similar to that of detuning but stronger. The increase in the Kerr parameter lowers the mean photon number since χ_1 rises the effective detuning through the intensity of the first mode. The reduction in $\langle n_1 \rangle$ when Kerr parameter increases from $\chi_1 = 0$ to $\chi_1 = 50\kappa$ is larger than the corresponding increase from $\chi_1 = 50\kappa$ to $\chi_1 = 100\kappa$ as shown in Figure 4.3(c). So, Mean photon number reduces nonlinearly with χ_1 which is consistent with the analytic result in Equation 4.46 and clearly depicted in Figure 4.4(c).

4.6.3.2 On $G^{(2)}$ and CSI

The effects of χ_1 on $g_{11}^{(2)}$ and $g_{22}^{(2)}$ dynamics are presented in Figures 4.5(c), 4.6(c). In the beginning, $g_{11}^{(2)}$ and $g_{22}^{(2)}$ are large for $\chi_1 = 0$ and become smaller as χ_1 increase. Soon, they reach a steady-state where the correlation for larger χ_1 is smaller in the first mode and the opposite in the second mode. Results display stronger effects on $g_{11}^{(2)}$ than on $g_{22}^{(2)}$ in contrast to the effects in the cases of injection rate and detuning. It also predicts that

statistics of the first mode are sub-Poissonian for large values of χ_1 but a little effect on the second mode. For $g_{12}^{(2)}$ and CSI, their dynamics are exhibited in Figures 4.7(c), 4.8(c) that show higher inter-mode correlation in the beginning similar to what is already observed in the effects of r_a and Δ but χ_1 almost has no effect. The effects on CSI is much similar to the effects of detuning in which a high violation in the beginning is seen then soon becomes weak. The weakness in the nonclassicality is due to the drop in inter-mode correlation. For steady-state, effects of Kerr parameter χ_1 on $g_{12}^{(2)}$ and F_{cs} are demonstrated in Figures 4.9(c). The inter-mode correlation, $g_{12}^{(2)}$ starts from $\kappa t = 1.1$ for $\chi_1 = 0$ and slowly rises with the increase in χ_1 . The single-mode correlation, $g_{11}^{(2)}$ starts from $g_{11}^{(2)} > 1$ which indicates super-Poissonian statistics and ends up with $g_{11}^{(2)} < 1$. Whereas, for the second mode it starts from $g_{22}^{(2)} < 1$ and reaches $g_{22}^{(2)} > 1$. This means that statistics of the two modes change from super-Poissonian to sub-Poissonian for the first mode but from sub-Poissonian to super-Poissonian for the second mode. The change happens when their $\chi_1 = \chi_2$. These changes are due to fluctuations that will be discussed in studying the effects on Q . The violation in CSI increases, approximately linearly; proportional to $g_{12}^{(2)}$.

4.6.3.3 On Entanglement

The correlation between modes rises and fluctuations decrease as χ_1 rises, so an increase in E is expected and this is the case as dynamics in Figures 4.2(c), 4.3(c) shows. The increase in χ_1 lowers mean photon numbers $\langle n_1 \rangle$, $\langle n_2 \rangle$ and, as was discussed earlier, the last term in the expression of E given by Equation 4.63 becomes less. The increase in E is nonlinear as the contribution comes to it almost from the last term that is exhibited in Figure 4.9(c) which was explained before. So, the results predicts no entanglement and Kerr parameter χ_1 boosts the field closely to an entangled state.

4.6.3.4 On Mandel Q Parameter

The effects of χ_1 on Q are prominent as results exhibit in Figures 4.10(c), 4.11(c) for their dynamics and in Figure 4.4(c) for their steady-state. The kinks in Q_1 and Q_2 are very obvious in which the lowest values of fluctuations take place. At the kink, Q_1 reaches its lowest value close to -0.30 . After that, fluctuations develop and reach their steady-state where χ_1 greatly reduces fluctuations in the first mode but lightly enhances fluctuations in the second mode. Fluctuations in the first mode are less than fluctuations in the second mode. As have been shown in the discussion of $G^{(2)}$, which is very obvious for Q , the two modes have statistics transition from super-Poissonian to sub-Poissonian in the first mode and from super-Poissonian to sub-Poissonian in the second mode; the magnitude of this change is large in the first mode. The transition occurs at $c\chi_1 = \chi_2$ and in which $Q_1 > Q_2$ for $\chi_1 < \chi_2$ and $Q_1 < Q_2$ for $\chi_1 > \chi_2$.

4.6.3.5 On Distribution $P_{n_1 n_2}$

The probability to measure a specific number of photons in the first mode in the cavity is higher than to measure them in the second mode. This means that at the same mean photon number, P_{n_1} is narrower than P_{n_2} for $\chi_1 > \chi_2$ and vice versa as was presented in the discussion of the effects of χ_1 on Q . This implies large squeezing in photon number for the first mode for $\chi_1 > \chi_2$ and small squeezing in photon number for the second mode for $\chi_1 < \chi_2$. This is exhibited in Figure 4.12iii(c) and the sizes of contours. The two crossed lines shown on the contours demonstrate the case as in the discussion of injection rate effects. In the present case, it is noticeable that the ellipse has been rotated clockwise as χ_1 increased (by symmetry, the rotation will be anticlockwise when χ_2). This makes the vertical line and the minor axis of the ellipse close to each other and the horizontal line and the major axis closer. The meaning is that the width of the distribution P_{n_1} is less than the width of P_{n_2} for this case $\chi_1 > \chi_2$. This is the breaking of symmetry that

was discussed early. It is to notice that the Kerr parameter χ_1 decrease the mean photon number of each mode simultaneously, $\langle n_1 \rangle = \langle n_2 \rangle$ but the fluctuations are different for $\chi_1 \neq \chi_2$. The implication of this result is variation in the field quadratures if each mode due to change in the phase.

4.6.4 Approximate Solution: Agreement and Justification

The point that is presented here is a discussion of the agreement between exact results from the simulation and analytic results from the approximation. Figure 4.13 shows a few exact and analytic results side by side. The comparison is to justify the assumptions that were made for deriving the analytic results and to what extent their validity and the discussion that can be built on. The upper panel of Figure 4.13(a, b) shows the agreement for the real part of the off-diagonal elements of the density matrix $\rho_{n_1 n_2; n_1+1 n_2+1}$ at steady-state for $n_1 = n_2 = 6$ against detuning and Kerr parameter χ_1 . The exact result comes from the solution of the density Equation 4.12 and the approximate solution given in Equation 4.26. The results show a good agreement, and this justifies the approximation used for the off-diagonal elements, which is given by Equation 4.26. The lower panel of Figure 4.13(a, b) shows the mean photon number $\langle n_1 \rangle$ against detuning Δ and Kerr parameter χ_1 for the exact and two expressions for the approximate solution; one is the solution of the quadratic expression, Equation 4.44, and the other is the solution of the fifth-degree polynomial, Equation 4.41. Also, there is a good agreement. Below, a possible explanation for the differences between the exact and approximate solutions is provided. On the right panel and at steady-state, Figure 4.13(c, d), the statistics function, mean photon number, and F_{cs} are depicted for $r_a = 40\kappa$, $\Delta = 0$ and for initial atom density matrix $\rho_{aa} = 1$, $\rho_{bb} = 0$, $\rho_{ab} = 0$. The atom density matrix element $\rho_{bb} = 0$ is chosen to abide by condition of validity of Equation 4.73. The statistics function $P_{n_1 n_2}$ at $\chi_1 = 50\kappa$ shows acceptable agreement. Also, the mean photon number $\langle n_1 \rangle$ and F_{cs} show a good agreement. The

mean $\langle n_1 \rangle$ on the right panel is greater than the one on the left because inversion on the right ($\rho_{aa} - \rho_{bb} = 1$) is higher than inversion for the left panel ($\rho_{aa} - \rho_{bb} = 0.8$) and the agreement is better since the part of the error due to approximation is removed.

Agreement: Exact and approximation at steady-state.

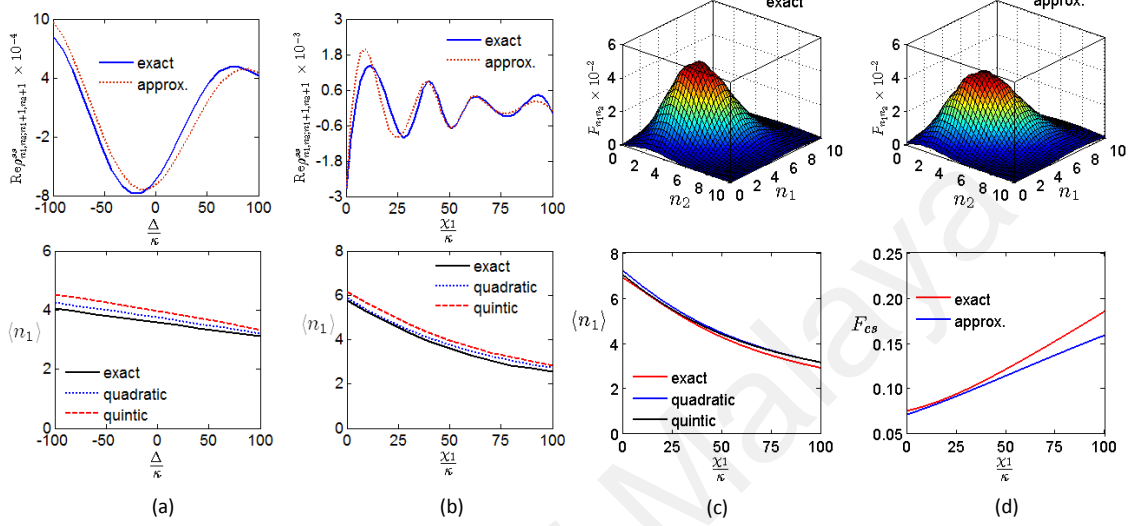


Figure 4.13: Agreement between the exact solution and the analytic approximation at steady-state: (a, b) real part of $\rho_{n_1 n_2; n_1+1 n_2+1}$ (Equations 4.12 and 4.26 at $n_1 = n_2 = 6$) and $\langle n_1 \rangle$ (solution of the quadratic and quintic expressions, Equation 4.44 and Equation 4.41) for (a) $r_a = 40\kappa$, $\chi_1 = 50\kappa$ and (b) $r_a = 40\kappa$, $\Delta = 0$. (c-d) for $r_a = 40\kappa$, $\Delta = 0$, $\rho_{bb} = 0$; $P_{n_1 n_2}$ (at $\chi_1 = 50\kappa$), $\langle n_1 \rangle$, and F_{CS} .

There are two likely causes for the differences between the exact and the analytic solutions:

First the analytic is valid above threshold for large number of photons which might be not fulfilled exactly in the exact solution due to computation capacity. The second reason is due to neglecting correlations in the solution for the moments. In order to solve the system of the moments in Equation 4.30, it was necessary to decouple them. The averages $\langle n_j L_{n_1, n_2} \rangle$ and $\langle n_j M_{n_1 n_2}^- \rangle$ are decorrelated to the first order. Then, to obtain a solution for the mean photon number $\langle n_j \rangle_{ss}$, the average $\langle L_{n_1, n_2} \rangle_{ss}$ (i.e. $\langle L_{n_1, n_2} \rangle_{ss} \approx L_{\langle n_1 \rangle_{ss} \langle n_2 \rangle_{ss}}$) is decorrelated in which the zeroth (uncorrelated) term was used. The source of the differences is due to ignoring the fluctuations in solving those equations. If one needs more accurate result one has to solve the coupled equations and keep the second order correlations in the Taylor

expansion of $\langle L_{n_1, n_2} \rangle_{ss}$ around the means

$$\begin{aligned} \langle L_{n_1, n_2} \rangle_{ss} &\approx L \langle n_1 \rangle_{ss} \langle n_2 \rangle_{ss} + l_{20} \left(\langle n_1^2 \rangle_{ss} - \langle n_1 \rangle_{ss}^2 \right) \\ &\quad + l_{02} \left(\langle n_2^2 \rangle_{ss} - \langle n_2 \rangle_{ss}^2 \right) \\ &\quad + l_{11} \left(\langle n_1 n_2 \rangle_{ss} - \langle n_1 \rangle_{ss} \langle n_2 \rangle_{ss} \right), \end{aligned} \tag{4.83}$$

where the coefficients l_{20} , l_{11} , and l_{02} are rational functions of $\langle n_1 \rangle_{ss}$ and $\langle n_2 \rangle_{ss}$. In solving for the mean the first term of the above equation was taken and the fluctuations are completely ignored.

University of Malaysia

CHAPTER 5: TWO-PHOTON LASER WITH (SELF & CROSS) KERR EFFECT AND IDC

5.1 Introduction

In Chapter 4, the role of the self-Kerr effect on the dynamics of the TPL is studied. The self-Kerr effect is a cause of many phenomena such as self-focusing. However, when the two modes interact, the mutual interaction energy must be included. This interaction energy or what is known by the cross-Kerr effect plays an important role also (Khan et al., 2015). Cross-phase modulation is one of them. Both self- and cross-Kerr effects have many applications in communication and fiber optics (Semiao et al., 2009). Since the Kerr effect is a result of third-order nonlinearity in the induced polarization of the medium, the interaction process is said to be intensity-dependent. The nonlinear part of the refractive index depends on the intensity. The TPL itself is considered as a nonlinear interaction process. These ideas lead researchers to investigate the role of the nonlinear interaction coupling strength, *i.e.* the intensity-dependence of the coupling between the field and the atoms of the medium (Bužek & Jex, 1990; Singh & Ooi, 2018; Singh et al., 2012; Singh & Gilhare, 2016a; Bartzis, 1990; Napoli & Messina, 1996; Gao et al., 2002). This kind of nonlinearity and its impact on entanglement and the dynamics and properties of the field and the atoms were investigated for a single atom (Faghihi et al., 2013) and two atoms (Ghorbani et al., 2017). In this chapter, the study in Chapter 4 is extended to investigate the role of the cross-Kerr effect and the IDC on the TPL. The role of both self- and cross-Kerr effects in the dynamics of the system is studied. How the properties of the field and statistics depend on the Kerr effect and IDC are investigated. A recent study of a single atom two-mode cavity field in a non-dissipative cavity filled with Kerr-like medium is investigated (Singh & Ooi, 2018). The researchers studied the dynamics of the atom and the field. These studies gave us the motivation to study the effect of the nonlinearity of

Kerr-type on the dynamics and nonclassicality of the TPL.

Along the same line in the previous chapter, the statistical properties of a nondegenerate TPL in Kerr-like medium in a dissipative cavity are studied and the effects of Kerr parameters on the statistical properties and distribution function of two modes of lasing photons are analyzed. In the second section, the model and its Hamiltonian in the interaction picture are presented. In the third section, the photon statistics equation is studied. The field characterization measures are calculated in the fourth section. The calculations carried out for the mean photon number, the moments, $G^{(2)}$, Q , the entanglement, and the CSI. The photon statistics function is presented in the fifth section. The last section is devoted to the discussion of the results of the numerical and analytic solutions.

5.2 Model and Laser Master Equation

In this model, the extension is in two directions. First, the two modes are allowed to have mutual interaction through the Kerr media. So, in the Hamiltonian, besides the self-Kerr, quantified by the parameters χ_1 and χ_2 , there is also the cross-Kerr, represented by the parameter χ . These parameters χ_1 , χ_2 , and χ are proportional to the third-order susceptibility of the medium $\chi^{(3)}$ (optical Kerr effect). The second, the coupling between the atoms and the field is assumed to be IDC represented by the function $F = F(a_1^\dagger a_1, a_2^\dagger a_2)$. In the analysis of the problem in this chapter, the effect of the coupling function of the form $F(a_1^\dagger a_1, a_2^\dagger a_2) = \sqrt{a_1^\dagger a_1 + 1} \sqrt{a_2^\dagger a_2 + 1}$ is studied, but in the general master equation, the function F is general and takes any form. The effective Hamiltonian of the system in the dipole approximation and rotating wave approximation is the sum of the free H_0 and interaction H_I Hamiltonians

$$H = H_0 + H_I, \quad (5.1a)$$

where

$$H_0 = \sum_j \frac{1}{2} \hbar \omega \sigma_j^z + \sum_{k=1,2} \hbar \left(\nu_k a_k^\dagger a_k + \chi_k a_k^{\dagger 2} a_k^2 \right) + \hbar \chi a_1^\dagger a_1 a_2^\dagger a_2, \quad (5.1b)$$

$$H_I = \sum_j \hbar \left[g \sigma_j^+ F(a_1^\dagger a_1, a_2^\dagger a_2) a_1 a_2 + g^* \sigma_j^- a_1^\dagger a_2^\dagger F^\dagger(a_1^\dagger a_1, a_2^\dagger a_2) \right]. \quad (5.1c)$$

Using the unitary transformation $U_0 = e^{-iH_0 t/\hbar}$, the Hamiltonian Equation 5.1b in the interaction picture takes the form (for the calculations, see Appendix B)

$$V = U_0^\dagger H_I U_0 = \sum_j V_j, \quad (5.2a)$$

$$V_j = \hbar g F \exp \left[-i2 \left(\delta + q_1 a_1^\dagger a_1 + q_2 a_2^\dagger a_2 \right) t \right] \sigma_j^+ a_1 a_2 + \text{h. c.} \quad (5.2b)$$

where (from Appendix B and for $k = 1, 2$)

$$q_k = \chi_k + \frac{1}{2} \chi, \quad (5.3)$$

$$\delta = \frac{1}{2} (\Delta + \chi). \quad (5.4)$$

The cross-Kerr effect has two actions as Equations 5.3 and 5.4 predict. It enhances the self-Kerr effect of each mode equally and modifies the detuning which means shifting the energy levels. Similar to the presentation given in Chapter 4 (see Appendices C and D for details), the laser master equation based on Scully-Lamb theory has the same form of the master equation in Equation 4.12. The difference is in the coefficients $D_{n_1 n_2}$ and $B_{n_1 n_2}$ that are modified by the cross-Kerr parameter χ and the IDC, F , where they become

$$D_{n_1 n_2} = \gamma^{-1} [\delta + q_1 (n_1 - 1) + q_2 (n_2 - 1)], \quad (5.5)$$

$$B_{n_1 n_2} = \gamma^{-1} g \sqrt{n_1 n_2} F(n_1 - 1, n_2 - 1). \quad (5.6)$$

These coefficients are used in Appendix C. Since there is no change in the general form of the density matrix by adding the cross-Kerr parameter and the IDC, the discussion refers to Equation 4.12 when the master equation is mentioned.

In the next section, the photon statistics, $P_{n_1 n_2} = \rho_{n_1 n_2; n_1 n_2}$ will be studied. Since the IDC function F appears explicitly in the coefficients $L_{n_1 n_2}$ and $K_{n_1 n_2}$ of the distribution equation $\dot{P}_{n_1 n_2}$, the statistics equation is rewritten for easy reference.

5.3 The Laser Rate Equation

The time evolution of the diagonal elements of the density matrix, Equation 4.23 with its modified coefficients, reads

$$\begin{aligned}
\dot{P}_{n_1 n_2} = & -r_a (\rho_{aa} L_{n_1+1 n_2+1} + \rho_{bb} L_{n_1 n_2}) P_{n_1 n_2} \\
& + r_a (\rho_{aa} L_{n_1 n_2} P_{n_1-1 n_2-1} + r_a \rho_{bb} L_{n_1+1 n_2+1} P_{n_1+1 n_2+1}) \\
& - i r_a (\rho_{ba} K_{n_1+1 n_2+1} \rho_{n_1+1 n_2+1; n_1 n_2} e^{-i2D_{n_1+1 n_2+1} \gamma t} + \text{h.c.}) \\
& + i r_a (\rho_{ba} K_{n_1 n_2} \rho_{n_1 n_2; n_1-1 n_2-1} e^{-i2D_{n_1 n_2} \gamma t} + \text{h.c.}) \\
& + \kappa_1 (n_1 + 1) P_{n_1+1, n_2} + \kappa_2 (n_2 + 1) P_{n_1, n_2+1} - \kappa_1 n_1 P_{n_1 n_2} - \kappa_2 n_2 P_{n_1 n_2},
\end{aligned} \tag{5.7}$$

where population and coherence coupling strength coefficients

$$L_{n_1 n_2} = \frac{2\gamma^{-2} |g|^2 n_1 n_2 |F_{n_1-1, n_2-1}|^2}{1 + 4\gamma^{-2} (\delta_q + q_1 n_1 + q_2 n_2)^2 + 4\gamma^{-2} |g|^2 n_1 n_2 |F_{n_1-1, n_2-1}|^2}, \tag{5.8a}$$

$$K_{n_1 n_2} = \frac{\gamma^{-1} g \sqrt{n_1 n_2} F_{n_1-1, n_2-1} [1 - i2\gamma^{-1} (\delta_q + q_1 n_1 + q_2 n_2)]}{1 + 4\gamma^{-2} (\delta_q + q_1 n_1 + q_2 n_2)^2 + 4\gamma^{-2} |g|^2 n_1 n_2 |F_{n_1-1, n_2-1}|^2}, \tag{5.8b}$$

and

$$\delta_q = \delta - q_1 - q_2 = \frac{\Delta - \chi}{2} - \chi_1 - \chi_2. \tag{5.9}$$

To shorten notations, the function $F(n_1, n_2)$ is written as F_{n_1, n_2} which is the matrix elements of the operator $F(a_1^\dagger a_1, a_2^\dagger a_2)$, i.e. $F_{n_1, n_2} = \langle n_1, n_2 | F(a_1^\dagger a_1, a_2^\dagger a_2) | n_1, n_2 \rangle$.

It is worth briefly discuss the effect of Kerr parameters and IDC on the probability transition flow in Equation 5.7 phenomenologically. From Equation 5.8, the values of the coefficients $L_{n_1 n_2}$ and $K_{n_1 n_2}$ become small by increasing the Kerr parameters. The cross Kerr parameter enhances the contributions of the self-Kerr parameters of each mode. Also, these parameters change the phase of the coefficient $K_{n_1 n_2}$ and then the total phase of the off-diagonal terms in Equation 5.7. The result will be reflected in the sign of the contribution of these terms. These parameters lessen the values of $L_{n_1 n_2}$ and so the probability flow will decrease and growth in mean photon number will decrease and the intensity becomes less. When it comes to the effect of the IDC, F , it decreases the absolute value of $K_{n_1 n_2}$ but accelerates the growth of $L_{n_1 n_2}$. The effect of F is much greater than that of the Kerr parameters since the gain and saturation (see the single-photon laser, Equation 3.66) depends on F and become nonlinear. So, the IDC is expected to increase the mean photon number greatly. Later, the reflection of these effects on the correlations, fluctuations, and statistics of the field and its consequences on the nonclassicality of the field will be addressed.

Equation of the cavity field distribution, Equation 5.7, shows explicitly the oscillating nature of the off-diagonal elements terms in the third and fourth lines due to the time-dependent factors. The oscillation becomes fast at high intensity or large detuning. This means that these terms become small at high intensity or detuning and the coherence vanishes. The oscillation time of these time-dependent factors is

$$\tau_{n_1, n_2} = \frac{\pi}{\gamma} \frac{1}{|D_{n_1, n_2}|} = \frac{\pi}{|\delta_q + q_1 n_1 + q_2 n_2|}. \quad (5.10)$$

Equation 5.10 shows how this oscillation becomes fast as Kerr parameters, detuning, and

intensity (average mean photon number) become high.

Until now, the IDC, F is general but for the particular choice in this study, its elements are $F_{n_1, n_2} = F(n_1, n_2) = \sqrt{(n_1 + 1)(n_2 + 1)}$. Without loosing generality, the coupling strength, g , is taken to be real. For this particular choice, Equation 5.8 becomes

$$L_{n_1 n_2} = \frac{2\gamma^{-2} g^2 n_1^2 n_2^2}{1 + 4\gamma^{-2} (\delta_q + q_1 n_1 + q_2 n_2)^2 + 4\gamma^{-2} g^2 n_1^2 n_2^2}, \quad (5.11a)$$

$$K_{n_1 n_2} = \frac{\gamma^{-1} g n_1 n_2 [1 - i2\gamma^{-1} (\delta_q + q_1 n_1 + q_2 n_2)]}{1 + 4\gamma^{-2} (\delta_q + q_1 n_1 + q_2 n_2)^2 + 4\gamma^{-2} g^2 n_1^2 n_2^2}, \quad (5.11b)$$

The photon statistics in Equation 5.7 can be rewritten to show the coherence terms clearly Lu & Bergou (1989). For this goal, the complex quantities are written in polar form to show the phase explicitly.

$$\rho_{ab} = |\rho_{ab}| e^{i\theta}, \quad (5.12a)$$

$$K_{n_1+1n_2+1}^* = |K_{n_1+1n_2+1}| e^{i \arctan 2D_{n_1+1n_2+1}}, \quad (5.12b)$$

$$\rho_{n_1 n_2; n_1+1n_2+1} = |\rho_{n_1 n_2; n_1+1n_2+1}| e^{i\varphi_{n_1+1, n_2+1}(t)}. \quad (5.12c)$$

The total phase will be

$$\vartheta_{n_1, n_2}(t) = \theta + \arctan(2D_{n_1, n_2}) + 2D_{n_1, n_2} \gamma t + \varphi_{n_1, n_2}(t). \quad (5.13)$$

The phase $\varphi_{n_1, n_2}(t)$ of the density matrix Equation 5.12c is time-dependent. Using Equation

5.12, the photon distribution function Equation 5.7 is rewritten in the form

$$\begin{aligned}
\dot{P}_{n_1 n_2} = & - (r_a \rho_{aa} L_{n_1+1 n_2+1} + r_a \rho_{bb} L_{n_1 n_2}) P_{n_1 n_2} \\
& + r_a \rho_{aa} L_{n_1 n_2} P_{n_1-1 n_2-1} + r_a \rho_{bb} L_{n_1+1 n_2+1} P_{n_1+1 n_2+1} \\
& - 2r_a |\rho_{ab} K_{n_1+1 n_2+1} \rho_{n_1 n_2; n_1+1 n_2+1}| \sin \vartheta_{n_1+1, n_2+1}(t) \\
& + 2r_a |\rho_{ab} K_{n_1 n_2} \rho_{n_1-1 n_2-1; n_1 n_2}| \sin \vartheta_{n_1, n_2}(t) \\
& + \kappa_1 (n_1 + 1) P_{n_1+1, n_2} + \kappa_2 (n_2 + 1) P_{n_1, n_2+1} - (\kappa_1 n_1 + \kappa_2 n_2) P_{n_1 n_2}.
\end{aligned} \tag{5.14}$$

In Equation 5.14, the total phase ϑ_{n_1, n_2} controls the contribution of coherence to cavity field distribution function, P_{n_1, n_2} . For the phase angle $2k\pi < \vartheta_{n_1, n_2} < (2k+1)\pi$ (K is an integer), the coherence contribution from states $|n_1-1, n_2-1\rangle$ and $|n_1, n_2\rangle$ enhances the rate, $\dot{P}_{n_1 n_2}$ by stimulation the emission from state $|an_1-1, n_2-1\rangle$ to $|bn_1, n_2\rangle$ state, yet this phase, in the meantime, reduces the rate since it boosts stimulation emission from state $|an_1, n_2\rangle$ to $|bn_1+1, n_2+1\rangle$ state. On the contrary, as long as the phase angle $(2k+1)\pi < \vartheta_{n_1, n_2} < 2(k+1)\pi$, its role is reversed. The time, t_r , it takes for the action to reverse between these two states is a solution of $\varphi_{n_1, n_2}(t_r) + 2D_{n_1, n_2} \gamma t_r + \arctan(2D_{n_1, n_2}) + \theta = \pi$. It can be said that the phase angle controls the competition of stimulation emission between states; when it reduces the stimulation from one state, it improves it by reversing its direction for the other state. The phase can be controlled through the atomic coherence ρ_{ab} , detuning and Kerr parameters in D_{n_1, n_2} . The time-dependence of the phase appears explicitly in the third term and implicitly in the fourth term in Equation 5.13. By adjusting the values of Kerr parameters and detuning, one can produce desirable nonclassical states or statistics of the field such as sub-Poissonian statistics.

It is worth to emphasize here that an analytic solution to Equation 5.14 is hard to obtain even in a steady state situation. However, above threshold with sufficient mean photon numbers, the oscillation in the system becomes small and the system reaches a stationary

state. In this case, the total phase becomes constant. To achieve this state, the phase of the density matrix element $\rho_{n_1-1, n_2-1; n_1, n_2}$ must be, $\varphi_{n_1, n_2}(t) \approx \varphi_{n_1, n_2}^0 - 2D_{n_1, n_2}\gamma t$ and the total phase becomes $\vartheta_{n_1, n_2}^{ss} = \theta + \arctan 2D_{n_1, n_2} + \varphi_{n_1, n_2}^0$ (phase-locked), where φ_{n_1, n_2}^0 is a constant phase. This section is concluded by approximating the coherence part of Equation 5.7 in terms of the populations.

The density matrix element $\rho_{n_1-1, n_2-1; n_1, n_2}$ is obtained in the same way as have been done in Chapter 4. For its extensive, it is repeated here but with a little modification in notation. Under the same conditions it can be written as

$$\rho_{n_1-1, n_2-1; n_1, n_2} \approx \frac{i\rho_{ba}e^{-i2D_{n_1, n_2}\gamma t}}{\Gamma_{n_1-1, n_2-1; n_1, n_2}} (K_{n_1, n_2; n_1-1, n_2-1}P_{n_1-1, n_2-1} - K_{n_1, n_2; n_1+1, n_2+1}P_{n_1, n_2}), \quad (5.15)$$

where

$$\Gamma_{n_1-1, n_2-1; n_1, n_2} = \rho_{aa}L_{n_1, n_2; n_1+1, n_2+1} + \rho_{bb}L_{n_1, n_2; n_1-1, n_2-1} + \frac{1}{r_a} \sum_{j=1,2} \kappa_j \left(n_j - \frac{1}{2} \right). \quad (5.16)$$

In deriving Equation 5.15, the relations $L_{n_1', n_2'; n_1, n_2}^* = L_{n_1, n_2; n_1', n_2'}$ and $M_{n_1', n_2'; n_1, n_2}^* = K_{n_1, n_2; n_1', n_2'}$ (Equation D.23, Appendix D) are used. By using Equations 5.15 and 5.16 in Equation 5.7, the approximated rate equation becomes

$$\begin{aligned} \dot{P}_{n_1, n_2} = & - \left(r_a \rho_{aa} L_{n_1+1, n_2+1} + r_a \rho_{bb} L_{n_1, n_2} + 2r_a |\rho_{ba}|^2 \Lambda_{n_1, n_2} \right) P_{n_1, n_2} \\ & + \left(r_a \rho_{aa} L_{n_1, n_2} + 2r_a |\rho_{ba}|^2 \Lambda_{n_1-1, n_2-1}^- \right) P_{n_1-1, n_2-1} \\ & + \left(r_a \rho_{bb} L_{n_1+1, n_2+1} + 2r_a |\rho_{ba}|^2 \Lambda_{n_1+1, n_2+1}^+ \right) P_{n_1+1, n_2+1} \\ & + \kappa_1 (n_1 + 1) P_{n_1+1, n_2} + \kappa_2 (n_2 + 1) P_{n_1, n_2+1} - (\kappa_1 n_1 + \kappa_2 n_2) P_{n_1, n_2}, \end{aligned} \quad (5.17)$$

with

$$\Lambda_{n_1 n_2}^+ = \text{Re} \left(\frac{K_{n_1 n_2}^*}{\Gamma_{n_1-1, n_2-1; n_1 n_2}} K_{n_1 n_2; n_1+1, n_2+1} \right), \quad (5.18a)$$

$$\Lambda_{n_1 n_2}^- = \text{Re} \left(\frac{K_{n_1+1, n_2+1}^*}{\Gamma_{n_1 n_2; n_1+1, n_2+1}} K_{n_1+1, n_2+1; n_1 n_2} \right), \quad (5.18b)$$

$$\Lambda_{n_1 n_2} = \Lambda_{n_1 n_2}^+ + \Lambda_{n_1 n_2}^-. \quad (5.18c)$$

The expression of Equation 5.17 can be rewritten in simpler form

$$\begin{aligned} \dot{P}_{n_1 n_2} = & - (r_a L_{n_1, n_2}^+ + \kappa_1 n_1 + \kappa_2 n_2) P_{n_1 n_2} + \kappa_1 (n_1 + 1) P_{n_1+1, n_2} \\ & + \kappa_2 (n_2 + 1) P_{n_1, n_2+1} + \frac{1}{2} r_a \left[\begin{aligned} & (L_{n_1-1, n_2-1}^+ + L_{n_1-1, n_2-1}^-) P_{n_1-1, n_2-1} \\ & + (L_{n_1+1, n_2+1}^+ - L_{n_1+1, n_2+1}^-) P_{n_1+1, n_2+1} \end{aligned} \right], \quad (5.19) \end{aligned}$$

where

$$L_{n_1, n_2}^\pm = \rho_{aa} L_{n_1+1, n_2+1} \pm \rho_{bb} L_{n_1, n_2} \pm 2 |\rho_{ba}|^2 (\Lambda_{n_1 n_2}^+ \pm \Lambda_{n_1 n_2}^-). \quad (5.20)$$

Analytic approximation for the moments and statistics in a special situation ($\rho_{bb} = 0$) coming from Equation 5.19 will be presented in the same foot as in Chapter 4.

5.4 Field Nonclassicality and its Measures

In this section, the measurable quantities are calculated to study the field properties. The moments, $G^{(2)}$, and Q are studied. Also, the nonclassicality is investigated by studying the F_{CS} function. The entanglement criterion E is investigated.

5.4.1 Moments

The calculations of the moments will enable us to obtain $G^{(2)}$ later. The calculations of moments are easily found by multiplying Equation 5.19 by $n_1^r n_2^s$ and doing the sum

$$\begin{aligned}
 \sum_{n_1 n_2=0}^{\infty} n_1^r n_2^s \dot{P}_{n_1 n_2} = & - \sum_{n_1 n_2=0}^{\infty} (r_a L_{n_1, n_2}^+ + \kappa_1 n_1 + \kappa_2 n_2) n_1^r n_2^s P_{n_1 n_2} \\
 & + \frac{1}{2} r_a \sum_{n_1 n_2=0}^{\infty} (L_{n_1-1, n_2-1}^+ + L_{n_1-1, n_2-1}^-) n_1^r n_2^s P_{n_1-1 n_2-1} \\
 & + \frac{1}{2} r_a \sum_{n_1 n_2=0}^{\infty} (L_{n_1+1, n_2+1}^+ - L_{n_1+1, n_2+1}^-) n_1^r n_2^s P_{n_1+1 n_2+1} \\
 & + \kappa_1 \sum_{n_1 n_2=0}^{\infty} (n_1 + 1) n_1^r n_2^s P_{n_1+1, n_2} + \kappa_2 \sum_{n_1 n_2=0}^{\infty} (n_2 + 1) n_1^r n_2^s P_{n_1, n_2+1}.
 \end{aligned} \tag{5.21}$$

From the definition of average and making the right shift of the indices to regain the definition of average, the following general formula for equations of moments is obtained

$$\begin{aligned}
 \frac{d}{dt} \langle n_1^r n_2^s \rangle = & - \langle (r_a L_{n_1, n_2}^+ + \kappa_1 n_1 + \kappa_2 n_2) n_1^r n_2^s \rangle + \kappa_1 \langle n_1 (n_1 - 1)^r n_2^s \rangle \\
 & + \kappa_2 \langle n_1^r n_2 (n_2 - 1)^s \rangle + \frac{1}{2} r_a \langle (L_{n_1, n_2}^+ + L_{n_1, n_2}^-) (n_1 + 1)^r (n_2 + 1)^s \rangle \\
 & + \frac{1}{2} r_a \langle (L_{n_1, n_2}^+ - L_{n_1, n_2}^-) (n_1 - 1)^r (n_2 - 1)^s \rangle.
 \end{aligned} \tag{5.22}$$

The solution for 5.22 is impossible unless specific assumptions are made as presented below for the first moments. A general solution is given in Appendix H for the case $\rho_{bb} = 0$ under the assumptions that are presented in what follows using the generating function.

The first few moments are

$$\frac{d}{dt}\langle n_j \rangle = -\kappa_j \langle n_j \rangle + r_a \langle L_{n_1, n_2}^- \rangle; \quad j = 1, 2, \quad (5.23a)$$

$$\frac{d}{dt}\langle n_j^2 \rangle = -2\kappa_j \langle n_j^2 \rangle + \kappa_j \langle n_j \rangle + 2r_a \langle n_j L_{n_1, n_2}^- \rangle + r_a \langle L_{n_1, n_2}^+ \rangle, \quad (5.23b)$$

$$\frac{d}{dt}\langle n_1 n_2 \rangle = -(\kappa_1 + \kappa_2) \langle n_1 n_2 \rangle + r_a \langle (n_1 + n_2) L_{n_1, n_2}^- \rangle + r_a \langle L_{n_1, n_2}^+ \rangle. \quad (5.23c)$$

The system in Equation 5.23 is difficult to solve as has been discussed in Chapter 4. Far from threshold (large mean photon-numbers), the quantities $L_{n_1, n_2}(\Lambda_{n_1 n_2}^\pm)$ are slowly growing (decaying) functions of orders $O(1)$ ($O(\langle n \rangle^{-3})$), where $\langle n \rangle = \langle n_1 + n_2 \rangle$, the total mean photon number. So at large values of photon numbers, the changes in these quantities are very small. Taking this into account, the averages $\langle L_{n_1, n_2}^\pm \rangle$ can be approximated by their steady-state values, $\langle L_{n_1, n_2}^\pm \rangle \approx \langle L_{n_1, n_2}^\pm \rangle_{ss}$ then decorrelate the averages such as $\langle n_j L_{n_1, n_2}^\pm \rangle \approx \langle L_{n_1, n_2}^\pm \rangle_{ss} \langle n_j \rangle$; $j = 1, 2$. Employing these arguments, Equation 5.23 are rewritten as

$$\frac{d}{dt}\langle n_j \rangle = -\kappa_j \langle n_j \rangle + r_a \langle L_{n_1, n_2}^- \rangle_{ss}; \quad j = 1, 2, \quad (5.24a)$$

$$\frac{d}{dt}\langle n_j^2 \rangle = -2\kappa_j \langle n_j^2 \rangle + \kappa_j \langle n_j \rangle + 2r_a \langle L_{n_1, n_2}^- \rangle_{ss} \langle n_j \rangle + r_a \langle L_{n_1, n_2}^+ \rangle_{ss}, \quad (5.24b)$$

$$\frac{d}{dt}\langle n_1 n_2 \rangle = -(\kappa_1 + \kappa_2) \langle n_1 n_2 \rangle + r_a \langle L_{n_1, n_2}^- \rangle_{ss} \langle n_1 + n_2 \rangle + r_a \langle L_{n_1, n_2}^+ \rangle_{ss}. \quad (5.24c)$$

The steady-state of moments in Equation 5.24 are

$$\kappa_j \langle n_j \rangle_{ss} = r_a \langle L_{n_1, n_2}^- \rangle_{ss}; \quad j = 1, 2, \quad (5.25a)$$

$$2\kappa_j \langle n_j^2 \rangle_{ss} = \kappa_j \langle n_j \rangle_{ss} + 2r_a \langle n_j \rangle_{ss} \langle L_{n_1, n_2}^- \rangle_{ss} + r_a \langle L_{n_1, n_2}^+ \rangle_{ss}, \quad (5.25b)$$

$$(\kappa_1 + \kappa_2) \langle n_1 n_2 \rangle_{ss} = r_a \langle n_1 + n_2 \rangle_{ss} \langle L_{n_1, n_2}^- \rangle_{ss} + r_a \langle L_{n_1, n_2}^+ \rangle_{ss}. \quad (5.25c)$$

The moments in Equation 5.25 can be rewritten as

$$\langle n_j \rangle_{ss} = \frac{r_a}{\kappa_j} \langle L_{n_1, n_2}^- \rangle_{ss} ; j = 1, 2, \quad (5.26a)$$

$$\langle n_j^2 \rangle_{ss} - \langle n_j \rangle_{ss}^2 = \frac{1}{2} \left(\langle n_j \rangle_{ss} + \kappa_j^{-1} r_a \langle L_{n_1, n_2}^+ \rangle_{ss} \right), \quad (5.26b)$$

$$\langle n_1 n_2 \rangle_{ss} - \langle n_1 \rangle_{ss} \langle n_2 \rangle_{ss} = \frac{r_a}{\kappa_1 + \kappa_2} \langle L_{n_1, n_2}^+ \rangle_{ss}. \quad (5.26c)$$

Using Equation 5.26, the moments in Equation 5.24 can be rewritten as

$$\frac{d}{dt} \langle n_j \rangle = -\kappa_j \left(\langle n_j \rangle - \langle n_j \rangle_{ss} \right); \quad j = 1, 2, \quad (5.27a)$$

$$\frac{d}{dt} \langle n_j^2 \rangle = -2\kappa_j \left(\langle n_j^2 \rangle - \langle n_j^2 \rangle_{ss} \right) + \kappa_j \left(2\langle n_j \rangle_{ss} + 1 \right) \left(\langle n_j \rangle - \langle n_j \rangle_{ss} \right), \quad (5.27b)$$

$$\begin{aligned} \frac{d}{dt} \langle n_1 n_2 \rangle &= -(\kappa_1 + \kappa_2) \left(\langle n_1 n_2 \rangle - \langle n_1 n_2 \rangle_{ss} \right) + \sum_{j=1,2} \kappa_j \langle n_j \rangle_{ss} \left(\langle n_j \rangle - \langle n_j \rangle_{ss} \right) \\ &= -(\kappa_1 + \kappa_2) \left(\langle n_j \rangle - \langle n_j \rangle_{ss} \right) + \kappa \langle n \rangle_{ss} \left(\langle n \rangle - \langle n \rangle_{ss} \right), \end{aligned} \quad (5.27c)$$

where κ and n are the same as in Chapter 4. Integrating Equation 5.27a gives

$$\langle n_j \rangle = \langle n_j \rangle_{ss} \left(1 - \exp(-\kappa_j t) \right). \quad (5.28)$$

Using this result in Equations 5.27b, 5.27c and integrating for $\langle n_j^2 \rangle$ and $\langle n_1 n_2 \rangle$ yields

$$\langle n_j^2 \rangle - \langle n_j \rangle^2 - \langle n_j \rangle = \left(\langle n_j^2 \rangle_{ss} - \langle n_j \rangle_{ss}^2 - \langle n_j \rangle_{ss} \right) \left(1 - e^{-2\kappa_j t} \right), \quad (5.29a)$$

$$\langle n_1 n_2 \rangle - \langle n_1 \rangle \langle n_2 \rangle = \left(\langle n_1 n_2 \rangle_{ss} - \langle n_1 \rangle_{ss} \langle n_2 \rangle_{ss} \right) \left(1 - e^{-(\kappa_1 + \kappa_2)t} \right). \quad (5.29b)$$

The time-dependence of fluctuations in Equation 5.29 reach their highest values in steady-state and the variance $(\Delta n_j)_{ss}^2 = \langle n_j^2 \rangle_{ss} - \langle n_j \rangle_{ss}^2$ attains its minimum when $\langle L_{n_1, n_2}^+ \rangle_{ss}$, in Equation 5.26b, reaches its lowest value (achieved for $\rho_{ba} = 0$, incoherent pumping).

For incoherent pumping, an atom must be prepared in one of its two states $|a\rangle$ or $|b\rangle$.

However, from Equation 5.26a, $\langle L_{n_1, n_2}^- \rangle_{ss}$ cannot be negative and then only $\rho_{bb} = 0$, the atom are prepared in the excited state $|a\rangle$. In this case, from Equation 5.20, $\langle L_{n_1, n_2}^+ \rangle_{ss} = \langle L_{n_1, n_2}^- \rangle_{ss} = r_a^{-1} \kappa_j \langle n_j \rangle_{ss}$ and the variance becomes $(\Delta n_j)_{ss}^2 = \langle n_j \rangle_{ss}$. This means that the fluctuations are minimum for the Poissonian statistics. The moments in steady-state, Equation 5.26 predict the statistics to be super-Poissonian and become Poissonian for incoherent pumping in which the atoms are prepared in their excited states. It is clear from Equation 5.11 and Equation 5.20 that the Kerr parameters decrease the average $\langle L_{n_1, n_2}^\pm \rangle_{ss}$, so the mean and fluctuations in Equation 5.26 decrease. One may ask, what is the role of the IDC? The answer to this question comes from the discussion made above about the role of F in L_{n_1, n_2} . Since F increases L_{n_1, n_2} then L_{n_1, n_2}^\pm (Equation 5.20) will increase too (atomic inversion is already assumed). From these observations, and from Equation 5.26, the mean photon number as well as fluctuations will increase.

So far, first moments are discussed, and now general expressions for moments, in the case $\rho_{bb} = 0$, are presented. The expressions can be obtained from the generating function, G ; the calculations are given in Appendix H in detail and the result is

$$\langle n_j^{r_j} \rangle = \sum_{k=0}^{r_j} \left\{ \begin{matrix} r_j \\ k \end{matrix} \right\} \langle n_j \rangle^k, \quad (5.30)$$

$$\langle n_1^{r_1} n_2^{r_2} \rangle = \sum_{k=0}^{r_2} \sum_{l=0}^{r_1} \sum_{s=0}^{r_1-l} \sum_{q=0}^l s! \binom{k}{s} \binom{r_1}{l} \left\{ \begin{matrix} r_2 \\ k \end{matrix} \right\} \left\{ \begin{matrix} l \\ q \end{matrix} \right\} \left\{ \begin{matrix} r_1-l \\ s \end{matrix} \right\} \langle n_1 \rangle^q \langle n_2 \rangle^{k-s} C_{12}^s, \quad (5.31)$$

where $\left\{ \begin{matrix} k \\ l \end{matrix} \right\}$ are Stirling numbers of the second kind given by (see Appendix H)

$$\left\{ \begin{matrix} k \\ l \end{matrix} \right\} = \frac{1}{l!} \sum_{m=0}^l (-1)^{l-m} \binom{l}{m} m^k. \quad (5.32)$$

Practically, the lowest order correlations are most important but the general relations for moments in Equations 5.30 and 5.31 are obtained for reference. The higher-order moments or correlations are expressed in terms of the mean photon numbers $\langle n_1 \rangle$, $\langle n_2 \rangle$ and the

correlation $\langle n_1 n_2 \rangle$.

5.4.2 Mean Photon Number

In the previous subsection, the time-dependent and the steady-state moments of the field were derived. They are expressed in terms of the mean photon numbers $\langle n_j \rangle$. The steady-state mean photon number $\langle n_j \rangle_{ss}$ can be obtained by using Equation 5.20 and solving Equation 5.26a. The resulting equation is not easy to solve, but with few reasonable assumptions, simple, but adequate, expressions to quantify the field properties are obtained. To this end, simple form for the averages $\langle L_{n_1, n_2}^\pm \rangle_{ss}$ are obtained by decorrelating them, $\langle L_{n_1, n_2}^\pm \rangle_{ss} \approx L_{\langle n_1 \rangle_{ss} \langle n_2 \rangle_{ss}}^\pm$. Similar to the treatment in Chapter 4, an effective expression for $\langle L_{n_1, n_2}^\pm \rangle_{ss}$ can be obtained by using Equation 5.25a to express $L_{\langle n_1 \rangle_{ss} \langle n_2 \rangle_{ss}}^\pm$ in terms of the total mean photon number $\langle n \rangle = \langle n_1 + n_2 \rangle = \langle n_1 \rangle + \langle n_2 \rangle$. From Equation 5.25a, Equation 4.36 are obtained. As discussed in the previous subsection, above threshold, the function $\langle L_{n_1, n_2} \rangle_{ss}$ changes very slowly which allows to write $\langle L_{n_1+1, n_2+1} \rangle_{ss} \approx \langle L_{n_1, n_2} \rangle_{ss}$. Also, the coherence contribution becomes very small and negligible compared to the contribution from population (since $\langle \Lambda_{n_1, n_2}^\pm \rangle$ are of order $\langle n \rangle_{ss}^{-3}$). Therefore, the last terms in Equation 5.20 are canceled safely, and Equation 5.20 is reduced to

$$\langle L_{n_1, n_2}^\pm \rangle_{ss} \approx (\rho_{aa} \pm \rho_{bb}) \langle L_{n_1, n_2} \rangle_{ss}. \quad (5.33)$$

By using Equations 5.33 and 5.11a in Equation 5.26a, the result becomes

$$\kappa \langle n \rangle_{ss} = \frac{2r_a \eta (\rho_{aa} - \rho_{bb}) \langle n \rangle_{ss}^4}{1 + 4\gamma^{-2} [\delta_q + (q_1 \kappa_1^{-1} + q_2 \kappa_2^{-1}) \kappa \langle n \rangle_{ss}]^2 + 4\eta \langle n \rangle_{ss}^4}, \quad (5.34a)$$

with

$$\eta = \left(\frac{g \kappa^2}{\gamma \kappa_1 \kappa_2} \right)^2. \quad (5.34b)$$

The trivial unimportant solution, $\langle n \rangle_{ss} = 0$, for Equation 5.34a is discarded. From Equation 5.34a, a quartic equation is obtained that has the form

$$c_0 + c_1 \langle n \rangle_{ss} + c_2 \langle n \rangle_{ss}^2 + c_3 \langle n \rangle_{ss}^3 + \langle n \rangle_{ss}^4 = 0, \quad (5.35)$$

with

$$c_0 = \frac{1}{\eta} \left(\delta_q^2 + \frac{1}{4} \right), \quad (5.36a)$$

$$c_1 = \frac{2\kappa\delta_q}{\eta} \left(\frac{q_1}{\kappa_1} + \frac{q_2}{\kappa_2} \right), \quad (5.36b)$$

$$c_2 = \frac{\kappa^2}{\eta} \left(\frac{q_1}{\kappa_1} + \frac{q_2}{\kappa_2} \right)^2, \quad (5.36c)$$

$$c_3 = -\frac{r_a (\rho_{aa} - \rho_{bb})}{2\kappa}. \quad (5.36d)$$

This equation has, in general, four real roots or two real roots and two complex conjugate roots. The physical solution is found to be in a good agreement with the numerical solution. A simpler expression for the mean, for strong coupling and detuning comparable with Kerr parameters, is obtained by ignoring the first and second terms in Equation 5.35. For this special case, the fourth-degree polynomial is reduced to a quadratic equation with the solution

$$\langle n \rangle_{ss} = -\frac{1}{2}c_3 \left(1 \pm \sqrt{1 - 4c_2c_3^{-2}} \right). \quad (5.37)$$

This expression requires $c_3 < 0$ and $4c_2c_3^{-2} < 1$ to have a physical solution. Explicitly, the two conditions are combined in the threshold condition

$$r_a (\rho_{aa} - \rho_{bb}) \geq \frac{4}{g} (q_1\kappa_2 + q_2\kappa_1). \quad (5.38)$$

The threshold condition Equation 5.38 predicts that Kerr parameters rise threshold. It also predicts the necessity of population inversion. The root of the positive sign represents the stable solution above the threshold and the other root is unstable and diminishes far above threshold. The mean photon numbers are

$$\langle n_j \rangle_{ss} = -\frac{\kappa c_3}{2\kappa_j} \left(1 + \sqrt{1 - 4c_2 c_3^{-2}} \right). \quad (5.39)$$

For large $\langle n_j \rangle_{ss}$ (very far from threshold) and small Kerr parameters, the means take the simpler form

$$\langle n_j \rangle_{ss} = \frac{r_a (\rho_{aa} - \rho_{bb})}{2\kappa_j}. \quad (5.40)$$

The expression in Equation 5.40 is the dominant zero-order approximation of Equation 5.39. Equation 5.39 says that Kerr parameters lessen the mean photon number as one can see from the first-order approximation

$$\langle n_j \rangle_{ss} = \frac{\kappa}{\kappa_j} \left(-c_3 + \frac{c_2}{c_3} \right), \quad (5.41)$$

which confirms the previous discussion. Here, it is important to emphasize that the IDC is dominant over the Kerr parameters. This is clear if the two expressions of the mean photon number, Equation 4.44 from Chapter 4 and Equation 5.39 and their zero-order approximations are examined. These two equations, for large photon number, are reduced forms of their corresponding higher-order polynomials, Equation 4.41 and Equation 5.35, respectively. One may notice that the Kerr parameters enter in the lower-degree terms (C_2 in Equation 5.35). At strong coupling, Equation 4.46 is reduced to Equation 5.40.

5.4.3 $G^{(2)}$ and CSI

The functional form of $G^{(2)}$ is maintained as in Chapter 4. The difference comes from the dependence of the mean photon numbers on the cross-Kerr parameter and the IDC, F .

At steady-state and from Equation 5.26, $g^{(2)}$ is written as

$$g_{jj}^{(2)ss} = 1 + \frac{1}{2} \left(\frac{\langle L_{n_1, n_2}^+ \rangle_{ss}}{\langle L_{n_1, n_2}^- \rangle_{ss}} - 1 \right) \frac{1}{\langle n_j \rangle_{ss}}, \quad (5.42a)$$

$$g_{12}^{(2)ss} = 1 + \frac{\langle L_{n_1, n_2}^+ \rangle_{ss}}{\langle L_{n_1, n_2}^- \rangle_{ss}} \frac{1}{\langle n_1 \rangle_{ss} + \langle n_2 \rangle_{ss}}. \quad (5.42b)$$

At far from threshold and using Equation 5.33, Equation 5.42 is reduced to

$$g_{jj}^{(2)ss} = 1 + \frac{\rho_{bb}}{\rho_{aa} - \rho_{bb}} \frac{1}{\langle n_j \rangle_{ss}}, \quad (5.43a)$$

$$g_{12}^{(2)ss} = 1 + \frac{1}{\rho_{aa} - \rho_{bb}} \frac{1}{\langle n_1 \rangle_{ss} + \langle n_2 \rangle_{ss}}. \quad (5.43b)$$

From Equation 5.43a, the $G^{(2)}$, $g_{jj}^{(2)ss} > 1$, $j = 1, 2$ predicts super-Poissonian statistics.

It takes its lowest value for incoherent pumping $\rho_{bb} = 0$ where statistics become Poissonian

$g_{jj}^{(2)ss} = 1$. So, statistics are not sub-Poissonian; however, the $G^{(2)}$ exhibits violation of CSI

(Walther et al., 2006; Klyshko, 1996) as demonstrated by Equation 4.52. The violation of

CSI does not require $\rho_{bb} = 0$ as shown below.

From Equation 5.42, and using Equations 4.36 and 4.37, $g_{11}^{(2)ss}$ and $g_{22}^{(2)ss}$ can be written in terms of $g_{12}^{(2)ss}$

$$g_{11}^{(2)ss} = \frac{\kappa_1}{2\kappa} \left[g_{12}^{(2)ss} - \frac{1}{\langle n \rangle_{ss}} - \frac{\kappa_1 - \kappa_2}{\kappa_1 + \kappa_2} \right], \quad (5.44a)$$

$$g_{22}^{(2)ss} = \frac{\kappa_2}{2\kappa} \left[g_{12}^{(2)ss} - \frac{1}{\langle n \rangle_{ss}} - \frac{\kappa_2 - \kappa_1}{\kappa_1 + \kappa_2} \right], \quad (5.44b)$$

and hence

$$\begin{aligned}
g_{11}^{(2)ss} g_{22}^{(2)ss} - \left(g_{12}^{(2)ss}\right)^2 &= \frac{\kappa_1 \kappa_2}{4\kappa^2} \left[\left(g_{12}^{(2)ss} - \frac{1}{\langle n \rangle_{ss}}\right)^2 - \left(\frac{\kappa_1 - \kappa_2}{\kappa_1 + \kappa_2}\right)^2 \right] - \left(g_{12}^{(2)ss}\right)^2 \\
&= \left(\frac{\kappa_1 \kappa_2}{4\kappa^2} - 1\right) \left(g_{12}^{(2)ss}\right)^2 - \frac{\kappa_1 \kappa_2}{4\kappa^2} \left(\frac{\kappa_1 - \kappa_2}{\kappa_1 + \kappa_2}\right)^2 \\
&\quad - \frac{\kappa_1 \kappa_2}{2\kappa^2} \frac{1}{\langle n \rangle_{ss}} \left(g_{12}^{(2)ss} - \frac{1}{2\langle n \rangle_{ss}}\right). \quad (5.45)
\end{aligned}$$

Since

$$\frac{\kappa_1 \kappa_2}{4\kappa^2} - 1 = \frac{(\kappa_1 + \kappa_2)^2}{4\kappa_1 \kappa_2} - 1 = \frac{(\kappa_1 - \kappa_2)^2}{4\kappa_1 \kappa_2},$$

Equation 5.45 takes the form

$$\begin{aligned}
g_{11}^{(2)ss} g_{22}^{(2)ss} - \left(g_{12}^{(2)ss}\right)^2 &= \frac{(\kappa_1 - \kappa_2)^2}{4\kappa_1 \kappa_2} \left(g_{12}^{(2)ss}\right)^2 - \frac{(\kappa_1 - \kappa_2)^2}{4\kappa_1 \kappa_2} \\
&\quad - \frac{(\kappa_1 + \kappa_2)^2}{2\kappa_1 \kappa_2} \frac{1}{\langle n \rangle_{ss}} \left(g_{12}^{(2)ss} - \frac{1}{2\langle n \rangle_{ss}}\right) \\
&= \frac{(\kappa_1 - \kappa_2)^2}{4\kappa_1 \kappa_2} \left[\left(g_{12}^{(2)ss}\right)^2 - 1 \right] \\
&\quad - \frac{(\kappa_1 + \kappa_2)^2}{2\kappa_1 \kappa_2} \frac{1}{\langle n \rangle_{ss}} \left(g_{12}^{(2)ss} - \frac{1}{2\langle n \rangle_{ss}}\right). \quad (5.46)
\end{aligned}$$

Since $\langle L_{n_1, n_2}^+ \rangle_{ss} \geq \langle L_{n_1, n_2}^- \rangle_{ss}$, and $g_{12}^{(2)ss} > 1 + \langle n \rangle_{ss}^{-1}$ (from Equation 5.42b), for not large difference in the cavity mode decay constants, the right-hand side of Equation 5.46 is negative, so the CSI is violated. The maximum of violation happens when $\kappa_1 = \kappa_2$ with amount of

$$\left(g_{12}^{(2)ss}\right)^2 - g_{11}^{(2)ss} g_{22}^{(2)ss} = \frac{2}{\langle n \rangle_{ss}} \left(g_{12}^{(2)ss} - \frac{1}{2\langle n \rangle_{ss}}\right); \quad (\kappa_1 = \kappa_2). \quad (5.47)$$

This violation is greater than $2\langle n \rangle_{ss}^{-1}$, which is similar to the result by Zubairy (1982). It reduces to Zubairy's result in the special situation $\rho_{bb} = 0$ with violation of amount $\langle n \rangle_{ss}^{-1}$.

As can be observed, the Kerr parameters decrease the mean photon number but the IDC increases it; therefore, the $G^{(2)}$ will increase due to the Kerr effect but will decrease due to IDC as Equation 5.43 predict. However, as discussed above, the IDC is dominant and the effective result is decreasing the $G^{(2)}$. From Equation 5.47, the violation of CSI becomes small at a large mean photon number. As a result, IDC weakens the nonclassicality of the field.

5.4.4 Mandel Q Parameter and Fluctuations

The important measure to characterize statistics is the Mandel Q parameter. The difference between the result here and that of Chapter 4 is the steady-state expressions. In the steady-state and from Equations 5.42, 4.53, Q becomes

$$Q_j^{ss} = \frac{1}{2} \left(\frac{\langle L_{n_1, n_2}^+ \rangle_{ss}}{\langle L_{n_1, n_2}^- \rangle_{ss}} - 1 \right). \quad (5.48)$$

Far from threshold and from Equation 5.43a, the Q parameter Equation 5.48 is reduced to

$$Q_j^{ss} = \frac{\rho_{bb}}{\rho_{aa} - \rho_{bb}}. \quad (5.49)$$

Since $\langle L_{n_1, n_2}^- \rangle_{ss}^{-1} \langle L_{n_1, n_2}^+ \rangle_{ss} > 1$, so that Q given by Equation 5.48 excludes any chance for sub-Poissonian statistics ($Q_j^{ss} < 0$) as seen clearly from Equation 5.49. It predicts Poissonian statistics ($Q_j^{ss} = 0$) when $\langle L_{n_1, n_2}^- \rangle_{ss} = \langle L_{n_1, n_2}^+ \rangle_{ss}$ which can be satisfied only at $\rho_{bb} = 0$. Other than this special case, the statistics are super-Poissonian ($Q_j^{ss} > 0$).

From Equation 5.48, the relative fluctuations of each single mode are easily written as

$$\frac{\langle (\Delta n_j)^2 \rangle_{ss}}{\langle n_j \rangle_{ss}} = \frac{1}{2} \left(\frac{\langle L_{n_1, n_2}^+ \rangle_{ss}}{\langle L_{n_1, n_2}^- \rangle_{ss}} + 1 \right). \quad (5.50)$$

These fluctuations, Equation 5.50, take their lowest values when $\langle L_{n_1, n_2}^+ \rangle_{ss} = \langle L_{n_1, n_2}^- \rangle_{ss}$

which is $\langle (\Delta n_j)^2 \rangle / \langle n_j \rangle = 1$. The relative fluctuations in the total photon number $\langle n \rangle = \langle n_1 \rangle + \langle n_2 \rangle$ could be written as

$$\frac{\langle (\Delta n)^2 \rangle_{ss}}{\langle n \rangle_{ss}} = \frac{1}{2} + \frac{1}{2} \left(1 + \frac{4\kappa}{\kappa_1 + \kappa_2} \right) \frac{\langle L_{n_1, n_2}^+ \rangle_{ss}}{\langle L_{n_1, n_2}^- \rangle_{ss}}. \quad (5.51)$$

The lowest value of the relative total fluctuations takes place when $\langle L_{n_1, n_2}^+ \rangle_{ss} = \langle L_{n_1, n_2}^- \rangle_{ss}$ which reduces to the result in Equation 4.59. Since the atomic coherence comes at the expense of atomic population inversion, so the effective result of coherence is to decrease correlations. This can be seen from Equation 5.20, where the increase in the atomic coherence ρ_{ab} increase L_{n_1, n_2}^+ and decrease L_{n_1, n_2}^- . The consequence of this is that the relative fluctuations increase as Equations 5.50 and 5.51 predict. So the coherence widens both the joint and the marginal photon distribution function.

5.4.5 Entanglement

To study the role of cross-Kerr effect and IDC on entanglement criterion, the final formula is written because its derivation is the same as that given in Chapter 4 and the final result has the same form as it was discussed earlier when deriving the approximation for the off-diagonal elements of density matrix. The entanglement criterion, the E function, has the expression

$$E(n_1, n_2) = \left| \rho_{ab} \langle \Xi_{n_1+1, n_2+1} K_{n_1+1, n_2+1; n_1 n_2}^* - \Xi_{n_1, n_2} K_{n_1 n_2; n_1+1, n_2+1}^* \rangle \right|^2 - \langle n_1 \rangle \langle n_2 \rangle, \quad (5.52)$$

where

$$\Xi_{n_1, n_2} = \frac{\sqrt{n_1 n_2}}{\Gamma_{n_1 n_2; n_1-1, n_2-1}} e^{i2D_{n_1 n_2} \gamma t}. \quad (5.53)$$

The last term in Equation 5.52 is the dominant and possibility to witness entanglement is faded similar to the result in Chapter 4. However, studying the effect of Kerr parameters and IDC on entanglement is useful for more understanding of their roles.

The effect of the Kerr parameters and IDC on the statistics function can be investigated by solving the statistics equation by following the same procedure that is used in Chapter 4. Since the equation has the same form, its solution has identical form with the solution obtained in Chapter 4 but with different coefficients as explained earlier. Therefore, it will not be repeated here, and the discussion refers to the expression of Chapter 4. The effect of the Kerr parameters and the IDC is through the mean photon numbers, as the analytic solution manifests. However, the correlation and coherence contribution to the exact solution cannot be neglected.

In this chapter, analytic expressions for the moments are derived; $G^{(2)}$ and Q are calculated and discussed. One of the main results of this section is the mean photon number expressed in Equation 5.35 which is in a very good agreement with the numerical solution over a large range of the parameters.

5.5 Results and Discussion

The effects of the detuning Δ , and the Kerr parameters, χ_1 , χ_2 , and χ on the dynamics of the field are studied through analysis of various measured quantities. The computed quantities are the same quantities that were studied in Chapter 4: the mean photon number $\langle n_j \rangle$, Q , $G^{(2)}$, CSI, Entanglement E , and the photon statistics $P_{n_1 n_2}$. The computations are for the same set of parameters and the same values but here the cross Kerr parameter χ is added to the set of the parameters similarly as χ_1 .

5.5.1 Effects of Injection Rate

In this subsection, the effects of the injection rate r_a on all quantities under the study mentioned above are discussed.

5.5.1.1 On Mean Photon Number

The dynamics in Figures 5.1(i) and 5.2(i) show the effects of r_a on mean photon number $\langle n_1 \rangle$. Mean photon number starts from zero and builds up quickly to reach steady-state. The amount of the increase in the mean photon number is greater than that is found in the absence of IDC. In the present situation, the mean photon number is approximately doubles that is because the IDC is proportional to the square root of field intensity and the effects of Kerr parameters that lower the average photon number are incomparable to the effects of IDC. In this situation, Equation 5.40 is almost satisfied. WE notice the delay in reaching steady-state and the reason of this may be attributed to the strong atom-field coupling that makes Rabi oscillations increase and rises the time of reaching steady-state. To reach steady-state with IDC, it requires more photons in the cavity to have a stationary exchange of energy between atom and cavity field which in turn rise mean photon number. The increase in injection rate results in a growth of mean photon number. In the steady-state, the mean photon number dependence on the injection rate is shown in Figure 5.3, where a large nonlinear growth in photon number is seen as explained. This in consistent with the predictions of Equation 5.39.

5.5.1.2 On $G^{(2)}$ and CSI

The dynamics of $G^{(2)}$ and its dependence on injection rate, r_a are shown in Figures 5.4(v), 5.5(i, v) for single-mode, and in Figures 5.6(i, v), 5.7(i, v) for inter-mode and CSI. The single-mode $G^{(2)}$, is, initially, high and then reduces fast to reach steady-state below the classical limit $g_{11}^{(2)} = g_{22}^{(2)} = 1$ at large injection rate. It is interesting to see the disappearance

Mean photon number and entanglement : Dynamics and effects of injection rate (r_a), detuning (Δ), self-Kerr effect (χ_1), and cross-Kerr effect (χ).

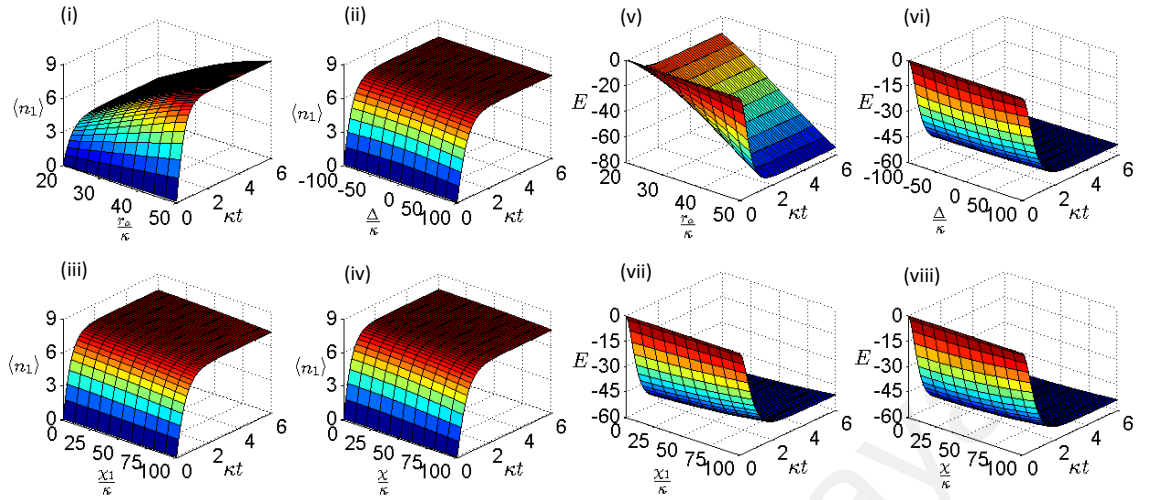


Figure 5.1: (i-iv) Mean photon $\langle n_1 \rangle$ and (v-viii) entanglement E ; the dynamics and parameter dependence are for: (i, v) $\Delta = 0$, $\chi_1 = 50\kappa$, $\chi = 0$, (ii, vi) $r_a = 40\kappa$, $\chi_1 = 50\kappa$, $\chi = 0$, (iii, vii) $r_a = 40\kappa$, $\Delta = 0$, $\chi = 0$, and (iv, viii) $r_a = 40\kappa$, $\Delta = 0$, $\chi_1 = 50\kappa$.

Effects of injection rate (r_a), detuning (Δ), self-Kerr effect (χ_1), and cross-Kerr effect (χ) on dynamics of the mean photon number and entanglement.

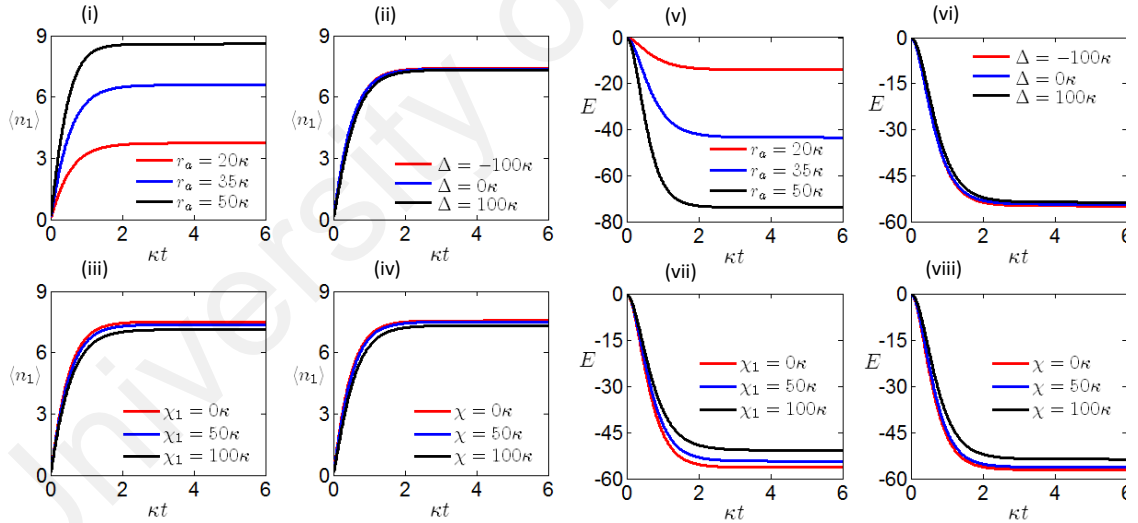


Figure 5.2: (i-iv) Mean photon number $\langle n_1 \rangle$ and (v-viii) entanglement E ; the dynamics for: (i, v) $\Delta = 0$, $\chi_1 = 50\kappa$, $\chi = 0$, (ii, vi) $r_a = 40\kappa$, $\chi_1 = 50\kappa$, $\chi = 0$, (iii, vii) $r_a = 40\kappa$, $\Delta = 0$, $\chi = 0$, and (iv, viii) $r_a = 40\kappa$, $\Delta = 0$, $\chi_1 = 50\kappa$.

of the kinks that was observe in the previous case without IDC. This is due to the fact that IDC dominates Kerr and detuning effects and fluctuations are become strong in the beginning before they settle down over time. What is noticeable here is that the IDC converts effects of injection rate such that r_a reduce distribution width and for large values of injection

Effects of injection rate (r_a), detuning (Δ), self-Kerr effect (χ_1), and cross-Kerr effect (χ) on steady-state of the mean photon number and photon number distribution (sub-Poissonian and super-Poissonian).

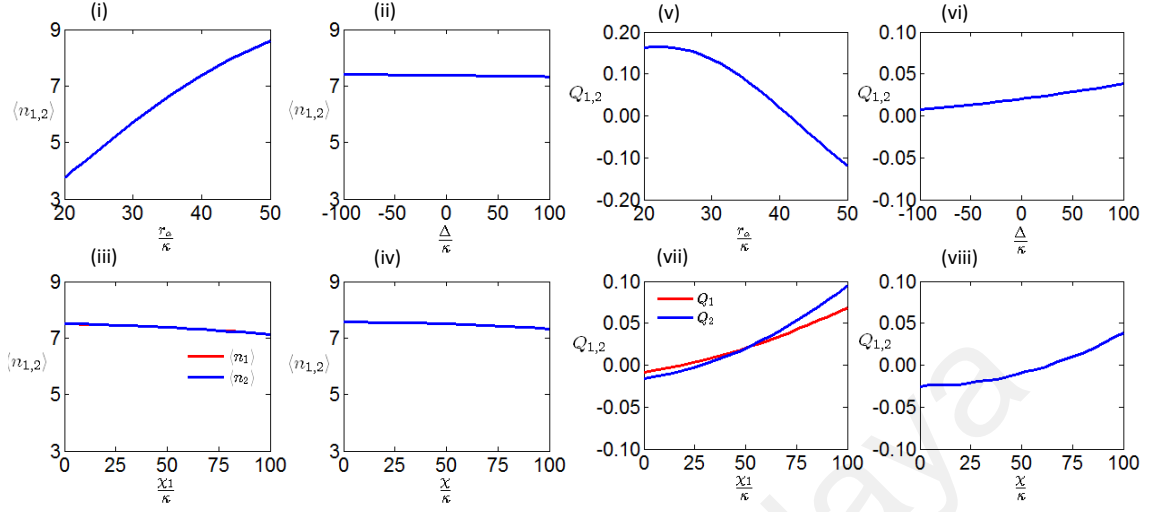


Figure 5.3: (i-iv) Mean photon numbers $\langle n_1 \rangle$, $\langle n_2 \rangle$, and (v-viii) Q_1 , Q_2 . The parameter dependence are for: (i, v) $\Delta = 0$, $\chi_1 = 50\kappa$, $\chi = 0$, (ii, vi) $r_a = 40\kappa$, $\chi_1 = 50\kappa$, $\chi = 0$, (iii, vii) $r_a = 40\kappa$, $\Delta = 0$, $\chi = 0$, and (iv, viii) $r_a = 40\kappa$, $\Delta = 0$, $\chi_1 = 50\kappa$.

rate, $g_{11}^{(2)} < 1$ indicating that the statistics are sub-Poissonian. This is completely opposite to the effects of injection rate in the previous case of non-IDC. However, fluctuations are still increasing by the rise in injection rate that can be obtained from Figures 5.5(i), 5.2(i) using Equations 4.53 and 4.56. For $r_a = 20\kappa$, the variance is $\langle n_1^2 \rangle - \langle n_1 \rangle^2 \approx 5$, and for $r_a = 50\kappa$, it is $\langle n_1^2 \rangle - \langle n_1 \rangle^2 \approx 7$. The inter-mode dynamics, in Figures 5.6(i), 5.7(i) 5.6(i) exhibit strong correlations in the beginning and decay swiftly with time to steady-state similarly to the non-IDC case. The violation of CSI, in Figures 5.6(v) and 5.7(v), is clear and persistent over time as in the previous results. The nonclassicality becomes less with IDC, since photon number and fluctuation increase, as correlation and violation of CSI become weak. These outcomes are seen obviously in steady-state from Figures 5.8(i, v). Thus the effect of r_a with IDC is to weaken the single-mode $G^{(2)}$ which means that the chance to measure two photons simultaneously is reduced or the light becomes antibunching in one sort of definition as discussed in Chapter 2. It also increases fluctuations, reduces the correlation between the two modes, and weakens the nonclassicality of the field. However, it leads to

driving statistics of the field towards sub-Poissonian.

Photon number distribution (sub-Poissonian and super-Poissonian) and self-mode second-order correlation function: Dynamics and effects of injection rate (r_a), detuning (Δ), self-Kerr effect (χ_1), and cross-Kerr effect (χ).

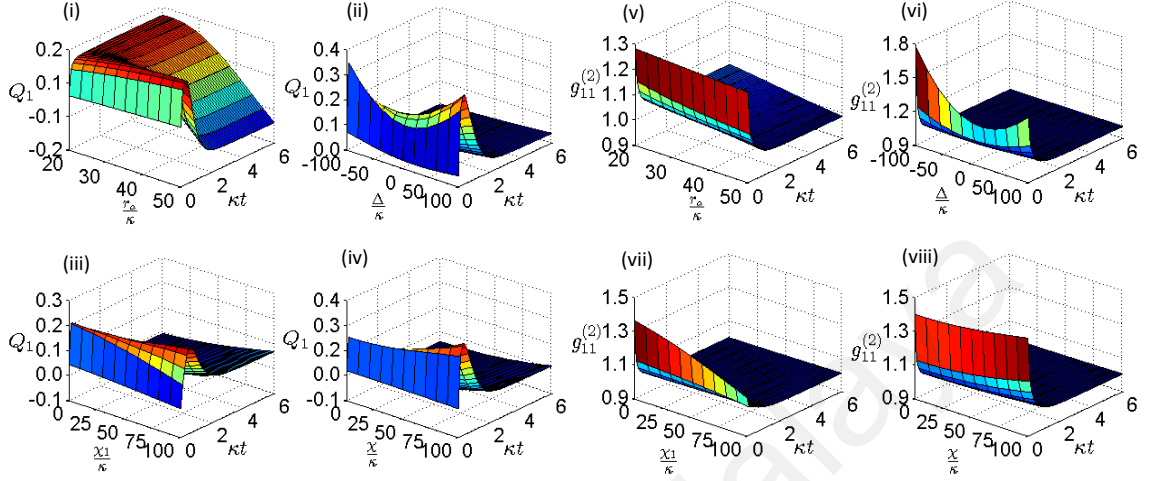


Figure 5.4: (i-iv) Q_1 and (v-viii) $g_{11}^{(2)}$; the dynamics and parameter dependence for: (i, v) $\Delta = 0$, $\chi_1 = 50\kappa$, $\chi = 0$, (ii, vi) $r_a = 40\kappa$, $\chi_1 = 50\kappa$, $\chi = 0$, (iii, vii) $r_a = 40\kappa$, $\Delta = 0$, $\chi = 0$, and (iv, viii) $r_a = 40\kappa$, $\Delta = 0$, $\chi_1 = 50\kappa$.

Effects of injection rate (r_a), detuning (Δ), self-Kerr effect (χ_1), and cross-Kerr effect (χ) on the dynamics of the self-mode second-order correlation functions.

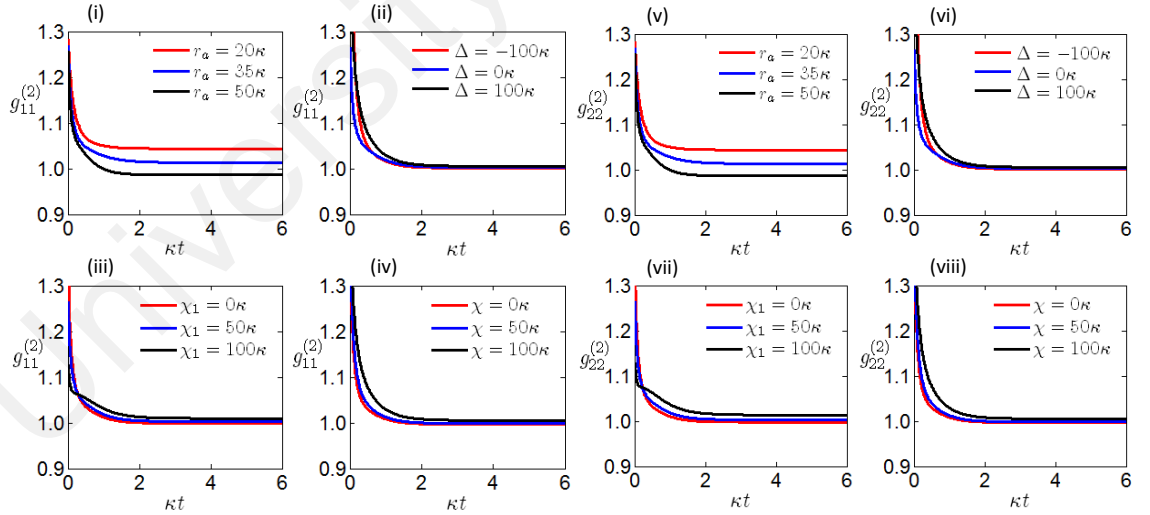


Figure 5.5: (i-iv) $g_{11}^{(2)}$ and (v-viii) $g_{22}^{(2)}$; the dynamics for: (i, v) $\Delta = 0$, $\chi_1 = 50\kappa$, $\chi = 0$, (ii, vi) $r_a = 40\kappa$, $\chi_1 = 50\kappa$, $\chi = 0$, (iii, vii) $r_a = 40\kappa$, $\Delta = 0$, $\chi = 0$, and (iv, viii) $r_a = 40\kappa$, $\Delta = 0$, $\chi_1 = 50\kappa$.

Inter-mode second-order correlation function and violation of CSI:
Dynamics and effects of injection rate (r_a), detuning (Δ), self-Kerr effect (χ_1), and cross-Kerr effect (χ).

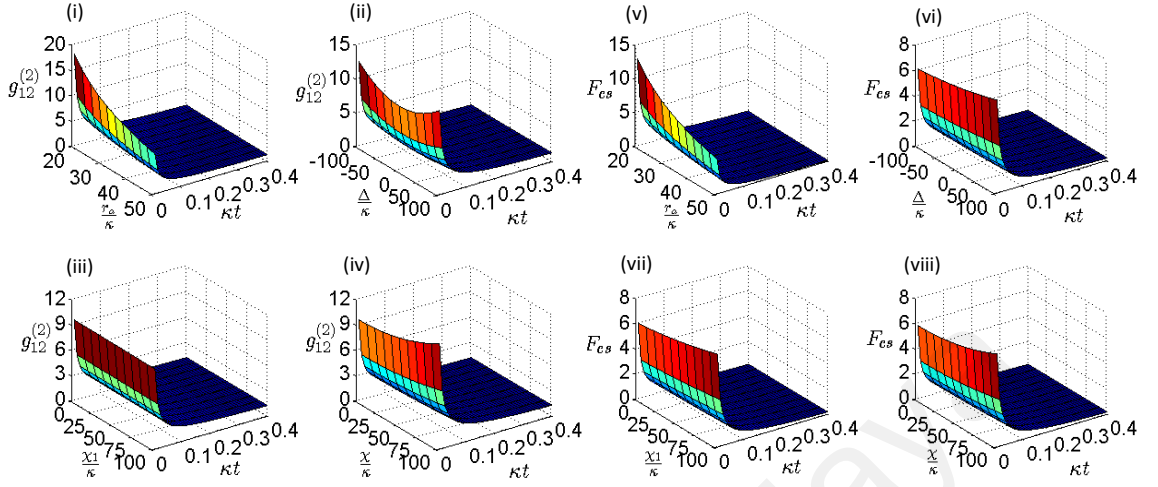


Figure 5.6: (i-iv) $g_{12}^{(2)}$ and (v-viii) CSI (F_{CS}); the dynamics and parameter dependence for: (i, v) $\Delta = 0$, $\chi_1 = 50\kappa$, $\chi = 0$, (ii, vi) $r_a = 40\kappa$, $\chi_1 = 50\kappa$, $\chi = 0$, (iii, vii) $r_a = 40\kappa$, $\Delta = 0$, $\chi = 0$, and (iv, viii) $r_a = 40\kappa$, $\Delta = 0$, $\chi_1 = 50\kappa$.

Effects of injection rate (r_a), detuning (Δ), self-Kerr effect (χ_1), and cross-Kerr effect (χ) on dynamics of inter-mode second-order correlation function and violation of the CSI.

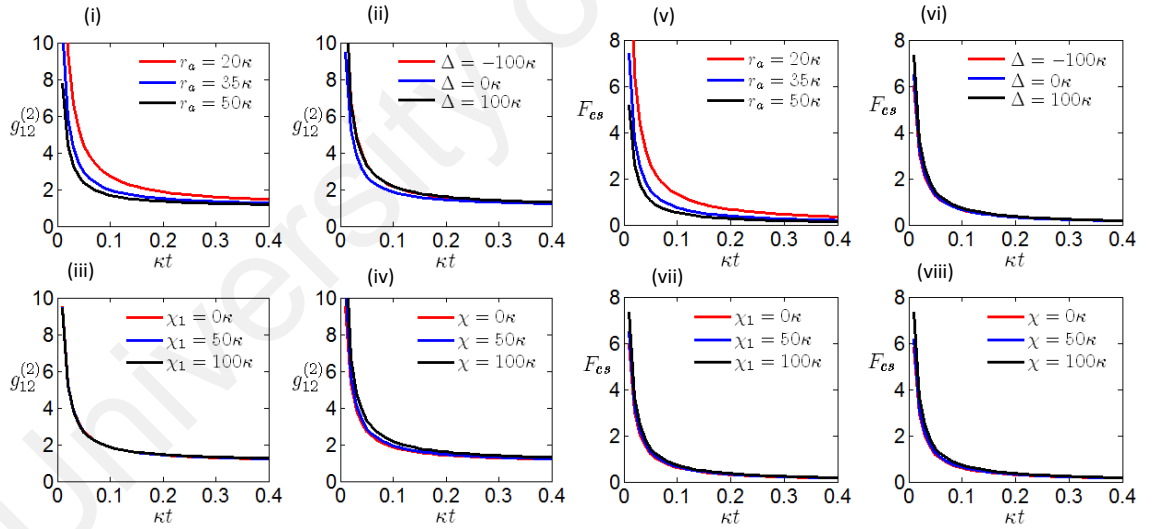


Figure 5.7: (i-iv) $g_{12}^{(2)}$ and (v-viii) CSI (F_{CS}). The dynamics for: (i, v) $\Delta = 0$, $\chi_1 = 50\kappa$, $\chi = 0$, (ii, vi) $r_a = 40\kappa$, $\chi_1 = 50\kappa$, $\chi = 0$, (iii, vii) $r_a = 40\kappa$, $\Delta = 0$, $\chi = 0$, and (iv, viii) $r_a = 40\kappa$, $\Delta = 0$, $\chi_1 = 50\kappa$.

5.5.1.3 On Entanglement

The increase in fluctuations and mean photon numbers as a result of the increase in the injection rate make reaching an entangled state unattainable. This result is shown in

Effects of injection rate (r_a), detuning (Δ), self-Kerr effect (χ_1), and cross-Kerr effect (χ) on the steady-state of the second-order correlation function and violation of the CSI.

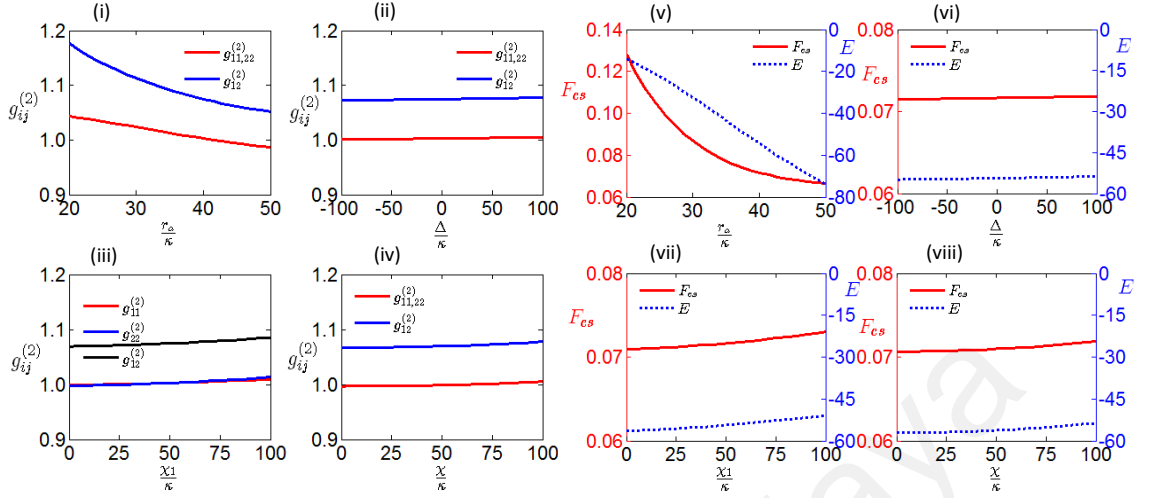


Figure 5.8: (i-iv) $g_{11}^{(2)}$, $g_{22}^{(2)}$, $g_{12}^{(2)}$. (v-viii) CSI (F_{cs} , on the left-hand side in red color) and entanglement E (on the right-hand side in blue). The parameter dependence for: (i, v) $\Delta = 0$, $\chi_1 = 50\kappa$, $\chi = 0$, (ii, vi) $r_a = 40\kappa$, $\chi_1 = 50\kappa$, $\chi = 0$, (iii, vii) $r_a = 40\kappa$, $\Delta = 0$, $\chi = 0$, and (iv, viii) $r_a = 40\kappa$, $\Delta = 0$, $\chi_1 = 50\kappa$.

Figures 5.1(v) and 5.2(v) which also predicts that over time and as injection rate increase, the two modes are more separable and far from being entangled. The presence of IDC enhances the effect of the injection rate for entanglement to be improbable. Again, from these figures and Figure 5.8(v), the last term in the expression of E , Equation 5.52, is dominant and changes almost quadratically as discussed earlier.

5.5.1.4 On Mandel Q Parameter

In the discussion of $G^{(2)}$, an increase in the field fluctuations was found, but a reduction in the single-mode $G^{(2)}$ was observed. The increase in fluctuations is also accompanied by a rise in the mean photon number. According to Equation 4.53, there is a competition between fluctuations and the average for Q . This competition dynamics are displayed in Figures 5.4(i), 5.9(i) which shows the prediction stated above. The results demonstrate rapid development in fluctuations which is faster than the growth in photon number average at the beginning which does not last for long and soon the average photon number exceeds

fluctuations and the relative fluctuations drop to a saturated steady-state value. These dynamics are shown through the sign change of Q with more reduction as an injection rate increases. Thus with IDC, the injection rate enhances nonclassicality of the field by switching statistics from super-Poissonian to sub-Poissonian which is distinctly depicted in Figure 5.3.

Effects of injection rate (r_a), detuning (Δ), self-Kerr effect (χ_1), and cross-Kerr effect (χ) on dynamics of photon number distribution (sub-Poissonian and super-Poissonian).

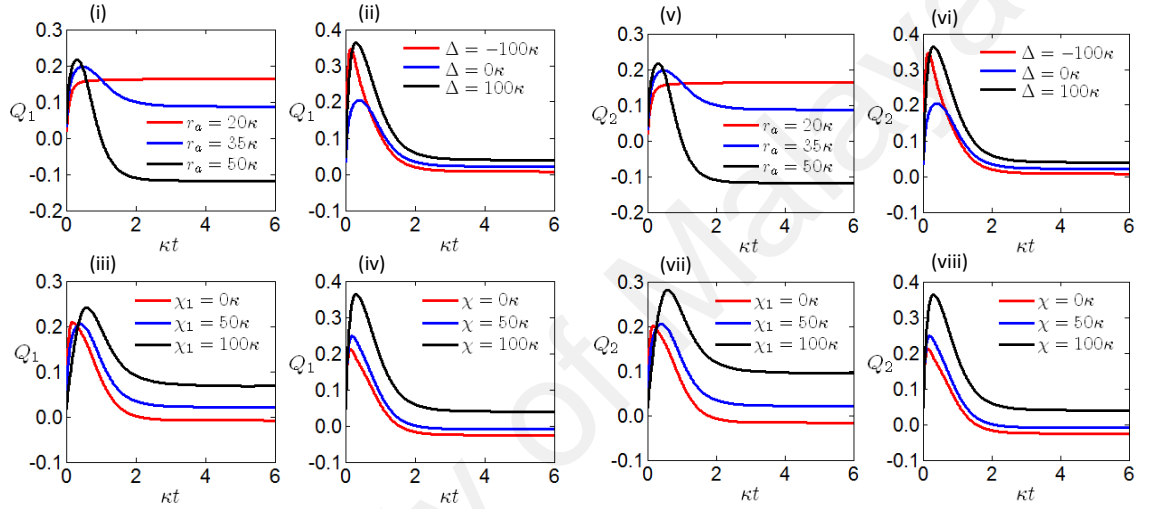


Figure 5.9: (i-iv) Q_1 and (v-viii) Q_2 ; the dynamics for: (i, v) $\Delta = 0$, $\chi_1 = 50\kappa$, $\chi = 0$, (ii, vi) $r_a = 40\kappa$, $\chi_1 = 50\kappa$, $\chi = 0$, (iii, vii) $r_a = 40\kappa$, $\Delta = 0$, $\chi = 0$, and (iv, viii) $r_a = 40\kappa$, $\Delta = 0$, $\chi_1 = 50\kappa$.

5.5.1.5 On Distribution $P_{n_1 n_2}$

The effects of the injection rate Δ on the quantities that have been discussed can be understood through the photon distribution function $P_{n_1 n_2}$ in Figure 5.10i. The displacement of the center of the distribution towards large values of photon numbers means the increase in the mean as r_a increase qualitatively similar, but greater than in the case without IDC in Figure 4.12i. The symmetry of the distribution about line of symmetry, $n_1 = n_2$, shows equal mean photon numbers, $\langle n_1 \rangle = \langle n_2 \rangle$ and from the projections on the planes $n_2 = 0$ and $n_1 = 0$, the single-mode distributions $P_{n_1} = P_{n_2}$ is obtained. Thus, it is most probable

to have more photons when the injection rate increases and with the increase in photon numbers, fluctuations grow also as can be seen from the broadening of the distribution.

5.5.2 Effects of Detuning

The effects of detuning, with IDC, on nonclassicality measures will be provided.

5.5.2.1 On Mean Photon Number

The detuning effects are reduced by IDC, and its effects on the dynamics of the mean photon number become insignificant compared to the injection rate as Figure 5.1(ii) and Figure 5.2(ii) show. The figures display a rapid growth of the average $\langle n_1 \rangle$ for all values of detuning. The increase in mean photon number due to the rise in detuning from $\Delta = -100\kappa$ to $\Delta = 100\kappa$ is tiny as depicted in Figure 5.3(ii). In the present case for IDC, the dynamics of mean photon number reach steady-state with higher value and in a longer time than in the previous case where the coupling is not intensity-dependent. The slight dependence of the mean photon number on detuning confirms its consistency with the analytic expressions, Equations 5.39, 5.40, and confirms the discussion at the end of the Subsection 5.4.2.

5.5.2.2 On $G^{(2)}$ and CSI

The effects of detuning on dynamics of $G^{(2)}$, $g_{11}^{(2)}$ and $g_{22}^{(2)}$ displayed in Figures 5.4(vi), 5.5(ii, vi) are, initially, larger especially for negative detuning. The single-mode correlations drop fast to reach their steady-state values with very small rise for the increase in detuning as shown in Figure 5.8(ii). Also, the inter-mode correlation, $g_{12}^{(2)}$ and F_{cs} start high and quickly drop to their steady-state similar to what is found in the non-IDC case. Also, the inter-mode correlation and violation of CSI are almost insensitive to the change in detuning as Figures 5.8(ii), 5.8(v) shows. The negligible response of $G^{(2)}$ to the change in detuning as a consequence of effect of IDC where intensity effects almost annihilate the small effects of detuning.

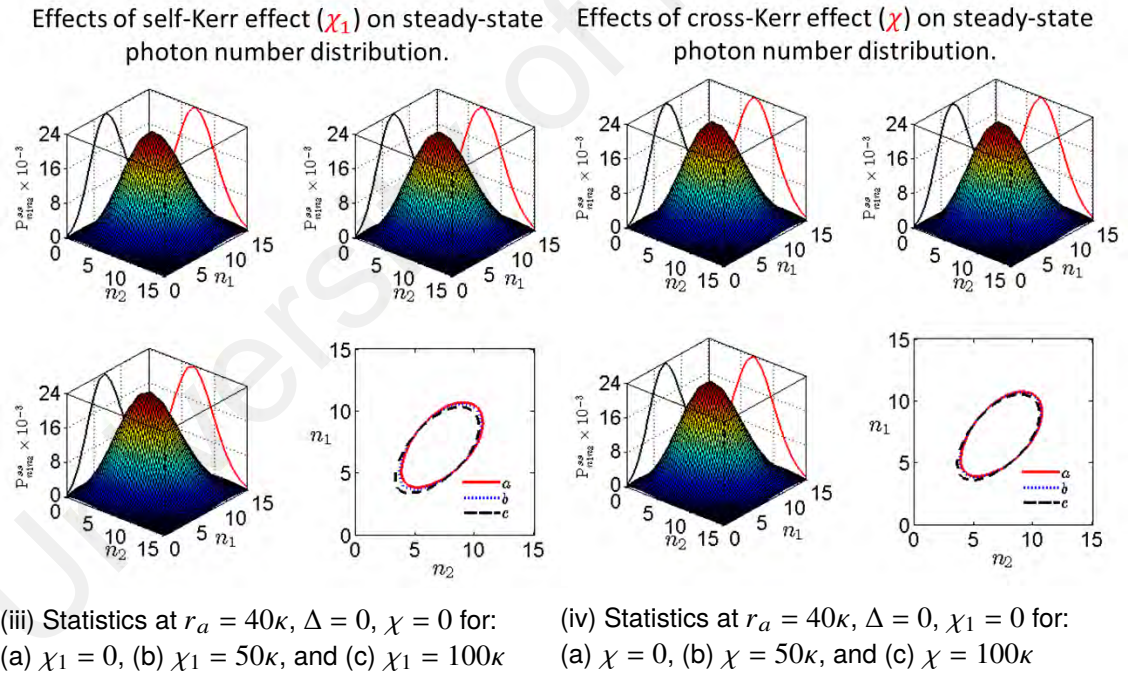
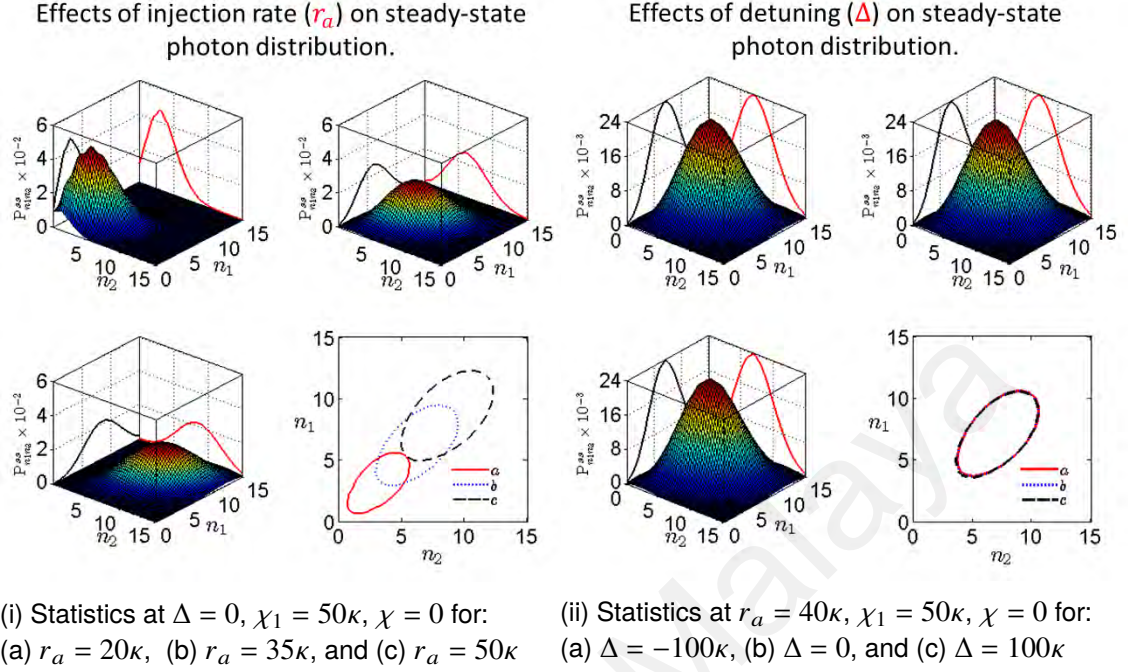


Figure 5.10: The statistics distribution function $P_{n_1 n_2}$, its contours at FWHM, and its two marginal distributions for each single mode for: (i) injection rate r_a , (ii) detuning Δ , (iii) Kerr parameter χ_1 , and (iv) Kerr parameter χ . The contours (ellipses) of the distributions and the single-mode distributions, P_{n_1} in black color and P_{n_2} in red color, for mode 1 and mode 2, respectively, evaluated at each of the three values.

5.5.2.3 On Entanglement

As time evolves, the function E takes large negative values and ends up in steady-state of showing a little difference to the changes in detuning, Figures 5.1(vi) and 5.2(vi). Two features can be highlighted, high negative amount of E and reversing change effects in E where the increase in detuning from negative values to positive values, E slightly increases as Figures 5.2(vi) and 5.8(vi) expose, oppositely to what happens if there is no IDC. So, in the IDC case, detuning has negligible effects on entanglement.

5.5.2.4 On Mandel Q Parameter

The Mandel Q parameter displays violent fluctuations in the beginning before they settle down over time to reach a steady-state. Fluctuations start larger for the off-resonance than for $\Delta = 0$ which exponentially decay to a stationary state, Figures 5.4(ii), 5.9(ii, vi). The stationary values of fluctuations grow when detuning increase as exhibited, also, in Figure 5.3(vi). The expectations state that statistics are super-Poissonian, and become close to Poissonian for large negative detuning. Moreover, fluctuations rise as detuning increases. Accordingly, IDC rises fluctuations ratio and the field is bunching with super-Poissonian statistics even for negative detuning.

5.5.2.5 On Distribution $P_{n_1 n_2}$

Figure 5.10ii displays effects of detuning on the the two-mode distribution function $P_{n_1 n_2}$ and the single-mode distribution functions P_{n_1} , P_{n_2} as well as their FWHM. In steady-state, detuning has a weak effect on photon distributions which means that the number of photons in a given state does not change appreciably by changing detuning. This is because of the intensity effect, through IDC, exceeds any finite change in detuning. So, the mean photon number has not affected, in a certain state is similar to the injection rate effect.

5.5.3 Effects of Kerr parameters

Here, a discussion on the effects of Kerr parameters, χ_1 and χ when the coupling is intensity-dependent is provided.

5.5.3.1 On Mean Photon Number

The dependence of the mean photon number $\langle n_1 \rangle$ on time and Kerr parameters χ_1 and χ are given in Figures 5.1(iii, iv) and 5.2(iii, iv). The results from these figures indicate that both self-Kerr and cross-Kerr effects are weak in the presence of IDC. However, the self-Kerr effect is a little stronger than the cross-Kerr effect for the same values of χ_1 and χ . This difference is due to the way they contribute to the total energy of the system. The cross-Kerr effect enhances one mode by half of its energy and the other half goes to the other mode. This means that the combined effect of the parameters χ_1 and χ_2 is larger than the effect of χ . Thus, Kerr parameters reduce the mean photon number slightly in the presence of IDC which is significantly different from their effects without IDC.

5.5.3.2 On $G^{(2)}$ and CSI

The results from Figures 5.4(vii, viii), 5.5(iii, iv), and 5.5(vii, viii), inform us how much weak are the effects of these parameters in the presence of IDC. The self-mode correlation decrease from large values in the beginning and almost reach the classical limit $g_{11}^{(2)} = g_{22}^{(2)} = 1$. The fluctuations are increased by the effect of IDC, so the statistics are sub-Poissonian only at small values for Kerr parameters and soon become super-Poissonian for larger values. This result is represented clearly in Figures 5.8(viii, iv). Therefore, the IDC lowers the role of the Kerr parameters and their contributions to the nonclassicality are decreased. Also, the inter-mode correlations reduce as exhibited in Figures 5.6(viii), 5.7(iv). They are high in the beginning and soon decrease but in the present situation, the χ_1 has no role, whereas χ shows a little difference where correlations increase slightly. The reason is

that the cross-Kerr effect couples the two modes through their intensities. Therefore, an increase in correlations and violation of CSI are expected, which is provided in Figures 5.6(vii), 5.7(viii). The steady-state of the correlations and violation of CSI are displayed in Figure 5.8(iii, iv), and 5.8(vii, viii). The results show a very small increase in $G^{(2)}$ and in violation of CSI. Thus, statistics become super-Poissonian and the field is still nonclassical, but the effects are weak.

5.5.3.3 On Entanglement

The dynamics and functional dependence of E on the Kerr parameters are similar to the effect of detuning on its dynamics but the effects of Kerr parameters are a little stronger. The Kerr effect rise values of E but the function is far from satisfying the entanglement criterion. The result are presented in Figures 5.1(vii, viii) and 5.2(vii, viii). The steady-state dependence of E on Kerr parameters are exposed in Figures 5.8(vii, viii). Therefore, Kerr parameters slightly improve the chance for the system to show entanglement but still far since the effect of IDC weaken their roles.

5.5.3.4 On Mandel Q Parameter

In the discussion of $G^{(2)}$, the self-mode correlations are found to be close to the classical limit and the statistics are sub-Poissonian only for small values of Kerr parameters. The dynamics of Q shown in Figures 5.4(iii, iv) and 5.9(iii, iv) are similar to its dynamics when effects of detuning are discussed. The effects in this situation are distinguished from that of the detuning. Here the effect is stronger and the important thing is that the statistics are sub-Poissonian for small Kerr parameters, whereas for the detuning, statistics always super-Poissonian. The results are displayed for the steady-state in Figures 5.3(vii, viii).

5.5.3.5 On Distribution $P_{n_1 n_2}$

The effect of IDC results in a weak change in the photon number distribution as in Figures 5.10iii, 5.10iv which is close to the effect of detuning, but here the effects are a little larger. From the shift in the ellipses towards smaller values of n_1 and n_2 , the mean photon numbers are reduced but with a small amount and the narrowing or broadening in the distribution is very small. The effect of Kerr parameters on the photon number distribution is widening the distribution which is contradictory to the situation when the coupling is not intensity dependent. So, the Kerr effect is not responsible for widening the distribution, but the effect of IDC is large such that the roles of Kerr parameters become very small.

5.5.4 Approximate Solution with IDC: Agreement and Justification

Now, a discussion on a few results from the analytic solution when the coupling is intensity-dependent is given. The effects of IDC on the validity of the assumptions made to derive the distribution equation are addressed. The results for the photon number distribution and the mean photon number are displayed in Figure 5.11 side-by-side to see how much these assumptions are valid. The figure shows an acceptable agreement if weak fluctuations are assumed. The results are not as good as in the case without IDC, but they are fairly useful to predict how the dynamics of the system are going to be. The reason for this error, which is larger than the error when the coupling is not intensity-dependent is the large fluctuations in the present case as was observed. The IDC increases the fluctuations that make neglecting correlation is not possible if more accurate results from the analytic solution are needed. However, as stated, the difficulty to solve the density matrix has the price in which one has to look for an approximate solution to have more insight into the dynamics and system behavior.

Agreement between the exact and approximate solutions for the photon number distribution, mean photon number, and violation of CSI (cross-Kerr χ dependence)

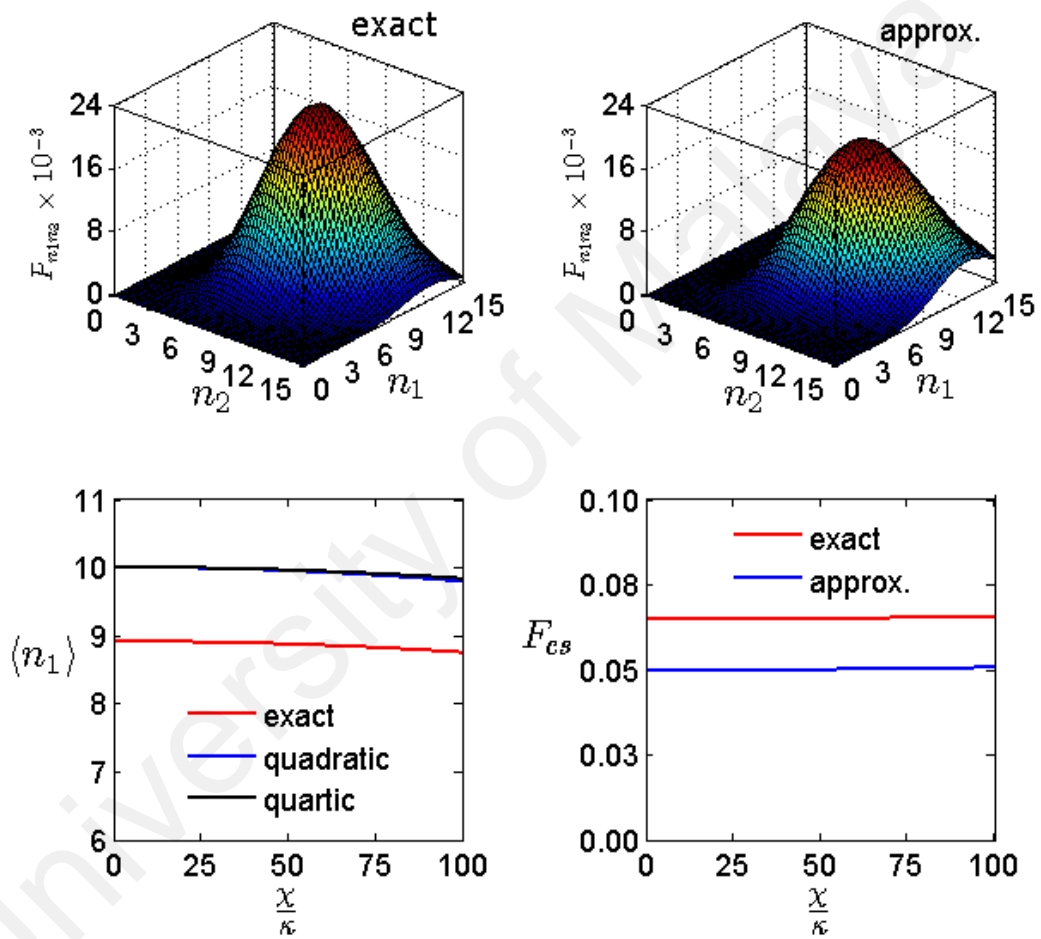


Figure 5.11: The distribution $P_{n_1 n_2}$ (upper panel for $\chi = 50\kappa$), $\langle n_1 \rangle$, and F_{CS} (lower panel) at $r_a = 40\kappa$, $\Delta = 0$, $\chi_1 = 0$. The approximate solutions are from Equation 5.39 for quadratic and from Equation 5.35 for quartic.

CHAPTER 6: CONCLUSION

In this thesis, the TPL in Kerr-like medium is studied. Effective two-level atoms injected in a dispersive cavity that emit nondegenerate two photons by stimulation emission is considered. The lasing medium is assumed to have a Kerr nonlinearity. A quantum theory of two-photon laser using the Scully-Lamb method is developed. A sophisticated program to obtain the exact numerical solution is developed too. Also, an approximate solution under certain assumptions, which is justified by comparison with the exact numerical results is obtained. The analytic solution enables having more insight into the physics of the problem. To study the statistical properties and nonclassicality of the laser, several measures are calculated. In addition to the numerical solution, explicit formulas for the mean photon number, $G^{(2)}$, Q , entanglement criterion, and photon number distribution are obtained. The effects of the injection rate, detuning, and Kerr parameters on the statistical properties of the field are studied for two cases of the atom-field coupling, intensity-free, and intensity-dependent. Statistics of the laser is found to be sub-Poissonian for different ranges of the Kerr parameters, and for small injection rate and not large positive detuning where the fluctuation ratio is below the classical limit. While the injection rate increases the mean photon number, the Kerr parameters and detuning reduce it. However, the Kerr parameters have a strong effect on the nonclassicality of the field. In the IDC case, the effects of the parameters changed dramatically. The effect of injection rate enhanced by the IDC become dominant, and with more injection rate, statistics transform to sub-Poissonian. However, the effects of Kerr parameters and detuning significantly reduced and limited, and statistics become sub-Poissonian only for small values of Kerr parameters. The results demonstrate strong competition between the Kerr effect, detuning, IDC, and injection rate. The ability to exploit and control the competition between the nonlinear processes of TPL, Kerr effect

and IDC is a fascinating subject for fundamental research. The light produced from such a device with nonclassical properties is promising for information science as well as chemical, biological and medical sciences. The search for entanglement does not succeed where the entanglement criterion does not fulfill due to low correlations and high fluctuations. However, the field exhibits nonclassicality through violation of CSI for all the time and all ranges of the parameters. In metrology, nonclassicality like squeezing or violation of CSI, rather than entanglement, is the necessary resource to achieve quantum advantages. The high nonclassicality is important to enhance the sensitivity of devices in quantum metrology. The need for photon number squeezing for accurate measurements is not avoidable as in interferometry. The nonclassicality in the TPL enhanced by the Kerr effect increases the reduction in the noise in photon number fluctuations that improves measurement tasks as in gravitational wave detection. It is expected that the results of this work will have some implications in this direction. One potential extension to this work is considering a few linear processes besides these nonlinear to achieve more understanding of the physical processes and using more sophisticated mathematical techniques.

REFERENCES

- Aasi, J., Abadie, J., Abbott, B., Abbott, R., Abbott, T., Abernathy, M., Adams, C., Adams, T., Addesso, P., Adhikari, R., et al. (2013). Enhanced sensitivity of the LIGO gravitational wave detector by using squeezed states of light. *Nature Photonics*, 7(8), 613–619.
- Abadie, J., Abbott, B. P., Abbott, R., Abbott, T. D., Abernathy, M., Adams, C., Adhikari, R., Affeldt, C., Allen, B., Allen, G. S., et al. (2011). A gravitational wave observatory operating beyond the quantum shot-noise limit. *Nature Physics*, 7(12), 962–965.
- Agarwal, G. S. (2013). *Quantum Optics*. Cambridge University Press, New York, USA.
- Agarwal, G. S. & Wolf, E. (1970a). Calculus for functions of noncommuting operators and general phase-space methods in quantum mechanics. I. mapping theorems and ordering of functions of noncommuting operators. *Physical Review D*, 2(10), 2161–2186.
- Agarwal, G. S. & Wolf, E. (1970b). Calculus for functions of noncommuting operators and general phase-space methods in quantum mechanics. II. quantum mechanics in phase space. *Physical Review D*, 2(10), 2187–2205.
- Agarwal, G. S. & Wolf, E. (1970c). Calculus for functions of noncommuting operators and general phase-space methods in quantum mechanics. III. a generalized wick theorem and multitime mapping. *Physical Review D*, 2(10), 2206–2225.
- Audretsch, J. (2008). *Entangled systems: new directions in quantum physics*. John Wiley & Sons.
- Bachor, H. & Ralph, T. (2004). *A Guide to Experiments in Quantum Optics*. Wiley-VCH Verlag GmbH & Co. KGaA, Weinheim, Germany.
- Bandilla, A. & Voigt, H. (1982). Quantum statistics of light after saturated two-photon emission processes and the photon statistics of a two-photon laser. *Optics Communications*, 43(4), 277–280.
- Barnett, S. (2009). *Quantum Information*. Oxford Master Series in Physics. Oxford University Press Inc., New York.

- Bartzis, V. (1990). Intensity dependent, two-photon Jaynes-Cummings model. *Physica A: Statistical Mechanics and its Applications*, 166(2), 347–360.
- Bay, S., Elk, M., & Lambropoulos, P. (1995). Aspects of the degenerate two-photon laser. *Journal of Physics B: Atomic, Molecular and Optical Physics*, 28(24), 5359–5376.
- Blaise, P. & Henri-Rousseau, O. (2011). *Quantum Oscillators*. John Wiley & Sons Inc., New Jersey, USA.
- Blum, K. (2012). *Density Matrix Theory and Applications* (3 ed.), volume 64. Springer Science & Business Media, Heidelberg, Germany.
- Boone, A. W. & Swain, S. (1989a). Effective hamiltonians and the two-photon laser. *Quantum Optics: Journal of the European Optical Society Part B*, 1(1), 27–47.
- Boone, A. W. & Swain, S. (1989b). Effective hamiltonians in two-photon laser theory. *Optics Communications*, 73(1), 47–50.
- Boone, A. W. & Swain, S. (1990). Theory of the degenerate two-photon laser. *Physical Review A*, 41(1), 343–351.
- Born, M. & Wolf, E. (1999). *Principles of Optics: electromagnetic theory of propagation, interference and diffraction of light*. Cambridge University Press, Cambridge, UK.
- Bouwmeester, D. & Zeilinger, A. (2000). The physics of quantum information: basic concepts. In *The physics of quantum information* (pp. 1–14). Springer.
- Boyd, R. W., Lukishova, S. G., & Zadkov, V. N. (2019). *Quantum photonics: pioneering advances and emerging applications*, volume 217. Springer, Switzerland.
- Brambilla, M., Castelli, F., Lugiato, L., Pessina, E., Prati, F., Strini, G., & Galatola, P. (1992). Generation of nonclassical states by nonlinear optical systems. *Applied Physics B*, 55(3), 190–201.
- Braunstein, S. L. & van Loock, P. (2005). Quantum information with continuous variables. *Reviews of Modern Physics*, 77, 513–577.

- Bužek, V. & Jex, I. (1990). Dynamics of a two-level atom in a Kerr-like medium. *Optics Communications*, 78(5-6), 425–435.
- Cahill, K. E. & Glauber, R. J. (1969a). Density operators and quasiprobability distributions. *Physical Review*, 177, 1882–1902.
- Cahill, K. E. & Glauber, R. J. (1969b). Ordered expansions in boson amplitude operators. *Physical Review*, 177, 1857–1881.
- Carmichael, H. (1993). *An open systems approach to quantum optics*. Springer Berlin Heidelberg.
- Carmichael, H. (2002). *Statistical Methods in Quantum Optics 1: Master Equations and Fokker-Planck Equations*. Corrected Second Printing 2002, Springer-Verlag, Berlin Heidelberg. First Edition 1999.
- Carmichael, H. (2008). *Statistical Methods in Quantum Optics 2: Non-Classical Fields*. Theoretical and Mathematical Physics. Springer Berlin Heidelberg.
- Caves, C. M. (1980). Quantum-mechanical radiation-pressure fluctuations in an interferometer. *Physical Review Letters*, 45, 75–79.
- Caves, C. M. (1981). Quantum-mechanical noise in an interferometer. *Physical Review D*, 23, 1693–1708.
- Cheng, W. Z. & Haken, H. (1988). Quantum theory of the two-photon laser. *Zeitschrift für Physik B Condensed Matter*, 71(2), 253–259.
- Cohen-Tannoudji, C., Dupont-Roc, J., & Grynberg, G. (1997). *Photons and Atoms: Introduction to Quantum Electrodynamics*. Wiley-VCH Verlag GmbH & Co. KGaA, Weinheim, Germany.
- Damanet, F., Kübler, J., Martin, J., & Braun, D. (2018). Nonclassical states of light with a smooth P function. *Physical Review A*, 97(2), 023832(1–12).
- Davidovich, L. (1996). Sub-poissonian processes in quantum optics. *Reviews of Modern Physics*, 68(1), 127–173.

- Denk, W., Strickler, J. H., & Webb, W. W. (1990). Two-photon laser scanning fluorescence microscopy. *Science*, 248(4951), 73–76.
- Dodonov, V. V. (2002). Nonclassical states in quantum optics: squeezed review of the first 75 years. *Journal of Optics B: Quantum and Semiclassical Optics*, 4(1), R1–R33.
- Dodonov, V. V., Klimov, A., & Man'ko, V. I. (1989). Photon number oscillation in correlated light. *Physics Letters A*, 134(4), 211–216.
- Dodonov, V. V. & Man'ko, V. I. (2003). *Theory of nonclassical states of light*. CRC Press, New York, USA.
- Dodonov, V. V. & Mizrahi, S. S. (1997a). Competition between one-and two-photon absorption processes. *Journal of Physics A: Mathematical and General*, 30(9), 2915–2935.
- Dodonov, V. V. & Mizrahi, S. S. (1997b). Exact stationary photon distributions due to competition between one-and two-photon absorption and emission. *Journal of Physics A: Mathematical and General*, 30(16), 5657–5667.
- Drummond, P. D. & Gardiner, C. W. (1980). Generalised p-representations in quantum optics. *Journal of Physics A: Mathematical and General*, 13(7), 2353–2368.
- Dung, H. T., Shumovsky, A. S., & Bogolubov Jr, N. N. (1992). Antibunching and sub-poissonian photon statistics in the Jaynes-Cummings model. *Optics Communications*, 90(4-6), 322–328.
- Einstein, A., Podolsky, B., & Rosen, N. (1935). Can quantum-mechanical description of physical reality be considered complete? *Physical Review*, 47(10), 777–780.
- Eremeev, V., Skipetrov, S., & Orszag, M. (2011). Quantum theory of a two-mode open-cavity laser. *Physical Review A*, 84(2), 023816(1–8).
- Esfandiari, R. S. (2017). *Numerical methods for engineers and scientists using MATLAB®*. CRC Press, New York, USA.
- Every, I. (1975). The production of photon antibunching by two-photon absorption. *Journal of Physics A: Mathematical and General*, 8(7), L69–L72.

- Fabre, C. (1992). Squeezed states of light. *Physics Reports*, 219(3-6), 215–225.
- Faghihi, M., Tavassoly, M., & Hooshmandasl, M. (2013). Entanglement dynamics and position-momentum entropic uncertainty relation of a Λ -type three-level atom interacting with a two-mode cavity field in the presence of nonlinearities. *Journal of the Optical Society of America B*, 30(5), 1109–1117.
- Fano, U. (1947). Ionization yield of radiations. II. the fluctuations of the number of ions. *Physical Review*, 72, 26–29.
- Fischer, K. (2018). Derivation of the quantum-optical master equation based on coarse-graining of time. *Journal of Physics Communications*, 2(9), 091001(1–10).
- Fox, M. (2006). *Quantum Optics: An Introduction*. Oxford Master Series in Physics. Oxford University Press, New York, USA.
- Friis, N., Skotiniotis, M., Fuentes, I., & Dür, W. (2015). Heisenberg scaling in Gaussian quantum metrology. *Physical Review A*, 92, 022106(1–8).
- Gao, Y.-F., Feng, J., & Shi, S.-R. (2002). Cavity field spectra of the intensity-dependent two-mode Jaynes–Cummings model. *International Journal of Theoretical Physics*, 41(5), 867–875.
- Gardiner, C. & Zoller, P. (2004). *Quantum noise: a handbook of Markovian and non-Markovian quantum stochastic methods with applications to quantum optics*, volume 56. Springer Science & Business Media.
- Garrison, J. & Chiao, R. (2008). *Quantum Optics*. Oxford Graduate Texts. Oxford University Press Inc., New York, USA.
- Gauthier, D. J. (2003). Two-photon lasers. In *Progress in Optics*, volume 45 (pp. 205–272). North-Holland Publishing Company - Amsterdam, Netherland.
- Ge, W., Jacobs, K., Eldredge, Z., Gorshkov, A. V., & Foss-Feig, M. (2018). Distributed quantum metrology with linear networks and separable inputs. *Physical Review Letters*, 121, 043604(1–6).
- Gerry, C. C. & Knight, P. L. (2005). *Introductory Quantum Optics*. Cambridge University

Press, New York, USA.

Ghorbani, M., Faghihi, M. J., & Safari, H. (2017). Wigner function and entanglement dynamics of a two-atom two-mode nonlinear Jaynes–Cummings model. *Journal of the Optical Society of America B*, 34(9), 1884–1893.

Glauber, R. J. (1963a). Coherent and incoherent states of the radiation field. *Physical Review*, 131(6), 2766–2788.

Glauber, R. J. (1963b). Photon correlations. *Physical Review Letters*, 10(3), 84–86.

Glauber, R. J. (1963c). The quantum theory of optical coherence. *Physical Review*, 130(6), 2529–2539.

Goldstein, H., Poole, C. P., & Safko, J. (2011). *Classical Mechanics*. Pearson Education India.

Göppert-Mayer, M. (1931). Über elementarakte mit zwei quantensprüngen. *Annalen der Physik*, 401(3), 273–294.

Greiner, W. & Reinhardt, J. (1996). *Field Quantization*. Springer-Verlag, Berlin-Heidelberg, Germany.

Grynberg, G., Aspect, A., & Fabre, C. (2010). *Introduction to Quantum Optics: From the Semi-classical Approach to Quantized Light*. Cambridge University Press.

Haar, D. T. (1961). Theory and applications of the density matrix. *Reports on Progress in Physics*, 24(1), 304–362.

Haken, H. (2012). *Laser Theory*. Springer Berlin Heidelberg, Germany.

Hassani, S. (2013). *Mathematical physics: a modern introduction to its foundations*. Springer Science & Business Media, Switzerland.

He, S. & Liu, S. (2017). *Advanced Nonlinear Optics*. World Scientific Publishing Company, Singapore.

- Hillery, M. (1987). Nonclassical distance in quantum optics. *Physical Review A*, 35(2), 725–732.
- Hillery, M. (2009). An introduction to the quantum theory of nonlinear optics. *Acta Physica Slovaca*, 59(1), 1–80.
- Hillery, M., O’Connell, R., Scully, M., & Wigner, E. (1984). Distribution functions in physics: Fundamentals. *Physics Reports*, 106(3), 121–167.
- Hillery, M. & Zubairy, M. S. (2006). Entanglement conditions for two-mode states. *Physical Review Letters*, 96(5), 050503(1–4).
- Horodecki, R., Horodecki, P., Horodecki, M., & Horodecki, K. (2009). Quantum entanglement. *Reviews of Modern Physics*, 81(2), 865–942.
- Inc, O. F. (2019). The on-line encyclopaedia of integer sequences. <https://oeis.org>. Accessed on 2019-11-10.
- Ivan, J. S., Chaturvedi, S., Ercolessi, E., Marmo, G., Morandi, G., Mukunda, N., & Simon, R. (2011). Entanglement and nonclassicality for multimode radiation-field states. *Physical Review A*, 83(3), 032118(1–20).
- Jackson, J. D. (1999). *Classical Electrodynamics* (3rd ed. ed.). Jon Wiley & Sons, New York, USA.
- Jaynes, E. T. & Cummings, F. W. (1963). Comparison of quantum and semiclassical radiation theories with application to the beam maser. *Proceedings of the IEEE*, 51(1), 89–109.
- Kaiser, W. & Garrett, C. G. B. (1961). Two-photon excitation in $\text{CaF}_2: \text{Eu}^{2+}$. *Physical Review Letters*, 7, 229–231.
- Khan, R., Massel, F., & Heikkilä, T. T. (2015). Cross-Kerr nonlinearity in optomechanical systems. *Physical Review A*, 91, 043822(1–6).
- Kheruntsyan, K., Jaskula, J.-C., Deuar, P., Bonneau, M., Partridge, G. B., Ruaudel, J., Lopes, R., Boiron, D., & Westbrook, C. I. (2012). Violation of the Cauchy-Schwarz inequality with matter waves. *Physical Review Letters*, 108(26), 260401(1–5).

- Kim, D. M., Scully, M. O., & Lamb, W. E. (1970). Quantum theory of an optical maser. V. atomic motion and recoil. *Physical Review A*, 2, 2534–2541.
- Kim, J., Somani, S., & Yamamoto, Y. (2012). *Nonclassical Light from Semiconductor Lasers and LEDs*. Springer Berlin Heidelberg.
- Kimble, H. J. (1992). Squeezed states of light: an (incomplete) survey of experimental progress and prospects. *Physics Reports*, 219(3-6), 227–234.
- Kimble, H. J., Dagenais, M., & Mandel, L. (1977). Photon antibunching in resonance fluorescence. *Physical Review Letters*, 39(11), 691–695.
- Kimble, H. J. & Mandel, L. (1976). Theory of resonance fluorescence. *Physical Review A*, 13(6), 2123–2144.
- Kimble, H. J. & Mandel, L. (1977). Resonance fluorescence with excitation of finite bandwidth. *Physical Review A*, 15, 689–699.
- Klaers, J., Schmitt, J., Vewinger, F., & Weitz, M. (2010). Bose–Einstein condensation of photons in an optical microcavity. *Nature*, 468(7323), 545–548.
- Klauder, J. & Skagerstam, B. (1985). *Coherent States: Applications in Physics and Mathematical Physics*. World Scientific Publishing Company, Singapore.
- Klauder, J. & Sudarshan, E. (2006). *Fundamentals of Quantum Optics*. Dover books on physics. Dover Publications, New York.
- Klyshko, D. (1996). The nonclassical light. *Physics-Uspekhi*, 39(6), 573–596.
- Knight, P. & Bužek, V. (2004). Squeezed states: Basic principles. In *Quantum Squeezing* (pp. 3–32). Springer, Berlin, Heidelberg.
- Knight, P. & Pegg, D. (1982). Double-photon transitions induced by antibunched light. *Journal of Physics B: Atomic and Molecular Physics*, 15(18), 3211–3222.
- Kozierowski, M. (1981). Photon antibunching in nonlinear optical processes. *Soviet Journal of Quantum Electronics*, 11(6), 695–701.

- Kreuzer, H. J. (1981). *Nonequilibrium thermodynamics and its statistical foundations*. Oxford University Press, New York, USA.
- Kryuchkyan, G. Y., Petrosyan, K., & Kheruntsyan, K. (1996). Critical effects in photon correlation for parametric generation. *Journal of Experimental and Theoretical Physics Letters*, 63(7), 526–531.
- Kühn, B. & Vogel, W. (2018). Preparation of arbitrary quantum states with regular P functions. *Physical Review A*, 98(5), 053807(1–12).
- Kwon, H., Tan, K. C., Volkoff, T., & Jeong, H. (2019). Nonclassicality as a quantifiable resource for quantum metrology. *Physical Review Letters*, 122(4), 040503(1–6).
- Landau, L. D. & Lifshitz, E. M. (1976). *Mechanics*. Butterworth-Heinemann, UK.
- Landau, L. D. & Lifshitz, E. M. (1981). *Quantum Mechanics; Non-relativistic Theory*. Pergamon Press, Oxford, England.
- Lax, M. & Louisell, W. H. (1969). Quantum noise. XII. density-operator treatment of field and population fluctuations. *Physical Review*, 185, 568–591.
- Loudon, R. (1980). Non-classical effects in the statistical properties of light. *Reports on Progress in Physics*, 43(7), 913–949.
- Loudon, R. (2000). *The Quantum Theory of Light*. Oxford University Press, Oxford.
- Loudon, R. & Knight, P. L. (1987). Squeezed light. *Journal of Modern Optics*, 34(6-7), 709–759.
- Louisell, W. H. (1973). *Quantum Statistical Properties of Radiation*, volume 7. John Wiley & Sons, Inc., Canada.
- Lu, N. & Bergou, J. A. (1989). Quantum theory of a laser with injected atomic coherence: Quantum noise quenching via nonlinear processes. *Physical Review A*, 40(1), 237–249.
- Lvovsky, A. I. (2015). Squeezed light. *Photonics: Scientific Foundations, Technology and*

Applications, 1, 121–163.

Mandel, L. (1976). The case for and against semiclassical radiation theory. In *Progress in Optics*, volume 13 (pp. 27–68). North-Holland Publishing Company - Amsterdam, Netherland.

Mandel, L. (1979). Sub-poissonian photon statistics in resonance fluorescence. *Optics Letters*, 4(7), 205–207.

Mandel, L. (1986). Non-classical states of the electromagnetic field. *Physica Scripta*, 1986(T12), 34–42.

Mandel, L. & Wolf, E. (1995). *Optical Coherence and Quantum Optics*. Cambridge University Press, New York, USA.

Mathkoor, F. H. A., Kam, C. H., & Ooi, C. H. R. (2020). Nonclassicality of the two-photon laser with Kerr nonlinearity. *Journal of the Optical Society of America B*, 37(3), 820–833.

McNeil, K. & Walls, D. (1975a). Quantum theory of multiphoton lasers. I. systems in detailed balance. *Journal of Physics A: Mathematical and General*, 8(1), 104–110.

McNeil, K. & Walls, D. (1975b). Quantum theory of multiphoton lasers. II. systems without detailed balance. *Journal of Physics A: Mathematical and General*, 8(1), 111–119.

McWeeny, R. (1960). Some recent advances in density matrix theory. *Reviews of Modern Physics*, 32, 335–369.

Mermin, N. D. (2007). *Quantum computer science: an introduction*. Cambridge University Press, New York, USA.

Meystre, P. & Sargent, M. (2007). *Elements of Quantum Optics*. Springer-Verlag Berlin Heidelberg.

Napoli, A. & Messina, A. (1996). Quantum effects in the dynamics of intensity-dependent two-mode two-photon models of radiation—matter interaction. *Nuclear Instruments and Methods in Physics Research Section B: Beam Interactions with Materials and Atoms*, 116(1-4), 465–472.

- Nielsen, M. & Chuang, I. (2010). *Quantum Computation and Quantum Information: 10th Anniversary Edition*. Cambridge University Press, New York, USA.
- Ooi, C. H. R. (2007). Continuous source of phase-controlled entangled two-photon laser. *Physical Review A*, 76(1), 013809(1–7).
- Ooi, C. H. R., Sun, Q., Zubairy, M. S., & Scully, M. O. (2007). Correlation of photon pairs from the double Raman amplifier: Generalized analytical quantum Langevin theory. *Physical Review A*, 75(1), 013820(1–13).
- Orszag, M. (2016). *Quantum Optics: Including Noise Reduction, Trapped Ions, Quantum Trajectories, and Decoherence*. Springer, Switzerland.
- Orszag, M. & Retamal, J. (1991). Reduction of photon-number fluctuations in two-photon lasers. *Physical Review A*, 43(11), 6209–6216.
- Parker, M. A. (2005). *Physics of Optoelectronics*. CRC Press, New York, USA.
- Paul, H. (1982). Photon antibunching. *Reviews of Modern Physics*, 54, 1061–1102.
- Pennini, F. & Plastino, A. (2010). Diverging Fano factors. In *Journal of Physics: Conference Series*, volume 246, (pp. 012030). IOP Publishing.
- Peřina, J., Hradil, Z., & Jurčo, B. (1994). *Quantum optics and fundamentals of physics*. Springer, Netherlands.
- Phoenix, S. J. D. & Knight, P. L. (1988). Fluctuations and entropy in models of quantum optical resonance. *Annals of Physics*, 186(2), 381–407.
- Prokhorov, A. (1965). Nobel prize lecture. *Science*, 149, 828–830.
- Puri, R. R. (2001). *Mathematical methods of quantum optics*, volume 79. Springer-Verlag Berlin, Heidelberg, Germany.
- Rand, S. C. (2016). *Lectures on light: nonlinear and quantum optics using the density matrix*. Oxford University Press, New York, USA.

- Reid, M. & Walls, D. (1986). Violations of classical inequalities in quantum optics. *Physical Review A*, 34(2), 1260–1276.
- Richter, T. & Vogel, W. (2002). Nonclassicality of quantum states: A hierarchy of observable conditions. *Physical Review Letters*, 89(28), 283601(1–4).
- Sahota, J. & Quesada, N. (2015). Quantum correlations in optical metrology: Heisenberg-limited phase estimation without mode entanglement. *Physical Review A*, 91, 013808(1–7).
- Sargent III, M., Scully, M., & Lamb Jr, W. (1974). *Laser physics*. Addison-Wesley, USA.
- Savage, C. M. & Walls, D. F. (1986). Squeezing via two-photon transitions. *Physical Review A*, 33, 3282–3291.
- Schleich, W. P. (2001). *Quantum Optics in Phase Space*. Wiley-VCH Verlag Berlin GmbH, Berlin, Germany.
- Schnabel, R. (2017). Squeezed states of light and their applications in laser interferometers. *Physics Reports*, 684, 1–51. Squeezed states of light and their applications in laser interferometers.
- Schrade, G., Akulin, V., Man'ko, V., & Schleich, W. (1993). Photon statistics of a two-mode squeezed vacuum. *Physical Review A*, 48(3), 2398–2406.
- Schrödinger, E. (1935). Discussion of probability relations between separated systems. In *Mathematical Proceedings of the Cambridge Philosophical Society*, volume 31, (pp. 555–563). Cambridge University Press.
- Schrödinger, E. (1936). Probability relations between separated systems. *Mathematical Proceedings of the Cambridge Philosophical Society*, 32(3), 446–452.
- Scully, M. O., Kim, D. M., & Lamb, W. E. (1970). Quantum theory of an optical maser. IV. generalization to include finite temperature and cavity detuning. *Physical Review A*, 2, 2529–2533.
- Scully, M. O. & Lamb, W. E. (1967). Quantum theory of an optical maser. I. general theory. *Physical Review*, 159, 208–226.

- Scully, M. O. & Lamb, W. E. (1968). Quantum theory of an optical maser. II. spectral profile. *Physical Review*, 166, 246–249.
- Scully, M. O. & Lamb, W. E. (1969). Quantum theory of an optical maser. III. theory of photoelectron counting statistics. *Physical Review*, 179, 368–374.
- Scully, M. O. & Zubairy, M. S. (1997). *Quantum Optics*. Cambridge University Press, Cambridge, UK.
- Semiao, F. L., Furuya, K., & Milburn, G. J. (2009). Kerr nonlinearities and nonclassical states with superconducting qubits and nanomechanical resonators. *Physical Review A*, 79(6), 063811(1–5).
- Shore, B. W. & Knight, P. L. (1993). The Jaynes-Cummings model. *Journal of Modern Optics*, 40(7), 1195–1238.
- Short, R. & Mandel, L. (1983). Observation of sub-poissonian photon statistics. *Physical Review Letters*, 51(5), 384–387.
- Simaan, H. (1975). Quantum statistics of the stimulated Raman effect. *Journal of Physics A: Mathematical and General*, 8(10), 1620–1637.
- Simaan, H. & Loudon, R. (1975a). Quantum statistics of double-beam two-photon absorption. *Journal of Physics A: Mathematical and General*, 8(7), 1140–1158.
- Simaan, H. & Loudon, R. (1975b). Quantum statistics of single-beam two-photon absorption. *Journal of Physics A: Mathematical and General*, 8(4), 539–554.
- Simaan, H. & Loudon, R. (1978). Off-diagonal density matrix for single-beam two-photon absorbed light. *Journal of Physics A: Mathematical and General*, 11(2), 435–441.
- Singh, S. (1983). Antibunching, sub-poissonian photon statistics and finite bandwidth effects in resonance fluorescence. *Optics Communications*, 44(4), 254–258.
- Singh, S. & Gilhare, K. (2016a). Dynamics for a two-atom two-mode intensity-dependent Raman coupled model. *Journal of Experimental and Theoretical Physics*, 122(6), 984–994.

- Singh, S. & Gilhare, K. (2016b). Influence of Kerr-like medium on the dynamics of a two-mode Raman coupled model. *Journal of Modern Optics*, 63(15), 1506–1520.
- Singh, S. & Ooi, C. H. R. (2018). Dynamics of Kerr-like medium with two-mode intensity-dependent cavity fields. *Laser Physics*, 29(1), 015202(1–12).
- Singh, S., Ooi, C. H. R., & Amrita (2012). Dynamics for two atoms interacting with intensity-dependent two-mode quantized cavity fields in the ladder configuration. *Physical Review A*, 86(2), 023810(1–12).
- Sorokin, P. P. & Braslau, N. (1964). Some theoretical aspects of a proposed double quantum stimulated emission device. *IBM Journal of Research and Development*, 8(2), 177–181.
- Sudarshan, E. C. G. (1963). Equivalence of semiclassical and quantum mechanical descriptions of statistical light beams. *Physical Review Letters*, 10(7), 277–279.
- Tan, K. C. & Jeong, H. (2019). Nonclassical light and metrological power: An introductory review. *AVS Quantum Science*, 1(1), 014701(1–28).
- Teich, M. C. & Saleh, B. E. A. (1985). Observation of sub-poisson Franck-Hertz light at 253.7 nm. *Journal of the Optical Society of America B*, 2(2), 275–282.
- Titulaer, U. & Glauber, R. (1965). Correlation functions for coherent fields. *Physical Review*, 140(3B), B676–B682.
- Ustione, A. & Piston, D. (2011). A simple introduction to multiphoton microscopy. *Journal of Microscopy*, 243(3), 221–226.
- Vedral, V. (2006). *Introduction to quantum information science*. Oxford University Press, New York, USA.
- Walls, D. F. (1983). Squeezed states of light. *Nature*, 306(5939), 141–146.
- Walls, D. F. & Milburn, G. J. (2008). *Quantum Optics*. Springer-Verlag Berlin, Heidelberg, Germany.

- Walther, H., Varcoe, B. T., Englert, B.-G., & Becker, T. (2006). Cavity quantum electrodynamics. *Reports on Progress in Physics*, 69(5), 1325–1382.
- Wang, Y. K. & Lamb, W. E. (1973). Quantum theory of an optical maser. VI. transient behavior. *Physical Review A*, 8, 866–873.
- Wang, Z. C. & Haken, H. (1984a). Theory of two-photon lasers I. *Zeitschrift für Physik B Condensed Matter*, 55(4), 361–370.
- Wang, Z. C. & Haken, H. (1984b). Theory of two-photon lasers II. *Zeitschrift für Physik B Condensed Matter*, 56(1), 77–82.
- Wang, Z. C. & Haken, H. (1984c). Theory of two-photon lasers III. *Zeitschrift für Physik B Condensed Matter*, 56(1), 83–90.
- Wigner, E. (1932). On the quantum correction for thermodynamic equilibrium. *Physical Review*, 40, 749–759.
- Wilf, H. (2006). *Generatingfunctionology* (3 ed.). A K Peters, Ltd., Wellesley, MA, USA.
- Yamamoto, Y., Machida, S., & Nilsson, O. (1986). Amplitude squeezing in a pump-noise-suppressed laser oscillator. *Physical Review A*, 34, 4025–4042.
- Yamamoto, Y. & Semba, K. (2015). *Principles and Methods of Quantum Information Technologies*. Lecture Notes in Physics. Springer, Tokyo, Japan.
- Yuen, H. P. (1976). Two-photon coherent states of the radiation field. *Physical Review A*, 13, 2226–2243.
- Yurke, B. & Stoler, D. (1986). Generating quantum mechanical superpositions of macroscopically distinguishable states via amplitude dispersion. *Physical Review Letters*, 57, 13–16.
- Zangwill, A. (2013). *Modern Electrodynamics*. Cambridge University Press, Cambridge, UK.
- Zhang, W.-M., Feng, D. H., & Gilmore, R. (1990). Coherent states: Theory and some

applications. *Reviews of Modern Physics*, 62, 867–927.

Zhu, S.-Y. & Li, X.-S. (1987). Quantum theory of a two-photon laser. *Physical Review A*, 36, 3889–3896.

Zou, X. & Mandel, L. (1990). Photon-antibunching and sub-poissonian photon statistics. *Physical Review A*, 41(1), 475–476.

Zubairy, M. (1980). Photon statistics of a two-photon laser. *Physics Letters A*, 80(4), 225–228.

Zubairy, M. (1982). Nonclassical effects in a two-photon laser. *Physics Letters A*, 87(4), 162–164.

Zubairy, M., Razmi, M., Iqbal, S., & Idress, M. (1983). Squeezed states in a multiphoton absorption process. *Physics Letters A*, 98(4), 168–170.

University of Malaya

LIST OF PUBLICATIONS AND PAPERS PRESENTED

Mathkooor, F. H. A., Kam, C. H., Ooi, C. H. R. (2020). Nonclassicality of the two-photon laser with Kerr nonlinearity. *Journal of the Optical Society of America B*, 37(3), 820–833.

Nahri, D. G., **Mathkooor, F. H. A.**, Ooi, C. H. R. (2016). Real-time path-integral approach for dissipative quantum dot-cavity quantum electrodynamics: impure dephasing-induced effects. *Journal of Physics: Condensed Matter*, 29(5), 055701(1–22).

University of Malaya